Computational and Matrix Isolation Studies of Heterocyclic Radicals and Azoheteroarene Photoswitches

CHITRANJAN SAH

A thesis submitted for the partial fulfillment of
the degree of Doctor of Philosophy

Department of Chemical Sciences

Indian Institute of Science Education and Research Mohali

Knowledge city, Sector 81, SAS Nagar, Manauli PO, Mohali 140306, Punjab, India.

December 2021

Dedicated to my family for their love and support

Declaration

The work presented in this thesis has been carried out by me under the guidance of Dr. Sugumar Venkataramani at the Indian Institute of Science Education and Research Mohali. This work has not been submitted in part or in full for a degree, a diploma, or a fellowship to any other university or institute. Whenever contributions of others are involved, every effort is made to indicate this clearly, with due acknowledgement of collaborative research and discussions. This thesis is a bonafide record of original work done by me and all sources listed within have been detailed in the bibliography.

Chitranjan Sah

In my capacity as the supervisor of the candidate's thesis work, I certify that the above statements by the candidate are true to the best of my knowledge.

Dr. Sugumar Venkataramani

Acknowledgements

Firstly, I want to express my gratitude towards my supervisor Dr. Sugumar Venkataramani for showing faith in my abilities, guiding and motivating me throughout the research journey. The independence provided by him to execute the research work helped me to develop the art of thinking and analysis to a much greater extent. Apart from science, under his guidance, I developed myself as a good presenter, a student with patience and a mature mind, and overall a much better human being. I also want to thank, Dr. P. Balanarayan and Dr. Arijit. K. De for being a part of thesis committee and for their valuable and fruitful discussions during the annual work assessment. I also want to thank Prof. K. S. Viswanathan for sharing his immense scientific experiences and helping in setting up of matrix isolation facility in lab. I am grateful to the former Director Prof. N. Sathyamurthy and also to the present Director Prof. J. Gowrishankar for the experimental and computational facilities. I am thankful to former HOD, Department of Chemical Sciences, Prof. K. S. Viswanathan and Dr. S A Babu along with the current HOD Dr. Sanjay Singh for granting the use of various departmental facilities. My sincere thanks to the faculty members of Department of Chemical Sciences for offering their teachings during my coursework.

I am thankful to Anjali Mahadevan and Pravesh Kumar for their efforts towards the synthesis of precursors used for the matrix isolation experiments. I would like to acknowledge Dr. Bhisma K Patel and Suresh Rajamanickam for giving me the opportunity to share my scientific and computational skills in encountering interesting problems. I am also thankful to Prof. K.S. Viswanathan and Dr. Ananth Venkatesan's lab for assisting with experimental advice and providing vacuum accessories whenever in need.

Contents

Chapter 1. Introduction

Chapter 2. Through space and through bond interactions of nitrogen lone pair with radical electron in pyridyl radical isomers

Chapter 3. Role of spin density in predicting the unimolecular and bimolecular reactivity patterns of pyridyl, pyridyl-*N*-oxide, and pyridinyl radical isomers

Chapter 4. Competition between delocalization and ring strain in determining the stability pattern of five-membered heterocyclic radicals

Chapter 5. Photochemistry of 2-hydroxyphenylazo-3,5-dimethylisoxazole under matrix isolation conditions

Chapter 6. Materials and Methods

Chapter 7. Summary and Outlook

List of Abbreviations

TS:	Through Space
TB:	Through Bond
BDE:	Bond Dissociation Energy
ESP:	Electrostatic Potential
NBO:	Natural Bond Orbital
(U)B3LYP:	(Unrestricted) Becke, 3-parameter, Lee-Yang-Parr
(U)M06:	(Unrestricted) Minnesota functional 06
(U)CCSDT:	(Unrestricted) Coupled Cluster Single and Double Substitutions with Triples
CC-pVDZ:	Correlation Consistent Polarized Valence only basis set Double-Zeta
CC-pVTZ:	Correlation Consistent Polarized Valence only basis set Triple-Zeta
CASSCF:	Complete Active Space Self Consistent Field
MCSCF:	Multi-configurational Self Consistent Field
SOMO:	Singly Occupied Molecular Orbital
LUMO:	Lowest Unoccupied Molecular Orbital
VIE:	Vertical Ionization Energy
VDE:	Vertical Detachment Energy
RSE:	Radical Stabilization Energy
NICS:	Nucleus-independent Chemical Shift
FTIR:	Fourier-Transform Infrared Spectroscopy
MM:	Molecular Mechanics
MD:	Molecular Dynamics
SEC:	Semiempirical Calculations
DFT:	Density Functional Theory
PES:	Potential Energy Surface
BHA:	Butylatedhydroxyanisole
BHT:	Butylatedhydroxytoluene
ROS:	Reactive Oxygen Species
RNS:	Reactive Nitrogen Species

SOD:	Superoxide Dismutase
GP$_X$:	Glutathione Peroxidase
CAT:	Catalase
STO:	Slater Type Orbitals
GTO:	Gaussian Type Orbitals
NHPI:	N-hydroxyphthalamide
PINO:	Phthalamido-N-Oxyl
TEMPO:	2,2,6,6-Tetramethyl Piperidine-N-Oxyl
HPAI:	2-Hydroxy Phenylazo-3,5-Dimethylisoxazole
AIM:	Atom In Molecule
ISM:	Interstellar Medium
EPR:	Electron Paramagnetic Resonance

List of Figures

energy, absolute energies are zero-point corrected. Thermal corrections to the Gibbs free energies has been considered for the relative population estimation.

Table 5.5 Computed frequency and intensity of 1Z-C3-*s* at M06-2X/cc-pVTZ level of theory along with the experimental frequency and intensity at 365 nm.

Table 5.6 Computed frequency and intensity of 1Z-C4-*s* at M06-2X/cc-pVTZ level of theory along with the experimental frequency and intensity at 365 nm.

Abstract

Free radicals are regarded as one of the important classes of highly reactive, short-lived intermediates containing an unpaired electron. The utility of these free radicals has been proposed by experimentalists and theoreticians in the field of organic synthesis, combustion chemistry, atmospheric chemistry, interstellar chemistry, and biological implications. Several approaches such as conjugation, spin delocalization, and introduction of heteroatoms have been adapted to enhance the stability as well as tuning the reactivity of radicals. In recent times, nitrogen-based heterocyclic radicals have gained immense importance for their various roles in reactive oxygen species (ROS), material chemistry, biofuels, and in constructing organic molecular-based magnets. Among the various heterocyclic radicals studied thus far, all of the radicals potentially resulted in two center-three electrons (2c-3e) interactions except for boryl and cyclopentadienyl radicals as shown in **Scheme A.1**.

$X = N, N\text{-}O \text{ and } N\text{-}H$

$X = BH, CH_2, NH, O, PH \text{ and } S$
$Y = B, CH, N \text{ and } P$
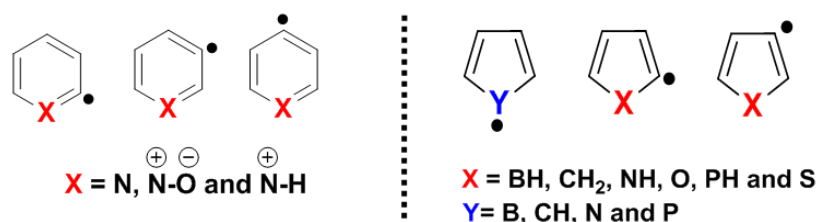
Scheme A.1. Five-and six-membered heterocyclic radicals exhibiting (2c-3e) interactions [exceptions are boryl and cyclopentadienyl radicals].

In this regard, the detailed investigation of the electronic structure and reactivity aspects were carried out using quantum chemical calculations. Through space (TS) and through-bond (TB) interactions prevailing between lone-pair and the radical electron provided valuable information regarding the thermodynamic stability of the isomeric radicals. Whereas, spin density value played a crucial role in predicting the bond cleavage in unimolecular decomposition channels as

well as in explaining the reactivity trend. Moreover, attempts have also been made towards the experimental characterization of 2- and 3-dehydropyridine-*N*-oxide radicals using matrix isolation (MI) technique assisted with infrared spectroscopy and computations. Based on the observations under photochemical conditions, we were able to identify the formation of 3-dehydropyridine-*N*-oxide radical in an inert gas matrix at 4 K. However, our attempts were not successful in the generation of 2-dehydropyridine-*N*-oxide radical, but, we did observe a few interesting species due to photoirradiation.
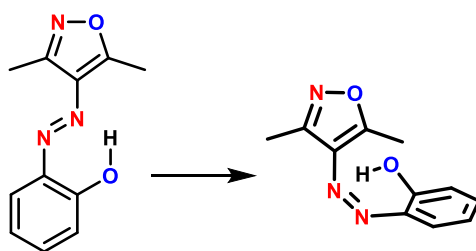
Scheme A.2. 2-Hydroxyphenylazo-3,5-dimethylisoxazole (HPAI) undergoing *E-Z* photoisomerization in an argon matrix at 4 K.

Recently, azoheteroarenes have been intensely studied due to their excellent photoswitching properties and exceptional thermal stability of the photoswitched state. Typically, photoisomerization of azo compounds is well known in the solution phase but their studies are limited under cryogenic conditions in the rigid matrix. In this regard, we explored azoheteroarene based photoswitch (i.e. 2-hydroxyphenylazo-3,5-dimethylisoxazole, HPAI) and successfully confirmed the *E-Z* photoisomerization in an argon matrix at 4 K as shown in **Scheme A.2**. The sharp spectral features at low temperature in combination with computations allowed us to understand the conformations for both *E*- and *Z*-isomers.

Overall, theoretical insights on five-and six-membered heterocyclic radicals, and matrix isolation studies of 2- and 3-iodopyridine-*N*-oxide, 2-hydroxyphenylazo-3,5-dimethylisoxazole will be presented.

Chapter 1

Introduction

1.1 Free radicals and its utility

Free radicals are one of the important and fascinating classes of reactive intermediates.[1-3] In general, a free radical can be defined as a species (atom or molecule) that contains unpaired electron in its valence shell. The names for free radicals have to end with 'yl' as per the nomenclature of organic molecules.[4] In general, the ground state of a radical is a doublet with magnetic quantum numbers ($m_s = \pm 1/2$). In principle, all the free radicals are paramagnetic due to the uncompensated spin of an unpaired electron. The paramagnetic nature is identified and characterized by electron paramagnetic resonance (EPR) spectrum.[5]

The presence of unpaired electron makes them highly reactive, unstable and short lived. In order to attain stability, it usually abstracts hydrogen atom or combines with other radical species. The stability of radicals is often influenced by spin delocalization and conjugation.[6,7] Apart from this, the stability of the radicals (usually carbon-centered) can be tuned by the incorporation of the heteroatom (i.e. O, N, P, S). The lone pair on heteroatom is mainly responsible for the radical stabilization by through space (i.e. direct interaction) or by through bond (i.e. by intervening bonds) interactions.[8,9] Moreover, heteroatom-centered radicals can be stabilized and form another class of stable radicals provided they have the possibility of the delocalization of free electron over the π cloud.[10,11] In this regard several stable radicals[12-14] were synthesized ranging from monoradical to polyradicals[15-18] owing to their potential applications in making molecular magnets and data storage.[19,20]

The free radical chemistry gathered the attention of synthetic chemists for their role in reaction mechanism, polymerization,[21] photoredox catalysis,[22] synthesis of natural products[23] and in explaining regio- and stereoselective outcomes.[24] Among the various types of reactions, free radicals can exhibit substitution, addition, elimination, isomerization, recombination, and disproportionation reactions. With its growing importance, they have been equally explored by biologists, and atmospheric chemists. Considerable attention has been given in envisaging their role in biochemistry of diseases, and aging in medicinal chemistry perspective,[25,26] and also in the cleansing action of the atmosphere.[27-29]

1.2 Historical background

The foundation of the term "radical" was laid in the late eighteenth century. In 1842, Bunsen obtained free cacodyl radical $(CH_3)_2As$ by the reaction of $(CH_3)_2AsCl$ with Zinc.[30] The radical obtained was unstable and resulted as a dimer, $(CH_3)_2AsAs(CH_3)_2$. A few years later in 1849, the existence of alkyl radicals came into picture with the contribution of Kolbe and Frankland. Kolbe reported the electrolytic decarboxylation of potassium acetate forming methyl as the free radical.[31] Frankland also reported the ethyl radical formation from the reaction of ethyl iodide with Zinc.[32] But to their surprise, the vapour pressure measurements showed a dimeric structure (i.e ethane and butane) for the obtained radicals. In 1879, Downes and Blunt reported the dissociation of hydrogen peroxide in solution to hydroxyl radical.[33] In 1891, the idea of generating radicals from electrolysis was reintroduced by Crum Brown and Walker.[34]

$$RCO_2H \xrightarrow[-H^+]{-e^-} RCO_2{}^\bullet \xrightarrow{-CO_2} R^\bullet \longrightarrow RR$$
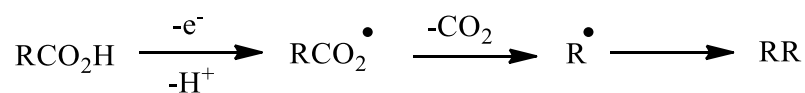
In the beginning of the 19th century, Gomberg and Paneth were the two leading pioneers in the field of free radical chemistry. In 1900, American chemist Gomberg came up with free radical generation in solution. In his attempt, he synthesized hexaphenylethane by the action of triphenylchloromethane with silver.[12,35]

$$2 \ (C_6H_5)_3CCl + 2 \ Ag \ \rightleftharpoons \ (C_6H_5)_3CC(C_6H_5)_3 + 2 \ AgCl$$

Gomberg was pretty sure that the product obtained in solution is a first stable free radical. Unfortunately, the product obtained by him showed characteristics of unsaturated compound by its reaction with halogen and oxygen. At this juncture, Weiland and Chichibabin closely inspected his work and revealed that the molecular mass of the new compound was almost double to the molecular mass of triphenylmethyl. The dimer obtained dissociated slightly into free radicals in solution. By now, Gomberg's valiant efforts gave an idea of obtaining radical which exists in a balance with its dimer in solution.

In 1929, Paneth led the discovery of aliphatic free radicals by passing tetramethyllead through a hot zone in a glass tube.[36,37] The technique was later adopted for the pyrolysis of many organic compounds.

$$(CH_3)_4Pb \xrightarrow{\Delta} 4 \ CH_3^{\bullet} + Pb$$
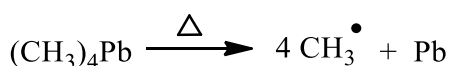
In 1911, Weiland generated diphenylaminyl radical in solution by reversible dissociation of tetraphenylhydrazine at 100 °C.[38,39]

$$(C_6H_5)_2NN(C_6H_5)_2 \ \rightleftharpoons \ 2 \ (C_6H_5)_2N^{\bullet}$$
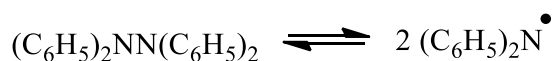
In 1965, Noygebauer with the help of EPR studies clearly revealed the non-existence of diphenylaminylic radical in solution and further pointed out the generation of radical would require much more rigorous conditions.

3

In 1922, the first stable free radical diphenylpicrylhydrazyl was prepared by Goldschmidt and Renn.[40] The radical has its application as a radical scavenger in the kinetic studies.[41] Several stable nitroxyl radicals are generated by the addition of transient radical to nitroso compounds[42] and nitrones.[43] In 1959, Lebedev and coworkers reported the preparation of the stable nitroxyl radical; 2,2,6,6-tetramethylpiperidine-*N*-oxyl (TEMPO).[44,45]

By now, many scientists had the common quest of understanding stable radicals. What makes radical stable in free state? The idea of stability of radicals is quite similar and relatable to the stability of three states of matter (i.e. solid, liquid and gas). All three states behave differently under the same temperature conditions. Therefore, a state of matter is stable till the time it is prone to its conditions. In a similar note, chemical bound systems behave quite differently than the chemical unbound (i.e. radical) system under the similar set of thermodynamic conditions.

Within the class of radicals itself, many are stable in aqueous solution and few are stable in air. The free radical stability in air was demonstrated by German chemists led by Piloty. The authors named the compound obtained by Piloty as porphyrexid, a red crystalline compound whose characteristics are attributed to the delocalization of free electron. The beginning of 1960s emerged as the era of the existence of stable radicals. At this juncture, free radicals of hydrazylic, phenoxylic, verdazylic and aminylic were found to be stable in air. By this time, majority of chemists believed that it is delocalization of unpaired electron with aromatic or conjugated double bond as observed in porphyrexid; which is responsible for the stability of organic radical in the free state.

1.3 State of the art on radical chemistry

Spin delocalization and conjugation are the popular strategies for enhancing the radical stability.[6,7] The other alternative approach is the introduction of a heteroatom in the ring containing the radical center. In our investigation on pyridyl radicals, the nitrogen lone pair provides a stabilizing effect if it is coplanar to the radical electron either by through space (TS) or through bond (TB) interactions.[9] Whereas, in the case of five-membered heterocyclic radicals the interactions between the radical electron and lone pair gets lowered due to the involvement of the latter in aromaticity. Apart from the orbital interactions, ring strain and resonance energy are the decisive factor which influences the stability that follows the order: heteroatom-centered > β-centered > α-centered radicals.[11] Despite the higher ring strain, dominating π-delocalization attributes to the higher stability of heteroatom-centered radicals. In this way, radicals can be structurally modified and tuned to obtain stable radicals. Due to the characteristic high reactivity of radicals, they have been proposed as intermediates in organic synthesis, atmospheric chemistry, interstellar chemistry and biological implications. In this aspect, the role of radicals has been discussed to shed light in these various perspectives.

1.3.1 Biological implications

Free radicals play a vital role in biological field due to their immune function and also due to implications of various diseases.[26,46] Free radicals are produced during the cellular metabolism in living organisms. Most commonly, free radicals produced are ROSs (reactive oxygen species) and RNSs (reactive nitrogen species).[46] The ROSs and RNSs are generally derived from endogenous sources (mitochondria, endoplasmic reticulum and peroxisomes)[47]

5

and from exogeneous sources (pollution, radiation, pesticides, industrial solvent, heavy metal and pesticides).[48] The ROSs and RNSs play a dual role ranging between, beneficial and disadvantageous to the living system. In a low or moderate concentration, they help in fighting against the foreign microorganisms, and cell signaling. ROSs being highly reactive, captures electron from the neighboring molecule in order to attain stability, in the process a new radical species is being generated. Such a cascade of radical generation at higher concentration leads to oxidative damage of biological molecules like lipids,[49] proteins[50] and DNA.[51]

The imbalance between the higher level of ROSs/RNSs and antioxidants (i.e. radical scavengers) leads to oxidative and nitrosative stress. The oxidative stress[52] is the cause for neurodegenerative disorders, cataract development, cancer, aging process and various cardiovascular and respiratory diseases.[53,54]Antioxidants inhibit the oxidative stress by scavenging the excessive concentration of radicals. In living organisms, the three enzymes namely superoxide dismutase (SOD), catalase (CAT) and glutathione peroxidase (GPx) constitute the antioxidant defense system. Few natural sources of antioxidant include β-carotene, vitamin E and C are quite important in diet.[55]Apart from this, the deterioration of food products due to oxidation is prevented by the use of synthetic oxidants such as butylatedhydoxyanisole (BHA), propyl gallate and butylatedhydroxytoluene (BHT).[56]

1.3.2 Interstellar Chemistry

The identification of OH radical in 1963 by radiotelescope technique marked the birth of interstellar chemistry.[57] Interstellar chemistry has contributed to our understanding of both chemistry and astronomy in the form of exploration of various exotic molecules,[58]

distribution of matter in galaxy, origin of stars and solar system. The milky way galaxy is distributed as 90% stars and 10% interstellar medium (ISM).[59] The relative abundances of elements in ISM are 0.9 H, 0.1 He, 0.001 C, N and O, and 0.0001 Mg, Al, Si, S, and Fe. The total mass of interstellar matter is comprised of 99% gas and 1% cosmic dust. The cosmic dust in the interstellar space leads to the formation of clouds. On the basis of physical properties and chemical composition, clouds are classified into three categories: (a) Intercloud (b) Diffuse clouds and (c) Dark clouds.[58-60]

(a) Intercloud has a temperature greater than 7000 K and density of less than 0.2 particles/cm^3.

(b) Diffuse clouds have temperature of 100 K and density of 1-100 particles/cm^3, due to low particle density they are easily penetrated by diffused starlight (1000-2000 Å range).

(c) Dark clouds are much colder (i.e. 10 K) and denser (i.e. 10^2-10^7 particles/cm^3), they are opaque to UV starlight and are penetrated by the cosmic rays (i.e. 1-100 MeV/nucleon) present in the galaxy.

The UV irradiation of nitrogen containing heterocycles such as pyridine, pyrimidine and s-triazine under matrix isolation conditions resulted in rapid destruction on photolysis, and the stability decreases with the increasing nitrogen atoms present in the ring.[61-63] Moreover, these molecules would be destroyed faster when scaled to the UV flux of diffuse interstellar clouds. However, only under dense cloud conditions; pyridine and pyrimidine can survive the average lifetime of the cloud. Nitrogen containing heterocycles have lower detactability in the interstellar medium owing to their low abundance compared to C, H and O.[61]

Interstellar medium is a home to open shell molecules.[60] The UV irradiation of interstellar ice (i.e. composed of water and other volatiles) can lead to radical generation.[64] The radicals

generated forms large complex molecules in the interstellar medium. In the context of radical chemistry; Cyano, ethinyl and phenyl radicals are one of the key reactants in the interstellar medium. The radicals generated by photolysis of HCN, C_2H_2 and C_6H_6 undergoes reaction with unsaturated hydrocarbons leading to the formation of nitriles and other complex hydrocarbons.[60]

1.3.3 Atmospheric Chemistry

Radical chemistry plays a huge role in controlling and preventing pollutants present in the atmosphere.[65,66,28] The atmospheric abundances of free radical is very small (less than one hundredth part per trillion of air), but their reactivity is responsible for transformation of most species in the atmosphere. The atmospheric radicals (i.e. HOx and NOx) plays a crucial role in maintaining atmospheric composition by controlling the oxidative capacity of the atmosphere.[29,67] In terms of reactivity, the most important is the hydroxyl radical. Hydroxyl radical was discovered in 1934 by Haber and Weiss in Fenton reaction.[68] In the upper troposphere, hydroxyl radical are generated by photolysis of ozone.

$$O_3 + h\nu \longrightarrow O(^1D_2) + O_2$$
$$O(^1D_2) + H_2O \longrightarrow 2\overset{\bullet}{O}H$$
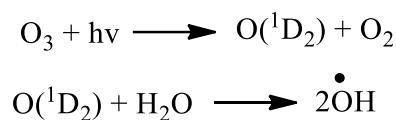
OH radical reacts with CO and CH_4 (greenhouse gas) radical and leads to the oxidation of tropospheric pollutants. Due to higher oxidative capacity hydroxyl radical is also coined as "detergent of the atmosphere".

$$\overset{\bullet}{O}H + CO \longrightarrow H + CO_2$$
$$\overset{\bullet}{O}H + CH_4 \longrightarrow \overset{\bullet}{C}H_3 + H_2O$$
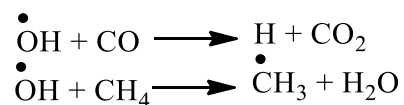
The mixing ratio of OH radical to CH_4 is 1 parts per trillion (ppt), but still due its extreme reactivity it manages to control the global level of CH_4 concentration.

Atmospheric radical chemistry works at day and as well as night time. During night; the oxidant is nitrate radical, and is formed by the slow oxidation of NO_2 by ozone.

$$N\overset{\bullet}{O}_2 + O_3 \longrightarrow N\overset{\bullet}{O}_3 + O_2$$
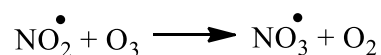
The nitrate radical has a reactivity towards organic compounds (mostly unsaturated hydrocarbons), producing hydroxyl peroxy radical.[69]

The reaction of HO_2 radical with ozone or NO_3 leads to the generation of night time OH radical.

$$H\overset{\bullet}{O}_2 + O_3 \longrightarrow \overset{\bullet}{O}H + 2O_2$$
$$H\overset{\bullet}{O}_2 + NO_3 \longrightarrow \overset{\bullet}{O}H + NO + O_2$$
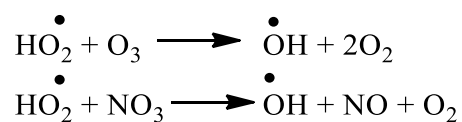
The OH radical generated during night also react with CO and CH_4 in a way similar to day time chemistry. In this way, not only nitrate radical has reactivity towards organic compounds but also leads to the production of night time source of HOx.

1.3.4 Organic Chemistry

The reemergence of free radicals in the field of organic synthesis was pioneered by Stork and coworkers. In their contribution, the best examined work was the potential of vinyl radical in organic synthesis.[70,71] One of the bigger challenge in organic synthesis is the formation of carbon-carbon bond. One way to construct carbon-carbon bond is by coupling of electrophile and nucleophile (i.e. polar process). The other two non polar processes are pericyclic reactions and free radical addition reactions. A free radical addition mechanism involves the following steps:

Initiation

$$R\text{-}X + \overset{\bullet}{In} \longrightarrow \overset{\bullet}{R} + In\text{-}X$$

Addition

$$\overset{\bullet}{R} + H_2C=CHR' \longrightarrow RH_2C-\overset{\bullet}{C}HR'$$
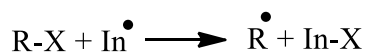
Chain Transfer

$$RH_2C-\overset{\bullet}{C}HR' + RX \longrightarrow RCH_2CH(X)R' + \overset{\bullet}{R}$$
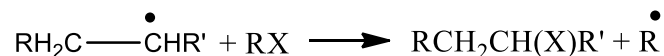
In general, the use of alkyl radicals leads to carbon-carbon bond formation with loss of functionality at the reacting centers. The other improved approach involves the generation of acyl radicals from phenyl selenoesters[72,73] and its participation in intermolecular, intramolecular alkene addition and macrocyclization reaction.[74] The acyl radical generated from phenyl selenoesters upon Bu_3SnH treatment provides a functionalized free radical for organic synthesis, and is regarded as a potential method for C-C bond formation.

The other major challenge in organic synthesis is the selective functionalization of C-H bond. N-hydroxyphthalimide (NHPI), a cheap and non-toxic organocatalyst prepared by reaction of phthalic anhydride and hydroxylamine acts as a precursor for phthalimido-N-oxyl (PINO) radical.[75] NHPI mediated free radical reactions is suitable for oxidation of alkenes,[76] alkylaromatics [77] and alcohols.[78] PINO radical is not only suitable for oxidation but is also an effective hydrogen abstraction species for C-H bond activation which leads to important synthetic transformations by forming C-C,[79] C-N[80] and C-Si bonds.[81]

Apart from this, free radicals are also widely used in the synthesis of natural products.[23,82] The most commonly used reagent for the purpose of natural product synthesis is Tributyltin hydride (Bu_3SnH). The reagent was first used in the construction of six membered ring in natural product synthesis. Radical cyclization in organic synthesis is mostly applied to the

cyclization of five membered ring compared to any other ring size. The reason being faster cyclization of five membered rings and their higher stereoselectivity.[83] The other most widely used reagent (TMS)$_3$SiH has its potential application in free radical polymerization and in the synthesis of nanomaterials.[84] Free radical reactions could be highly selective if it meets two conditions: (i) of the two radical intermediates formed during the reaction progress, one should be persistent and other transient. (ii) Both persistent and transient radical intermediates must be formed at equal rates. The above mentioned conditions collectively constitutes the persistent radical effect (PRE), which explains the formation of highly selective cross-coupling product.[85] Thus, one can conclude that free radical chemistry has developed enough to become an integral part of organic chemistry.

1.4 Heterocyclic radicals

Heterocyclic radicals are the radicals which incorporates a heteroatom in a cyclic ring. The introduction of heteroatom can perturb the stability of the radicals.[86] In principle, the nature and position of the heteroatom relative to the radical center, and orbital interactions between the heteroatom lone pair and the radical electron can influence the stability of carbon-centered radicals.[8] The orbital interactions can be either through space (direct overlap) or through-bond (indirect interaction via intervening bonds). The extent of such interactions in heterocyclic radicals can be realized from the delocalization of the spin density.[10,87] In this unique way, radical properties are generally tuned by incorporating heteroatom or by creating radical center at the heteroatom. Recently, heterocyclic radicals have acquired immense fascination of theoreticians and experimentalists for their various roles in material

chemistry[88,89], biofuels[90,91], free radical reactions[92], reactive oxygen species (ROS)[93] and in tuning of reactivity[94,95].

Pyridyl radicals are one of the simplest heterocyclic radicals, it has been proposed as a possible intermediate in combustion processes and laser IR pyrolysis.[96,97] The generation of pyridyl radicals using photolysis from their corresponding iodides in argon matrices and their ESR spectra have been studied by Kasai et al.[98] Sander and coworkers have also generated 2-, 3-, and 4-dehydropyridine radicals under matrix conditions by flash vacuum pyrolysis of their respective iodopyridine precursors.[99] Keifer et al. revealed the C-H BDE (bond dissociation energy) of pyridyl radicals by thermal decomposition of pyridine using laser-schlieren densitometry and time-of-flight mass spectrometry.[100]

Shlotani and coworkers employed ESR technique to investigate heterocyclic radical cation of pyrrole, furan, thiophene and related derivatives that exhibited π-centered radicals.[101] Similarly, Aramaki et al. have synthesized and characterized a stable B-heterocyclic π-radical.[102] Pyrrolyl radical has been characterized through the pyrolysis of 3-methoxypyridine using threshold photoelectron spectroscopy.[103] Using the same technique, Lineberger and coworkers have determined the electron affinity of pyrrolyl radical.[104]

1.5 Measure of radical character and detection techniques used

1.5.1 Spin density

Spin density is the measure of unpaired electron density in a molecule, which is the difference in the distribution of alpha spin over beta spin.[105] This dimensionless quantity with a maximum value of one at a given center is an indication of localization of the radical character, whereas, a lowering of it means spatial delocalization of the radical character.[106,107]

The stability of many radicals under thermodynamic considerations has been discussed through the spin density distribution or delocalization. Compared to π-delocalized radicals such as benzyl radical, allyl radical, etc., the corresponding σ-radicals (e.g. phenyl radical) are found to be less stable, due to higher localization of the radical character.[108,109] Polarized neutron diffraction is a major experimental technique for spin density estimation, whereas, computations play a key role in predicting it.[110,111]

1.5.2 Computational and experimental techniques

Computations have also played a major role in predicting the structural, stability, and reactivity aspects of several heterocyclic radicals. Either independently or in combination with experiments, computational studies have been reported on the stability of isomeric radicals of several heterocycles, bond dissociation energies (BDEs), electronic structure, stereoelectronic effects on reactivity, and unimolecular decomposition studies on selected heterocyclic radicals.[112-118] Conversely, bimolecular reactions of heterocyclic radicals have been experimentally and theoretically investigated only to a limited extent.[99,119] Apart from this, reactivity studies have been experimentally explored using techniques such as shock tube pulsed pyrolysis,[96] mass spectrometry,[120] photoelectron spectroscopy,[103] matrix isolation,[99,121,122] and UV photodissociation studies,[123] etc. The exploration of the reactivity aspects provides many insights, in particular, related to the combustion chemistry in petrochemical industries, where heterocyclic radicals are commonly encountered as reactive intermediates.[96,97]

1.5.3 EPR spin trapping

Electron paramagnetic resonance (EPR) is a spectroscopic technique which detects unpaired electrons and provides valuable structural information of paramagnetic species like organic radicals and transition metal ions.[124,125] The technique is concerned with the splitting of electronic spin states in a magnetic field which is analogous to the splitting of nuclear spin state in NMR.[124] EPR method detects radicals directly but it is limited to relatively stable radicals. Many radical species are highly reactive and short-lived, the concentration of these radicals in the biochemical systems is too small to be detected by EPR.[126]

EPR becomes much more powerful technique when it gets combined with spin traps to detect reactive oxygen species (ROS) and reactive nitrogen species (RNS) by using biological systems such as mitochondria, endothelial cells and human neutrophils.[127] The most popular spin traps used for ROS detection are pyrroline-based cyclic nitrones such as DMPO (5,5-dimethyl-1-pyrroline-*N*-oxide) and DEPMPO (5-diethoxyphosphoryl-5-methyl-1-pyrroline-*N*-oxide).[128] as depicted in **Figure 1.1.**

Nitrone spin trap
(DMPO)

Nitroxide
(Spin adduct)
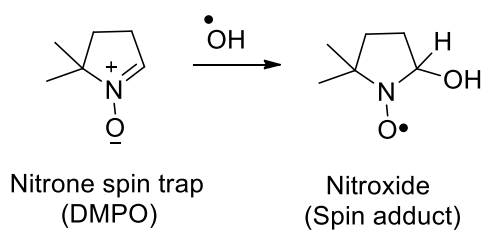
Figure 1.1 DMPO (5,5-dimethyl-1-pyrroline-*N*-oxide) used as an spin trap for ROS detection.

Thus, coupling of EPR spectroscopy with spin trapping technique provides a sensitive probe for the characterization of radical production in complex biological systems.[129,130]

1.5.4 Laser-induced fluorescence (LIF)

The spectroscopic method was first reported by Zare and coworkers in 1968.[131,132] The method involves the absorption of laser light that excites the atom or molecule to higher energy level followed by detection of subsequent emission.[133] The excited molecule or atom after few femtoseconds to nanoseconds, gets de-excited and emits light of longer wavelength than the excitation wavelength. The fluorescent light is recorded by the photomultiplier tube (PMT). The technique has a good detection sensitivity and due to delay between excitation and detection; it is also possible to study the processes which the excited molecule underwent. The technique is widely used for the detection of free radicals. The technique has played a pivotal role in detection of $SiCF$[134] and hydroxyl (OH) radical[135]; and also in the measurement of tropospheric RO_2 and HO_2 radicals.[136]

1.5.5 Laser Flash Photolysis (LFP)

The two pioneers Norrish and Porter laid the foundation of flash photolysis in the era between 1950s and 1960s.[137] The technique allowed the detection of intermediates on the microseconds and milliseconds timescales using UV-Vis spectroscopy. The major obstacle in detection on shorter timescales was overcomed by the introduction of the short-duration (i.e. nanoseconds and other shorter timescales) laser pulses produced by laser emission led to the development of laser flash photolysis (LFP) technique.[138,139] Under this technique, the molecule absorbs intense flash of light to give excited states. The excited molecule loses energy by nonradiative decay to give radical species. Several carbon, nitrogen, oxygen and sulfur based radicals are identified using LFP.[140-142]

1.5.6 Matrix Isolation Infrared Spectroscopy

Matrix isolation is one of the best experimental spectroscopic technique for the characterization of radical intermediates.[143] The technique in combination with photolysis and flash vacuum pyrolysis allows the detection of reactive intermediates in real-time measurements by using spectroscopic techniques such as FT-IR, UV/Vis and ESR. Under this technique, the precursor molecule (i.e. guest) is deposited with excess of inert host gas (1:1000) in a cold spectroscopic window at cold temperatures. The precursor deposited on a cold KBr window can be converted into reactive species either by photolysis or pyrolysis. The extreme cold temperature (i.e. 4 K) and dilution not only isolates the reactive species in the rigid matrix and arrests the intermolecular interactions but also allows the gases like argon and nitrogen to form transparent matrices in the UV and IR regions. Under the matrix isolation conditions, the molecule of interest containing the photo-labile groups undergoes photolysis which leads to the generation of transient species. In principle, the kinetically stable products can be isolated in inert gas matrices at low temperature; and further photochemistry can give insights with regard to the reactivity.

The technique can be very useful for the study of heterocyclic radicals with regard to their characterization and the reactivity channel on photolysis. On this aspect, Kasai and McLeod generated ESR spectra of 2-, 3-, and 4-pyridyl radicals within argon matrices by photoelectron transfer process and further carried out the photolysis of these radicals.[98] Sander and coworkers synthesized three isomeric pyridyl radicals using flash vacuum pyrolysis and characterized them by using infrared spectroscopy.[99] Furthermore, the reaction of these radicals with molecular oxygen lead to the formation of pyridylperoxy radicals. The same group carried out the photolysis of 3-iodo-2,5,6-trifluoropyridyl azide in argon matrix

leading to the formation of a high-spin nitrene radical (i.e. 2,5,6-trifluoropyridylnitren-3-yl) with a quartet ground state.[144] Morris et al, reported the matrix isolation study of the thermal decomposition of pyridine at a temperature range 700-900 $^{\circ}$C leading to the formation of bipyridine and cyanomethylene as the major products.[145] In another report, extensively delocalized heterocycle-substituted stable thioaminyl radical was matrix isolated and characterized using ESR.[146] Several hydrogen bonded complexes of heterocyclic compounds such as furan, 2,5-dihydrofuran, pyrrole and thiophene with methanol;[147] and the first report on a strong hydrogen bond between N-Heterocyclic carbene with water and methanol have also been studied using matrix isolation infrared spectroscopy.[148] The novel methodology was also helpful in generation and isolation of protonated polycyclic nitrogen heterocycles (H+PANH), a interstellar ion in para-hydrogen matrices.[149]

The solution phase chemistry of the isomerization of planar *trans* azo molecule to *cis* isomer by light is well established. However, the photochemistry of azo compounds under cryogenic conditions are limited in study. At this juncture, the technique can be pivotal for the study of photoisomerization of azo compounds at cryogenic temperature looking at the potential applications of photoswitching molecules such as in data storage[150], molecular switches[151], sensors,[152] catalysis[153] and drug delivery.[154] Photochemical transformation of azobenzene and its derivatives in matrix are reported in literature.[155,156] The study provides a insight on the structural property of the molecule that can undergo the photoisomerization process under low temperature conditions. Based on these reports; photochemistry of azoheteroarenes can be explored as they are one of the most popular classes of photoswitches in recent times.

1.6 Objective to the thesis

The primary objective of this thesis work is to understand the effects of heteroatom and their influence on the stability pattern of the isomeric heterocyclic radicals through theoretical and experimental techniques. In order to understand the influence of various factors in the kinetic and thermodynamic stability of the heterocyclic radicals, we have explored five- and six membered heteroatom containing ring systems with unpaired electron at different position.

1. In the first part of the thesis, we investigated the system that includes the heterocyclic isomeric radicals of pyridine, pyridine-*N*-oxide and pyridine cation. The availability of the lone pair in isomeric pyridyl radicals makes it an interesting candidates for the lone pair and radical interaction. Qualitative information regarding lone pair-radical interactions for pyridyl radicals was provided in a report by Roald Hoffmann.[8] However, the mode of operation of these interactions (Through space or through bond) and magnitude of its strength was unclear. Thus, exploration and quantification of these interactions as a determinantal factor for the thermodynamic (existence) and the kinetic stability (reactivity) was our primary objective. Moreover, in order to obtain evidence of such interactions we considered isomeric radicals of pyridine-*N*-oxide and pyridine cation.

2. The mode of interaction between the radical and the lone pair in the five-membered heterocyclic radicals of pyrrole, furan, thiophene, borole, phosphorole, have been the motivation for the second part of the thesis work. Besides the influence of the ring size/geometrical constraints and also by the internuclear distance between the radical and the heteroatom, the influence of delocalization of radical electron has been considered as major factors towards stability.

3. The next research objective was towards photoisomerization of azoheteroarene at matrix isolation conditions. Since the isomerization processes have been restricted to solution phase, or ambient temperature, the experimental data on low temperature phenomena and condensed phase is restricted to few system. In this regard, we attempted for photoswitching studies of 2-hydroxyphenylazo-3,5-dimethylisoxazole. To execute this objective, the matrix isolation infrared spectroscopic technique has been set up from scratch.

1.7 Mode of execution

1.7.1 Computations: Computationally, our objective is to deeply address the structural, stability and reactivity aspects of various isomeric radicals. The understanding of structural properties of isomeric radicals involves the following (i) Comparison of geometrical changes in the radical isomer as compared to the parent molecule (ii) Bond dissociation energies of radical (iii) Electrostatic potential surfaces and spin densities of radical (iv) Natural bond orbital analysis of radicals. Apart from this, five-membered heterocyclic radicals do involve resonance energy, ring strain and NICS calculations for further quantification. The above-mentioned calculations helped in explaining the overall thermodynamic stability order of isomeric heterocyclic radicals.

1.7.2 Matrix isolation infrared spectroscopy: The photoswitching behavior of azobenzene and its derivatives are well established in solution phase but not much of it is explored under cryogenic conditions. In recent times, azoheteroarenes are one of the elusive class of photoswitches due to its better photoswitching efficiency in solution phase. In this regard, we wanted to investigated 2-hydroxy-phenylazo-3,5-dimethylisoxazole as one of the

azoheteroarene based photoswitch under matrix isolation conditions. The structural diversity of the molecule opens up the possibility of tautomerization, *E-E* conformational change and *E-Z* photoisomerization on photolysis. Through this study, we wanted to investigate the dominating channel among the possible competing channels. We intended to explore this study using matrix isolation IR spectroscopy in combination with computations, which can clearly exhibit vibrational features that can be used to differentiate between the competing channels.

1.8 REFERENCES

1. Wentrup, C. From Reactive Intermediates to Stable Compounds. *Science.* **2002**, *295*, 1846−1847.

2. Moss, R. A.; Platz, M. S.; Jones, M., Jr *Reactive Intermediates in Chemistry*; John Wiley & Sons, Ltd: New York, 2003.

3. Stephenson, C. R. J.; Studer, A.; Curran, D. P. The Renaissance of Organic Radical Chemistry−Deja vu All Over Again. *Beilstein J. Org. Chem.* **2013**, *9,* 2778−2780.

4. Powell, W. H. Revised nomenclature for radicals, ions, radical ions and related species. *Pure & Appl. Chem.* **1993**, *65*, 1357−1455.

5. Gerson, F., Huber, W. *Electron Spin Resonance Spectroscopy of Organic Radicals*; Wiley-VCH: Weinheim, Germany, 2003.

6. *Conjugated Carbon Centered Radicals, High-Spin System and Carbenes*; Fischer, H; Eds.; Academic: Berlin, 2002.

7. Trinquier, G.; Malrieu, J. –P. Spreading out spin density in polyphenalenyl radicals. *Phys. Chem. Chem. Phys.* **2017**, *19*, 27623–27642.

8. Hoffmann, R. Interaction of Orbitals Through Space and Through Bond. *Acc. Chem. Res.* **1971**, *4*, 1−9.

9. Sah, C.; Jacob, L.; Saraswat, M.; Venkataramani, S. Does a Nitrogen Lone Pair Lead to Two Centered−Three Electron (2c−3e) Interactions in Pyridyl Radical Isomers? *J. Phys. Chem. A.* **2017**, *121,* 3781−3791.

10. Lu, D.; Wu, C.; Li, P. 3-Center-5-Electron Boryl Radicals with $\sigma^0\pi^1$ Ground State Electronic Structure. *Org. Lett.* **2014**, *16*, 1486−1489.

11. Sah, C.; Yadav, A. J.; Venkataramani, S. Deciphering Stability of Five-Membered Heterocyclic Radicals: Balancing Act Between Delocalization and Ring Strain. *J. Phys. Chem. A*. **2018**, *122*, 5464−5476.

12. Gomberg, M. An Instance of Trivalent Carbon: Triphenylmethyl. *J. Am. Chem. Soc.* **1900**, *22*, 757−771.

13. De Vleeschouwer, F.; Chankisjijev, A.; Yang, W.; Geerlings, P.; De Proft, F. Pushing the Boundaries of Intrinsically Stable Radicals: Inverse Design Using the Thiadiazinyl Radical as a Template. *J. Org. Chem.* **2013**, *78*, 3151−3158.

14. Matuschek, D.; Eusterwiemann, S.; Doerenkamp, C.; Stegemann, L.; Strassert, C. A.; Wibbeling, B.; Daniliuc, C. G.; Doltsinis, N. L.; Eckert, H.; Studer, A. Profluorescent Verdazyl Radicals - Synthesis and Characterization. *Chem. Sci.* **2015**, *6*, 4712−4716.

15. Dougherty, D. A. Spin Control in Organic Molecules. *Acc. Chem. Res.* **1991**, *24*, 88−94.

16. Rajca, A. Organic Diradicals and Polyradicals: From Spin Coupling to Magnetism? *Chem. Rev.* **1994**, *94*, 871−893.

17. Krylov, A. I. Triradicals. *J. Phys. Chem. A*. **2005**, *109*, 10638−10645.

18. Ma, H.; Liu, C.; Zhang, C.; Jiang, Y. Theoretical Study of Very High Spin Organic π - Conjugated Polyradicals. *J. Phys. Chem. A*. **2007**, *111*, 9471−9478.

19. Constantinides, C. P.; Koutentis, P. A.; Krassos, H.; Rawson, J. M.; Tasiopoulos, A. J. Characterization and Magnetic Properties of a "Super Stable" Radical 1,3-Diphenyl-7-trifluoromethyl-1,4-dihydro- 1,2,4-benzotriazin-4-yl. *J. Org. Chem.* **2011**, *76*, 2798−2806.

20. Imada, Y.; Nakano, H.; Furukawa, K.; Kishi, R.; Nakano, M.; Maruyama, H.; Nakamoto, M.; Sekiguchi, A.; Ogawa, M.; Ohta, T.; et al. Isolation of Hypervalent Group-16 Radicals and Their Application in Organic-Radical Batteries. *J. Am. Chem. Soc.* **2016**, *138*, 479−482.

21. Matyjaszewski, K.; Xia, J. Atom Transfer Radical Polymerization. *Chem. Rev.* **2001**, *101*, 2921−2990

22. Stache, E. E.; Ertel, A. B.; Rovis, T.; Doyle, A. G. Generation of Phosphoranyl Radicals via Photoredox Catalysis Enables Voltage–Independent Activation of Strong C–O Bonds. *ACS Catal.* **2018**, *12*, 11134–11139.

23. Romero, K. J.; Galliher, M. S.; Pratt, D. A.; Stephenson, C. R. J. Radicals in natural product synthesis. *Chem. Soc. Rev.* **2018**, *47*, 7851−7866.

24. Giese, B. The Stereoselectivity of Intermolecular Free Radical Reactions. *Angew. Chem. Int. Ed. Engl.* **1989***, 28,* 969−980.

25. Imlay, J. A.; Linn, S. DNA Damage and Oxygen Radical Toxicity. *Science.* **1988**, *240*, 1302−1309.

26. Davies, K. J.; Pryor, W. A. The Evolution of Free Radical Biology and Medicine: A 20-Year History. *Free Radical Biol. Med.* **2005**, *39*, 1263−1264.

27. Orlando, J. J.; Tyndall, G. S.; Wallington, T. J. The Atmospheric Chemistry of Alkoxy Radicals. *Chem. Rev.* **2003**, *103*, 4657−4689.

28. Berndt, T.; Richters, S.; Kaethner, R.; Voigtlander, J.; Stratmann, F.; Sipila, M.; Kulmala, M.; Herrmann, H. Gas-Phase Ozonolysis of Cycloalkenes: Formation of Highly Oxidized RO_2 Radicals and Their Reactions with NO, NO_2, SO_2, and Other RO_2 Radicals. *J. Phys. Chem. A.* **2015**, *119*, 10336−10348.

29. Gligorovski, S.; Strekowski, R.; Barbati, S.; Vione, D. Environmental Implications of Hydroxyl Radicals (•OH). *Chem. Rev.* **2015**, *115*, 13051−13092.

30. Bunsen, R.; von Baeyer, A. Untersuchungen Über Die Kakodylrheihe; W. Engelmann: Leipzig, Germany, **1891**.

31. Kolbe, H. Investigations into the electrolysis of organic links. *Justus Liebigs Ann. Chem.* **1849**, *69*, 257–294.

32. Frankland, E. On the isolation of organic radicals. *Justus Liebigs Ann. Chem.* **1849**, *71*, 171–213.

33. Downes, A.; Blunt, T. P. The effect of sunlight upon Hydrogen Peroxide. *Nature.* **1879**, *20(517)*, 521.

34. Crum Brown, A.; Walker, J. *Justus Liebigs Ann. Chem.* **1891**, *261*, 107–128.

35. Gomberg, M. Radicals in Chemistry, Past and Present. *Ind. Eng. Chem.* **1928**, *20*, 159–164.

36. Paneth, F. A.; Hofeditz, W. About the preparation of free methyl. *Ber. Dtsch. Chem. Ges.* **1929**, *62*, 1335–1347.

37. Paneth, F. A.; Lautsch, W. Free organic radicals in the gaseous state. Part VI. Attempts to prepare various free radicals: the existence of free benzyl. *J. Chem. Soc.* **1935**, 380–383.

38. Wieland, H. *Justus Liebigs Ann. Chim.* **1911**, *381*, 200–216.

39. Wieland, H.; Lecher, H. *Ber. Dtsch. Chem. Ges.* **1912**, *45*, 2600–2605.

40. Goldschmidt, S.; Renn, K. Bivalent nitrogen: via the α, α-diphenyl-β-trinitrophenyl-hydrazyl. *Ber. Dtsch. Chem. Ges.* **1922**, *55*, 628–643.

41. Bartlett, P. D.; Funahashi, T. Galvinoxyl (2, 6-Di-tert-butyl-α-(3,5-di-tert-butyl-4-oxo-2,5-cyclohexadiene-1-ylidene)-p-tolyloxy) as a Scavenger of Shorter-lived Free Radicals. *J. Am. Chem. Soc.* **1962**, *84*, 2596–2601.

42. Mackor, A.; Wajer, Th. A. J. W.; de Boer, Th. J.; van Voorst, J. D. W. C-nitroso compounds. Part III. Alkoxy-alkyl-nitroxides as intermediates in the reaction of alkoxy-radicals with nitroso compounds. *Tetrahedron Lett.* **1967**, *8*, 385–390.

43. Iwamura, M.; Inamoto, N. Novel formation of nitroxide radicals by radical addition to nitrones. *Bull. Chem. Soc. Jpn.* **1967**, *40*, 703.

44. Lebedev, O. L.; Kazarnovsky, S. N. *Tr. Chem. Chem.Technol. (Gorky)* **1959**, *3*, 649.

45. Zhou, Z.; Liu, L. TEMPO and its Derivatives: Synthesis and Applications. *Current Organic Chemistry.* **2014**, *18,* 459–474.

46. Phaniendra, A.; Jestadi, D. B.; Periyasamy, L. Free Radicals: Properties, Sources, Targets, and Their Implication in Various Diseases. *Ind J Clin Biochem.* **2015**, *30*, 11–26.

47. Sastre, J.; Pallardo, F. V.; Asuncion, J. G. D. L.; Vina, J. Mitochondria, oxidative stress and aging. *Free Radical Research.* **2000**, *32*, 189–198.

48. Thomas, C. E.; Aust, S. D. Free radicals and environmental toxins. *Annals of Emergency Medicine.* **1986**, *15*, 1075–1083.

49. Yla-Herttuala, S. Oxidized LDL and atherogenesis. *Ann NY Acad Sci.* **1999**, *874*, 134–137.

50. Stadtman, E. R.; Levine, R. L. Protein oxidation. *Ann NY Acad Sci.* **2000**, *899*, 191–208.

51. Marnett, L. J. Oxyradicals and DNA damage. *Carcinogenesis*. **2000**, *21*, 361–370.

52. Mc Cord, J. M. The evolution of free radicals and oxidative stress. *The American Journal of Medicine.* **2000**, *108*, 652–659.

53. Beebe, D. C.; Holekamp, N. M.; Shui, Y. B. Oxidative damage and the prevention of age-related cataracts. *Ophthalmic Res.* **2010**, *44*, 155–165.

54. Dreher, D.; Junod, A. F. Role of oxygen free radicals in cancer development. *Eur J Cancer*. **1996**, *32A*, 30–38.

55. Ping Xu, D.; Li, Y.; Meng, X.; Zhou, T.; Zhou, Y.; Zheng, J.; -Jiao Zhang, J.; -Bin Li, H. Natural Antioxidants in Foods and Medicinal Plants: Extraction, Assessment and Resources Int. *J. Mol. Sci.* **2017**, *18*, 96–127.

56. Shahidi, F. Antioxidants in food and food antioxidants. *Food/Nahrung.* **2000**, *44*, 158–163.

57. Weinreb, S.; Barrett, A. H.; Meeks, M. L.; Henry, J. C. Radio Observations of OH in the Interstellar Medium. *Nature*. **1963**, *200*, 829–831.

58. Green, S. Interstellar Chemistry: Exotic Molecules in Space. *Ann. Rev. Phys. Chem.* **1981**, *32*, 103–138.

59. Carbo, R.; Ginebreda, A. Interstellar Chemistry. *Journal of Chemical Education.* **1985**, *62*, 832–836.

60. Kaiser, R. I. Experimental Investigation on the Formation of Carbon-Bearing Molecules in the Interstellar Medium via Neutral-Neutral Reactions. *Chem. Rev.* **2002**, *102,* 1309–1358.

61. Peeters, Z.; Botta1, O.; Charnley, S. B.; Kisiel, Z.; Kuan, Y. J.; Ehrenfreund, P. Formation and photostability of N-heterocycles in space I.The effect of nitrogen on the photostability of small aromatic molecules. *A&A*. **2005**, *433*, 583–590.

62. Destexhe, A.; Smets, J.; Adamowicz, L.; Maes, G. Matrix Isolation FT-IR Studies and ab Initio Calculations of Hydrogen-Bonded Complexes of Molecules Modeling Cytosine or Isocytosine Tautomers. 1. Pyridine and Pyrimidine Complexes with H_2O in Ar Matrices. *J. Phys. Chem.* **1994**, *98,* 1506–1514.

63. Peeters, Z.; Botta, O.; Charnley, S.; Ruiterkamp, R., & Ehrenfreund, P. The Astrobiology of Nucleobases. *APJ*. **2003**, *593*, L129-L132.

64. Oberg, K. I. Photochemistry and Astrochemistry: Photochemical Pathways to Interstellar Complex Organic Molecules. *Chem. Rev.* **2016**, *116*, 9631−9663.

65. Mellouki, A.; Wallington, T. J.; Chen, J. Atmospheric Chemistry of Oxygenated Volatile Organic Compounds: Impacts on Air Quality and Climate. *Chem. Rev.* **2015**, *115*, 3984−4014.

66. Glasson, W. A. Methoxyl radical reactions in atmospheric chemistry. *Environ. Sci. Technol.* **1975**, *9*, 1048–1053.

67. George, C.; Ammann, M.; Anna, B. D.; Donaldson, D. J.; Nizkorodov, S. A. Heterogeneous Photochemistry in the Atmosphere. *Chem. Rev.* **2015**, *115*, 4218−4258.

68. Fenton, H. J. H. LXXIII.-Oxidation of Tartaric Acid in Presence of Iron. *J. Chem. Soc., Trans.* **1894**, *65*, 899−910.

69. Monks, P. S. Gas-phase radical chemistry in the troposphere. *Chem. Soc. Rev.* **2005**, *34*, 376–395.

70. Stork, G.; Baine, N. H. Cyclization of vinyl radicals: a versatile method for the construction of five- and six-membered rings. *J. Am. Chem. Soc.* **1982**, *104*, 2321–2323.

71. Stork, G.; Baine, N. H. Vinyl radical cyclization in the synthesis of natural products: Seychellene. *Tetrahedron Lett.* **1985**, *26*, 5927–5930.

72. Boger, D. L.; Mathvink, R. J. Acyl radicals: functionalized free radicals for intramolecular cyclization reactions. *J. Org. Chem.* **1988**, *53*, 3377–3379.

73. Boger, D. L.; Mathvink, R. J. Phenyl selenoesters as effective precursors of acyl radicals for use in intermolecular alkene addition reactions. *J. Org. Chem.* **1989**, *54*, 1777–1779.

74. Boger, D. L. Applications of Free Radicals in Organic Synthesis. *Israel Journal of Chemistry.* **1997**, *37*, 119–129.

75. Karakurt, A.; Dalkara, S.; Ozalp, M.; Ozbey, S.; Kendi, E.; Stables, J. P. Synthesis of some 1-(2-naphthyl)-2-(imidazole-1-yl)ethanone oxime and oxime ether derivatives and their anticonvulsant and antimicrobial activities. *Eur. J. Med. Chem.* **2001**, *36*, 421.

76. Masui, M.; Rosomi, K.; Tsuchida, K.; Ozaki, S. Electrochemical Oxidation of Olefins Using N-Hydroxyphthalimide as a Mediator. *Chem. Pharm. Bull.* **1985**, *33*, 4798.

77. Yoshino, Y.; Hayashi, Y.; Iwahama, T.; Sakaguchi, S.; Ishii, Y. Catalytic Oxidation of Alkylbenzenes with Molecular Oxygen under Normal Pressure and Temperature by *N*-Hydroxyphthalimide Combined with $Co(OAc)_2$. *J.Org. Chem.* **1997**, *62*, 6810–6813.

78. Grochowski, E.; Boleslawska, T.; Jurczak, J. Reaction of Diethyl Azodicarboxylate with Ethers in the presence of N-Hydroxyimides as Catalysts. *Synthesis.* **1977**, 718–720.

79. Kato, S.; Iwahama, T.; Sakaguchi, S.; Ishii, Y. *N*-Hydroxyphthalimide-Catalyzed Carboxylation of Polycyclic Alkanes with Carbon Monoxide in the Presence of Dioxygen. *J. Org. Chem.* **1998**, *63*, 222–223.

80. Ishii, Y.; Sakaguchi, S.; Nishiwaki, Y.; Kitamura, T. Efficient Catalytic Alkane Nitration with NO_2 under Air Assisted by N-Hydroxyphthalimide. *Angew. Chem., Int. Ed.* **2001**, *40*, 222–224.

81. Tayama, O.; Iwahama, T.; Sakaguchi, S.; Ishii, Y. The First Hydroxysilylation of Alkenes with Triethylsilane under Dioxygen Catalyzed by *N*-Hydroxyphthalimide. *Eur. J. Org. Chem.* **2003**, 2286–2289.

82. Jasperse, C. P.; Curran, D. P.; Fevig, T. L. Radical Reactions in Natural Product Synthesis. *Chem. Rev.* **1991**, *91*, 1237–1286.

83. Beckwith, A. L. J.; Schiesser, C. H. Regio- and stereo-selectivity of alkenyl radical ring closure: A theoretical study. *Tetrahedron.* **1985**, *41*, 3925–3941.

84. Chatgilialoglu, C.; Ferreri, C.; Landais, Y.; Timokhin, V. I. Thirty Years of $(TMS)_3SiH$: A Milestone in Radical-Based Synthetic Chemistry. *Chem. Rev.***2018**, *118*, 6516−6572.

85. Studer, A. The Persistent Radical Effect in Organic Synthesis. *Chem. Eur. J.* **2001**, *7*, 1159–1164.

86. Rakitin, O. A. Stable heterocyclic radicals. *Russ. Chem. Rev.* **2011**, *80(7)*, 647–659.

87. Hioe, J.; Sakic, D.; Vrcek, V.; Zipse, H. The Stability of Nitrogen-Centered Radicals, *Org. Biomol. Chem.* **2015**, *13*, 157–169.

88. Du, G. H.; Li, W. Z.; Liu, Y. Q.; Ding, Y.; Wang, Z. L. Growth of Carbon Nanotubes by Pyrolysis of Thiophene. *J. Phys. Chem. C.* **2007**, *111*, 14293−14298.

89. Qiu, Y. Q.; Fan, H. L.; Sun, S. L.; Liu, C. G.; Su, Z. M. Theoretical Study on the Relationship Between Spin Multiplicity Effects and Nonlinear Optical Properties of the Pyrrole Radical (C4H4N·). *J. Phys. Chem. A*. **2008**, *112*, 83−88.

90. Vasiliou, A.; Nimlos, M. R.; Daily, J. W.; Ellison, G. B. Thermal Decomposition of Furan Generates Propargyl Radicals. *J. Phys. Chem. A*. **2009**, *113*, 8540−8547.

91. Fan, X.; Wang, X.; Wang, J.; Yang, K. Comparative Shock Tube and Kinetic Study on High-temperature Ignition of 2,3-Dihydrofuran and 2,5-Dihydrofuran. *Energy Fuels*. **2016**, *30*, 8727−8736.

92. Gritter, R. J.; Chriss, R. J. Free-Radical Reactions of Pyrroles. *J. Org. Chem.* **1964**, *29*, 1163−1167.

93. Kanzler, C.; Haase, P. T.; Schestkowa, H.; Kroh, L. W. Antioxidant Properties of Heterocyclic Intermediates of the Maillard Reaction and Structurally Related Compounds. *J. Agric. Food Chem.* **2016**, *64*, 7829−7837.

94. Ueng, S. H.; Solovyev, A.; Yuan, X.; Geib, S. J.; Fensterbank, L.; Lacote, E.; Malacria, M.; Newcomb, M.; Walton, J. C.; Curran, D. P. N-Heterocyclic Carbene Boryl Radicals: A New Class of Boron-Centered Radical. *J. Am. Chem. Soc.* **2009**, *131*, 11256−11262.

95. Wu, C.; Hou, X.; Zheng, Y.; Li, P.; Lu, D. Electrophilicity and Nucleophilicity of Boryl Radicals. *J. Org. Chem.* **2017**, *82*, 2898−2905.

96. Mackie, J. C.; Colket, M. B., III; Nelson, P. F. Shock Tube Pyrolysis of Pyridine. *J. Phys. Chem.* **1990**, *94*, 4099−4106.

97. Hore, N. R.; Russell, D. K. Radical pathways in the thermal decomposition of pyridine and diazines: a laser pyrolysis and semiempirical study. *J. Chem. Soc., Perkin Trans. 2* **1998**, *2*, 269−276.

98. Kasai, P. H.; McLeod, D., Jr. Electron Spin Resonance Study of Heterocycles; Pyridyl Radicals. *J. Am. Chem. Soc.* **1972**, *94*, 720−727.

99. Korte, A.; Mardyukov, A.; Sander, W. Pyridyl- and Pyridylperoxy Radicals: A Computational and Matrix Isolation Study. *Aust. J. Chem.* **2014**, *67*, 1324−1329.

100. Kiefer, J. H.; Zhang, Q.; Kern, R. D.; Yao, J.; Jursic, B. Pyrolyses of Aromatic Azines: Pyrazine, Pyrimidine, and Pyridine. *J. Phys. Chem. A*. **1997**, *101*, 7061−7073.

101. Shiotani, M.; Nagata, Y.; Tasaki, M.; Sohma, J.; et al. Electron Spin Resonance Studies on Radical Cations of Five-Membered Heteroaromatics. Furan, Thiophene, Pyrrole, and Related Compounds. *J. Phys. Chem.* **1983**, *87*, 1170−1174.

102. Aramaki, Y.; Omiya, H.; Yamashita, M.; Nakabayashi, K.; Ohkoshi, S.; Nozaki, K. Synthesis and Characterization of B-Heterocyclic π-Radical and Its Reactivity as a Boryl Radical. *J. Am. Chem. Soc*. **2012**, *134*, 19989−19992.

103. Holzmeier, F.; Wagner, I.; Fischer, I.; Bodi, A.; Hemberger, P. Pyrolysis of 3-Methoxypyridine. Detection and Characterization of the Pyrrolyl Radical by Threshold Photoelectron Spectroscopy. *J. Phys. Chem. A*. **2016**, *120*, 4702−4710.

104. Gianola, A. J.; Ichino, T.; Hoenigman, R. L.; Kato, S.; Bierbaum, V. M.; Lineberger, W. C. Thermochemistry and Electronic Structure of the Pyrrolyl Radical. *J. Phys. Chem. A*. **2004**, *108*, 10326−10335.

105. McNaught, A. D.; Wilkinson, A. *IUPAC Compendium of Chemical Terminology;* Blackwell Scientific Publications; Oxford: 1997.

106. Gatti, C.; Orlando, A. M.; Presti, L. L. Insights on Spin Polarization through the Spin Density Source Function. *Chem. Sci.* **2015**, *6*, 3845–3852.

107. Makarova, T.; Palacio, F. *Carbon-based magnetism : an overview of the magnetism of metal free carbon-based compounds and materials*; Elsevier: 2014.

108. Tang, B.; Zhao, J.; Xu, J. F.; Zhang, X. Tuning the stability of organic radicals: From covalent approaches to non-covalent approaches. *Chem. Sci.* **2020**, *11*, 1192–1204.

109. Hicks, R. G. *Stable Radicals: Fundamentals and Applied Aspects of Odd-Electron Compounds*; John Wiley & Sons, Ltd: Wiltshire, U.K.,2010.

110. Ressouche, E.; Schweizer, J. Ab Initio Calculations Versus Polarized Neutron Diffraction for the Spin Density of Free Radicals. *Monatshefte fur Chemie.* **2003***, 134(2),* 235–253*.

111. Boguslawski, K.; Marti, K. H.; Legeza, O.; Reiher, M. Accurate ab Initio Spin Densities. *J. Chem. Theory Comput.* **2012**, *8(6),* 1970–1982.

112. Feng,Y.; Wang, J. T.; Liu, L.; Guo, Q. X. C-H and N-H bond dissociation energies of five- and six-membered ring aromatic compounds. *J. Phys. Org. Chem.* **2003**, *16*, 883–890.

113. Liu, R.; Huang, T. T. S.; Tittle, J.; Xia, D. A Theoretical Investigation of the Decomposition Mechanism of Pyridyl Radicals. *J. Phys. Chem. A.* **2000**, *104*, 8368–8374.

114. Mukhopadhyay, A.; Jacob, L.; Venkataramani, S. Dehydro-Oxazole, Thiazole and Imidazole Radicals: Insights into the Electronic Structure, Stability and Reactivity Aspects. *Phys. Chem. Chem. Phys.* **2017**, *19*, 394−407.

115. Barckholtz, C.; Barckholtz, T. A.; Hadad, C. M. C-H and N-H Bond Dissociation Energies of Small Aromatic Hydrocarbons. *J. Am. Chem. Soc.* **1999**, *121*, 491–500.

116. Fadden, M. J.; Hadad, C. M. Rearrangement Pathways of Arylperoxy Radicals. 2. Five-Membered Heterocycles. *J. Phys. Chem. A.* **2000**, *104*, 6324–6331.

117. Gomes, G. d. P.; Loginova, Y.; Vatsadze, S. Z.; Alabugin, I. V. Isonitriles as Stereoelectronic Chameleons: The Donor–Acceptor Dichotomy in Radical Additions. *J. Am. Chem. Soc.* **2018**, *140*, 14272– 14288.

118. Šakić, D.; Zipse, H. Radical Stability as a Guideline in C–H Amination Reactions. *Adv. Synth. Catal.* **2016**, *358*, 3983–3991.

119. Thompson, R. A.; Francisco, J. S.; Grutzner, J. B. Dimerization and trapping of diazirinyl radicals. *Phys. Chem. Chem. Phys.* **2004**, *6*, 756–765.

120. Turecek, F.; Wolken, J. K.; Sadilek, M. Distinction of isomeric pyridyl cations and radicals by neutralization-reionization mass spectrometry, abinitio and density functional theory calculations. *Eur. Mass Spectrom.* **1998**, *4*, 321–332.

121. Winkler, M.; Cakir, B.; Sander, W. 3,5-Pyridyne A Heterocyclic *meta*-Benzyne Derivative. *J. Am. Chem. Soc.* **2004**, *126*, 6135–6149.

122. Rostkowskaa, H.; Lapinskiaand, L.; Nowaka, J. UV-induced transformations of matrix-isolated 1,3,4-thiadiazole-2-thiones. *J. Phys. Org. Chem.* **2010**, *23*, 56–66.

123. Lucas, M.; Minor, J.; Zhang, J.; Brazier, C. Ultraviolet Photodissociation Dynamics of the *o*-Pyridyl Radical. *J. Phys. Chem. A.* **2013**, *117*, 12138–12145.

124. Roessler, M. M.; Salvadori, E. Principles and applications of EPR spectroscopy in the chemical sciences. *Chem. Soc. Rev.* **2018**, *47*, 2534–2553.

125. Chechik, V.; Carter, E.; Murphy, D. Electron paramagnetic resonance, Oxford University Press, Oxford, 2016.

126. Khan, N.; Wilmot, C. M.; Rosen, G. M.; Demidenko, E.; Sun, J.; Joseph, J.; O'Hara, J.; Kalyanaraman, B.;Swartz, H.M. In vitro toxicity and stability of radical adducts. *Free Radic. Biol. Med*. **2003**, *34*, 1473–1481.

127. Suzen, S.; Orhan, H. G.; Saso, L. Detection of Reactive Oxygen and Nitrogen Species by Electron Paramagnetic Resonance (EPR) Technique. *Molecules*. **2017**, *22*, 181–189.

128. Kim, S. U.; Liu, Y.; Nash, K. M.; Zweier, J. L.; Rockenbauer, A.; Villamena, F. A. Fast Reactivity of CyclicNitrone-Calix(4)Pyrrole Conjugate with Superoxide Radical Anion: Theoretical and Experimental Studies. *J. Am. Chem. Soc*. **2010**, *132*, 17157–17173.

129. Brackett, D. J.; Wallis, G.; Wilson, M. F.; McCay, P. B. Spin Trapping and Electron Paramagnetic Resonance Spectroscopy. In Free Radical and Antioxidant Protocols; Humana Press, 1998.

130. Davies, M. J.; Hawkins, C. L. EPR Spin Trapping of Protein Radicals. *Free Radic. Biol. Med*. **2004**, *36*, 1072–1086.

131. Tango, W. J.; Link, J. K.; Zare, R. N. Spectroscopy of K_2 Using Laser Induced Fluorescence. *J. Chem. Phys.* **1968**, *49*, 4264–4268.

132. Zare, R. N. My Life with LIF: A Personal Account of Developing Laser-Induced Fluorescence. *Annu. Rev. Anal. Chem.* **2012**, *5*, 1–14.

133. Kinsey, J. L. Laser induced fluorescence. *Ann. Rev. Phys. Chem.* **1977**, *28*, 349–372.

134. Rothschopf, G.; Smith, T. C.; Clouthier, D. J. Laser-induced fluorescence detection of the elusive SiCF free radical. *J. Chem. Phys.* **2018**, *149*, 024301.

135. Stauffer, H. U.; Kulatilaka, W. D.; Gord, J. R.; Roy, S. Laser-induced fluorescence detection of hydroxyl (OH) radical by femtosecond excitation. *Opt. Lett.* **2011**, *36*, 1776–1778.

136. Fuchs, H.; Holland, F.; Hofzumahaus, A. Measurement of tropospheric RO_2 and HO_2 radicals by a laser-induced fluorescence instrument. *Rev. Sci. Instrum*. **2008**, *79*, 084104.

137. J. C. Scaiano, in Reactive Intermediate Chemistry, ed. R. A. Moss, M. S. Platz and M. Jones Jr., Wiley-Interscience, Hoboken, NJ, 2004, 847.

138. N. P. Schepp and F. L. Cozens, in *Lasers in Chemistry*, ed. M. Lackner, Wiley-VHC, Weinheim, 2008, *2*, 1073.

139. Y. A. Gaudel, in *Lasers in Chemistry*, ed. M. Lackner, Wiley-VCH, Weinheim, 2008, *2*, 861.

140. Yamashita, H.; Ikezawa, T.; Kobayashi, Y.; Abe, J. Photochromic Phenoxyl-Imidazolyl Radical Complexes with Decoloration Rates from Tens of Nanoseconds to Seconds. *J. Am. Chem. Soc.* **2015**, *137*, 4952–4955.

141. Bonesi, S. M.; Crespi, S.; Merli, D.; Manet, I.; Albini, A. Direct irradiaton of aryl sulfides. Homolytic fragmentation and sensitized S-oxidation. *J. Org. Chem.* **2017**, *82*, 9054–9065.

142. Ye, J.; Hatano, S.; Abe, M.; Kishi, R.; Murata, Y.; Nakano, M.; Adam, W. A Puckered Singlet Cyclopentane-1,3-diyl: Detection of the Third Isomer in Homolysis. *Chem. Eur. J.* **2016**, *22*, 2299–2306.

143. Whittle, E.; Dows, D. A.; Pimentel, G. C. Matrix Isolation Method for the Experimental Study of Unstable Species. *J. Chem. Phys.* **1954**, *22*, 1943.

144. Grote, D.; Finke, C.; Neuhaus, P.; Sander, W. Matrix Isolation and Spectroscopic Characterization of 2,5,6-Trifluoropyridylnitren-3-yl. *Eur. J. Org. Chem.* **2012**, *17*, 3229–3236.

145. Morris, V. R.; Bhatia, S. C.; Stelson, A. W.; Hall, J. H. Matrix-isolation study of the thermal decomposition of pyridine. *Energy Fuels.* **1991**, *5* (1), 126–133.

146. Yozo Miura, Y.; Tomimura,T.; Teki, Y. Heterocycle-Substituted Stable Thioaminyl Radicals: Isolation, ESR Spectra, and Magnetic Properties[1]. *J. Org. Chem.* **2000**, *65* (23), 7889–7895.

147. Jiang, X.; Liu, S.; Tsona, N. T.; Tang, S.; Ding, L.; Zhao, H.; Du, L. Matrix isolation FTIR study of hydrogen-bonded complexes of methanol with heterocyclic organic compounds. *RSC Adv.* **2017**, *7*, 2503–2512.

148. Raut, A. H.; Karir, G.; Viswanathan, K. S. Matrix Isolation Infrared and *Ab Initio* Study of the Interaction of N-Heterocyclic Carbene with Water and Methanol: A Case Study of a Strong Hydrogen Bond. *J. Phys. Chem. A*. **2016**, *120*, 9390–940.

149. Tsuge, M.; Tseng, C. Y.; Lee, Y. P. Spectroscopy of prospective interstellar ions and radicals isolated in *para*-hydrogen matrices. *Phys. Chem. Chem. Phys.* **2018**, *20*, 5344–5358.

150. Irie, M. Diarylethenes for Memories and Switches. *Chem. Rev.* **2000**, *100*, 1685−1716.

151. Osorio-Planes, L.; Espelt, M.; Pericas, M. A.; Ballester, P. Reversible photocontrolled disintegration of a dimeric tetraurea-calix[4]pyrrole capsule with all-*trans* appended azobenzene units. *Chem. Sci.* **2014**, *5*, 4260–4264.

152. Do, K.; Boxer, S. G. GFP Variants with Alternative β-Strands and Their Application as Light-driven Protease Sensors: A Tale of Two Tails. *J. Am. Chem. Soc.* **2013**, *135*, 10226−10229.

153. Stoll, R. S.; Hecht, S. Artificial light-gated catalyst systems. *Angew. Chem. Int. Ed.* **2010**, *49*, 5054−5075.

154. Velema, W. A.; Szymanski, W.; Feringa, B. L. Photopharmacology: Beyond Proof of Principle. *J. Am. Chem.Soc.* **2014**, *136*, 2178−2191.

155. Duarte, L.; Khriachtchev, L.; Fausto, R.; Reva, I. Photoisomerization of Azobenzenes Isolated in Cryogenic Matrices. *Phys. Chem. Chem. Phys.* **2016**, *18*, 16802−16811.

156. Duarte, L.; Fausto, R.; Reva, I. Structural and spectroscopic characterization of *E*- and *Z*-isomers of azobenzene. *Phys. Chem. Chem. Phys.* **2014**, *16*, 16919−16930.

Chapter 2

Through Space and Through Bond Interactions of Nitrogen Lone pair with Radical Electron in Pyridyl Radical Isomers

2.1 INTRODUCTION

The study of heterocyclic radicals is of immense importance to experimentalist and theoreticians as the radical properties can be tuned by the incorporation of heteroatom. Such studies are not only fundamentally important but also insightful in the fields of organic magnets[1,2] and in the making of stable radicals.[3,4] Pyridyl radicals are one of the simplest heterocyclic radicals, containing nitrogen as a lone heteroatom. The pyridyl radicals exist in three isomeric forms, namely, 2-, 3-, and 4-dehydropyridine radicals relative to the nitrogen. All of these isomers possess the radical centers (occupying σ-orbital) in the same plane as the nitrogen lone pair, and are classified as σ-radicals. Due to the geometrical arrangements, either direct (through-space, TS) and/or through intervening bonds (through-bond, TB) coupling between the lone pair and the radical electron presumably lead to two center-three electron interactions in pyridyl radicals. Although Hoffmann has discussed about such interactions and the mode of operation of TS and TB interactions, a thorough study in explaining the radical stability has not been documented.[5] In this regard, we have attempted an investigation on how TS and TB interactions between the lone pair and radical electron can influence the relative stability of the isomeric pyridyl radicals.

In order to obtain evidence for such interactions, protonated and *N*-oxide analogues of the corresponding isomeric pyridyl radicals have been considered in such a way to understand

the consequences due to unavailability of the lone pair. For the better understanding of the nature and strength of such interactions, detailed studies have been attempted. In this regard, various properties of the isomeric pyridyl radicals have been compared with the respective pyridinyl and pyridyl-N-oxide radicals. These include geometrical parameters, stability order, thermodynamic stability, spin densities, and electrostatic potential mapping. Qualitative information of such interactions has been obtained from multiconfigurational CASSCF calculations. To quantify and also to understand the mode of the interactions, NBO analysis has been performed. Furthermore, vertical ionization (VIE) and vertical detachment (VDE) energies have been calculated to verify and also to understand the nature of interactions. The detailed insights that we obtained in these studies are described in the proceeding sections of this chapter.

2.2 RESULTS AND DISCUSSION

The main objective in this study is to understand the interaction between the radical center and the nitrogen lone pair in pyridyl radicals, in order to arrive at a conclusion, the study has been extended to pyridyl-N-oxide and pyridinyl radicals. The outcome of these studies in particular to obtain the quantitative information on the interaction between the lone pair and the radical electron and a comparative studies on the radicals of pyridine, protonated pyridine and pyridine-N-oxide are given in detail. (**Scheme 2.1**)
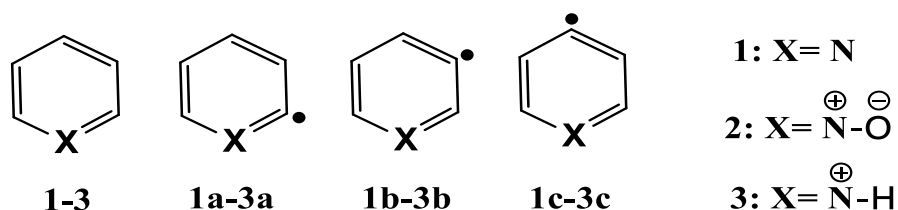
Scheme 2.1 Pyridine, Pyridine-N-oxide, Protonated pyridine and Their Corresponding Radicals.

2.2.1 Geometry

The isomeric radicals of dehydro-pyridine, pyridine-*N*-oxide and protonated pyridine have been investigated using different levels of theory. All the electronic states that we optimized are found to have a doublet spin and falls either in C_s ($^2A'$) or C_{2v} ($^2A_1$) point group symmetries. The electronic and thermodynamic parameters of the parent and their respective radicals have also been provided. (**Table A2.1** in Appendix) The minimal energy structures for each radical along with their respective parent molecules are given in **Figure 2.1**. Structural aspects of these species can be better compared through a closer look at their geometrical parameters. In this regard, we compared the key geometrical parameters of the optimized structures of all the radicals with their respective parent compounds at (U)B3LYP/cc-pVTZ and (U)M06/cc-pVTZ levels of theory.

We have observed that all the radical isomers follow some general trends in changes with respect to their parent. Both the immediate bond lengths from the radical center got shortened in all the radical isomers as compared to parent compound except **1a**, in which one of the bond lengths (C-N) got shortened while the other (C-C) was almost unaffected. Concomitantly, the alternate bond shows an increase in the bond length compared to the parent molecules and the bond distances opposite to the radical center remains almost the same. On the other hand, bond angle at the radical centers are found to increase in all the radicals as compared to the parent system.

In a similar way, comparison of the N-H bond lengths of the pyridinyl radical isomers show only a negligible increase as compared to the parent molecule. However, in case of pyridine-*N*-oxide radical isomers, the *meta* isomer shows a decrease in N-O bond length, whereas the *ortho* and *para* isomers show an increase in the corresponding bond lengths with

respect to their parent molecule. In general, all the radicals species that we investigated show a small shortening in almost all bond distances at (U)M06 level (with parameterized functions for long range dispersion corrections) compared to the (U)B3LYP level (without dispersion corrections). Also, both the levels predict nearly the same bond angles at radical centers in all the cases, except in the case of **1a**.
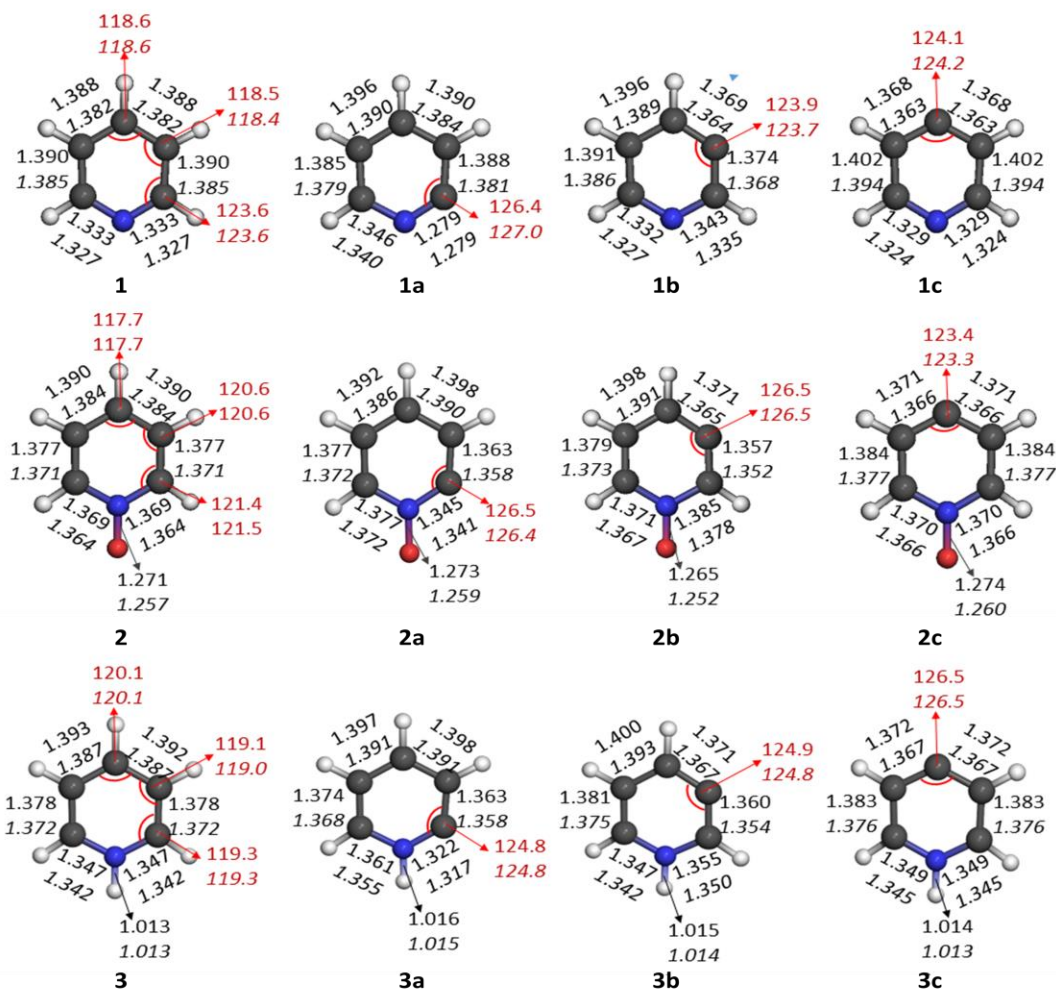
Figure 2.1 Optimized structures of pyridine **1**, pyridine-*N*-oxide **2** and protonated pyridine **3** and their corresponding radical isomers **1a-c, 2a-c** and **3a-c**. Selected geometrical parameters (bond distances in Å and bond angles in degrees) corresponding to the computed geometries at (U)B3LYP/cc-pVTZ (normal font) and (U)M06/cc-pVTZ (italics) levels of theory are indicated.

2.2.2 Stability order

The data on relative stability of all the isomeric radicals can provide insights into the influence of the heteroatom(s) on the radicals and also the interaction between the lone pair and the radical electron. In order to understand the stability order, pyridyl (**1a-c**), pyridyl-*N*-oxide (**2a-c**) and pyridinyl (**3a-c**) radicals have been optimized at different levels of theory and the relative energy values have been listed in **Table 2.1**. In case of pyridyl radicals, isomer **1a** has minimum energy and is found to be the most stable isomer, whereas **1b** and **1c** lie energetically close to each other with an energy difference ranging between 0.8 and 1.5 kcal/mol in favor of **1c**. Higher stability of isomer **1a** can be attributed to the stabilizing interaction between radical center and lone pair of heteroatom. Among the pyridinyl radicals, **3c** is the most stable isomer and the least stable one is **3a**. The positive charge on the N atom operating either inductively and/or through field effect withdraws the electron density from the radical center and as a consequence the stability falls in the order **3c** > **3b** > **3a**. On the other hand, for pyridyl-*N*-oxide radicals, isomer **2b** is the most stable isomer followed by **2c** and **2a**, respectively. A 1,3- repulsive interaction operated by one of the lone pairs of oxygen on the radical electron might be the plausible reason for the destabilization of **2a**. Among the two competing properties of oxygen in *N*-oxides, i.e. π-donation of oxygen and its σ-electron withdrawing through inductive effect, the former dominates and as a result, **2b** gathers extra stabilization. All the levels of theory follow the same energetic order in all the radical isomers.

Table 2.1 Relative Stability Order of Isomeric Pyridyl **1a-c**, Pyridyl-*N*-oxide **2a-c** and Pyridinyl **3a-c** Radicals at Different Levels of Theory.

Level of theory	Relative energy[a] (kcal/mol)								
	Pyridyl radicals			Pyridyl-*N*-oxide radicals			Pyridinyl radicals		
	1a	1b	1c	2a	2b	2c	3a	3b	3c
(U)B3LYP/6-311++G(d,p)	0.0	6.0	4.7	5.0	0.0	1.5	3.1	2.3	0.0
(U)B3LYP/cc-pVDZ	0.0	6.0	4.8	5.3	0.0	1.9	3.0	2.3	0.0
(U)B3LYP/cc-pVTZ	0.0	6.2	4.9	5.1	0.0	1.7	3.1	2.4	0.0
(U)B3LYP/cc-pVQZ	0.0	6.2	4.9	5.0	0.0	1.6	3.1	2.4	0.0
(U)B3LYP/aug-cc-pVDZ	0.0	5.8	4.6	4.9	0.0	1.5	3.1	2.4	0.0
(U)B3LYP/aug-cc-pVTZ	0.0	6.1	4.8	4.9	0.0	1.5	3.1	2.4	0.0
(U)B3LYP/aug-cc-pVQZ	0.0	6.2	4.9	5.0	0.0	1.5	3.1	2.4	0.0
(U)BLYP/cc-pVTZ	0.0	5.7	4.9	5.8	0.0	2.8	2.9	2.1	0.0
(U)M06/cc- pVTZ	0.0	5.3	3.9	5.3	0.0	1.4	3.2	2.2	0.0
CBS-QB3	0.0	6.8	5.4	5.8	0.0	1.8	3.8	2.6	0.0
(U)CCSD(T)/cc-pVTZ//(U)B3LYP/cc-pVTZ[b]	0.0	5.8	4.3	4.4	0.0	0.4	3.4	2.7	0.0

[a]Zero-point energy corrected; [b]Single point energy calculation performed at (U)CCSD(T)/cc-pVTZ using (U)B3LYP/cc-pVTZ optimized geometry.

2.2.3 Isodesmic reactions

Comparison of thermodynamic stability of different species can be achieved by an isodesmic reaction, where the species of interest hypothetically reacts with a reference molecule that involves cleavage and formation of same kind of bonds.[6,7] We have taken benzene as the reference molecule and assumed that the C-H bond in benzene gets cleaved leading to the formation of phenyl radical, which accompanied the formation of parent heterocycle from the corresponding radical species. Through this method radical stabilization energy (RSE) can be calculated, which is the enthalpy change for the isodesmic reactions at standard temperature (298.15 K) and pressure (1 atm). We have estimated the RSE at composite CBS-QB3 levels of theory for predicting accurate energies and the data are listed in **Table 2.2**. The values suggest that **2a** is the least stable isomer as it is having the highest negative ΔH value, which in turn implies that the reaction is favorable in the forward direction towards formation of the parent heterocycle. Similarly, the most stable isomer is **1a** among all the radical isomers with a positive ΔH value of 6.3 kcal/mol. The stability order estimated from these isodesmic reactions are consistent with the one obtained from the comparison of absolute energies within the respective isomers.

Table 2.2 Radical Stabilization Energies (RSE's) of Isomeric Pyridyl **1a-c**, Pyridyl-*N*-oxide **2a-c** and Pyridinyl **3a-c** radicals at CBS-QB3 Level of Theory.

$\Delta H_{product-reactant}$ **(kcal/mol)**

Pyridyl radicals			Pyridyl-*N*-oxide radicals			Pyridinyl radicals		
1a	**1b**	**1c**	**2a**	**2b**	**2c**	**3a**	**3b**	**3c**
6.3	-0.5	0.9	-8.9	-3.1	-4.9	-5.9	-4.7	-2.1

2.2.4 Spin density

The electron density distribution pattern of the difference in α and β spin state electrons can be identified through analysis of the spin density values at each radical center. This information will directly imply the extent of delocalization as a result of interactions with neighboring atoms. In order to understand whether the spins are localized at the radical center and to estimate the extend of delocalization, we calculated spin densities of all the radicals at (U)B3LYP/cc-pVTZ and (U)M06/cc-pVTZ levels of theory and the corresponding spin density values are listed in **Figure2**.**2**. A high positive spin density value has been observed for all the radical isomers at their respective carbon centers, where the unpaired electron is located. This clearly implies that the electron density is localized at each carbon radical center, however, delocalization has been observed to a smaller extent for few radicals. The isomeric 2, 3, and 4-pyridyl radicals have spin densities at the formal radical carbon

atoms, 0.80, 0.89 and 0.92, respectively. Interestingly, both **1a** and **1b** show a non-zero spin density at nitrogen center strongly supporting a possible interaction between radical center and the nitrogen. At few centers negative spin density values have also been observed as a consequence of spin polarization effect due to the interaction of singly occupied (SOMO) orbital with the fully filled (doubly occupied) inner orbitals.[8]
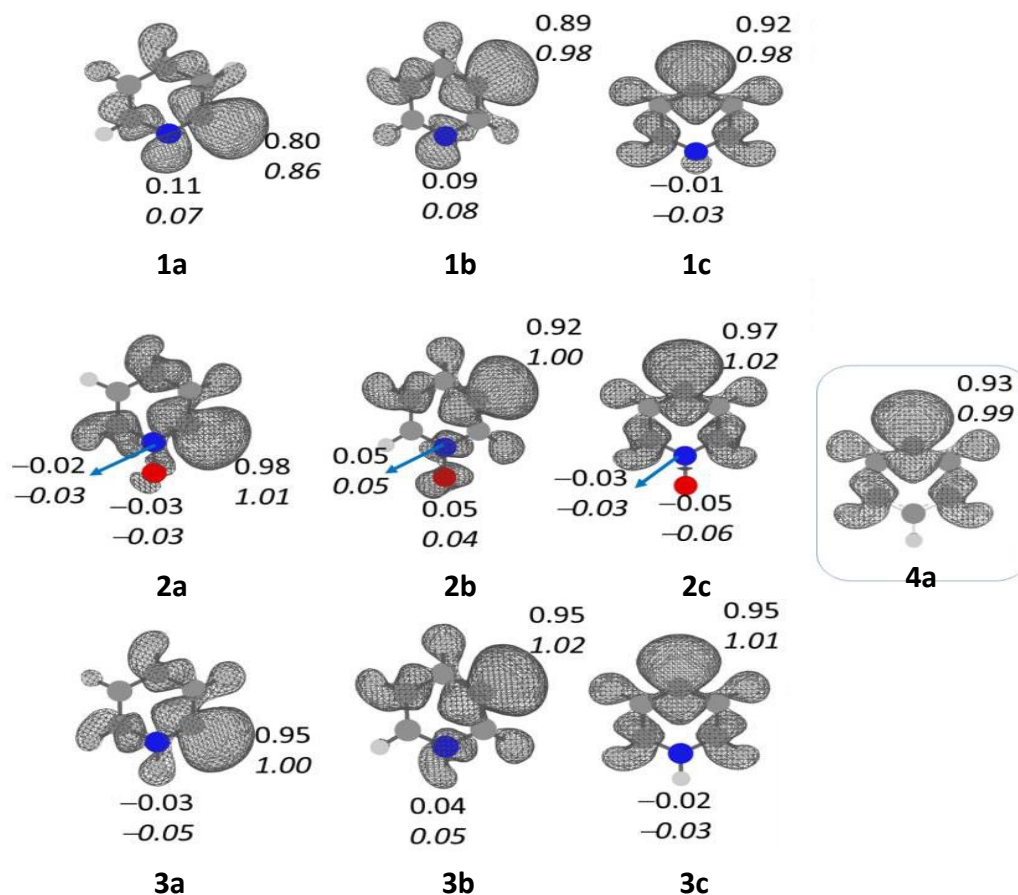
Figure 2.2 Spin density values of isomeric pyridyl **1a-c**, pyridyl-*N*-oxide **2a-c** and pyridinyl radicals **3a-c** at different levels of theory. (The values indicated in the normal font are estimated at (U)B3LYP/cc-pVTZ and those in italics belong to (U)M06/cc-pVTZ level of theories) For comparison, the spin density values for phenyl radical **4a** are also provided.

Upon protonation, all the three isomeric pyridinyl radical isomers show not only increase in the spin density values but also have an equal value of 0.95. Both the increase and

attainment of equal spin density value (a value very close to that of phenyl radical) can be attributed to the elimination of interaction of radical electron with the lone pair as the later is no longer available. Similarly the pyridyl-*N*-oxide radicals also show an increase in the spin density values as compared to the pyridyl radicals. Nevertheless, the amount of increase is relatively larger in the case of both pyridyl-*N*-oxide radicals **2a** and **2c**, whereas **2b** shows a increase to a smaller extent in comparison to the respective pyridinyl radicals. As in the case of pyridinyl radicals, pyridyl-*N*-oxide radicals also show higher spin densities that can be explained again on the basis of non-availability of nitrogen lone pair, which is involved in the bonding with oxygen. Since two contrasting forces are possible due to oxygen in *N*-oxide, i.e. π-donation and inductive effect, the resulting electronic effect is complex one. However, based on the spin density values, it is very clear that the π-donation is the dominating force, which results in an *ortho* and *para* directing effect.

2.2.5 Electrostatic potential

The electrostatic potential map for all the radical isomers have been assessed at (U)B3LYP/cc-pVTZ level of theory. (**Figure 2.3**) A negative potential has been observed at the lone pair of electron and radical center in the pyridyl radical isomers. Upon protonation, the resulting pyridinyl radical isomers show uniform positive potential through out the molecule, which indicates the equal distribution of the charge in all the three isomers. Similarly, pyridyl-*N*-oxide radicals showed a negative potential corresponding to the lone pair of oxygen atoms. Unlike pyridyl radicals, the negative potential was recessed at the radical centers in pyridyl-*N*-oxide radicals due to the high intense electronegative potential of oxygen lone pairs. Analysis of this electrostatic potential map gives a clear indication of the

relative distribution of electron density over the molecule and the overlap between the lone pair electrostatic potential with the adjacent radical center designates the existence of a through space interaction between them.
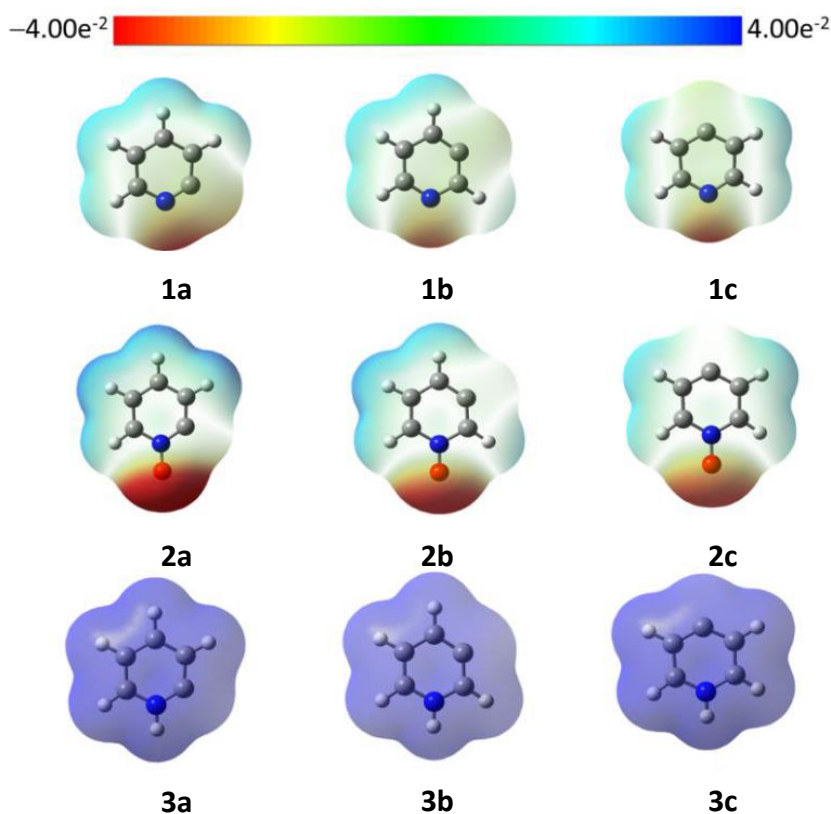
Figure 2.3 Electrostatic potential map of the isomeric pyridyl **1a-c**, pyridyl-*N*-oxide **2a-c** and pyridinyl radicals **3a-c** at (U)B3LYP/cc-pVTZ level of theory.

2.2.6 Multireference calculations

Qualitative study of the interaction between lone pair and radical electron is required in order to understand the mode of operation and also their influence in stability. In this regard, we performed optimization followed by frequency calculations at multireference electronic structure mode using CASSCF method. The CASSCF orbitals have been calculated using (9, 8), (11, 9) and (7, 7) active spaces for **1a-c**, **2a-c** and **3a-c** radical isomers, respectively. The

complete results of the muticonfiguration calculations are given in the Appendix. (**Figure A2.1**) Earlier, spin density calculations showed that the electron density is localized at radical centers. This result has been further supported by multireference calculations, as all the radical species showed singly occupied molecular orbital (SOMO) corresponding to localization of σ-orbitals. For all the radicals, lone pair orbitals are found to be low lying below the filled π-orbitals. Parent compounds **1**, **2** and **3** possess a $^1A_1$ ground state with C_{2V} symmetry. Similarly, all the 2-dehydro and 3-dehydro radicals (**1a, 1b**, **2a, 2b**, **3a** and **3b**) have attained a C_S symmetric structure and are found to possess $^2A'$ electronic state, whereas, C_{2V} symmetric radicals **1c-3c** attain a $^2A_1$ ground state electronic structure. In order to understand the bonding or antibonding interaction between lone pair of heteroatom and radical electron, we inspected singly occupied molecular orbital (SOMO) of all the radical species. (**Figure 2.4**) Through this, we found out that the radicals **1a**, **1b**, **2a**, **2b**, **3a** and **3b** have an antibonding interaction between radical center and lone pair of electrons. Such nodal character at the SOMO indicates that the unpaired electron is localized at the radical center with a weak spin distribution towards nitrogen center in the ground electronic state. Also, based on the orbital coefficient at the nitrogen atom, it is clear that the extend of localization at formal radical center increases in the order **1a** < **1b** < **1c**.

   The LUMO and SOMO orbitals with their orbital energies are shown in **Figure 2.4**. For the pyridyl radicals, the SOMO-LUMO energy gap is in the order **1a** > **1b** > **1c**. If the lone pair is made unavailable (either through protonation or *N*-oxide formation), the changes in such energy gaps can be an indication of the interactions between the radical electron and the nitrogen lone pair. In this regard, CASSCF calculations have been performed for the pyridinyl and pyridyl-*N*-oxide radicals. Interestingly, both the LUMO and SOMO are

relatively well stabilized upon protonation or *N*-oxide formation at the nitrogen center in all the cases. The stabilization of SOMO can be attributed to the enhancement in the stability due to electrostatic and electronic effects of the resulting pyridinyl and pyridyl-*N*-oxide radicals, respectively. Presumably, delocalization of the charge and extended π-conjugation are reasons for the stabilization of the LUMO in pyridinyl and pyridyl-*N*-oxide radicals, respectively. However, the extent of SOMO-LUMO separation varies from one radical to another.
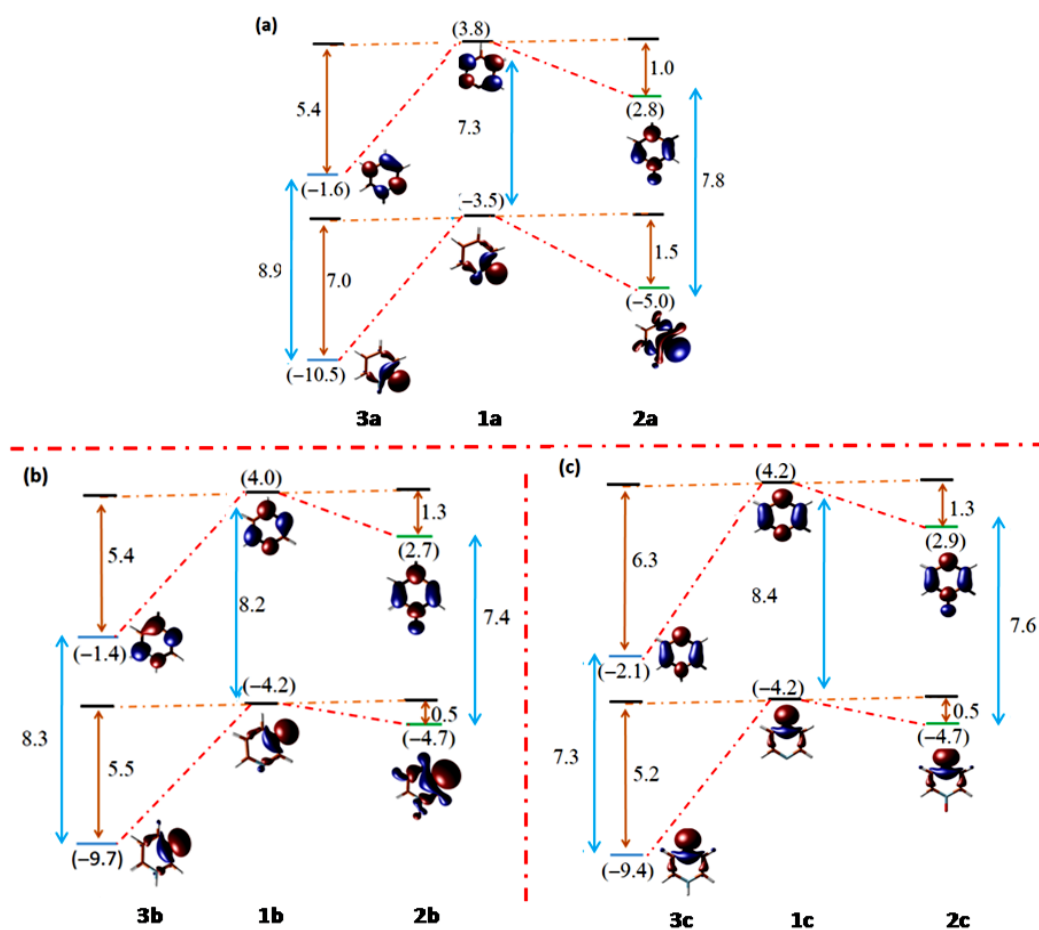
Figure 2.4 Relative SOMO-LUMO energy gaps (eV) in pyridyl **1a-c**, pyridyl-*N*-oxide **2a-c** and pyridinyl **3a-c** radical isomers. The SOMO and LUMO orbitals along with their orbital energies are indicated. All the orbitals have been rendered at an isovalue of 0.05. (Color code: Blue = negative; Red = positive)

Protonation leads to an electrostatic interaction between the radical electron and the positively charged nitrogen center, which decreases over the distance. Consequently, the SOMO-LUMO gap decreases in the order **3a** > **3b** > **3c**, which is the same for the relative stabilization of SOMO in those species with respect to the corresponding pyridyl radicals. The LUMO, on the other hand, showed a higher stabilization only in the case of **3c** compared to that of **3a** and **3b**, where the relative stabilization is the same with respect to the LUMO of corresponding pyridyl radicals. On contrary, pyridyl-*N*-oxide radicals show no particular trend in the SOMO-LUMO gap, due to contrasting push-pull electronic effects. However, a marginal *ortho*-, *para*- directive effect of *N*-oxide is the feature of such changes. All these results show that the 2-dehydropyridine undergoes the strongest perturbation upon protonation or *N*-oxide formation, an indication of stronger interaction between the lone pair and the radical center. Whereas, the 3- and 4-pyridyl radicals undergo relatively lesser changes, a consequence of moderate to weak interactions between them.

From the spin density calculations, we observed that the delocalization of spin at the formal radical center is observed only in the cases of 2- and 3- pyridyl (**1a** and **1b**) radicals. On the other hand, 4-pyridyl radical **1c,** *N*-oxide (**2a-c**) and protonated radicals (**3a-c**) show more localization. The MCSCF calculations support a dominant through bond interactions between nitrogen lone pair and radical electron in the 4-pyridyl radical (**1c**) on the basis of orbital ordering (out-of-phase combination orbital is lower than the in-phase combination orbital) as shown in **Figure 2.5.** However, the 2- and 3-pyridyl radicals show an anti-symmetric combination in the SOMO orbital, an indication of the presence of dominant through space interaction (considering the fact that the symmetric combination is more stabilized in both cases) that may lead to delocalization. Based on these facts, the character

and wavefunction of SOMO can be correlated to the extend of through space interaction. As the through space interaction follows the order **1a** > **1b** > **1c**, the delocalization of spin density also follows the same trend.
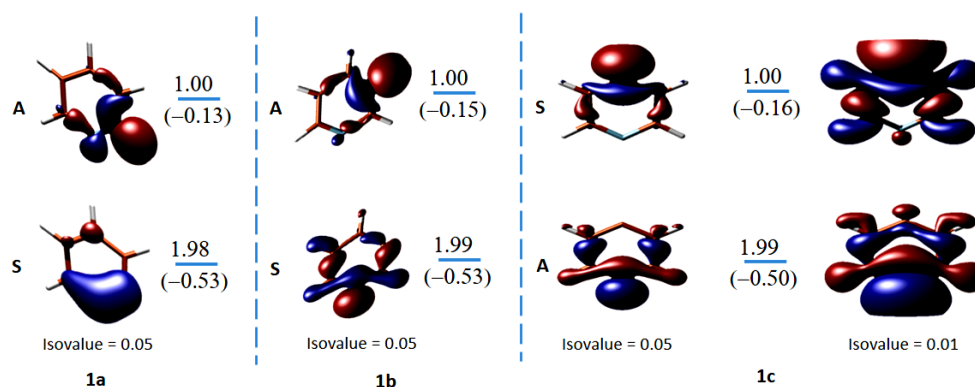
Figure 2.5 Molecular orbitals representing symmetric and antisymmetric combinations of lone pair and radical electron at CASSCF(3,2)/cc-pVTZ//(U)B3LYP/cc-pVTZ level of theory for pyridyl radicals **1a-c**.The values in normal font indicate orbital occupancies and values in parenthesis represent the orbital energies (in hartree). All the orbitals are rendered at an isovalue 0.05. For clarity, the SOMO and SOMO-1 orbitals of **1c** were rendered at an isovalue 0.01.
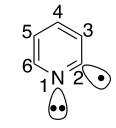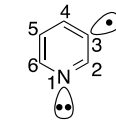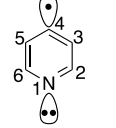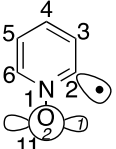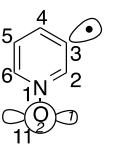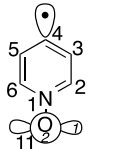
2.2.7 NBO analysis

The data from thermodynamic stability, geometrical parameters, spin density and electrostatic potential mapping evidently reveal the existence of an interaction between nitrogen lone pair and radical electron. In order to quantify the interactions and also to identify the type, the natural bond orbital (NBO) calculations have been performed at (U)B3LYP/cc-pVTZ, (U)M06/cc-pVTZ and (U)CCSD(T)/cc-pVTZ//(U)B3LYP/cc-pVTZ level of theories. The NBO calculations have been carried out for all the pyridyl, pyridyl-*N*-oxide and pyridinyl radical isomers and the results reveal the interaction energies between different orbitals involved using second order perturbation energy are listed in **Table 2.3**. In

the case of 2-pyridyl radical **1a**, the N-atom lone pair depicts a substantial amount of through-space (TS) interaction with the radical center, whereas such interactions are found to be insignificant and completely absent in **1b** and **1c**, respectively. Similarly the lone pair stabilizes radical isomer by through bond (TB) interaction also. Unlike TS interaction, there is a considerable amount of TB interaction energies is observed in all the radical isomers, of which the order varies as **1a** < **1b** < **1c**. These observations suggest that in the case of pyridyl radicals TB interactions are found to be comparable, however, a dominant TS interactionis the pivotal reason for the stabilization of **1a** among the isomers. Despite the absence of TS interactions, the large TB interaction energy explains the stability of **1c** over **1b**.

Upon protonation, no significant TS or TB interactions have been observed in case of pyridinyl radical isomers due to the lack of lone pair. In the same way, through space interactions are either insignificant or absent in the case of pyridyl-*N*-oxide radicals as the oxygen lone pairs lie at larger distances. Even the radical **2a**, which lies in the close proximity of lone pairs compared to other isomers shows a negligible amount of TS interaction energy of 1.1 kcal/mol. Interestingly, the TB interaction of the lone pair with the antibonding orbital of radical has considerably high interaction energy values, out of which **2b** has the highest value followed by **2c** and **2a**. The TB interaction energy order directly follows the stability order of the radical isomers, which infers that through bond interaction is the predominant stabilizing factor in pyridyl-*N*-oxide radical isomers.

Table 2.3 The Second Order Perturbation Energy from the NBO Analysis at Different Levels of Theory.

1a			1b			1c		
Donor	Acceptor	<E>[a,b]	Donor	Acceptor	<E>[a,b]	Donor	Acceptor	<E>[a,b]
$n_{(N1)}$	$n^*_{(C2)}$	**20.8** *20.6* 23.5	$n_{(N1)}$	$n^*_{(C3)}$	**0.7** *0.8* 0.7	$n_{(N1)}$	$n^*_{(C4)}$	-
$n_{(N1)}$	$\pi^*_{(C5-C6)}$	**5.0** *5.1* 6.6	$n_{(N1)}$	$\pi^*_{(C5-C6)}$	**5.1** *5.4* 5.2	$n_{(N1)}$	$\pi^*_{(C5-C6)}$	**6.2** *6.3* 5.8
$n_{(N1)}$	$\pi^*_{(C2-C3)}$	**3.3** *3.5* 5.5	$n_{(N1)}$	$\pi^*_{(C2-C3)}$	**5.8** *5.7* 6.2	$n_{(N1)}$	$\pi^*_{(C2-C3)}$	**6.2** *6.3* 5.8
$\pi^*_{(C5-C6)}$	$\pi^*_{(C2-N1)}$	**30.2** *29.7* 16.1	$\pi^*_{(C5-C6)}$	$\pi^*_{(C4-C3)}$	**38.6** *38.3* 51.6	$\pi^*_{(C2-N1)}$	$\pi^*_{(C4-C3)}$	**30.5** *31.1* 42.8
$\pi^*_{(C4-C3)}$	$\pi^*_{(C2-N1)}$	**41.7** *39.8* 18.3	$\pi^*_{(C2-N1)}$	$\pi^*_{(C4-C3)}$	**37.6** *39.8* 24.3	$\pi^*_{(C5-C6)}$	$\pi^*_{(C4-C3)}$	**39.8** *39.3* 71.6

2a			2b			2c		
Donor	Acceptor	<E>[a,b]	Donor	Acceptor	<E>[a,b]	Donor	Acceptor	<E>[a,b]
$n_{1(O11)}$	$n^*_{(C2)}$	**1.1** *0.7*	$n_{1(O11)}$	$n^*_{(C3)}$	-	$n_{1(O11)}$	$n^*_{(C4)}$	-
$n_{1(O11)}$	$\pi^*_{(C2-N1)}$	**5.7** *7.0*	$n_{1(O11)}$	$\pi^*_{(C2-C3)}$	**0.4** *0.4*	$n_{1(O11)}$	$\pi^*_{(C2-C3)}$	**0.4** *0.5*
$n_{1(O11)}$	$\pi^*_{(C5-C6)}$	**0.4** *0.5*	$n_{1(O11)}$	$\pi^*_{(C2-N1)}$	**7.4** *8.0*	$n_{1(O11)}$	$\pi^*_{(C2-N1)}$	**5.4** *6.2*
$n_{1(O11)}$	$\pi^*_{(C6-N1)}$	**5.0** *6.7*	$n_{1(O11)}$	$\pi^*_{(C5-C6)}$	**0.4** *0.4*	$n_{1(O11)}$	$\pi^*_{(C5-C6)}$	**0.4** *0.5*
$n_{2(O11)}$	$\pi^*_{(C2-C3)}$	**0.4** *0.4*	$n_{1(O11)}$	$\pi^*_{(C6-N1)}$	**4.5** *5.5*	$n_{1(O11)}$	$\pi^*_{(C6-N1)}$	**5.4** *6.2*
$n_{2(O11)}$	$\pi^*_{(C6-N1)}$	**26.9** *59.5*	$n_{2(O11)}$	$\pi^*_{(C6-N1)}$	**34.8** *39.6*	$n_{2(O11)}$	$\pi^*_{(C2-N1)}$	**26.7** *13.9*
$\pi^*_{(C6-N1)}$	$\pi^*_{(C2-C3)}$	**13.9** *23.7*	$\pi^*_{(C6-N1)}$	$\pi^*_{(C2-C3)}$	**10.7** *10.6*	$\pi^*_{(C2-N1)}$	$\pi^*_{(C4-C3)}$	**21.1** *0.85*

[a]Interaction energies expressed in kcal/mol [b]Bold = (U)B3LYP/cc-pVTZ; Italics = (U)M06/cc-pVTZ; Normal = (U)CCSD(T)/cc-pVTZ//(U)B3LYP/cc-pVTZ.

49

2.2.8 Vertical ionization energy (VIE) and vertical detachment energy (VDE)

To gain further insights, VIE and VDE calculations have been performed to cut-off the interaction between the radical center and the heteroatom by converting the radical to attain either cation (vacant) or anion (doubly occupied) as shown in the Appendix (**Scheme A2.1**). In this regard, the electronic structures of cations and anions of pyridine, pyridine-*N*-oxide and protonated pyridine (three isomers each) have been computed. The relative stability order of the cations and anions can provide the insights into the change in interaction energy between the radical center and lone pair. The resulting VIE and VDE for each isomeric pyridyl, pyridyl-*N*-oxide and pyridinyl radicals are indicated in **Figure 2.6**.
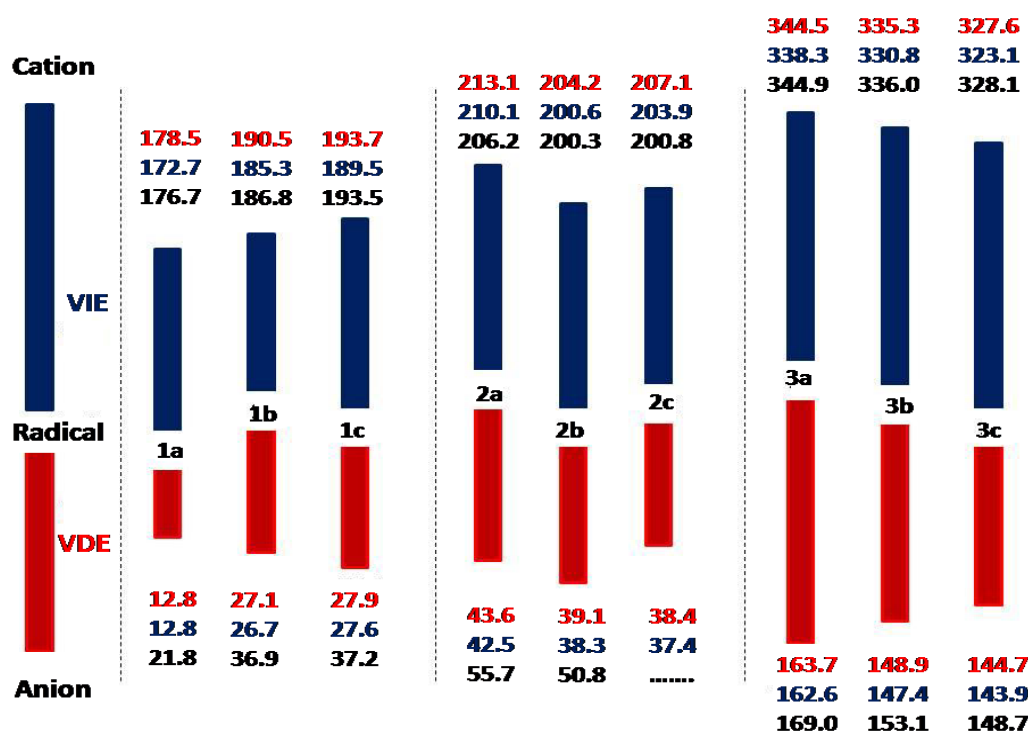
Figure 2.6 Schematic diagram representing VIE and VDE of the isomeric pyridyl **1a-c**, pyridyl-*N*-oxide **2a-c** and pyridinyl **3a-c** radicals (All the values indicated are in kcal/mol; Red color – (U)B3LYP/cc-pVTZ; Blue color – (U)M06/cc-pVTZ; Black color– CBS-QB3).

For each isomer, the VIE has a larger value compared to the VDE, i.e the removal of unpaired electron needs higher energy relative to addition of electron into the radical orbital. Among the three pyridyl radicals, the VIE varies in the order **1a** < **1b** < **1c**. This trend can be expected since the creation of positive center stabilized by through space interaction of the nitrogen lone pair. Since the strength decrease from *ortho* to *meta* to *para*, **1a** has the lowest value and **1c** has the highest.

Due to the unavailability of lone pair as a result of positive charge at nitrogen atom such TS interactions are non-existing in the pyridinyl radicals. Apart from that, the repulsive forces between the two positively charged centers destabilizes at proximal distances. As a result, they showed a reversal of the trend, i.e. **3a** > **3b** > **3c**. On the other hand, the electronic effect of the *N*-oxide substituent primarily influences through π-donation that results in stabilization of the cationic center at 3-position of **2b** rather than **2a** or **2c**. Consequently, the trend varies in the pyridyl-*N*-oxide radicals as **2b** < **2c** < **2a**. Except in the case of **2b** and **2c**, where it showed a reversal with a smaller variation (<1 kcal/mol), the VDE follows the same trend as VIE. All these clearly indicate a strong TS interaction between the lone pair and the radical center at 2-position (**1a**), which weakens as it moves to 3-position (**1b**) and completely disrupts at 4-position (**1c**).

2.3 CONCLUSIONS

Based on the studies, we have found out that the pyridyl radicals have a relative stability order: **1a** < **1c** < **1b**, an indication of stabilizing interactions between the radical center and the nitrogen atom. The protonation and *N*-oxide formation disrupt those interactions, as a result, the stability order changes. Spin density calculations showed a high value of spin at

radical center along with a non-zero spin density at nitrogen in **1a** and **1b**, a clear evidence for the interaction. Again the protonation and *N*-oxide formation significantly increases the spin density values at the radical center that clarifies the enhancement in localization of spin upon breaking the radical electron – lone pair interaction. Electrostatic potential mapping is also consistent with this. Through the multireference calculations, it was found out that all the radicals are highly localized and are σ-radicals. However, no conclusive evidences for the mode of interactions between the nitrogen and the radical center have been observed.

On contrast, the NBO analysis provides a complete picture of the interactions including the *modus operandi*. In general, through space interaction is the most important mode, which can stabilize the radical center, whereas the through bond interactions are providing overall stability to the radicals. In the case of 2-pyridyl radical, the through space interaction is found to have a maximum contribution, whereas a weak interaction has been observed in the case of 3-pyridyl radical. Due to geometric constraints, it is completely absent in the case of 4-pyridyl radical. Since through bond interaction is the prevailing mode in **1c**, it has a marginal favor over **1b**. By *N*-oxide and protonation formations, the lone pair interactions are made unavailable at nitrogen center and so only through bond interactions are the major contributors for stabilization in the cases of pyridyl-*N*-oxide and pyridinyl radicals. Furthermore, the interactions are also confirmed using the VIE and VDE calculations and also vibrational analysis of selected normal modes.

In summary, varying through bond interactions between nitrogen lone pair and the radical electron are the major contributors to the overall stability of the three isomeric pyridyl radicals. On the other hand, a strong and stabilizing through space interaction is predicted in the case of 2-pyridyl radical, whereas such interaction weakens in the case of 3-pyridyl

radical and completely absent in the case of 4-pyridyl radical. Protonation disrupts those through space interactions and leading to a change in stability order, which entirely depends on the cation–radical electron interaction. In the case of pyridyl-*N*-oxide radicals, the electronic effects, in particular the combination of π-donation and σ-withdrawing (push-pull) effects play a major role in determining the stability order.

2.4 REFERENCES

1. Constantinides, C. P.; Koutentis, P. A.; Krassos, H.; Rawson, J. M.; Tasiopoulos, A. J. Characterization and Magnetic Properties of a "Super Stable" Radical 1,3-Diphenyl-7-trifluoromethyl-1,4-dihydro-1,2,4-benzotriazin-4-yl. *J. Org. Chem.* **2011**, *76*, 2798−2806.

2. Imada, Y.; Nakano, H.; Furukawa, K.; Kishi, R.; Nakano, M.; Maruyama, H.; Nakamoto, M.; Sekiguchi, A.; Ogawa, M.; Ohta, T.; et al. Isolation of Hypervalent Group-16 Radicals and Their Application in Organic-Radical Batteries. *J. Am. Chem. Soc*. **2016**, *138*, 479−482.

3. Ullman, E. F.; Osiecki, J. H.; Boocock, D. G. B.; Darcy, R. Studies of Stable Free Radicals. Nitronyl Nitroxide Monoradicals and Biradicals as Possible Small Molecule Spin Labels. *J. Am. Chem. Soc*. **1972**, *94*, 7049−7059.

4. Xie, C. J.; Lahti, P. M.; George, C. Modulating Spin Delocalization in Phenoxy Radicals Conjugated with Heterocycles. *Org. Lett*. **2000**, *2*, 3417−3420.

5. Hoffmann, R. Interaction of Orbitals Through Space and Through Bond. *Acc. Chem. Res*. **1971**, *4*, 1−9.

6. Ponomarev, D. A.; Takhistov, V. V. What are Isodesmic Reactions? *J. Chem. Educ*. **1997**, *74*, 201−203.

7. Colson, A.; Becker, D.; Eliezer, I.; Sevilla, M. D. Application of Isodesmic Reactions to the Calculation of the Enthalpies of H• and OH• Addition to DNA Bases: Estimated Heats of Formation of DNA Base Radicals and Hydrates. *J. Phys. Chem. A*. **1997**, *101*, 8935–8941.

8. Glaser, R.; Choy, G. S. –C. Spin Polarization versus Spin Delocalization. Topological Electron and Spin Density Analysis of the Rotational Automerization of Allyl Radical Including Electron Correlation Effects. *J. Phys. Chem.* **1994**, *98*, 11379–11393.

9. Venkataramani, S.; Winkler, M.; Sander, W. 1,2,3-Tridehydrobenzene. *Angew. Chem. Int. Ed. Engl.* **2005,** *44*, 6306–6311.

10. Koziol, L.; Winkler, M.; Houk, K. N.; Venkataramani, S.; Sander, W.; Krylov, A. I. The 1,2,3-Tridehydrobenzene Triradical: ^{2}B or not ^{2}B? The Answer is ^{2}A! *J. Phys. Chem. A.* **2007**, *111*, 5071–5080.

11. Sander, W.; Exner, M.; Winkler, M.; Balster, A.; Hjerpe, A.; Kraka, E.; Cremer, D. Vibrational Spectrum of *m*-Benzyne: A Matrix Isolation and Computational Study. *J Am. Chem. Soc.* **2002,** *124*, 13072–13079.

12. Korte, A.; Mardyukov, A.; Sander, W. Pyridyl- and Pyridylperoxy Radicals – A Matrix Isolation Study. *Austr. J. Chem.* **2014,** *67*,1324–1329.

13. Scott, A. P.; Radom, L. Harmonic Vibrational Frequencies: An Evaluation of Hartree-Fock, Møller-Plesset, Quadratic Configuration Interaction, Density Functional Theory, and Semi-empirical Scale Factors. *J. Phys. Chem.* **1996**, *100,* 16502–16513.

Chapter 3

Role of Spin Density in Predicting the Unimolecular and Bimolecular Reactivity patterns of Pyridyl, Pyridyl-N-oxide, and Pyridinyl Radical Isomers

3.1 INTRODUCTION

Spin density is the measure of unpaired electron density in a molecule, which is the difference in the distribution of alpha spin over beta spin at any given center.[1] This dimensionless quantity with a maximum value of one at a given center is an indication of localization of the radical character, whereas, a lowering of it means spatial delocalization of the radical character.[2-4] Through spin polarization mechanisms and dipolar coupling, the spin density within a molecule can acquire negative values as well. The sign and magnitude of the spin density distributions have experimental relevance, particularly in the prediction and simulation of hyperfine splitting, a characteristic feature obtained from the ESR spectroscopy that can be useful in understanding the electronic structure of the radicals.[5,6] The hyperfine coupling constant (a_H) and the spin density (ρ_C) are related by McConnel's relation, $a_H = Q\rho_C$, where Q is an empirical constant. Polarized neutron diffraction is a major experimental technique for spin density estimation, whereas, computations play a key role in predicting it (**Appendix, A3.1**).[7,8] The stability of many radicals under thermodynamic considerations has been discussed through the spin density distribution. Compared to π-delocalized radicals such as benzyl radical, allyl radical, etc., the corresponding localized σ-radicals (e.g. phenyl radical) are found to be less stable, due to higher localization of the radical character.[9,10]

Based on our previous work on the isomeric pyridyl radicals, we reported the type and also the magnitude of orbital interactions in determining the stability order of them.[11] The extent of such interactions in heterocyclic radicals can be realized from the delocalization of the spin density.[12,13] Despite these investigations accounted for the thermodynamic stability order, the kinetic stability based on the reactivity aspects of them is yet to be explored. Reactivity studies have been experimentally explored using techniques such as shock tube pulsed pyrolysis,[14] mass spectrometry,[15] photoelectron spectroscopy,[16] matrix isolation,[17] and UV photodissociation studies,[18] etc. The exploration of the reactivity aspects provides many insights, in particular, related to the combustion chemistry in petrochemical industries, where heterocyclic radicals are commonly encountered as reactive intermediates.[19,20]

Indeed, our major intention is to understand the relationship between spin density and reactivity patterns, particularly in the heterocyclic radicals, and correlating them with the changes in the properties associated with reactions profile, and predicting low energy pathway among the various potential pathways, etc. In this regard, we explored the unimolecular and bimolecular reactivity studies on the three isomers each of pyridyl **1a-c**, pyridyl-*N*-oxide **2a-c**, and pyridinyl **3a-c** radicals and monitored the spin density (**Scheme 3.1**). The bimolecular reactions have been investigated with selected small molecules H_2, H_2O, CO, CO_2, CH_4, and CH_3OH. In this contribution, we investigated the unimolecular and bimolecular reactivity aspects of the pyridyl, pyridyl-*N*-oxide, and pyridinyl radical isomers, with a major focus on the spin density as a predictive tool for their kinetic stability.
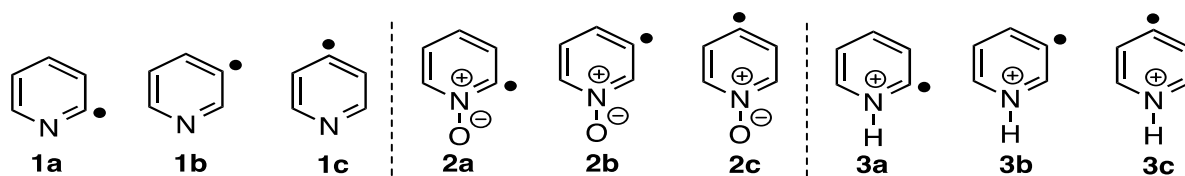
Scheme 3.1 Isomers of pyridyl **1a-c**, pyridyl-*N*-oxide **2a-c**, and pyridinyl **3a-c** radicals

56

3.2 RESULTS AND DISCUSSION

Table 3.1 Bond Dissociation Energies (BDEs) of Isomeric Pyridyl (**1a-c**), Pyridyl-*N*-oxide (**2a-c**), and Pyridinyl (**3a-c**) Radicals at Different Levels of Theory.

{X = N (**1a-c**); N+-O- (**2a-c**); NH+ (**3a-c**)}
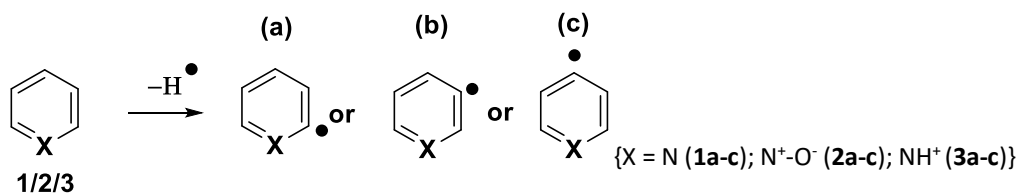
First C-H bond dissociation energy[a] (kcal/mol)

Level of theory	pyridyl radicals			pyridyl-*N*-oxide radicals			pyridinyl radicals		
	1a	**1b**	**1c**	**2a**	**2b**	**2c**	**3a**	**3b**	**3c**
(U)B3LYP/cc-pVTZ	104.9	111.0	109.7	116.7	111.5	113.2	117.6	116.9	114.4
(U)M06-2X/cc-pVTZ	106.2	112.3	110.5	117.0	112.5	113.3	117.5	117.1	114.5
CBS-QB3	109.1	115.9	114.5	124.3	118.5	120.4	121.3	120.1	117.5
Experimental[b,][18,31]	105	112	112	-	-	-	-	-	-

N-O bond dissociation energy[a] (kcal/mol)

Level of theory				
(U)B3LYP/cc-pVTZ	126.4	114.5	125.9	122.9
(U)M06-2X/cc-pVTZ	121.3	110.5	121.1	118.5
CBS-QB3	112.8	97.6	110.2	107.0

[a]Zero-point energy corrected; [b]Experimental BDEs have been reported in kcal/mol with an error ± 2 kcal/mol.

The main objective of this work is to understand and compare the kinetic stability of radical isomers derived from pyridine **1a-c**, pyridine-*N*-oxide **2a-c**, and protonated pyridine **3a-c**. Also, we intended to correlate their reactivity patterns either directly or with the changes in the spin density associated with the reactions. In this regard, we considered the following reactions: (a) homolytic C-H bond breaking towards the generation of dehydro-radical isomers from their respective parents through BDE calculations, (b) isomerization pathways through 1,2-H shifts, (c) unimolecular decomposition channels, and (d) bimolecular reactions with small molecules. The proceeding section will give details of such reactions.

3.2.1 Bond Dissociation Energies (BDEs)

Bond dissociation energy (BDE) is the enthalpy change associated with the reaction involving homolytic cleavage of the specific bond where the molecule results in the pair of radicals. It can be estimated by measuring the enthalpy of the given molecule and also the resulting radical pairs. This can be estimated either experimentally or using computations. As a starting point, we estimated the first C-H BDEs of the parent compounds pyridine **1**, pyridine-*N*-oxide **2**, and protonated pyridine **3** in the generation of all the radical species of our interest. Depending on the position of the C-H bond relative to the nitrogen, homolytic dissociation can lead to three possible radical isomers each, namely **1a-c** in pyridine, **2a-c** in pyridine-*N*-oxide, and **3a-c** in protonated pyridine, respectively. At (U)B3LYP and (U)M06-2X levels, the first C-H BDE values were found to be lowest for the pyridyl radicals, followed by pyridyl-*N*-oxide radicals and then pyridinyl radicals (**Table 3.1**). However, the estimated C-H BDEs at the CBS-QB3 level in **2a** and **2c** showed a higher value compared to

3a and **3c**, respectively, which was opposite to the other levels of theory. Whereas, the order is maintained for **2b** and **3b** in all the levels of theory.

The comparison of BDEs across all the radical isomers exhibits the same trend as that of the stability order. In our earlier work, the stability order for pyridyl isomers was found to be **1a** > **1c** > **1b**, which is consistent with the increasing BDEs in the same order.[11] The lowest BDE value for **1a** favors higher radical stabilization arising due to through space stabilizing interaction between nitrogen lone pair and the radical center. On the other hand, **1c** has a reasonable stabilization arising due to the through-bond interaction. The C-H BDE is highest for **1b** among the pyridyl radicals. This can be attributed to the absence of a strong stabilization arising from either through space or through bond interactions. Conversely, the 2-dehydro-pyridyl-*N*-oxide **2a** has the highest C-H BDE, which is attributable to a 1,3 anomeric type interaction between lone pair of oxygen with the radical center.[11] Again, the C-H BDE value decreases for **2c** and least for **2b**. A strong through-bond interaction between the radical center and the oxygen lone pair could be accounted for stabilization of the radical **2b** and lowering of C-H BDE. In the case of pyridinyl radicals, the complete quenching of the lone pair over nitrogen atom (i.e. protonation) prevents the stabilization arising due to orbital interactions. The resulting electronic effect and charge delocalization is decisive in the higher C-H BDE values in those isomers **3a-c**. The C-H BDE value gets lowered with the increasing distance of the radical center from the protonated nitrogen atom. On comparison, the C-H BDE values increase with a partial quenching of nitrogen lone pair (i.e. with the introduction of N-O moiety) and reach a maximum value with the complete quenching of it. Hence, C-H BDEs can be comparable to the relative stability within the isomeric radicals based on lone pair-radical interactions. All these results are consistent with the earlier studies

59

on pyridine-based radicals.[14] Similarly, the N-O BDEs corresponding to the deoxygenation step for the dehydro pyridyl-*N*-oxide radicals **2a-c** relative to the corresponding parent **2** have also been estimated. The resulting N-O BDEs showed lower values in **2a-c** compared to the corresponding value of the parent **2**. This supports the existence of stabilizing interaction between the lone pair of nitrogen with the radical centers in the products **1a-c**.
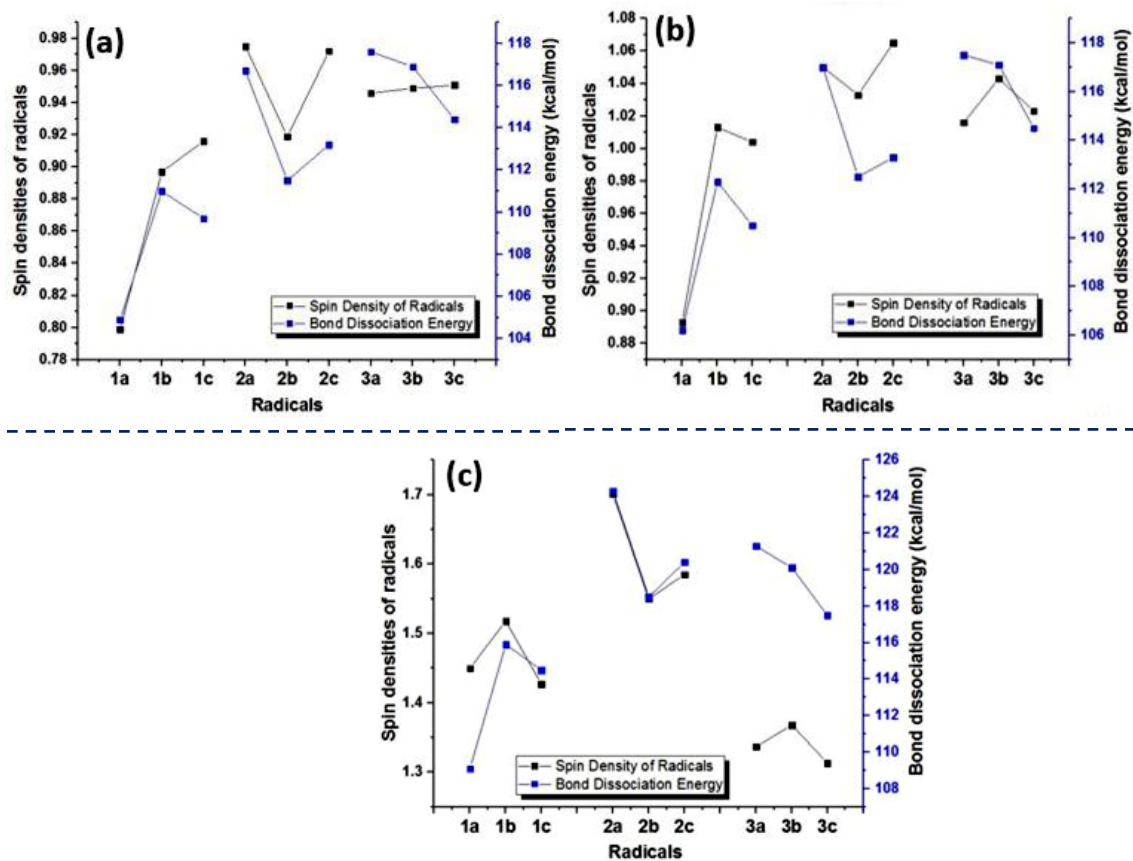
Figure 3.1 Trends in the first C-H BDEs of the parent compounds **1-3** relative to the spin densities at the radical centers in isomeric pyridyl (**1a-c**), pyridyl-*N*-oxide (**2a-c**) and pyridinyl (**3a-c**) radicals at (a) (U)B3LYP/cc-pVTZ, (b) (U)M06-2X/cc-pVTZ, and (c) CBS-QB3 levels of theory.

For obtaining further insights, we compared the trends in C-H BDEs with that of spin densities of each radical isomers. Except for the pyridinyl radical isomers **3a-c**, the spin

densities exhibited a similar variation as in the case of their respective C-H BDEs (**Figure 3.1**). Presumably, the delocalization of the charge (inferred from the electrostatic potential) influences the spin densities in the pyridinyl radicals.

3.2.2 Isomerization through 1, 2-H shifts

Among the unimolecular reactivity channels, a concerted 1, 2-H shift of the radicals can lead to isomerization. Due to the presence of nitrogen atom in the ring, such 1, 2-H shifts lead to a maximum of two radical isomers depending on the position of the radical center. Having optimized the transition states connecting such channels, we estimated the activation barriers for various 1, 2-H shifts (**Figure 3.2**). For pyridyl radicals (**1a-c**), the activation barrier is higher for **1b** to **1a** (66.1 kcal/mol) as compared to **1b** to **1c** (62.1 kcal/mol). The observed barriers have a direct correlation with the difference (between the reactant and the transition state) in the spin density values of radical centers, that is, lower spin (0.897 – 0.467 = 0.430) for **1b-1a** and a relatively higher value (0.897–0.455 = 0.442) for **1b-1c** isomerization channels. In the case of pyridyl-*N*-oxide radicals (**2a-c**), isomerization pathway **2b** to **2a** had a barrier 64.9 kcal/mol, which was found to be slightly higher than **2b** to **2c** (63.8 kcal/mol), which is consistent with the observed spin density differences, 0.413 and 0.449, respectively. This correlation is also valid for pyridinyl radicals (**3a-c**), where the difference in spin densities are estimated to 0.419 and 0.448 that corroborates well with computed barriers for the **3b** to **3a** (66.9 kcal/mol) and **3b** to **3c** (64.1 kcal/mol), respectively. The results of isomerization pathways at different levels of theory are shown in **figure 3.2**.

The comparison of those barriers supports our assumption regarding the lowering of kinetic stability upon *N*-oxidation in the radicals. This trend can be attributed to decrease in the through space and through-bond orbital interactions. However, the protonation of pyridyl

radicals did not affect the barriers drastically. The isomerization from a more stable radical to less stable radical was endothermic, and the conversion was less facile due to higher barriers.
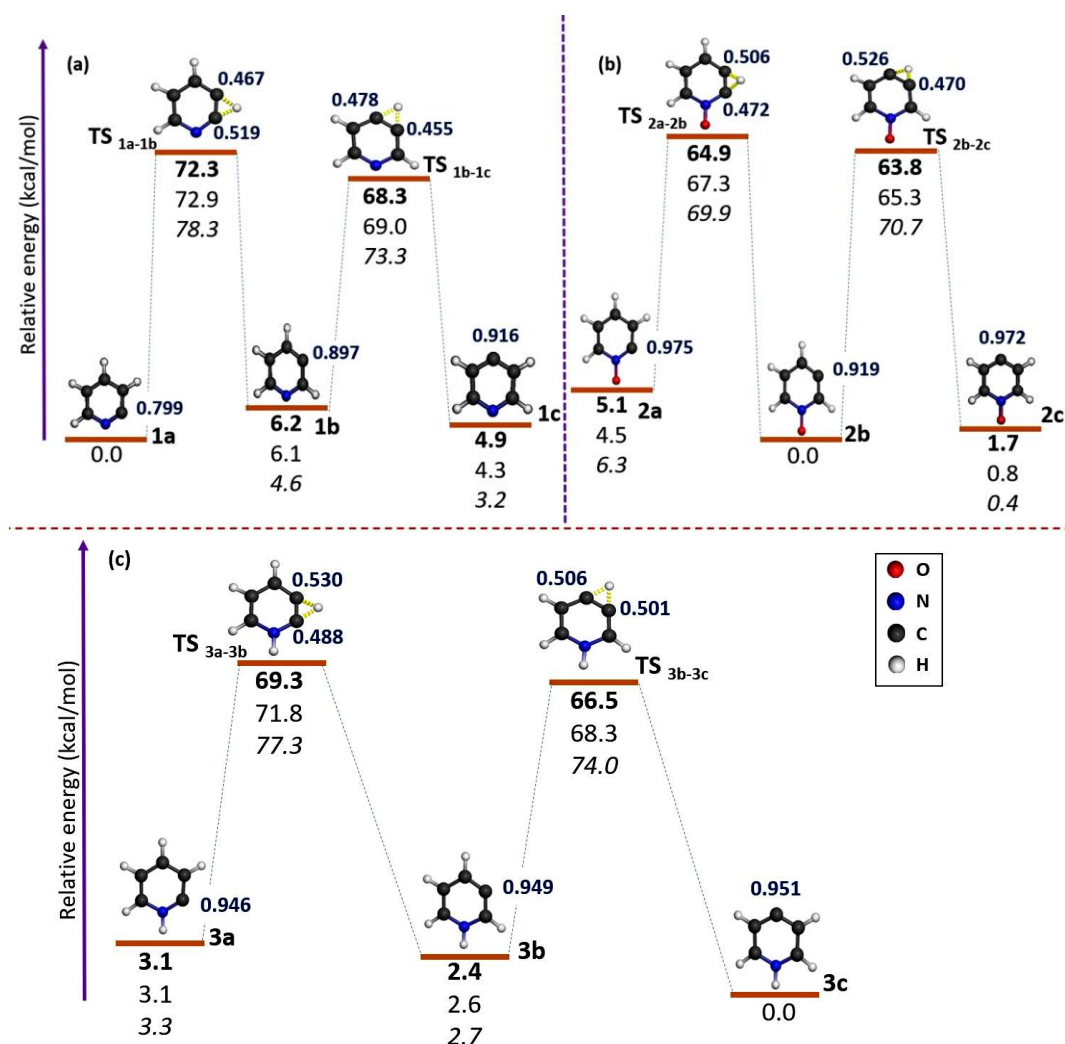
Figure 3.2 Isomerization through 1,2 H-shift in isomeric (a) pyridyl (**1a-c**), (b) pyridyl-*N*-oxide (**2a-c**), and (c) pyridinyl (**3a-c**) radicals at different levels of theory. Bold: (U)B3LYP/cc-pVTZ, normal: (U)M06-2X/cc-pVTZ, and italics: (U)CCSD(T)/cc-pVTZ//(U)B3LYP/cc-pVTZ. (Spin densities at the radical centers are indicated for the reactants, products and the transition states)

The measure of the spin density transfer (the difference in the spin densities between the reactant and transition state) helps in explaining the reactivity pattern. A higher difference will lead to a lower activation barrier and higher reactivity.

3.2.3 Unimolecular dissociation pathways

Higher first C-H BDEs of the radicals, and high activation barriers (>59 kcal/mol) in the isomerization channels through 1, 2-H shift make them minor pathways in the unimolecular reactivity considerations. Hence, we paid our attention to the alternative channels in the form of unimolecular dissociation pathways. We mainly considered the ring-opening pathways of those radical isomers through step-wise bond scission, followed by fragmentation channels. All our attempts on concerted ring-opening were unsuccessful and did not lead to any transition state. In majority of the radical isomers, the ring-opening step was found to be the rate-limiting. Primarily the loss of aromatic stabilization could be responsible for it. Also, the consecutive fragmentation steps exhibit lower barrier relative to the first step. As a result, the barrier for first ring-opening step is reflective of the kinetic stability of the radicals under unimolecular reactivity consideration. The ring-opening can be initiated from multiple locations, and so attempts have been made in the optimization of the corresponding transition states. Almost in each radical isomer, we observed a maximum of two bonds, which were found to be weaker. Indeed, the ring-openings were initiated from those bonds. Such bonds can be easily identified based on the inspection of elongation in bond lengths upon the creation of the radical centers.[11] Previously, different groups have reported the unimolecular decomposition pathways of pyridyl radicals.[21-23] For comparison, we have included our results with the previously reported data which showed consistency (Appendix **Table A3.2**).

However, we have reinvestigated all the possible decomposition pathways of pyridyl radicals (i) at different levels of theory, (ii) compared the results with that of pyridyl-*N*-oxide and pyridinyl radicals: (a) to understand the effect of the nitrogen lone pair in the unimolecular decomposition channels, and (b) understanding the kinetic stability of all those radical isomers, and (iii) also to obtain the insights on spin density towards reactivity. (**Figure 3.3-3.5** and **Section 1A** and **Section 2A** in Appendix).

3.2.3.1 Dissociation pathways in 2-pyridyl 1a, 2-pyridyl-*N*-oxide 2a, and 2-pyridinyl 3a radicals

For these 2-dehydro radical isomers **1a**, **2a**, and **3a**, the inspection of spin density and the bond distance characteristics identified two weak bonds alternative to the radical center on either side of it. It envisages the possibility of unimolecular decomposition channels through these two bonds, namely C3-C4 and C6-N1. Such bond scissions have been illustrated by using the spin density mapping in the case of **1a**. (**Figure 3.3**) We were able to obtain the transition states for both the channels in all the three radicals. Interestingly, the C6-N1 cleavage was found to be the low energy channel in all the three isomeric radicals. In the case of pyridyl radical **1a**, C6-N1 bond cleavage led to a ring-opening product through a transition state **TS$_{1a-9}$** with an estimated barrier of 42.5 kcal/mol. Further, the ring-opened product **9** led either to a β-cyanovinyl radical **10** or (2*Z*)-penten-4-ynenitrile **12**. Both these channels can be predicted based on the spin density of **9**, which is localized at the terminal carbon. As a result, the alternate bonds of **9** has been predicted as the sites of cleavage. This led to the products **10** and **12** through the fragmentation of acetylene or C-H bond cleavage, respectively. Both the channels were found to have a low barrier. The resulting radical **10** loses a hydrogen to form cyanoacetylene, which can be predicted by inspecting the spin

density of **10**, and the weak alternate bond relative to the radical center. In the case of pyridyl-*N*-oxide radical **2a**, the first ring opening pathway along the C6-N1 bond cleavage leads to a linear nitrile oxide radical **23**. This happens through the transition state **TS₂ₐ₋₂₃** with an energy barrier of 39.5 kcal/mol relative to **2a**, which is 3.0 kcal/mol lower than that of pyridyl radical **1a**.
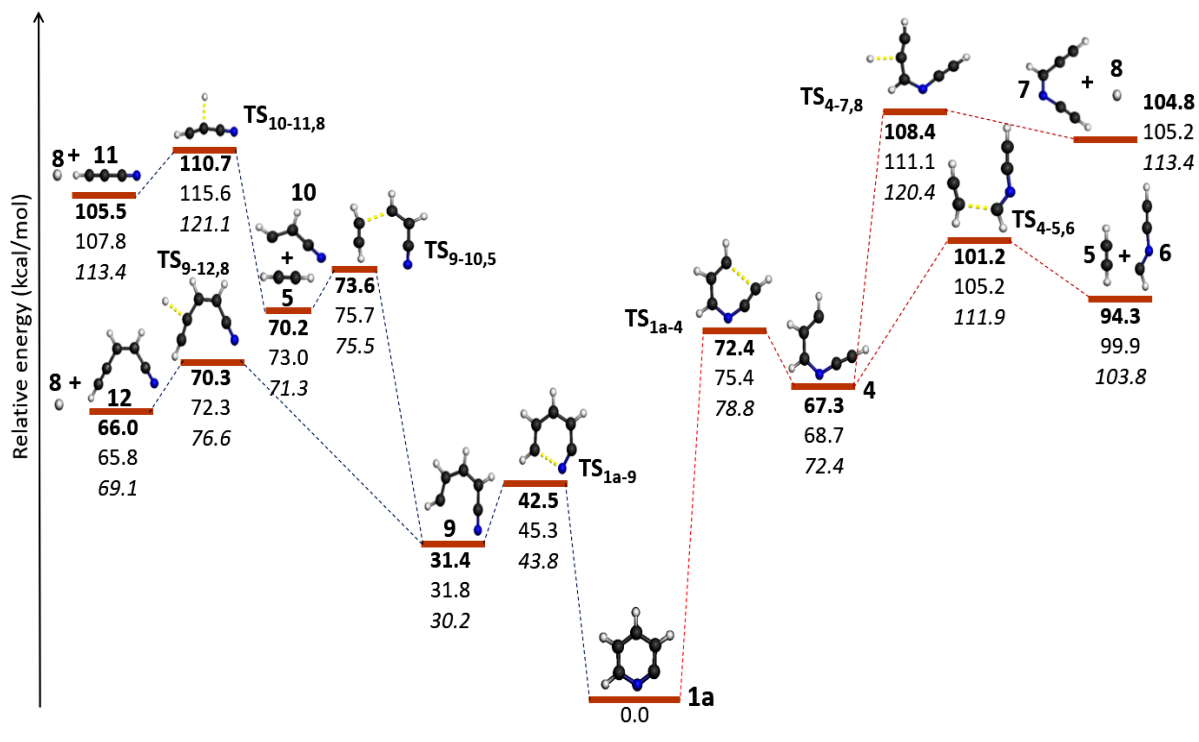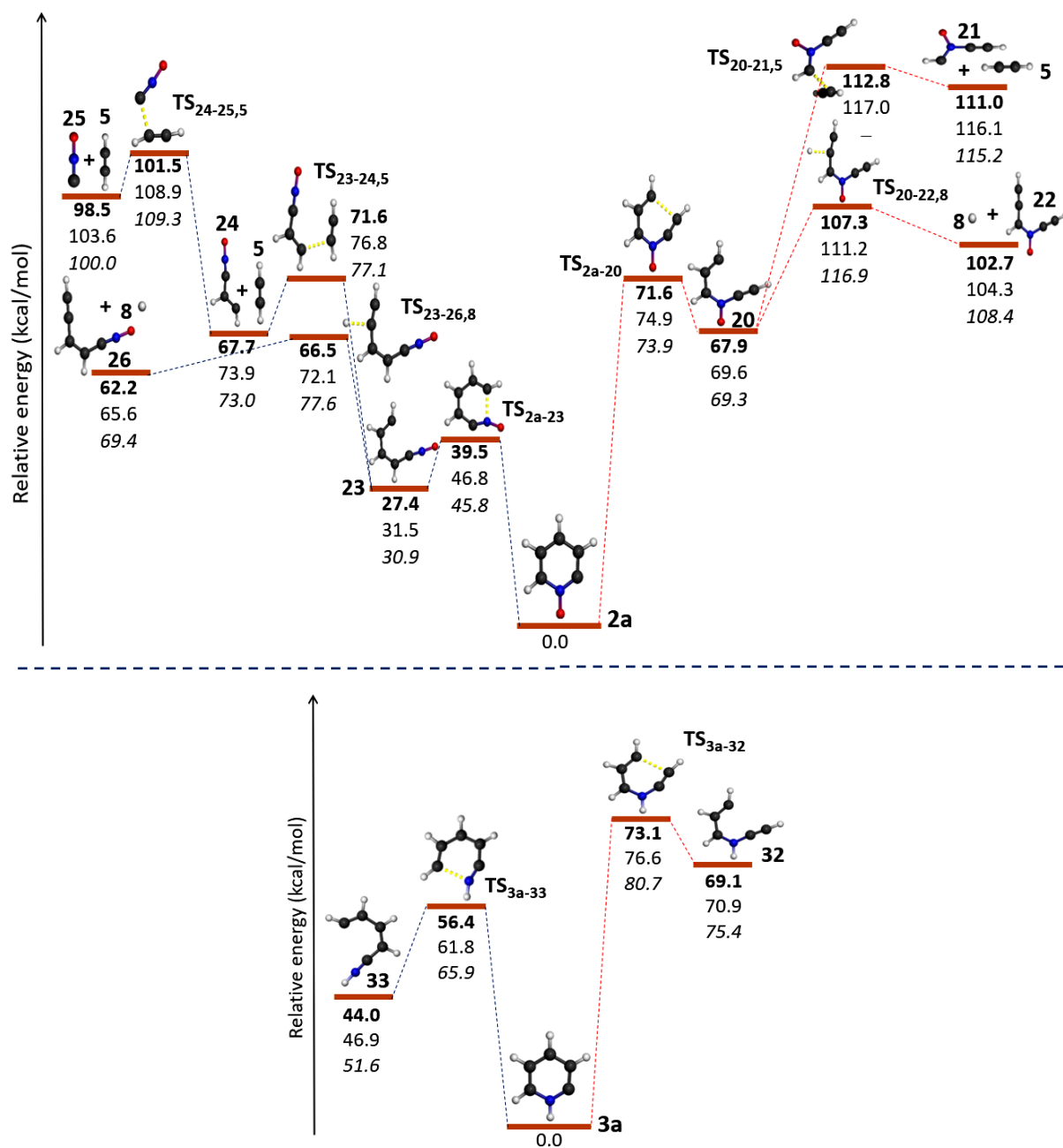
Figure 3.3 Unimolecular decomposition channels of 2-pyridyl **1a**, 2-pyridyl-*N*-oxide **2a**, and 2-pyridinyl **3a** radicals. (The optimized structures, barriers (kcal/mol) Bold: (U)B3LYP/cc-pVTZ; normal: (U)M06-2X/cc-pVTZ and italics: (U)CCSD(T)/cc-pVTZ//(U)B3LYP/cc-pVTZ level of theory). The spin density at the radical centers are indicated based on (U)B3LYP/cc-pVTZ level of theory listed in **Section 1A** in Appendix.

Similar to the case of **2a**, this intermediate **23** can also further undergo further fragmentation either by C-C or C-H bond cleavage. Again, this can be recognized by using the spin density estimation at the radical center of **23**. Furthermore, the C-C bond cleavage of intermediate **23** led to the formation of acetylene **5**, and CNO radical **25** as the end products. In the case of pyridinyl radical **3a**, the C6-N1 bond cleavage once again led to a lower energy pathway with an estimated barrier of 56.4 kcal/mol. However, we were unable to obtain further fragmentation products in this case.

Apart from the C6-N1 bond cleavage, all the three radicals **1a**, **2a**, and **3a** exhibited an alternative ring-opening channel through the C3-C4 bond scission. However, this channel was found to have estimated barriers of 72.4, 71.6, and 73.1 kcal/mol for **1a**, **2a**, and **3a**, respectively. (**Figure 3.3**) Interestingly, both the channels involve late transitions states in all the cases. Hence, the difference in the product stability could be one of the factors for the preference towards C6-N1 scission over the C3-C4 bond cleavage. The selectivity in such ring-opening steps leading to the product pairs **4/9**, **20/23**, and **32/33**. Both thermodynamic stabilization of the ring-opened products (thermodynamic control, driven by exergonic process) accompanied by early transition states (kinetic control, driven by the stabilization of the transition states) could be responsible for it. In the case of pyridyl radical **1a**, the C3-C4 bond cleavage led to the radical intermediate **4**. This further fragmented to **6** and **7** either by acetylene formation or a C-H bond scission. The decomposition through C3-C4 bond cleavage in pyridyl-*N*-oxide radical **2a** led to radical intermediate **20** via **TS$_{2a-20}$**. Surprisingly, the further fragmentation of intermediate **20** through the C-H bond cleavage is more favorable compared to the fragmentation through acetylene formation. On contrary, the further fragmentation of **32** in the case of **3a** was unsuccessful even after several attempts.

67

Among the unimolecular decomposition pathways in 2-pyridyl, 2-pyridyl-*N*-oxide, and 2-pyridinyl radicals, the first and the low energy step involves the C6-N1 bond cleavage. The barrier corresponding to this step increases in the order: **2a** < **1a** < **3a**. Such a trend correlates well with the spin density at the radical center. However, the influence of the charge might be responsible for a higher barrier in the case of **3a**, whereas the anomeric interaction between radical electron and the oxygen lone pair favors the higher reactivity in **2a**. The schematic unimolecular decomposition channels of all the three isomeric radicals are indicated in **Figure 3.3**, and the corresponding spin density data and IRC are available in the Appendix (**Section 1A** and **2A**).

3.2.3.2 Dissociation pathways in 3-pyridyl 1b, 3-pyridyl-*N*-oxide 2b and 3-pyridinyl 3b radicals

The investigations on the decomposition pathways for **1b**, **2b**, and **3b** revealed C2-N1 and C4-C5 bond scissions as the possible channels. They were identified based on the spin density at the radical centers and also the weakening of the alternate bonds with respect to it. Similar to 2-dehydro isomeric radicals, once again the C2-N1 bond cleavage is found to be kinetically more favorable than the C4-C5 bond cleavage pathways. (**Figure 3.4**)

Ring-opening through C2-N1 bond scission in **1b** led to the radical intermediate **13** via **TS$_{1b-13}$** having an energy barrier of 45.2 kcal/mol. This species **13** can further be decomposed either by C-C bond or C-H bond cleavage. Indeed, the cleavage at C-C bond led to HCN **14** along with an enyne type radical **15**, which further led to the formation of diacetylene **16** through a C-H bond breaking. In yet another channel, a C-H bond cleavage of the radical intermediate **13** led to the (**2Z**)**-penten-4-ynenitrile 12**, which is also an end

product of 2-pyridyl radical **1a** decomposition. The decomposition through C2-N1 bond cleavage in 3-pyridyl-*N*-oxide **2b** radical led to the radical intermediate **27**. This happened via the **TS₂ᵦ₋₂₇** with an energy barrier of 27.2 kcal/mol, which is kinetically more favorable compared to 3-pyridyl **1b** radical. However, the subsequent C-H scission from the intermediate **27** requires a higher barrier leading to the product **26**. The formation of HCNO (a similar channel like the formation of HCN in **1b**) was unsuccessful in this case. Conversely, all our attempts in locating the transition state corresponding to the C2-N1 bond cleavage pathway in 3-pyridinyl radical **3b** was failed.
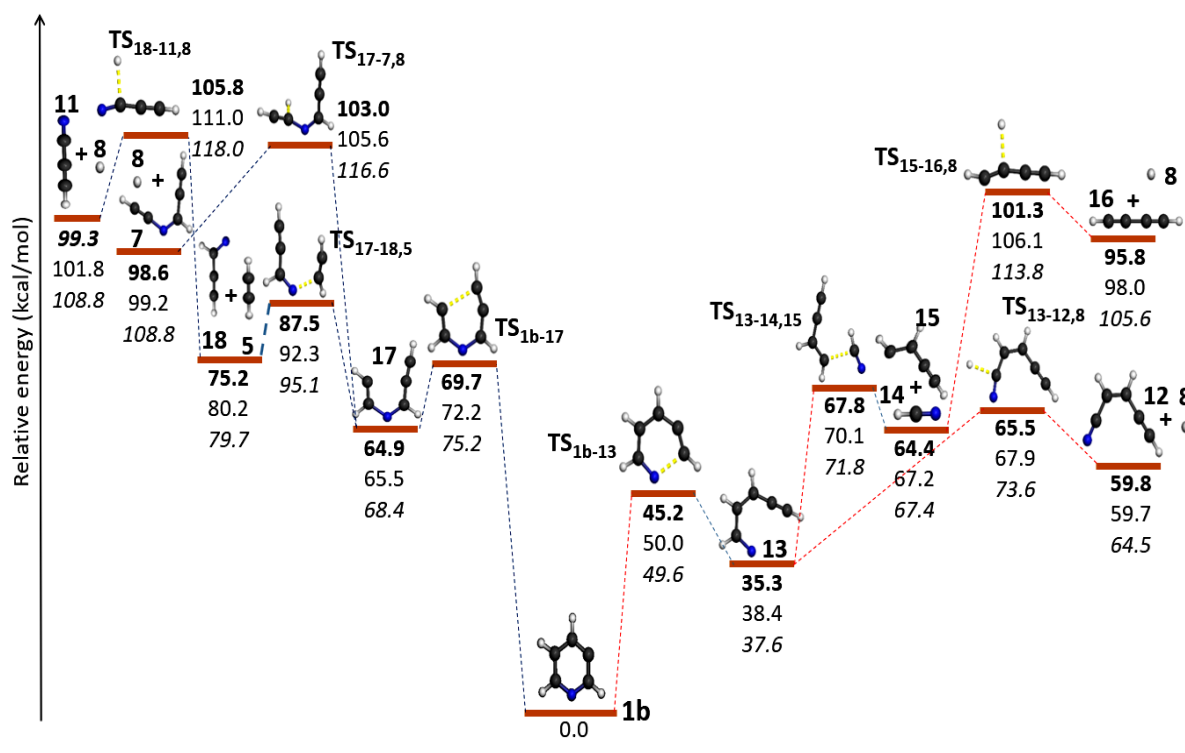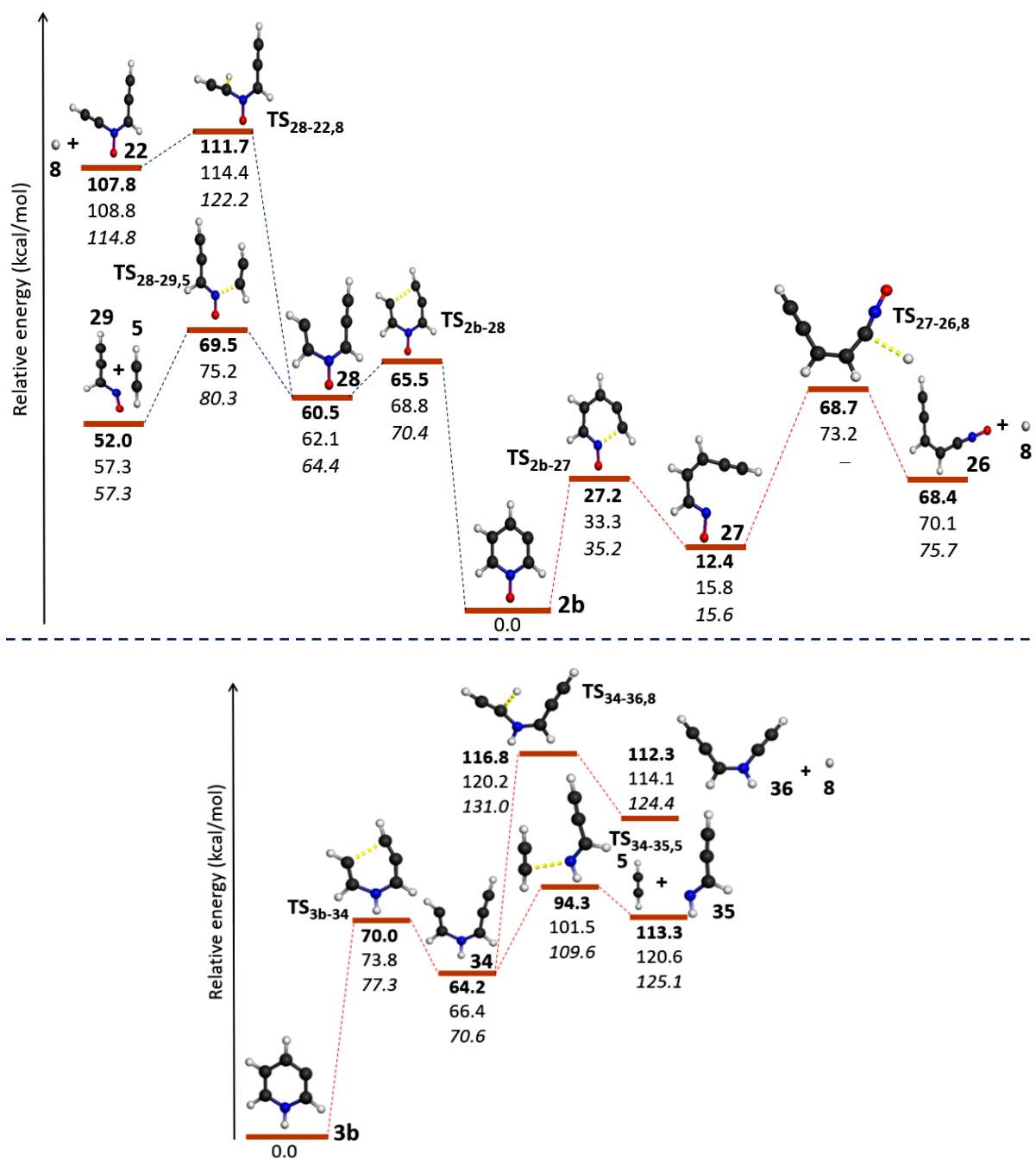
Figure 3.4 Unimolecular decomposition channels of 3-pyridyl **1b**, 3-pyridyl-*N*-oxide **2b**, and 3-pyridinyl **3b** radicals. (The optimized structures, barriers (kcal/mol) Bold: (U)B3LYP/cc-pVTZ; normal: (U)M06-2X/cc-pVTZ and italics: (U)CCSD(T)/cc-pVTZ//(U)B3LYP/cc-pVTZ level of theory). The spin density at the radical centers are indicated based on (U)B3LYP/cc-pVTZ level of theory listed in **Section 1A** in Appendix.

An alternative decomposition channel in all the isomeric radicals **1b**, **2b**, and **3b** was observed through the C4-C5 bond cleavage having barriers of 69.7, 65.5, and 70.0 kcal/mol, respectively. Similar to the previous cases, all of the radical intermediates **17**, **28**, and **34** can further undergo fragmentation either by C-C bond or C-H bond cleavages. Indeed, those bonds are located at the alternate position relative to the new radical center having more localized spin density. Both **17** and **28** undergo further fragmentation with the release of acetylene as the low barrier channels among the two possibilities, whereas **34** exhibited this as the higher energy channel by 22.5 kcal/mol. Furthermore, the C-H bond cleavage in **17** led to the formation of (**Z**)**-7**. Meanwhile, the C-H bond cleavage in **18** (formed through the fragmentation of acetylene from **17**) led to the formation of cyanoacetylene **11** as the end product. The radical intermediate **28** formed by the decomposition of pyridyl-*N*-oxide radical isomer **2b** through a C-C bond cleavage. This further led to the (**Z**)**-22** by C-H bond breaking, which is also one of the end products in the decomposition of **2a**. Apart from this, an alternative mode of cleavage in the intermediate **28** led to the acetylene **5** and a radical **29** (having a molecular formula C_3H_2NO).

Thus, all three 3-dehydro analogous radicals **1b**, **2b**, and **3b** undergo decomposition through the C4-C5 bond cleavage pathways. However, the other channel through the C2-N1 bond cleavage is found to be the kinetically favored channel. Indeed, the spin density of the radicals **1b** and **2b** corroborates very well with the barriers in the low energy pathways. This confirms the localization of higher spin density favors the lower energy pathway and *vice-versa*.

3.2.3.3 Dissociation pathways in 4-pyridyl 1c, 4-pyridyl-*N*-oxide 2c and 4-pyridinyl 3c radicals

Due to symmetry, the radical analogs, 4-pyridyl **1c** and 4-pyridyl-*N*-oxide **2c**, and 4-pyridinyl **3c** radicals undergo unimolecular decomposition only through the C2-C3 bond cleavage. The C2-C3 bond scission in the radical analogs **1c**, **2c**, and **3c** exhibited estimated barriers of 57.6, 70.1, and 70.4 kcal/mol, respectively. (**Figure 3.5**) Such a bond breaking leads to the ring-opening intermediates directly in the radicals **1c** and **2c**, whereas, the **3c** involves an additional ring contraction step. In the cases of **1c** and **2c**, the resulting intermediates **19** and **30** further lose HCN, and fulminic acid (HCNO), respectively. The corresponding fragmentations involve the barriers of 30.6 and 23.5 kcal/mol, respectively.
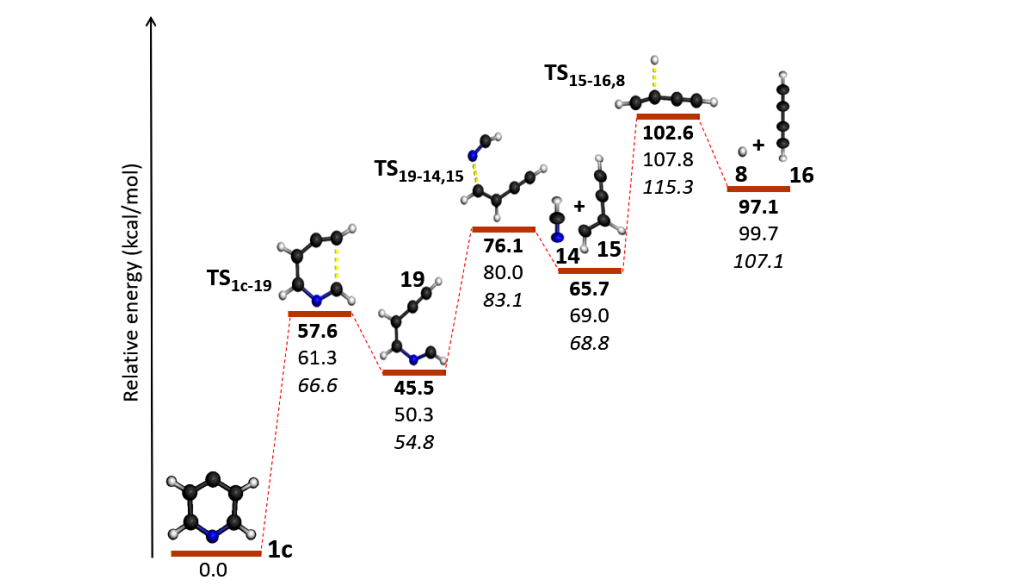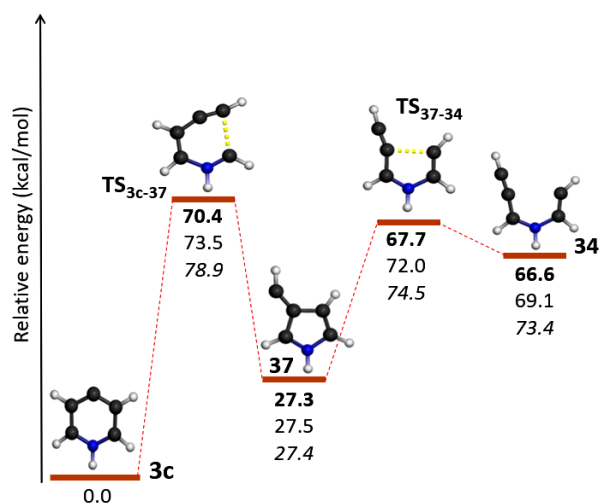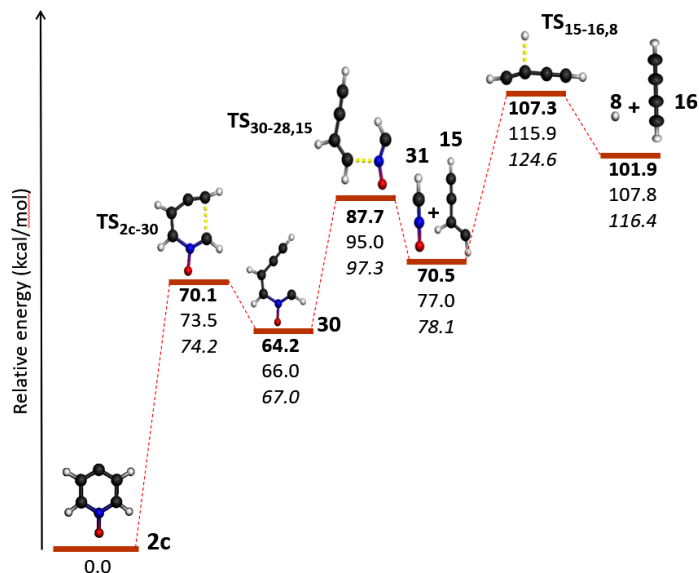
Figure 3.5 Unimolecular decomposition channels of 4-pyridyl **1c**, 4-pyridyl-*N*-oxide **2c**, and 4-pyridinyl **3c** radicals. (The optimized structures, barriers (kcal/mol) Bold: (U)B3LYP/cc-pVTZ; normal: (U)M06-2X/cc-pVTZ and italics: (U)CCSD(T)/cc-pVTZ//(U)B3LYP/cc-pVTZ level of theory). The spin density at the radical centers are indicated based on (U)B3LYP/cc-pVTZ level of theory listed in **Section 1A** in Appendix.

On the other hand, the ring contracted radical **37** undergoes ring opening to form a radical **34** with a barrier of 40.4 kcal/mol. The common product **15** in the decomposition

channels of **1c** and **2c**, loses hydrogen and forms the diacetylene as the end product with a barrier of 36.8 kcal/mol.

The inspection of the spin density once again provides the insights on the mode of ring-opening. Moreover, the interaction of the nitrogen lone pair with the radical center is equally critical in the observed trends associated with the barriers. Presumably, the through-bond interaction assists the ring-opening with lower barriers in **1c** compared to **2c** and **3c**. Indeed, a strong through-bond interaction in 4-pyridyl radical **1c** was inferred from the NBO analysis.[11] Once the through-bond interaction is prevented by the *N*-oxidation or protonation, the barrier increases in the cases of **2c** and **3c**.
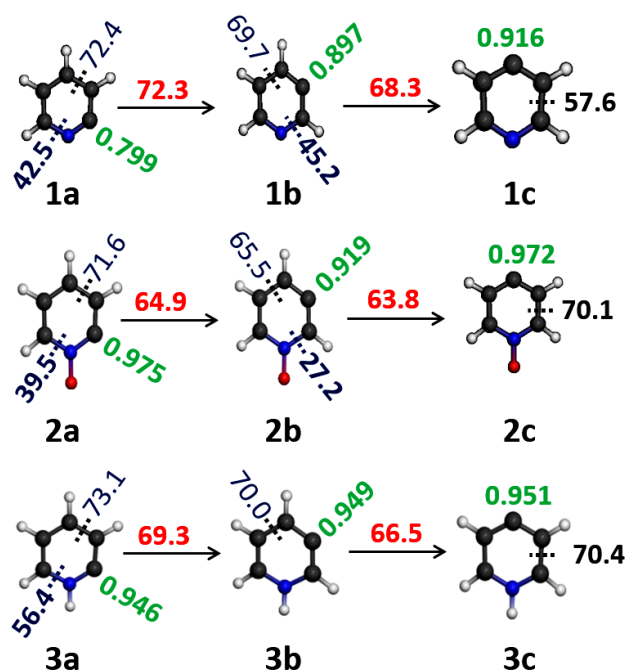
Figure 3.6 Summary of spin densities and barriers related to the first step in the unimolecular reactions (spin densities are indicated in green at the radical centers; The barriers corresponding to unimolecular ring-opening steps (bold–low energy channel) and isomerization reaction (red) are depicted.

The overall summary of the unimolecular decomposition channels pertaining the kinetic stability, and the importance of spin density in understanding reactivity patterns are depicted in **Figure 3.6**. In all the cases, the C-N bond cleavage is found to be a low energy pathway compared to the C-C bond breaking, which has both thermodynamic as well as kinetic control. Based on the lowest barriers at (U)B3LYP/cc-pVTZ in all possible unimolecular reactions, the kinetic stability order in pyridyl radicals is found to be **1a** < **1b** < **1c**, which got changed from that of the thermodynamic stability order, **1a** > **1c** > **1b**.(**Figure 3.6**) In a similar way, the pyridyl-*N*-oxide and pyridinyl radicals have the kinetic stability order as, **2b** < **2a** < **2c**, and **3a** < **3b** < **3c**, whereas their relative stability order was **2b** > **2c** > **2a** and **3c** > **3b** > **3a**, respectively. These trends are consistent with the changes in the spin density transfer.

3.2.4 Bimolecular reactions

An alternative reactivity perspective in understanding the kinetic stability of the target radicals is to investigate their reactions with small molecules. In this regard, the transition state barriers have been estimated for the reactions of pyridyl **1a-c**, pyridyl-*N*-oxide **2a-c**, and pyridinyl **3a-c** radical isomers with selected small molecules H_2, CO, CO_2, CH_4, H_2O, and CH_3OH. (**Figure 3.7**, **Section 3A** and **Table A3.1** in Appendix) These small molecules have been chosen in such a way that the bimolecular reactions can be diverse. Differences such as, the type of reaction viz, radical addition, H-abstraction, loss of H-atom, etc., and also the site of reaction have been explored. Likewise, in the unimolecular reactions, our primary intention was to understand the bimolecular reactivity through spin density as well as their changes at the transition state (relative to the reactant radical). Apart from that, we attempted

at predicting the role of the heteroatom in the bimolecular reactivity. In this regard, a comparison for all the bimolecular reactions was made with respect to phenyl radical. All such studies have been carried out at different levels of theory. The barriers for these reactions were ranging between −4.5 and 35.4 kcal/mol at (U)B3LYP/cc-pVTZ level of theory. Interestingly, molecules such as CO and CH_3OH resulted in exothermic and barrierless reactions.

Sander and coworkers have studied the interactions in phenyl radical-water and the formation of benzene and hydroxyl radical under low temperature matrix isolation and photochemical conditions.[24,25] However, thermal reactivity of phenyl radical with water is unknown. Interestingly, reactions of radical with water molecule opened up two possibilities, namely, (a) formation of hydroxyl radical, and (b) formation of hydrogen atom (radical). The formation of hydroxyl radicals was found to be kinetically much more favored than the latter.

(a)

(b)

(c)
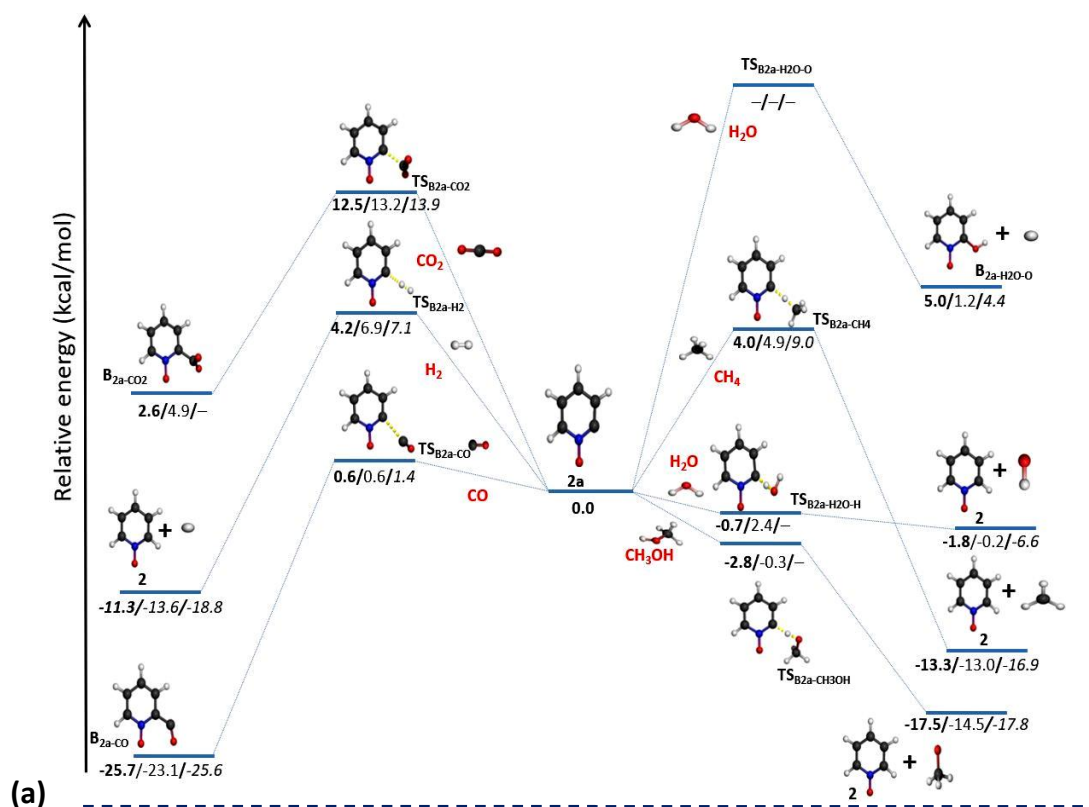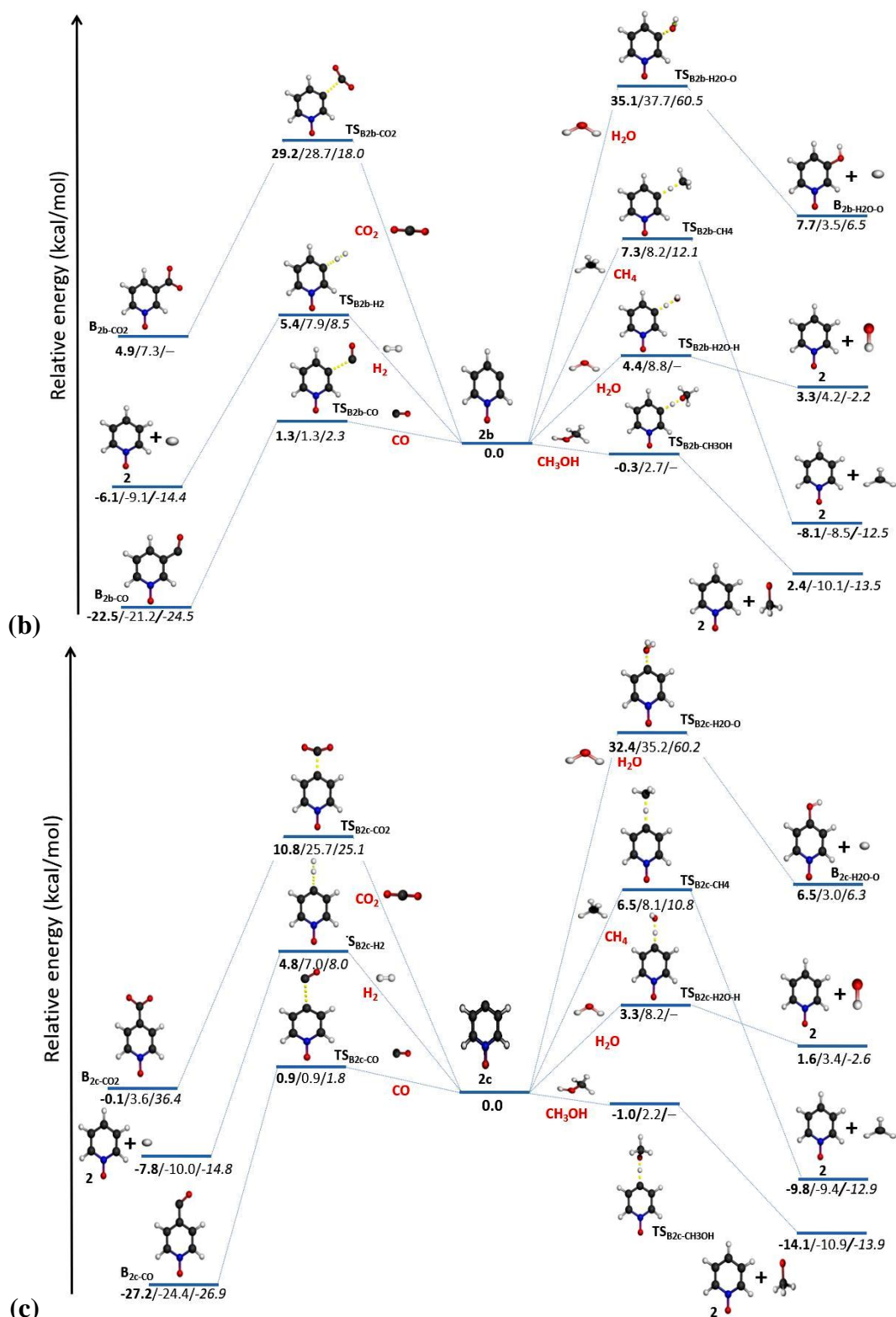
Figure 3.7 Bimolecular reactions of pyridyl-*N*-oxide radical isomers (a) **2a**; (b) **2b** and (c) **2c** with small molecules (CO, H₂, CO₂, H₂O, CH₄, and CH₃OH). (For water, both H-atom

abstraction, as well as OH abstraction channels by the radical isomers, have been indicated separately; The energy values (in kcal/mol) are indicated in Bold – (U)B3LYP/cc-pVTZ; Normal font – (U)M06-2X/cc-pVTZ and italics – (U)CCSD(T)/cc-pVTZ//(U)B3LYP/cc-pVTZ). At few places the energies are missing as the structures failed to optimize even after several attempts. (The corresponding bimolecular reactions of pyridyl **1a-c**, and pyridinyl **3a-c** radical isomers are given in **Section 3A** in the Appendix).

The activation barrier for the former was less than 10 kcal/mol, whereas the latter resulted in the highest activation barriers (16.9–35.4 kcal/mol) among all the bimolecular reactions explored in the current investigation. The products formed by both possibilities are endothermic.The bimolecular reactions of the target radicals with molecules like H_2, CH_4, and CO_2 also exhibited low kinetic energy barriers. The reactions were exothermic in the cases of H_2 and CH_4, while it turned out to be endothermic for CO_2. Due to lower spin density distribution, the pyridyl radicals **1a-c** were expected to have the maximum barriers. Since spin densities got localized at the radical center upon protonation or *N*-oxide formation in pyridyl radicals, higher reactivity (that is lower activation barrier) is expected for pyridyl-*N*-oxide **2a-c** and pyridinyl **3a-c** radicals as compared to pyridyl **1a-c** radical isomers. Through our reactivity studies, the expected trend fits very well for molecules such as CO, CH_3OH, H_2, CH_4, and H_2O (OH abstraction) (**Figure 3.8**). However, a marginal discrepancy was observed in the case of CO_2 and H_2O (hydrogen abstraction).
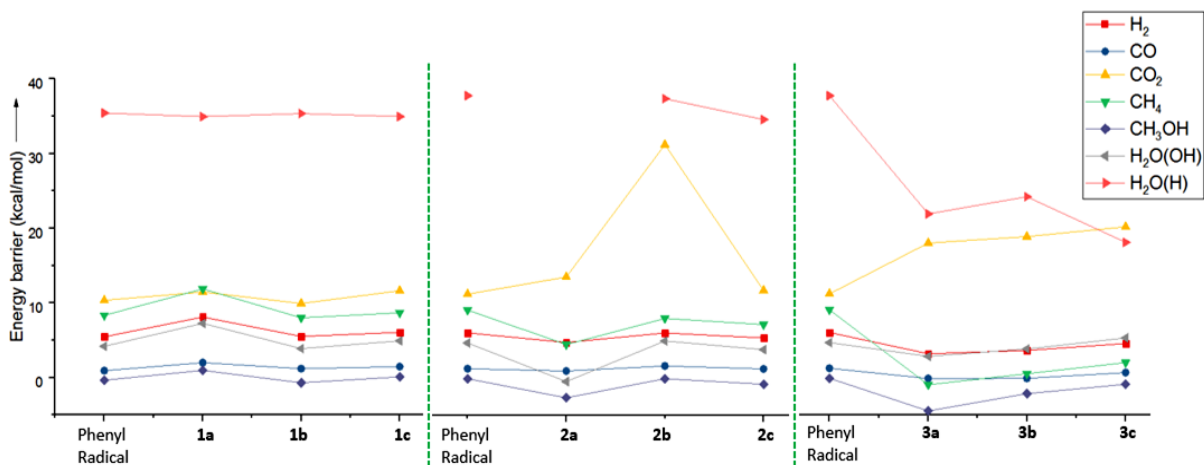
Figure 3.8 Overall bimolecular reactivity pattern of pyridyl (**1a-1c**), pyridyl-*N*-oxide (**2a-2c**), and pyridinyl (**3a-3c**) radical isomers with small molecules at (U)B3LYP/cc-pVTZ level of theory.

Alternatively, the bimolecular reactivity pattern can also be explained in terms of direct consequence of lone pair-radical interactions in the radical isomers. As a consequence of such through space and through-bond orbital interactions, the radical character is delocalized in pyridyl radicals **1a-c**, and so hinders the reactivity. Since the *N*-oxidation in **2a-c** and protonation in **3a-c** cut off those interactions, the reactivity increases, otherwise the barrier decreases. Interestingly, pyridinyl radical isomers **3a-c** and a phenyl radical have a comparable spin density at the radical centers. Despite this situation, a remarkable difference in their reactivity pattern has been observed, which might primarily arise due to the delocalized positive charge over the ring. However, the inspection of spin density at the radical centers corresponding to each transition state revealed a very interesting perspective. The activation barriers corresponding to these bimolecular reactions were found to be inversely proportional to the spin densities at the transition states. (**Figure 3.9**) Such correlations between the activation barrier and the spin densities corresponding to the transition state at the reaction center exhibited consistency at different levels of theory. The

complete data have been tabulated (**Table A3.1** in the Appendix). Except for pyridinyl radicals **3a-c** (having charge delocalization), the plots on the activation barrier against the spin density for bimolecular reaction with each of the individual smaller molecules exhibited a very good correlation for pyridyl **1a-c** and pyridyl-*N*-oxide **2a-c** radicals.
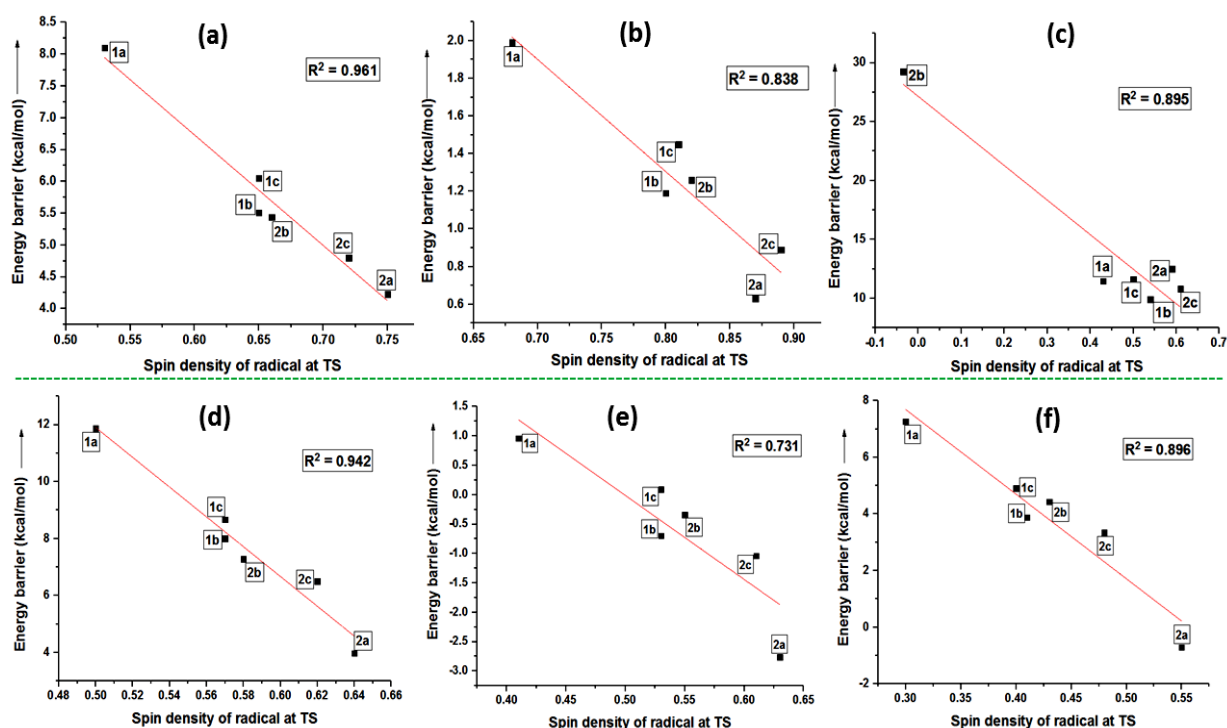
Figure 3.9 Overall bimolecular reactivity pattern of pyridyl (**1a-1c**), and pyridyl-*N*-oxide (**2a-2c**) radicals with small molecules at (U)B3LYP/cc-pVTZ level of theory: (a) with H_2; (b) with CO; (c) CO_2; (d) with CH_4; (e) CH_3OH; (f) H_2O (OH).

3.3 Photochemical reactions and Matrix Isolation (MI) experiments

Generation of isomeric pyridyl radicals from its corresponding iodo precursors using flash vacuum pyrolysis have been reported by Sander and coworkers.[17] Pyridyl radicals generated in argon matrix were characterized by the aid of infrared spectroscopy. Moreover, Kasai and McLeod generated ESR spectra of 2-, 3-, and 4-pyridyl radicals in argon matrices by photoelectron transfer process and further carried out the photolysis of these radicals.[26] So

far, there are no such reports based on the experimental investigation of pyridyl-*N*-oxide radicals under the matrix isolation conditions. In this regard, we wanted to explore these interesting radical species, and further understanding the role of N-O moiety in the reactivity channels under photochemical conditions. In principle, iodo precursors are well known for their photochemistry. Therefore, the matrix isolation experiments including their generation, characterization and their photochemistry using appropriate iodo precursors have been carried out.[17,27] Thus, attempts have been made towards the experimental characterization of 2- and 3-dehydropyridine-*N*-oxide radicals using matrix isolation (MI) technique assisted with infrared spectroscopy and computations. The insights that we obtained in these studies are described in the proceeding sections of this chapter.

3.4 Matrix isolation IR spectroscopic studies

3.4.1 Deposition of 3-iodopyridine-*N*-oxide

The precursor (3-iodopyridine-*N*-oxide) molecule was heated at 155 $^{\text{O}}$C for 90 minutes duration and was deposited with large excess of nitrogen gas at 4 K. The spectral features were compared with the calculated spectra of the precursor molecule at B3LYP/DGTZVP level of theory. The most intense signal in the deposited spectra appeared at 1007.0 cm^{-1}. However, computationally we observed the most intense peak at 1348.0 cm^{-1} corresponding to N-O stretching with C-H in plane bending. This signal has been tentatively assigned to a pair of experimentally observed signals at 1302.0 and 1271.0 cm^{-1}. Presumably, the splitting arises due to the Fermi resonance of the overtone of the normal mode (v_{10}) with that of N-O stretching (v_{22}). On the other hand, the deposition spectrum was found to be in good

agreement with the calculated spectrum within the limits of experimental shifts as given in **Figure 3.10**

Figure 3.10 (a) Deposition spectrum of 3-iodopyridine-*N*-oxide (N$_2$, 4 K, 90 min, 155 $^\circ$C); **(b)** Calculated spectrum of 3-iodopyridine-*N*-oxide (B3LYP/DGTZVP, unscaled).

3.4.2 Photochemistry of the deposited 3-iodopyridine-*N*-oxide

The deposited precursor was irradiated with xenon lamp (λ=283 nm) at different time intervals (i.e 0.5, 1.5, 3.5, 7.5 and 15.5 min). The purpose of irradiation at short time intervals was to witness the kinetic growth of new signals and the bleaching of signals corresponding to the precursor. The changes in the signals after irradiation is shown in **Figure 3.11**
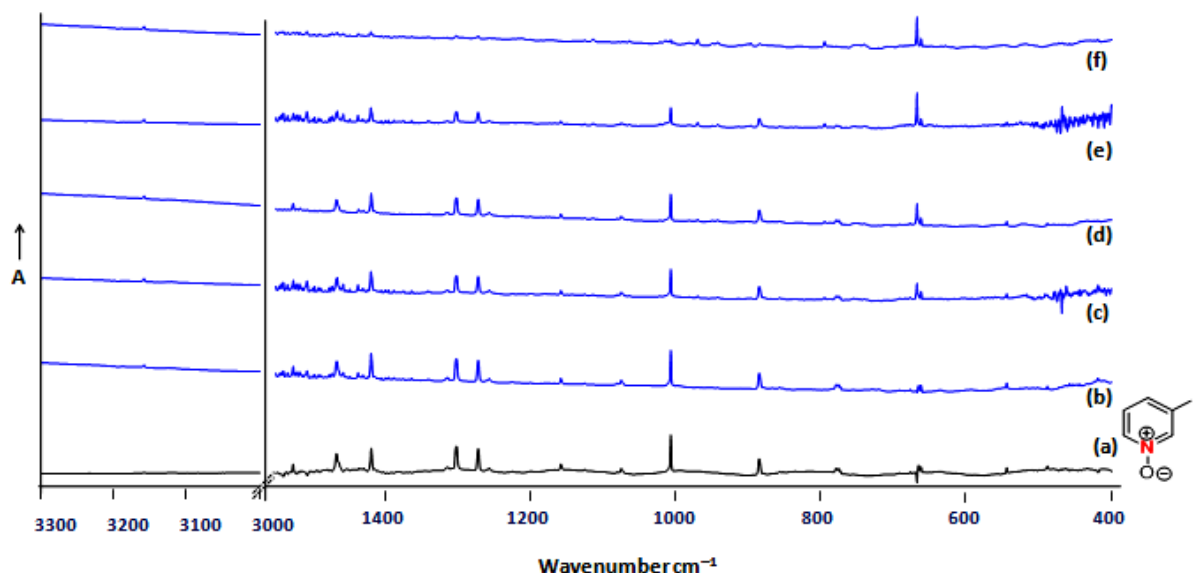
Figure 3.11 (a) Deposited spectra of 3-iodopyridine-*N*-oxide (N$_2$, 4 K, 90 min, 155 ^{O}C); **(b-f)** Spectra obtained on irradiation with 283 nm at different time intervals (i.e 0.5, 1.5, 3.5, 7.5 and 15.5 min).

On irradiation for 15.5 minutes, the precursor signals got almost bleached and new peaks appeared. The photochemical cleavage of either C-I or N-O bond are the two potential pathways on photolysis as depicted in **scheme 3.2**.
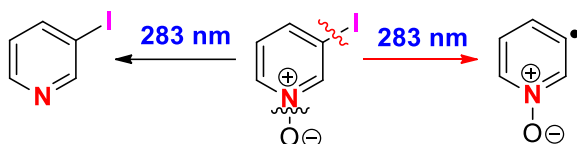
Scheme 3.2 Potential pathways on irradiation with 283 nm light.

Furthermore, the ring opening channels of 3-dehydropyridine-*N*-oxide were also considered. The new peaks were compared with the calculated spectra of 3-dehydropyridine-*N*-oxide and 3-iodopyridine at (U)B3LYP/cc-pVTZ level and B3LYP/DGTZVP of theory as shown in **Figure 3.12.** The signals appearing downwards in the difference spectra corresponds to the precursor whereas those appearing upwards could be due to ring opening channel, 3-

dehydropyridine-*N*-oxide or 3-iodopyridine. So far, a few new signals could be tentatively assigned to 3-dehydropyridine-*N*-oxide. The other signals are smaller in intensity; thus the segregation based on the growth rate was difficult to follow. Also, there is no evidence for assigning the ring-opening/fragmented products since none of them have any characteristic IR frequency like acetylenic C-H stretch which should be prominent in the case of ring-opening.
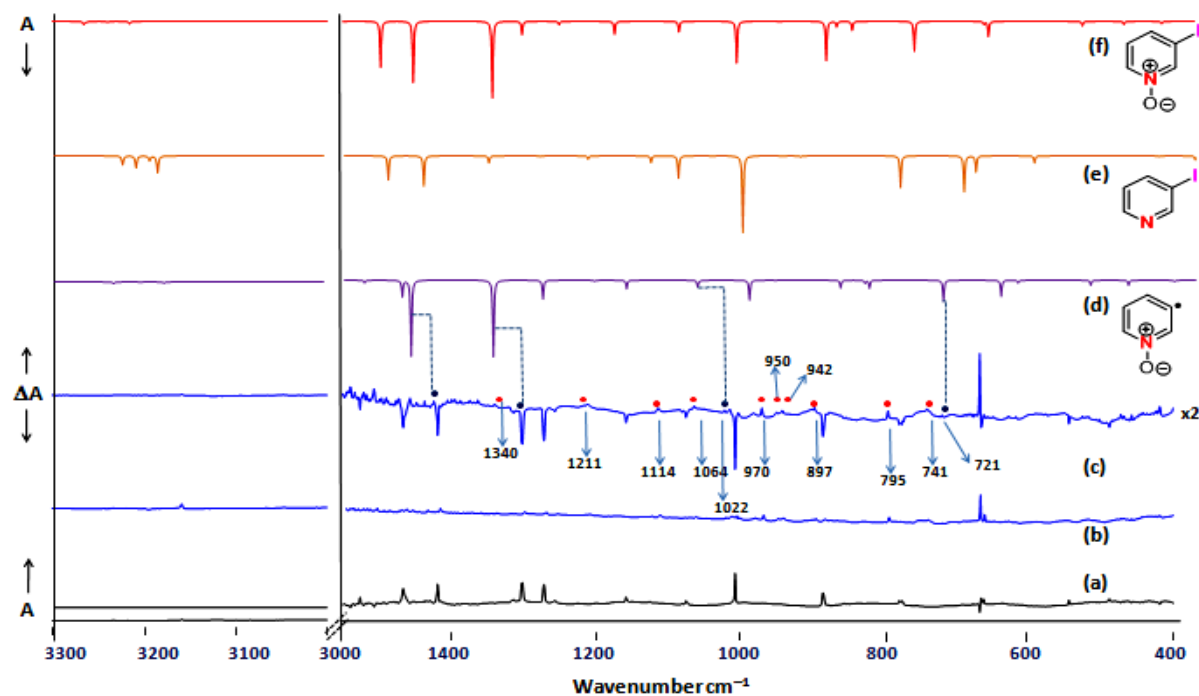
Figure 3.12 (a) Deposited spectra of 3-iodopyridine-*N*-oxide (N₂, 4 K, 90 min, 155 °C); **(b)** Spectra obtained on irradiation with 283 nm; **(c)** Difference spectrum after irradiation at 283 nm {(b)-(a)}; **(d)** Calculated spectra of 3-dehydropyridine-*N*-oxide at (U)B3LYP/cc-pVTZ, unscaled; **(e, f)** Calculated spectra of 3-iodopyridine and 3-iodopyridine-*N*-oxide at B3LYP/DGTZVP, unscaled.

The matrix containing the photoproducts was further irradiated with 345 nm for 20 minutes. On irradiation, we observed rising of the precursor signals accompanied by the bleaching of the some of the signals which were formed during irradiation at 283 nm as shown in **Figure**

3.13. In this process, iodine radical recombines with 3-dehydropyridine-*N*-oxide which leads to the formation of the precursor as represented in **scheme 3.3**.
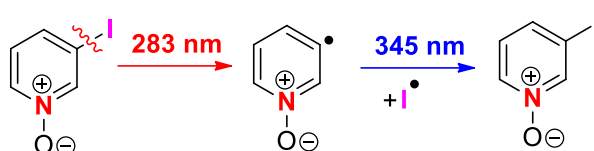
Scheme 3.3 Regeneration of the precursor molecule on irradiation with 345 nm light.

However, due to the lower signal intensity of the photoproducts at 283 nm, the bleaching of the signals was very small. On the basis of this study, the only evidence of 3-dehydropyridine-*N*-oxide is the regeneration of the precursor molecule at 345 nm. However, the smaller intensity new signals did not allow us to unambiguously assign the signals to the desired radicals. Further the formation of 3-iodopyridine by the loss of oxygen at 283 nm, followed by the recombination at 345 nm cannot be ruled out. Furthermore, there is no direct mechanism available for the photochemical recombination of radical pair although such process is well-known in the literature.[28,29] Possibly the excited radical on relaxation gains excess energy that may lead to a localized annealing effect. However, there is no other evidence for such mechanism. The relative yields on getting the precursor through traditional annealing, on the other hand, is relatively less. Due to the poor signal-to-noise ratio and small changes in the signals due to the newly formed photoproducts, the annealing experiments were unsuccessful in this case.
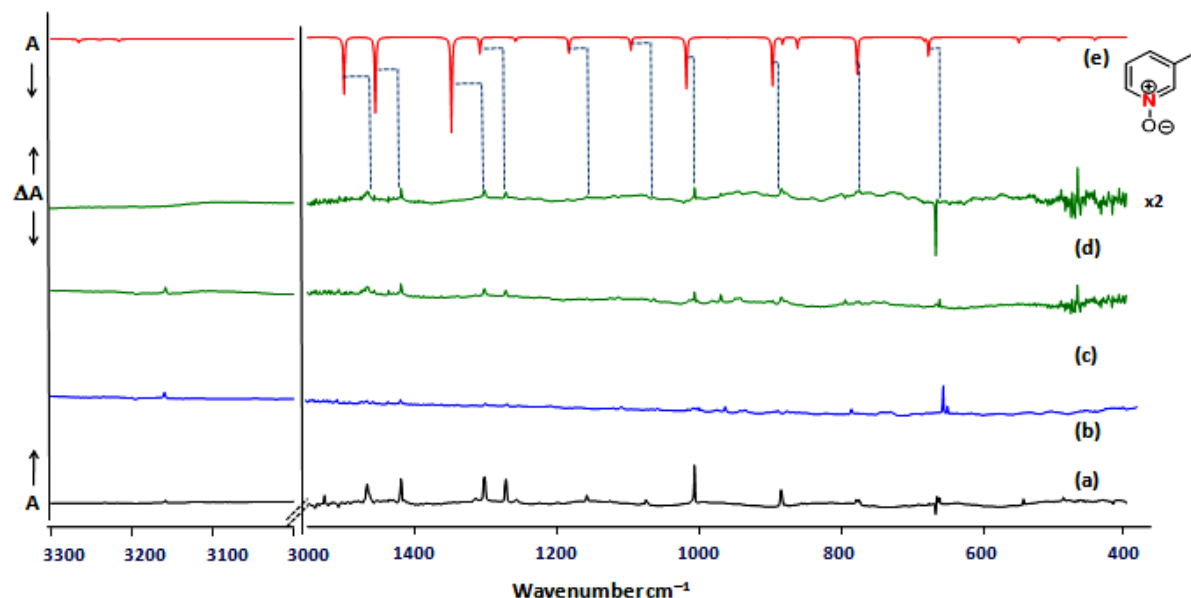
Figure 3.13 (a) Deposited spectra of 3-iodopyridine-*N*-oxide (N$_2$, 4K, 90 min, 155 $^{\circ}$C); **(b)** Spectra obtained on irradiation with 283 nm; **(c)** Spectra obtained on irradiation with 345 nm for 60 min duration; (d) Difference spectrum after irradiation at 345 nm {(c)-(b)}; The signals pointing upwards are due to the formation of the precursor, whereas the small changes in the downward direction are due to the photoproducts formed after irradiation at 283 nm; **(e)** Calculated spectrum of 3-iodopyridine-*N*-oxide (B3LYP/DGTZVP, unscaled).

3.4.3 Deposition of 2-iodopyridine-*N*-oxide

The precursor (2-iodopyridine-*N*-oxide) molecule was heated at 180 $^{\circ}$C for 4 hours duration and was deposited with large excess of argon gas at 4 K. The spectral features were compared with the calculated spectra of the precursor molecule at B3LYP/DGTZVP level of theory. The most intense signal in the deposited spectrum appeared at 1290.0 cm^{-1}. The deposited spectra was found to be in good agreement with the calculated spectrum within the limits of experimental shifts as given in **Figure 3.14**
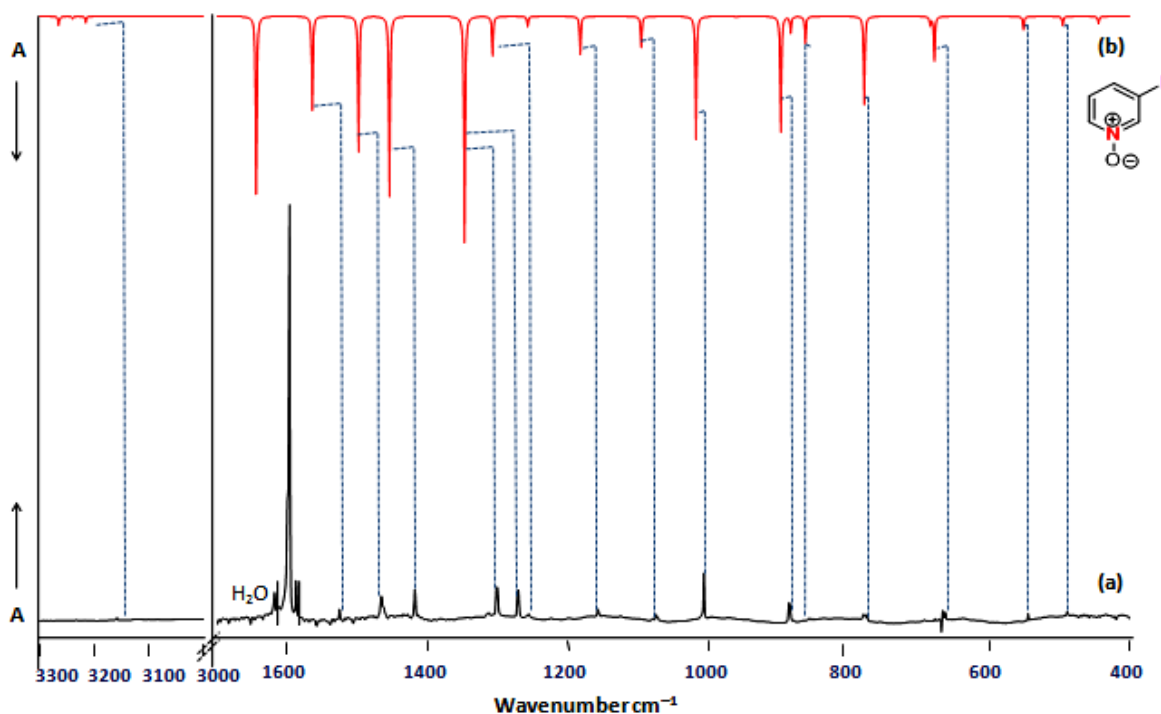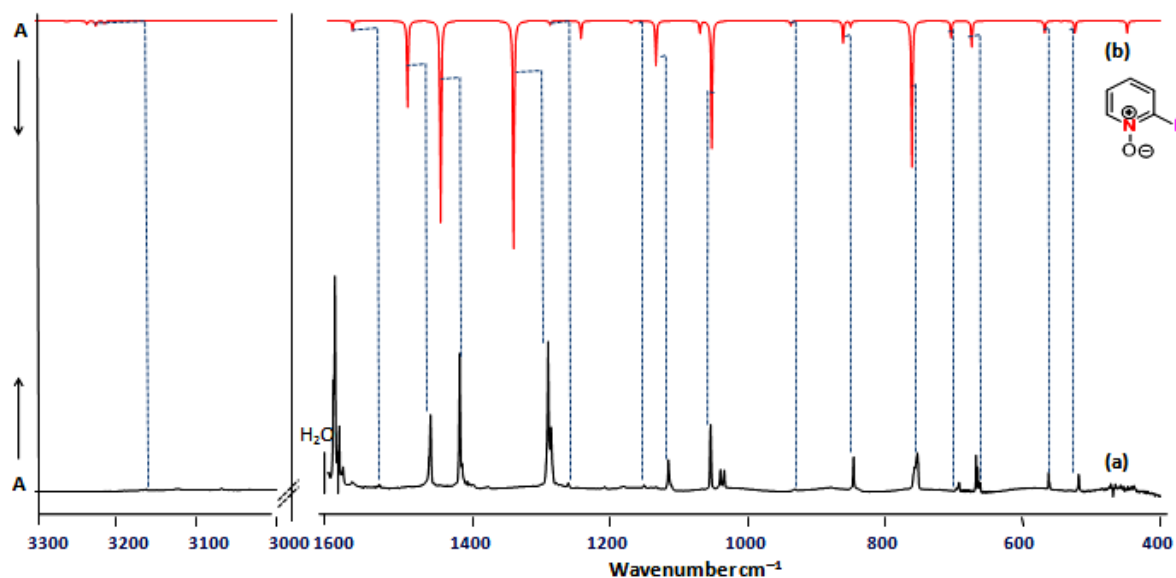
Figure 3.14 (a) Deposition spectrum of 2-iodopyridine-*N*-oxide (Ar, 4 K, 4 hr, 180 °C); **(b)** Calculated spectrum of 2-iodopyridine-*N*-oxide (B3LYP/DGTZVP, unscaled).

3.4.4 Photochemistry of the deposited 2-iodopyridine-*N*-oxide

The deposited precursor was irradiated with low pressure mercury lamp (λ=254 nm) at different time intervals (i.e. 5, 15, 45, 105 and 165 min). Homolysis of C-I bond is one of the potential pathway on photolysis. The purpose of irradiation at short time intervals was to witness the radical formation, kinetic growth of new signals and the bleaching of signals corresponding to the precursor. The changes in the signals after irradiation is shown in **Figure 3.15**.

At each time interval, we looked for the formation of 2-dehydropyridine-*N*-oxide. On photolysis for 165 minutes, the precursor signals got completely bleached and a few new signals were obtained. The new signals obtained were compared with the computed spectra of 2-dehydropyridine-*N*-oxide at (U)B3LYP/cc-pVTZ level of theory but none of them matches with that of 2-dehydropyridine-*N*-oxide radical.
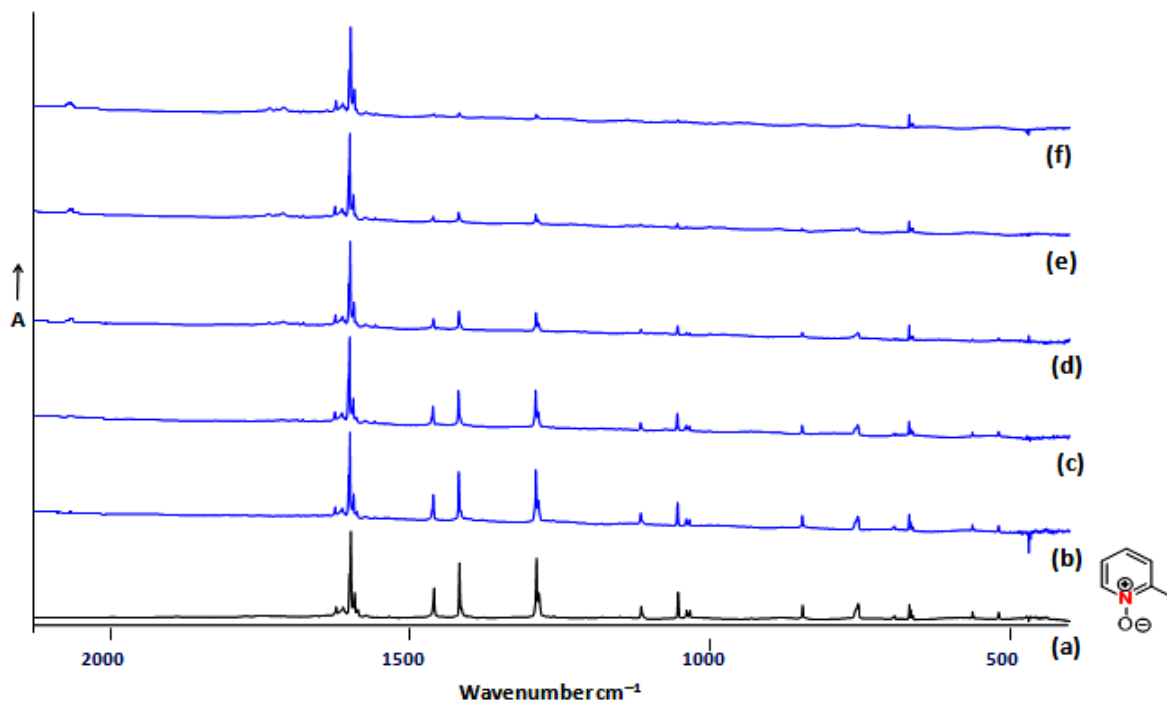
Figure 3.15 (a) Deposition spectrum of 2-iodopyridine-*N*-oxide (Ar, 4 K, 4 hr, 180 °C); **(b-f)** Spectra obtained on irradiation with 254 nm at different time intervals (i.e. 5, 15, 45, 105 and 165 min).

As per the electronic and reactivity studies, 2-dehydropyridine-*N*-oxide was found to be the less stable isomer among the series, however, it was predicted to be the most reactive. In this regard, the reactive nature of 2-dehydropyridine-*N*-oxide is depicted in the possible photochemical channels of 2-iodopyridine-*N*-oxide as represented in **Figure 3.16**
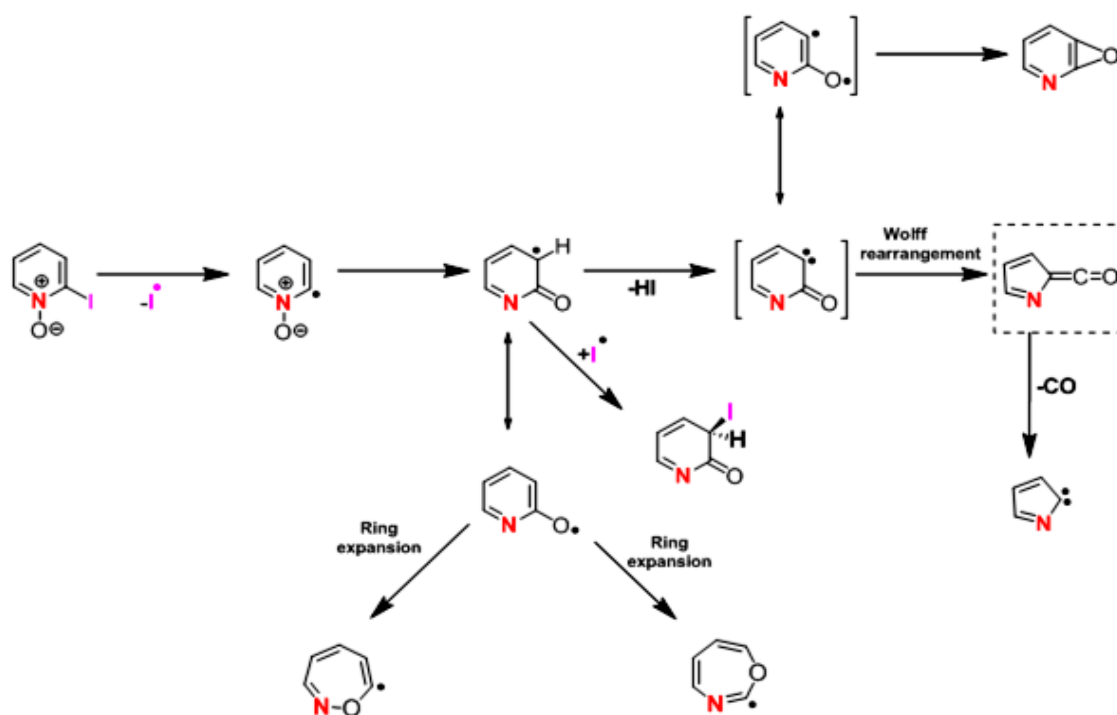
Figure 3.16 Possible photochemical channels for 2-iodopyridine-*N*-oxide.

On irradiation with 254 nm, a prominent signal with split band was observed around 2128.0 and 2134.0 cm^{-1}, and also a peak at 2143.0 cm^{-1}. The signal at 2143.0 cm^{-1} has been tentatively assigned to CO. However, the blue shift from the free CO in argon matrix (2138.5 cm^{-1}) is possibly due to a complexation with the other species within the matrix cage.[30] Interestingly, the loss of CO indicates that a carbene might also be formed, however the intensity might be too weak to detect. On the other hand, the irradiation at 365 nm led to the enhancement in the signal at 2134.0 cm^{-1} which could be a ketene. The formation of the ketene (i.e. 2H-pyrrol-2- ylidene methanone) was further confirmed by calculated spectra at B3LYP/cc-pVTZ level of theory as shown in **Figure 3.17**. Apart from this, spectral features at 1735.0 and 1711.0 cm^{-1} were difficult to assign as per the possible products that could be formed on the basis of photochemical channels as shown in **Figure 3.16.**
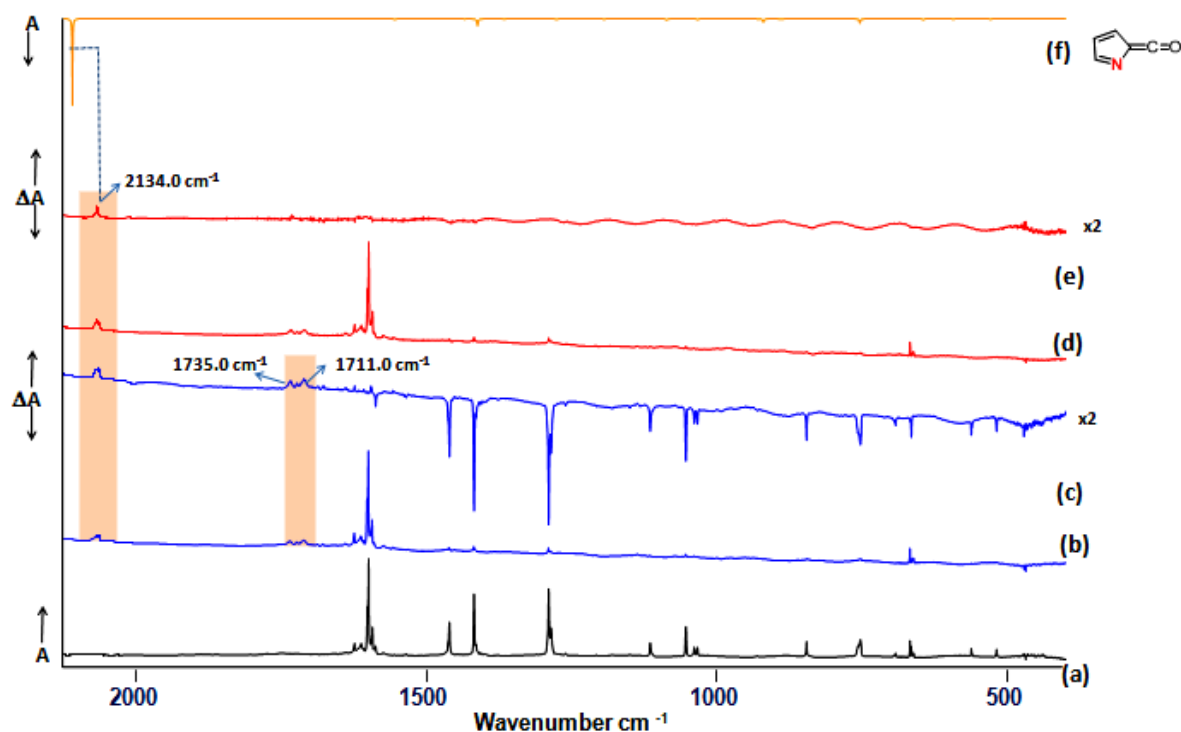
Figure 3.17 (a) Deposition spectrum of 2-iodopyridine-*N*-oxide (Ar, 4K, 4 hr, 180 °C); **(b)** Spectra obtained on irradiation with 254 nm for 165 minutes; **(c)** Difference spectrum after irradiation at 254 nm {(b)-(a)}; **(d)** Spectra obtained on irradiation with 365 nm for 60 minutes; **(e)** Difference spectrum after irradiation at 365 nm {(d)-(b)}; **(f)** Calculated spectrum of (2H-pyrrol-2-ylidene) methanone at (B3LYP/cc-pVTZ, unscaled).

Based on this study, our attempts were not successful in characterization of 2-dehydropyridine-N-oxide radical, but we were able to identify the formation of ketene (i.e 2H-pyrrol-2- ylidene methanone) on photoirradiation.

3.5 CONCLUSIONS

A systematic computational investigation on the reactivity aspects of pyridyl **1a-c**, pyridyl-*N*-oxide **2a-c**, and pyridinyl **3a-c** radical isomers has been carried out. Both unimolecular channels and bimolecular reactions with small molecules have been explored.

Based on these studies, we have concluded the following:

(a) The first C-H BDEs for the formation of radical species (from their parent) follow the same trend as their respective spin densities. Exceptions are felt in the cases of pyridinyl radicals **3a-c**. Also, the increasing order of BDEs is in line with the decreasing order of their thermodynamic stability.

(b) The radicals with more localization of spin density distribution exhibit higher reactivity (lower barrier) for the isomerization through a 1, 2-H shift. Also, the difference in the spin density between the reactant (*meta* isomer) and the transition state involved in the isomerization channel correlates well with the barriers.

(c) The identification of radical center through the maximum spin density distribution, and the alternate bonds relative to the radical center can be useful in predicting possible reaction steps. Apart from the ring-opening, such predictions can also be extended to fragmentation steps. This general trend is observed in all the radicals except in the case of pyridyl-*N*-oxide radicals **2a-c**, presumably due to the role of the oxygen atom.

(d) For bimolecular reactions, the changes in the spin density during the reaction are a direct measure of the reactivity of the radicals. The only exception is pyridinyl radicals **3a-c**. Based on the bimolecular reaction studies, the kinetic stability of the three sets of isomeric radicals have an excellent agreement with the thermodynamic stability order of these radicals. However, a small discrepancy of this correlation was observed for the reactions of pyridinyl radical with CO_2, and H_2O in the hydrogen atom formation possibility.

(e) Based on the experimental observations under photochemical conditions, we were able to identify the formation of 3-dehydropyridine-*N*-oxide radical in nitrogen matrix at 4 K. Whereas, our attempts were not successful in the generation of 2-dehydropyridine-*N*-oxide

radical. However, we were able to characterize ketene (i.e. 2H-pyrrol-2-ylidene methanone) on photolysis.

Overall, we concluded that the spin density plays a significant role in predicting the reactivity pattern of radicals. The localization or spin density transfer in the transition states can be useful in explaining observed reactivity patterns, and the deviations in spin density vs reactivity can occur with the involvement of charge delocalization.

3.6 REFERENCES

1. McNaught, A. D.; Wilkinson, A. *IUPAC Compendium of Chemical Terminology;* Blackwell Scientific Publications; Oxford: 1997.
2. Lund, A.; Shiotani, M.; Shimada, S. *Principles and Applications of ESR Spectroscopy*; Springer: 2011.
3. Gatti, C.; Orlando, A. M.; Presti, L. L. Insights on Spin Polarization through the Spin Density Source Function. *Chem. Sci.* **2015**, *6*, 3845–3852.
4. Makarova, T.; Palacio, F. *Carbon-based magnetism : an overview of the magnetism of metal free carbon-based compounds and materials*; Elsevier: 2014.
5. Munzarova, M. L.; Engels, B.; Rassolov, V. A.; Chipman, D. M.; Patchkovskii, S. S., Lushington, G.; Neese, G. H. *EPR Parameters, Methodological Aspects. In Calculation of NMR and EPR Parameters. Theory and Applications*; 1st ed.; Kaupp, M.; Buhl, M.; Malkin V. G. Eds.; Wiley-VCH: Weinheim, Germany, 2004, 461–564.
6. McConnell, H. M. Indirect Hyperfine Interactions in the Paramagnetic Resonance Spectra of Aromatic Free Radicals. *J. Chem. Phys.* **1956**, *24*, 764-766.
7. Ressouche, E.; Schweizer, J. Ab Initio Calculations Versus Polarized Neutron Diffraction for the Spin Density of Free Radicals. *Monatshefte fur Chemie.* **2003***, 134(2),* 235–253.
8. Boguslawski, K.; Marti, K. H.; Legeza, O.; Reiher, M. Accurate ab Initio Spin Densities. *J. Chem. Theory Comput.* **2012**, *8(6),*1970–1982.
9. Tang, B.; Zhao, J.; Xu, J. F.; Zhang, X. Tuning the stability of organic radicals: From covalent approaches to non-covalent approaches. *Chem. Sci.* **2020**, *11*, 1192–1204.

10. Hicks, R. G. *Stable Radicals: Fundamentals and Applied Aspects of Odd-Electron Compounds*; John Wiley & Sons, Ltd: Wiltshire, U.K., 2010.

11. Sah, C.; Jacob, L.; Saraswat, M.; Venkataramani, S. Does a Nitrogen Lone Pair Lead to Two Centered−Three Electron (2c−3e) Interactions in Pyridyl Radical Isomers? *J. Phys. Chem. A*. **2017**, *121*, 3781−3791.

12. Lu, D.; Wu, C.; Li, P. 3-Center-5-Electron Boryl Radicals with $\sigma^0\pi^1$ Ground State Electronic Structure. *Org. Lett*. **2014**, *16*, 1486−1489.

13. Hioe, J.; Sakic, D.; Vrcek, V.; Zipse, H. The Stability of Nitrogen-Centered Radicals. *Org. Biomol. Chem*. **2015**, *13*, 157−169.

14. Kiefer, J. H.; Zhang, Q.; Kern, R. D.; Yao, J.; Jursic, B. Pyrolyses of Aromatic Azines: Pyrazine, Pyrimidine, and Pyridine. *J. Phys. Chem. A*. **1997**, *101*, 7061−7073.

15. Turecek, F.; Wolken, J. K.; Sadilek, M. Distinction of isomeric pyridyl cations and radicals by neutralization-reionization mass spectrometry, abinitio and density functional theory calculations. *Eur. Mass Spectrom*. **1998**, *4*, 321–332.

16. Holzmeier, F.; Wagner, I.; Fischer, I.; Bodi, A.; Hemberger, P. Pyrolysis of 3-Methoxypyridine. Detection and Characterization of the Pyrrolyl Radical by Threshold Photoelectron Spectroscopy. *J. Phys. Chem. A*. **2016**, *120*, 4702–4710.

17. Korte, A.; Mardyukov, A.; Sander, W. Pyridyl- and Pyridylperoxy Radicals – A Matrix Isolation Study. *Aust. J. Chem*. **2014**, *67*, 1324–1329.

18. Lucas, M.; Minor, J.; Zhang, J.; Brazier, C. Ultraviolet Photodissociation Dynamics of the *o*-Pyridyl Radical. *J. Phys. Chem. A*. **2013**, *117*, 12138–12145.

19. Mackie, J. C.; Colket, M. B., III; Nelson, P. F. Shock Tube Pyrolysis of Pyridine. *J. Phys. Chem*. **1990**, *94*, 4099−4106.

20. Hore, N. R.; Russell, D. K. Radical pathways in the thermal decomposition of pyridine and diazines: a laser pyrolysis and semiempirical study. *J. Chem. Soc., Perkin Trans. 2* **1998**, *2*, 269−276.

21. Liu, R.; Huang, T. T. S.; Tittle, J.; Xia, D. A Theoretical Investigation of the Decomposition Mechanism of Pyridyl Radicals. *J. Phys. Chem. A*. **2000**, *104*, 8368–8374.

22. Cheng, X. L.; Zhao, Y. Y.; Zhou, Z. Y. Theoretical Studies on p-Pyridyl Radical Decomposition Reactions. *J. Mol. Struct.: THEOCHEM*. **2004**, *678*, 17−21.

23. Cheng, X. L. Reaction Mechanism of Decomposition System of m-Pyridyl Radical: A Theoretical Investigation. *J. Mol. Struct.:THEOCHEM*. **2005**, *731*, 89−99.

24. Mardyukov, A.; Crespo-Otero, R.; Sanchez-Garcia, E.; Sander, W. Photochemistry and Reactivity of the Phenyl Radical-Water System: A Matrix Isolation and Computational Study. *Chem. Eur. J.* **2010**, *16*, 8679–8689.

25. Mardyukov, A.; Sanchez-Garcia, E.; Crespo-Otero, R.; Sander, W. Interaction and reaction of the phenyl radical with water: a source of OH radicals. *Angew. Chem. Int. Ed.* **2009**, *48*, 4804–4807.

26. Kasai, P. H.; McLeod, D., Jr. Electron Spin Resonance Study of Heterocycles; Pyridyl Radicals. *J. Am. Chem. Soc.* **1972**, *94*, 720−727.

27. Haupa, K. A.; Chen, K.-P.; Li, Y.-K.; Lee, Y.-P. Infrared spectra of (*Z*)- and (*E*)-$C_2H_3C(CH_3)I$ radicals produced upon photodissociation of (*Z*)- and (*E*)-$(CH_2I)HCC(CH_3)I$ in solid para- hydrogen. *J. Phys. Chem. A.* **2020**, *124*, 5887−5895.

28. Butscher, T.; Duvernay, F.; Theule, P.; Danger, G.; Carissan, Y.; Hagebaum-Reignier, D.; Chiavassa, T. Formation mechanism of glycolaldehyde and ethylene glycol in astrophysical ices from $HCO^\bullet$ and $^\bullet CH_2OH$ recombination: an experimental study. *Monthly Notices of the Royal Astronomical Society*. **2015**, *453*, 1587–1596.

29. Butscher, T.; Duvernay, F.; Rimola, A.; Segado-Centellas, M.; Chiavassa, T. Radical recombination in interstellar ices, a not so simple mechanism. *Phys. Chem. Chem. Phys.* **2017**, *19*, 2857–2866.

30. Raducu, V.; Jasmin, D.; Dahoo, R.; Brosset, P.; Gauthier-Roy, B.; Abouaf-Marguin, L. The $CO:CO_2$ complex in argon matrices: Experimental evidence for two conformations with spontaneous interconversion. *J. Chem. Phys*. **1995**, *102*, 9235–9239.

Chapter 4

Competition Between Delocalization and Ring Strain in determining the stability pattern of Five-membered Heterocyclic Radicals.

4.1 INTRODUCTION

The stability and the transient character of radicals is often influenced by conjugation, spin delocalization and orbital interactions.[1-3] On these aspects, structural modification or tuning to obtain stable radicals is an strategy for making organic based molecular magnets.[4,5] Various approaches such as enhancing delocalization through resonance, and hindering the reactivity through steric bulkiness have been explored.[6,7] Alternatively, creating radicals at the heteroatoms and enhancing resonance stabilization have also been attempted.[8,9] Our previous investigations on six-membered heterocyclic radicals clarified that the nitrogen lone pair provides a stabilizing effect if it is coplanar to the radical electron.[10,11]

However, in the case of five-membered heterocyclic radicals with one heteroatom, the interactions between the radical electron and the lone pair will be lowered due to the involvement of the latter in the aromaticity. At this juncture; orbital interactions, resonance energy[12-15] and ring strain[16-18] are the decisive factors that needs to be considered. The sole purpose is to understand the interplay between delocalization (stabilizing effect) and ring strain (destabilizing effect) which dictates the overall stability order of the isomeric radicals. In this regard, we investigated the simplest five-membered dehydro-borole **1a–1c**, pyrrole **3a–3c**, furan **4b–4c**, phosphole **5a–5c**, and thiophene **6b–6c** radicals (**Scheme 4.1**). For

comparison, we have utilized the dehydroradicals of cyclopentadiene **2a–2c** as well. The outcomes of these studies are discussed in detail.
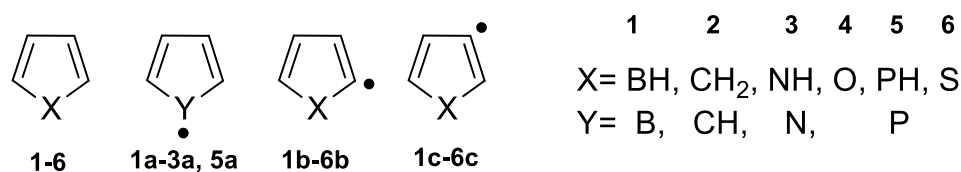
Scheme 4.1 Five Membered Hetero- and Carbocyclics, Borole **1**, Cyclopentadiene **2**, Pyrrole **3**, Furan **4**, Phosphole **5**, Thiophene **6** and Their Corresponding Dehydro Radical Isomers.

4.2 RESULTS AND DISCUSSION

4.2.1 Geometry

Computational studies of dehydro-borole **(1a-c)**, cyclopentadiene **(2a-c)**, pyrrole **(3a-c)**, furan **(4b-c)**, phosphole **(5a-c)** and thiophene **(6b-c)** have been carried out at different levels of theory (**Figure 4.1**). Key features like change in bond length, bond angle and planarity in radical isomers have been compared with their respective parent analogues. Parent compounds as well as majority of their radical analogues have been optimized to C_{2v} or C_s point group symmetries. The exceptions are **5b** and **5c**, which attained C_1 symmetry. All of the radical species are found to be spin doublets at their ground states. Structures **1a** and **5** were found to be saddle points at C_{2v} geometries and so optimized at C_s point group. The electronic and thermodynamic parameters of the parent and their respective radicals have also been provided. (**Table A4.1** in Appendix) Likewise, in our previous studies, we found out that the bond lengths adjacent to the radical centers got shortened, whereas the inter-nuclear distances alternate to the radical position got elongated relative to the parent.[10,11,19]

Similarly, bond angles at radical centers increased except in **3a** (*N*-centered radical), for which it got decreased, whereas in the case of **5a**, the bond angle was found to be nearly the same. Interestingly, the angle at heteroatom connecting two-carbon atoms $\angle$CXC (X=heteroatom) strongly depends on the position of the radical center. Among the various radicals, the *B*-centered and *N*-centered radicals exhibited the maximum angle change at the radical center, *viz* $+15.2°$ and $-5.1°$, respectively with respect to the parent as listed in **Table 4.1.** In the case of *C*-centered radical, it is less positive, whereas the *P*-centered radical showed almost no change. These changes are mainly a consequence of the heteroatom/carbon atom to adopt a geometry in such a way to satisfy Bent'rule. The expanded version of the rule states that the electronegativity and covalent radii is crucial for an atom to gain and impart s- or p-character to the bonds it form with the substituents.[20-21] For *B*- and *N*-centered radicals, the angle of deviation leads to the attainment of more s- and p-characters, respectively. Also, α-radicals exhibit a decrease in those bond angles, whereas they increase in the case of β-radicals as compared to $\angle$CXC of their respective parents. Presumably the change in the ring strain can be the reason for it. The geometrical parameters at both (U)B3LYP/cc-pVTZ and (U)M06-2X/cc-pVTZ levels of theory predict the similar trend.

Table 4.1 Deviation in Bond Angles (in degrees) for Radical Isomers as Compared to Their Respective Parent Analogue. The Values Indicated are at (U)B3LYP/cc-pVTZ Level of Theory.

Y= B, CH, N, P   X= BH, CH_2, NH, O, PH, S
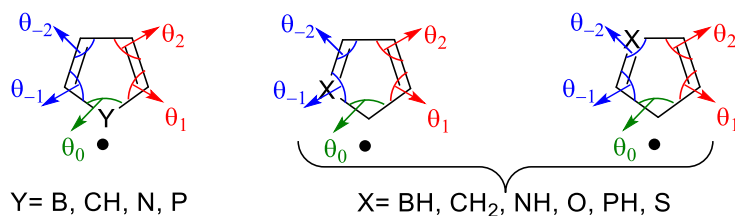
Compound	Atom -2 θ_{-2}		Atom -1 θ_{-1}		Radical Atom θ_0		Atom 1 θ_1		Atom 2 θ_2	
1a	C4	2.2	C5	-11.8	B1	15.2	C2	-11.8	C3	2.2
1b	C5	0.9	B1	-2.8	C2	4.4	C3	-3.5	C4	0.8
1c	B1	1.8	C2	-4.4	C3	5.7	C4	-2.9	C5	-0.2
2a	C4	-1.7	C5	-0.3	C1	3.9	C2	-0.4	C3	-1.6
2b	C5	0.4	C1	-2.5	C2	4.4	C3	-3.1	C4	0.9
2c	C1	0.7	C2	-3.3	C3	4.6	C4	-2.6	C5	0.7
3a	C4	-2.1	C5	4.7	N1	-5.1	C2	4.7	C3	-2.1
3b	C5	-0.1	N1	-1.9	C2	3.7	C3	-2.8	C4	1.1
3c	N1	0.3	C2	-2.5	C3	3.7	C4	-2.5	C5	0.9
4b	C5	-0.9	O1	-1.3	C2	3.7	C3	-2.8	C4	1.1
4c	O1	0.4	C2	-2.8	C3	3.8	C4	-2.5	C5	0.9
5a	C4	-0.8	C5	1.4	P1	-0.1	C2	1.4	C3	-0.8
5b	C5	0.6	P1	-2.4	C2	3.8	C3	-3.1	C4	0.5
5c	P1	0.7	C2	-3.9	C3	6.0	C4	-2.9	C5	0.5
6b	C5	0.2	S1	-2.1	C2	4.3	C3	-3.2	C4	0.9
6c	S1	0.4	C2	-3.6	C3	5.4	C4	-3.0	C5	0.8
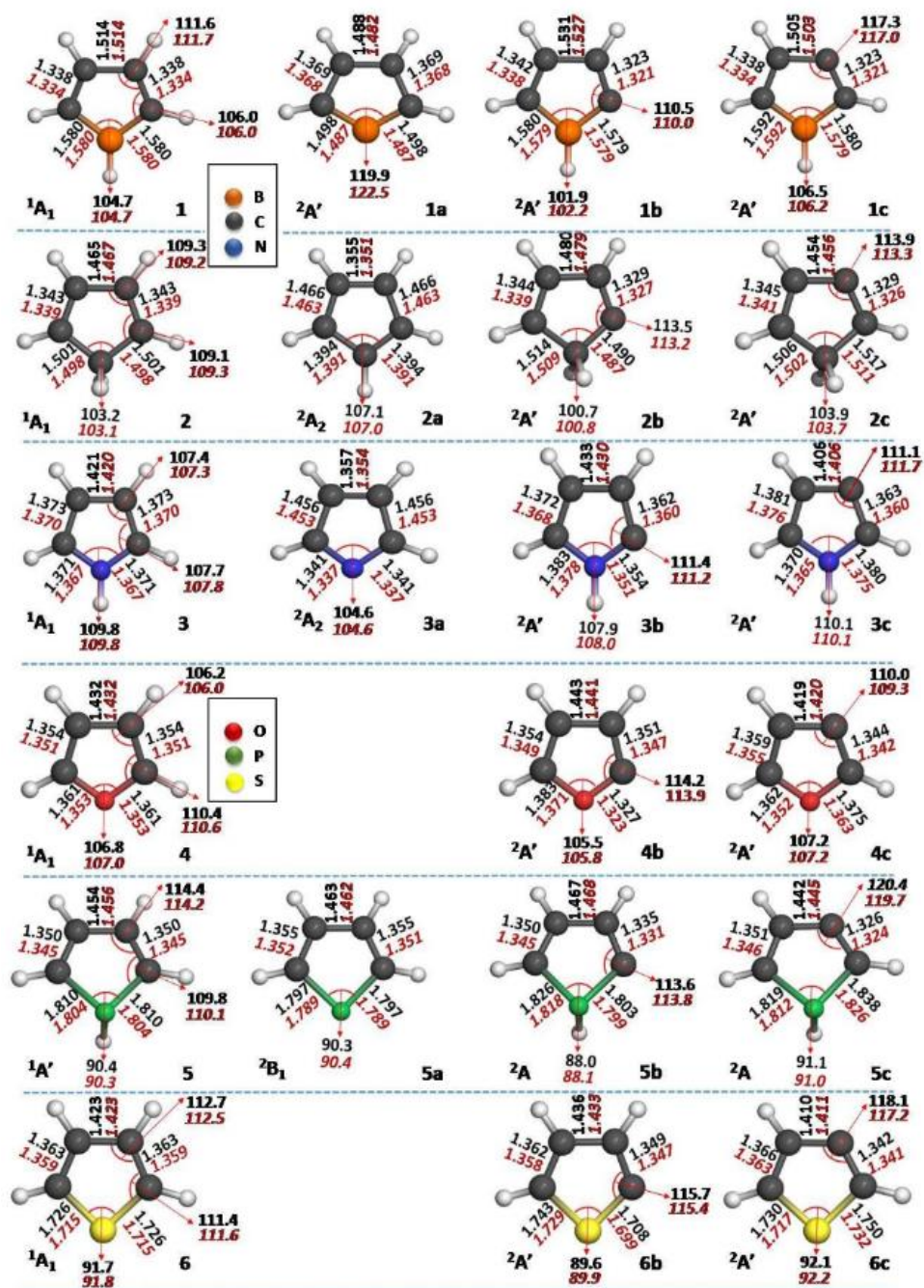
Figure 4.1 Optimized structures of borole **1**, cyclopentadiene **2**, pyrrole **3**, furan **4**, phosphole **5**, thiophene **6** and their corresponding radical isomers **1a-c**, **2a-c**, **3a-c**, **4b**-**c**, **5a-c** and **6b**-**c**. Selected geometrical parameters (bond distances in Å and bond angles in degrees) corresponding to the computed geometries at (U)B3LYP/cc-pVTZ (black) and (U)M06-2X/cc-pVTZ (red) levels of theory are indicated.

4.2.2 Stability aspects

4.2.2.1 Relative Stability order

In order to understand the influence of heteroatoms on the stability aspects of various heterocyclic radicals, we compared the relative stability among the individual heterocyclic radical isomers. These data have been obtained by comparing the absolute energies within the individual sets of isomeric radical species. For dehydro- borole (**1a-c**), cyclopentadiene (**2a-c**), pyrrole (**3a-c**), furan (**4b-c**), phosphole (**5a-c**) and thiophene (**6b-c**), the relative energies have been estimated at different levels of theory and are listed in **Table 4.2.** Based on these data, insights into the influence of the heteroatom on the radicals and also the interaction between the lone pair and the radical electron can be envisaged. Particularly, nitrogen and phosphorus with one lone pair and oxygen and sulphur with two lone pairs can interact with radical centers in different ways. On contrast, the presence of an empty π-orbital in the case of borolyl radicals, and the sp^3 center in the case of cyclopentadienyl radical isomers provide entirely different situation, where no such interactions are possible. Interestingly, the radicals **1a**, **2a**, **3a** and **5a** are found to have their radical centers located at the heteroatoms, possesses π–character. During our investigations, the default optimization of the radicals **3a** and **5a** led to π-centered radicals. However, we tried to optimize them by swapping the orbitals to attain σ-centered radicals. Although it worked for **3a** at lower basis set (ST0-3G), we could not optimize the σ-centered radical at higher basis sets. Similarly, the orbital swapping strategy failed in the case of **5a** as well. At this juncture, we expect the delocalization of radical electron in the π-orbital governs more stability than the availability of it in the σ-orbital, irrespective of the stabilization through aromaticity. All of the other radicals are carbon-centered and σ-radicals, which differ in their relative position with

respect to heteroatom. In all of the cases, heteroatom centered radicals are found to be more stable than their respective carbon centered isomers. The reason for their enhanced stability can be attributed to the ease of delocalization in π–centered radicals.

Surprisingly, in all of the cases, a significant preference in stability for the β-centered radicals over α-centered radicals has been observed that range between near degenerate (in furan) to substantial difference in other cases. This is in contrast to the stability of six membered heterocyclic radicals such as pyridyl and diazinyl radicals, where the α-centered radicals are found to be more stable. Among the radical pairs (**2b**, **2c**) and (**3b**, **3c**) pairs, different levels of theory predict the energy difference ranging between 0.3 to 0.9 kcal/mol favoring the β-centered radicals. The preference for β-centered radical is still maintained in the cases of (**1b**, **1c**), (**5b**, **5c**), and (**6b**, **6c**) pairs with an energy difference ranging between 2.0 to 3.7 kcal/mol. On the other hand, either **4b** or **4c** attained minima depending on the level of the theory. At B3LYP level, the β-centered was found to be more stable, whereas with the dispersion corrected M06-2X or CBS-QB3 level, the α-centered radical was found to be stabilized. Also, single point energy calculations at (U)CCSD(T) level predict a degeneracy between α- and β-centered radicals. Considering the fact that the energy differences at different levels are too small, it will be difficult to find the exact reason for this discrepancy. However, the amount of dispersive forces involved between the radical center and oxygen lone pair could be responsible in the furanyl radical isomers **4b** and **4c**.

Table 4.2 Relative Stability of Isomeric Dehydro- Borole **1a-c**, Cyclopentadiene **2a-c**, Pyrrole **3a-c**, Furan **4b-c**, Phosphole **5a-c** and Thiophene **6b-c** Radicals at Different Levels of Theory.
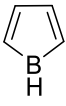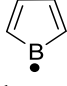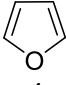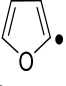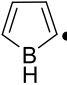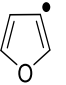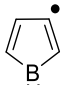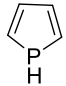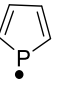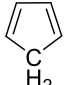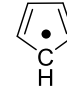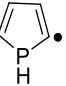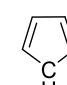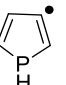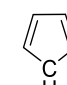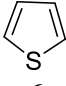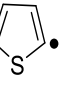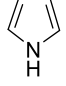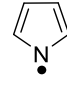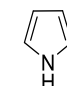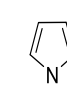
Level of theory	Relative Energy (kcal/mol)								
	1a	1b	1c	2a	2b	2c	3a	3b	3c
A	0.0	11.1	7.4	0.0	35.5	34.6	0.0	24.7	24.3
B	0.0	12.4	9.1	0.0	33.2	32.5	0.0	21.9	21.5
C	0.0	8.2	6.1	0.0	32.8	32.5	0.0	25.0	24.5
D	0.0	8.3	5.2	0.0	33.6	33.0	0.0	24.4	24.1
	4b	4c	5a	5b	5c	6b	6c		
A	0.1	0.0	0.0	40.8	37.4	2.9	0.0		
B	0.0	0.4	0.0	40.9	38.0	2.5	0.0		
C	0.0	0.0	0.0	43.5	41.2	2.0	0.0		
D	0.0	0.2	0.0	40.7	37.6	2.4	0.0		

A= (U)B3LYP/cc-pVTZ; B= (U)M06-2X/cc-pVTZ; C= (U)CCSD(T)/cc-pVTZ//(U)B3LYP/cc-pVTZ; D = CBS-QB3

4.2.2.2 Bond Dissociation Energy (BDE)

In order to examine the thermodynamic stability order, bond dissociation energies (BDE) for each radical species have been estimated. In this regard, the enthalpy changes accompanying the reactions, where C-H or X-H bond dissociation of the parent heterocycle leading to the heterocyclic radical and hydrogen atom as products have been considered. The estimated BDEs at (U)B3LYP/cc-pVTZ, (U)M06-2X/cc-pVTZ and CBS-QB3 levels of theory are listed in **Table 4.3.**

Table 4.3 Bond Dissociation Energies (BDE's) of Isomeric Dehydroborole **1a-1c**, Cyclopentadiene **2a-2c**, Pyrrole **3a-3c**, Furan **4b-4c**, Phosphole **5a-5c** and Thiophene **6b-6c** Radicals at (U)B3LYP/cc-pVTZ (in bold), UM06-2X/cc-pVTZ (in italics) and CBS-QB3 (in normal) levels of theory.

Reactant	Products	$\Delta H_{product-reactant}$ (kcal/mol)	Reactant	Products	$\Delta H_{product-reactant}$ (kcal/mol)
1	**1a** + H•	**101.2** / *100.3* / 104.9	**4**	**4b** + H•	**118.6** / *118.1* / 120.3
	1b + H•	**112.4** / *112.7* / 113.2		**4c** + H•	**118.5** / *118.5* / 120.5
	1c + H•	**108.8** / *109.5* / 110.1		**5a** + H•	**72.4** / *72.6* / 74.0
2	**2a** + H•	**79.7** / *81.8* / 82.3	**5**	**5b** + H•	**113.2** / *113.6* / 114.7
	2b + H•	**114.8** / *114.8* / 115.9		**5c** + H•	**109.8** / *110.7* / 111.6
	2c + H•	**113.9** / *114.1* / 115.3	**6**	**6b** + H•	**116.6** / *116.7* / 118.4
3	**3a** + H•	**93.5** / *96.2* / 96.0		**6c** + H•	**113.7** / *114.3* / 115.9
	3b + H•	**118.3** / *118.1* / 120.4			
	3c + H•	**117.8** / *117.7* / 120.1			

In general, lower the BDE value, the reaction is more favorable that accounts for higher thermodynamic stability of the radical. On the basis of BDE values, **5a** was found to be the

most stable radical followed by **2a**, **3a** and **1a**. On the other hand, **4b** was the least stable among all of the computed radicals. Indeed, the thermodynamic stability order predicted by the estimation of BDE's for individual heterocyclic/carbocylic radicals follow the same trend as compared to the order predicted based on their relative energies. This is in line with our earlier work, where the thermodynamic relative stability order is in the same trend as the BDEs.[10,11] However, factors such as bond strengths and steric bulkiness can influence the BDEs leading to incorrect qualitative behavior particularly when DFT methods have been adopted. Hence, we computed the same using composite CBS-QB3 level of theory as well.[22] The results revealed that CBS-QB3 values are consistent with the DFT methods, however, with a slight underestimation of energy in relative terms.

4.2.3. Factors influencing stability order of radical isomers

4.2.3.1 Spin density, Electrostatic potential and Multireference character

The difference in the electron density of one spin (β spin) relative to the opposite spin (α spin) is known as the spin density, which is a measure of the radical character. The understanding of the spin density will provide additional insights into the stability aspects such as delocalization of the electron spin. Larger the spin density values, localization of the spin at the radical center will be more, and the resulting species will be expected to have a higher reactivity. On the other hand, those with more delocalization of the spin thrive to enhanced stability of the resulting radicals. In this regard, we have calculated spin densities of all the radicals at (U)B3LYP/cc-pVTZ and (U)M06-2x/cc-pVTZ levels of theory. The spin density values are listed in **figure 4.2**. Through these values, we found out that all of the carbon-centered radicals except **2a** have large positive spin densities indicating a high radical

character. Based on the orientation of the spin lobe, all of the carbon-centered radicals except **2a** can be ascertained as σ–radicals. On the other hand, *N*-centered **3a**, *B*-centered **1a**, *C*-centered **2a** and *P*-centered **5a** follow a different trend. Among them, the radicals **3a** and **2a** possess a negative spin density values at nitrogen and carbon atoms, respectively, whereas the other carbon atoms of the ring show positive values. The negative spin density values at the carbon and nitrogen atoms are due to the polarization effect, as a consequence of interaction of singly occupied molecular orbital (SOMO) with the fully filled inner orbitals. Both **2a** and **3a** have nearly the same spin density values since both are isoelectronic species. Interestingly, both of them possesses no significant spin density values at the radical centers, which are indeed completely delocalized. On contrast, elements that are less electronegative than carbon such as B, and P gets a non-zero coefficient in their SOMO i.e *B*-centered **1a** and *P*-centered **5a** radicals, and accumulating partial spins at σ– and π–orbitals of the radical centers. In the case of **1a**, a competition between the configurations $\sigma^0\pi^1$ and $\sigma^1\pi^0$ leading to a slightly dominating π-character with a spin density value of 0.63 at *B*-center. By achieving this, not only the ring strain gets relieved in **1a**, but also the molecule attains non-planarity (as a consequence of Jahn-Teller distortion) that overcomes the anti aromaticity. As a result, the extent of spin delocalization is less in those radicals compared to the *N*-centered (**3a**) and *C*-centered (**2a**) radicals. The stability order among these radicals follows the trend: **5a** > **2a** > **3a** > **1a**. The higher stability of *P*-centered radical **5a** indicates the possible involvement of d-orbital for the spin delocalization. Many boryl radicals, in particular with electron withdrawing groups and π-conjugation have been reported to attain stability on the basis of flipping of radical electron from σ–orbital to an π–orbital.[23] However, in the case of **1a**, due to partial delocalization, the radical was found to be the least stable. Again, the involvement

of π–orbitals and delocalization of spin are attributed to the stability of *C*-centered **2a** and *N*-centered **3a** radicals. Except in the cases of pyrrolyl (**3b**, **3c**) and furanyl (**4b**, **4c**) radicals, spin density values are also supportive of the higher stability of β-centered over α-centered radicals. As indicated before, α-centered and β-centered isomeric pyrrolyl and furanyl radicals are close in energy at different levels of theory with an energy difference equal or less than 0.5 kcal/mol.

In line with these observations, the multireference CASSCF calculations have also been performed to understand the nature of the radical orbitals. The complete active space for the heterocyclic radicals were constructed by including the π orbitals of the ring systems, the radical orbital and also the orbitals corresponding to lone pair(s) of heteroatom, wherever necessary. Active space for borolyl (**1a-1c**) and cyclopentadienyl (**2a-2c**) radicals have been constructed using five electrons and five orbitals. For all these radicals, four of the chosen orbitals are π-type related to ring, whereas the other orbital is corresponding to radical (σ–type). The only exception is **2a,** where all the five orbitals correspond to the π orbitals. For pyrrolyl (**3a-3c**) and phospholyl (**5a-5c**) radicals, we have considered seven electrons (four π, one lone pair, and one radical electron) and six orbitals (four π, one lone pair and one radical orbital) in its active space. Since furanyl (**4b, 4c**) and thiophenyl (**6b, 6c**) contains two lone pairs, their active space has been constructed using nine electrons and seven orbitals. In all the radicals except **1a-1c** and **2a-2c**, lone pair orbitals were found to be low lying followed by π–orbitals and the SOMO orbital. SOMO orbitals were σ–centered for all the α- and β-centered radicals. On contrast, SOMO orbitals for **2a** and **3a** were completely π centric, whereas it has more σ–character in **1a** and **5a**. The resulting singly occupied

molecular orbitals (SOMO) from those calculations have confirmed that all of the carbon-centered radicals except **2a** are σ–radicals, whereas, the *C*-centered **2a** and *N*-centered **3a** radicals are π–radicals. On contrast, *B*-centered **1a**, and *P*-centered **5a** radicals possess orbital coefficients at the ring as well as at the heteroatoms. All of the SOMO's are indicated in **figure 4.2** and the complete active space orbitals are provided (**Figure A4.1** in Appendix).
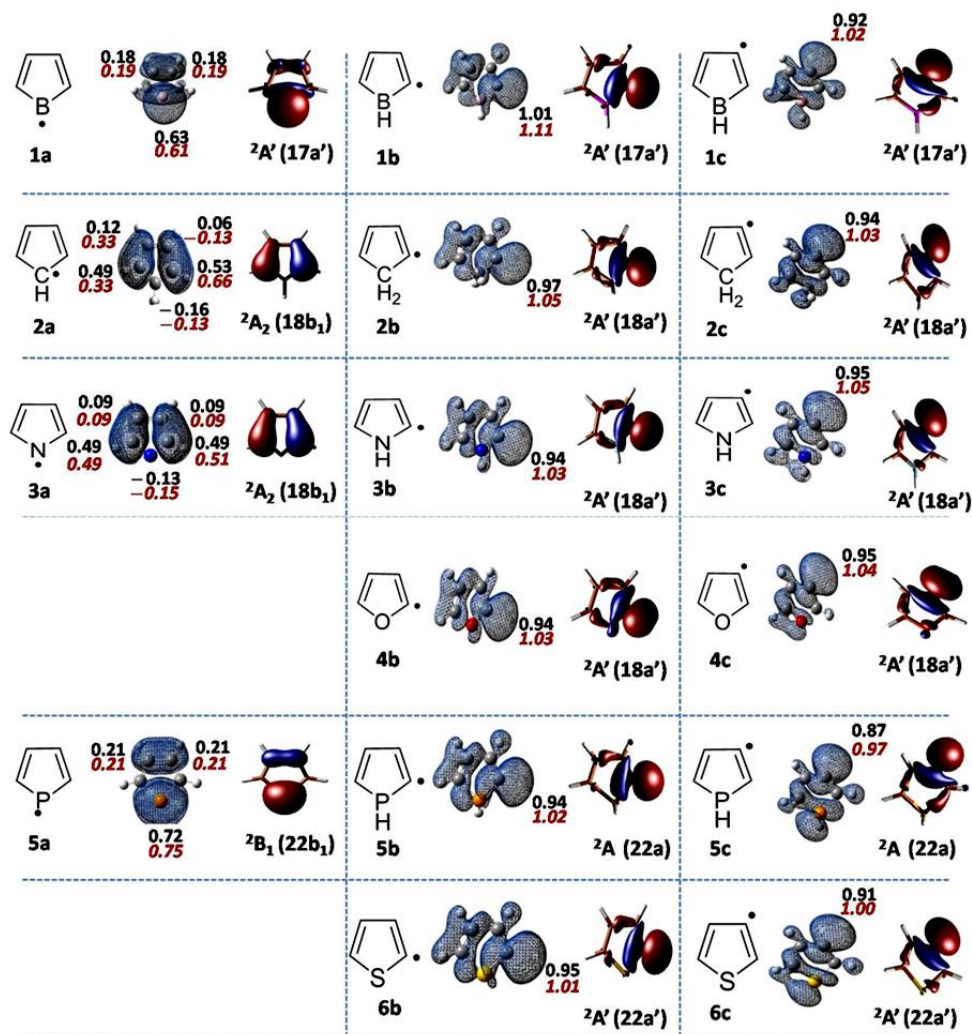
Figure 4.2 Spin density values (at (U)B3LYP/cc-pVTZ (black) and (U)M06-2X/cc-pVTZ (red) levels of theory) and SOMO (at CASSCF/cc-pVTZ) of isomeric borole **1a-c**, cyclopentadiene **2a-c**, pyrrole **3a-c**, furan **4b-c**, phosphole **5a-c** and thiophene **6b-c** radicals. (The electronic state of the radicals and the orbital number corresponding to the SOMO are indicated)

Apart from these, we have inspected at the electrostatic potential surfaces of all the radicals at (U)B3LYP/cc-pVTZ level of theory as shown in **Figure 4.3.** The results suggest that except in the case of the three-pyrrolyl radical isomers, all other radicals gain only a minimal negative potential at their respective radical centers. However, all of the radical centers of the pyrrolyl radicals are observed with a maximum negative charge. In the case of **3a**, the observed maximum negative charge at the nitrogen (radical) center can be attributed to the presence of lone pair at the σ–orbital of the *N*-center, which can be rationalized based on the spin density and the SOMO. However, the **3b** and **3c** radical isomers also gained more negative charges at the radical centers that can be due to the involvement of the lone pair of electrons of nitrogen in the aromaticity. As a result, the nitrogen atom is no longer a negative center that implies the accumulation of more negative charge at the radical center. Apparently, the N-H part of the molecule gains a positive potential in a relative scale, which is nearly of the same order of magnitude as the negative charge at the radical center.
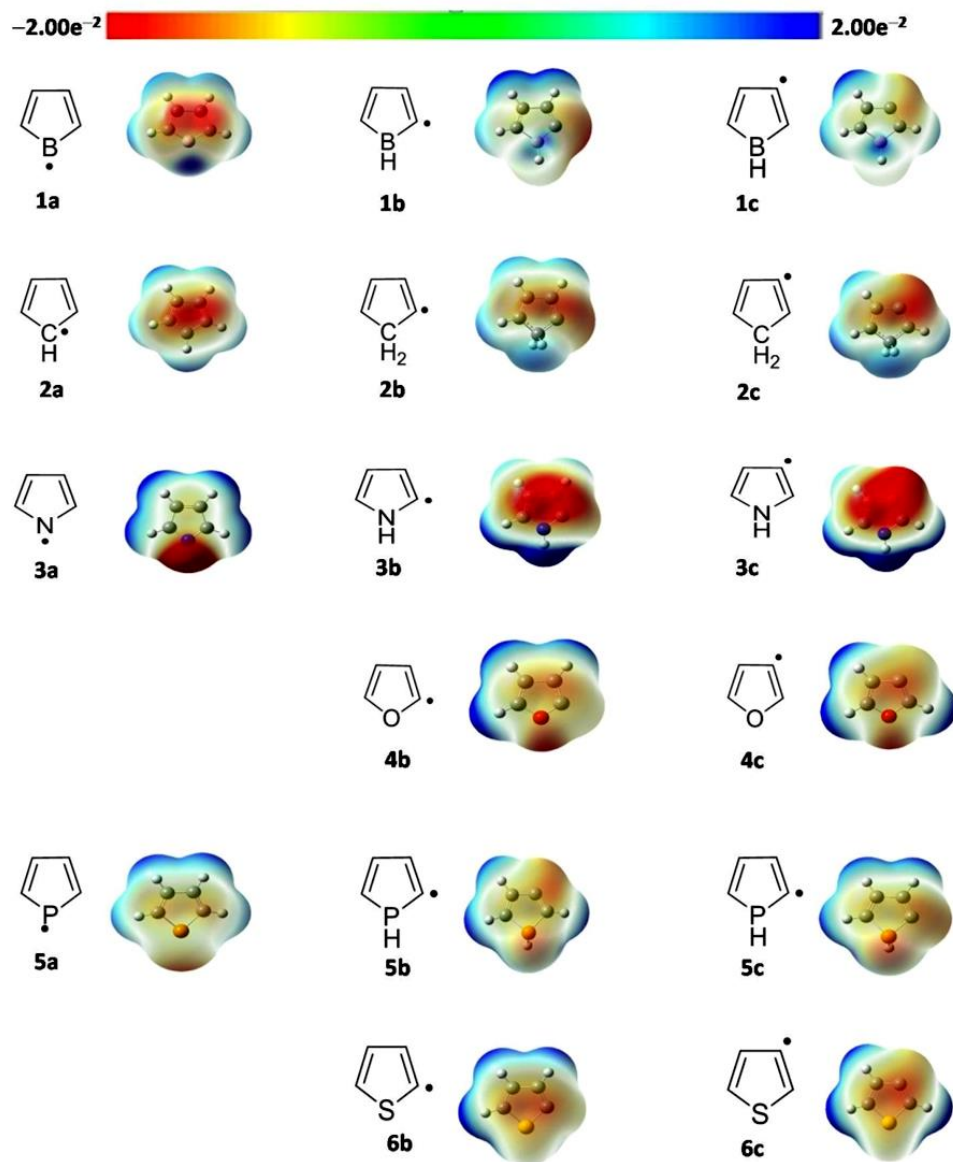
Figure 4.3 Electrostatic potential surfaces of isomeric borole **1a-1c**, cyclopentadiene **2a-2c**, pyrrole **3a-3c**, furan **4b-4c**, phosphole **5a-5c** and thiophene **6b-6c** radicals at (U)B3LYP/cc-pVTZ level of theory.

4.2.3.2 NBO analysis
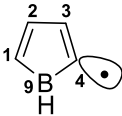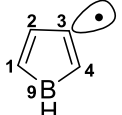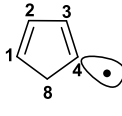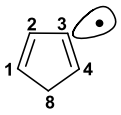
On the basis of optimized geometries, stability order, spin density and electrostatic potential mapping, qualitative aspects with respect to the interactions between heteroatoms and the radical center have been rationalized thus far. NBO analysis has been carried out to
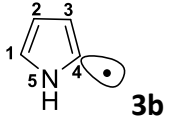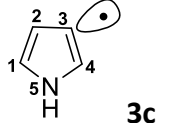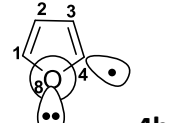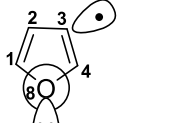
estimate the interactions between the radical centers and the heteroatoms, to quantify hyperconjugation and also to understand those interactions stabilizing β-centered radicals over α-centered radicals. Since the heteroatom centered or π–centered radicals are found to have a delocalized radical electron, the NBO analysis has been focused on the C-centered or σ–radicals. In the case of borolyl radicals **1b**, and **1c**, we observed no direct interaction between the radical electron and the boron atom, possibly due to an empty π–orbital at boron center. Indeed, all of the major interactions at the radical centers are mainly through intervening bonds. The same trend is followed in the case of **2b** and **2c**, as there is no availability of lone pair. However, in the pyrrolyl and phospholyl radicals, the presence of one lone pair at the heteroatom, opens up a possibility for through space interactions. Still only in the case of **5b**, a very weak through space interaction (0.75 kcal/mol) has been observed, whereas in **3b**, **3c** and **5c**, no TS interactions have been observed. This can be rationalized on the basis of geometrical changes in **5b** and **5c** due to the possible d-orbital involvement that forces the hydrogen connected to the phosphorus to deviate from the planarity. As a result, the phosphorus lone pair can possibly have a slight overlap with the radical orbital. Due to the increased distance, no such interactions are possible in the case of **5c**. Similarly, the involvement of additional lone pairs of oxygen and sulfur leads to furanyl and thiophenyl radicals exhibiting through space (TS) interactions. Indeed, **4b** showed significant TS interaction, whereas a weak TS interaction was observed for **6b**. Similarly, a weak TS interaction has also been observed for **4c** that was completely absent in the case of **6c**. Due to the greater internuclear distances in C-P and C-S bonds, the orbital overlap weakens between the lone pair and the radical leading to weak interactions.[24,25] As expected, in all of the cases, TB interactions are found to be the important stabilizing interactions
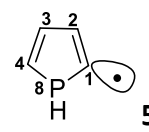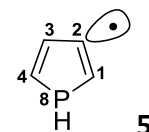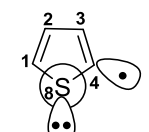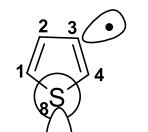
between the radical center and the lone pairs or heteroatoms. The most significant interactions involving either the radical center or the heteroatoms in this regard are tabulated in **Table 4.4.** Based on the analysis for all of the radicals, the TS interactions are either weak or non-existent. Despite the presence of stronger TB interactions, no general trend has been observed for various radicals. Hence, the orbital interactions alone cannot provide the evidences favoring β-centered over α-centered radicals.

For the stability of all these radicals, we have also considered the possibility of hyperconjugation. Since all of the radicals possess C-H or X-H (X=B, N, P) bonds in either side of the radical center, the interaction between the radical electron and the C/X-H σ^* bond was considered in this regard. Although all of the radical isomers showed the presence of hyperconjugation, the interaction energies were observed in the range of 0.3 and 1.1 kcal/mol. We have also considered the situations where the radical electron is having an α-spin (Donor) or a β-spin (Acceptor). In both the cases such interactions were found to be in the same range. In order to address the effect of hyperconjugation on the radical stability, we considered the following situations in the NBO analysis. In the analysis of orbital interactions using α-spin, the radical is treated as a donor that interacts with $\sigma^*_{(C-H)}$. Whereas, in consideration of β-spin, the radical center is treated as an acceptor that interacts with $\sigma_{(C-H)}$. The low values of hyperconjugation interactions in these radicals can be attributed to the geometrical constraints and hybridization. In the case of phosphole and thiophene based radicals, such interactions have still appeared to be small, although the bond distances between the radical center and the adjacent C-H bonds are relatively small. This situation clearly demonstrates that the hyperconjugation is not a major stabilizing factor.

Table 4.4 The Second Order Perturbation Energy (in kcal/mol) from the NBO Analysis at (U)B3LYP/cc-pVTZ and (U)M06-2X Levels of Theory. Energies in Bold Indicates (U)B3LYP and in Italics Represents (U)M06-2X.

	1b				1c				2b				2c		
Donor	Acceptor	$\langle E\rangle^a$	$\langle E\rangle^b$	Donor	Acceptor	$\langle E\rangle^a$	$\langle E\rangle^b$	Donor	Acceptor	$\langle E\rangle^a$	$\langle E\rangle^b$	Donor	Acceptor	$\langle E\rangle^a$	$\langle E\rangle^b$
$\pi_{(C2\text{-}C3)}$	$n^*_{(C4)}$	**9.86** / *10.44*	....	$\pi_{(C1\text{-}C2)}$	$n^*_{(C3)}$	**5.53** / *5.90*	....	$\pi_{(C2\text{-}C3)}$	$n^*_{(C4)}$	**11.23** / *11.80*	....	$\pi_{(C1\text{-}C2)}$	$n^*_{(C3)}$	**7.12** / *7.27*	....
$\pi_{(C1\text{-}B9)}$	$n^*_{(C4)}$	**6.67** / *6.63*	....	$\pi_{(C4\text{-}B9)}$	$n^*_{(C3)}$	**22.98** / *24.70*	....	$\pi_{(C1\text{-}C8)}$	$n^*_{(C4)}$	**9.13** / *9.36*	....	$\pi_{(C1\text{-}C2)}$	$\pi^*_{(C3\text{-}C4)}$	**8.77** / *10.32*	**7.34** / *8.93*
$\sigma_{(C3\text{-}H8)}$	$n^*_{(C4)}$	**1.15** / *1.56*	....	$\sigma_{(C4\text{-}H8)}$	$n^*_{(C3)}$	**0.43** / *0.76*	....	$\pi_{(C1\text{-}C2)}$	$\pi^*_{(C3\text{-}C4)}$	**4.81** / *5.63*	**6.96** / *8.79*	$\pi_{(C4\text{-}C8)}$	$n^*_{(C3)}$	**12.51** / *13.07*	....
$\pi_{(C1\text{-}C2)}$	$\pi^*_{(C3\text{-}C4)}$	**2.50** / *2.63*	**5.11** / *5.57*	$\pi_{(C1\text{-}B9)}$	$\pi^*_{(C2\text{-}C3)}$	**0.41** / *0.52*	**0.39** / *0.46*	$\sigma_{(C3\text{-}H7)}$	$n^*_{(C4)}$	**0.47** / *0.69*	....	$\sigma_{(C4\text{-}H7)}$	$n^*_{(C3)}$	**0.44** / *0.68*	....
$n^*_{(C4)}$	$\sigma^*_{(C3\text{-}H8)}$	**0.68** / *0.63*		$n^*_{(C3)}$	$\sigma^*_{(C2\text{-}H7)}$	**0.65** / *0.61*		$n^*_{(C4)}$	$\sigma^*_{(C3\text{-}H7)}$	**0.64** / *0.58*		$n^*_{(C3)}$	$\sigma^*_{(C2\text{-}H6)}$	**0.45** / *0.41*	
				$n^*_{(C3)}$	$\sigma^*_{(C4\text{-}H8)}$	**1.09** / *0.99*						$n^*_{(C3)}$	$\sigma^*_{(C4\text{-}H7)}$	**0.67** / *0.61*	

3b

Donor	Acceptor	$\langle E\rangle^a$	$\langle E\rangle^b$
n (N5)	π* (C3-C4)	**19.79** / _26.11_	.... / ....
π (C2-C3)	n* (C4)	**11.60** / _12.02_	.... / ....
π (C1-N5)	n* (C4)	**7.16** / _7.36_	.... / ....
π (C1-C2)	π* (C3-C4)	**6.39** / _8.74_	**8.65** / _12.29_
σ(N5-H6)	n* (C4)	**0.35** / _0.56_	.... / ....
n (N5)	π* (C1-C2)	**15.85** / _21.66_	**16.90** / _23.58_
π* (C1-C2)	π* (C3-C4)	**27.03** / _30.75_	.... / ....
n* (C4)	σ* (C3-H9)	**0.41** / _0.38_	
n* (C4)	σ* (C5-H6)	**0.39** / _0.37_	

3c

Donor	Acceptor	$\langle E\rangle^a$	$\langle E\rangle^b$
n (N5)	π* (C3-C4)	**13.25** / _17.94_	.... / ....
π (C4-N5)	n* (C3)	**5.86** / _6.04_	.... / ....
π (C1-C2)	n* (C3)	**8.95** / _9.16_	.... / ....
π (C1-C2)	π* (C3-C4)	**11.09** / _14.69_	**9.58** / _13.12_
n (N5)	π* (C1-C2)	**20.03** / _28.04_	**18.51** / _25.46_
π* (C1-C2)	π* (C3-C4)	**32.35** / _36.67_	.... / ....
n* (C3)	σ* (C2-H8)	**0.31** / _0.28_	
n* (C3)	σ* (C4-H9)	**0.39** / _0.36_	

4b

Donor	Acceptor	$\langle E\rangle^a$	$\langle E\rangle^b$
n1(O8)	n* (C4)	**2.51** / _3.74_	.... / ....
n1(O8)	π* (C3-C4)	**1.75** / _2.02_	**2.25** / _2.51_
n2(O8)	π* (C3-C4)	**16.64** / _21.40_	**14.88** / _19.63_
π (C2-C3)	n* (C4)	**12.39** / _12.82_	.... / ....
π (C1-O8)	n* (C4)	**6.71** / _6.97_	.... / ....
π (C1-C2)	π* (C3-C4)	**5.04** / _6.91_	**7.27** / _10.26_
n2(O8)	π* (C1-C2)	**11.44** / _15.74_	**12.11** / _16.95_
π* (C1-C2)	π* (C3-C4)	**21.13** / _21.60_	.... / ....
n* (C4)	σ* (C3-H7)	**0.48** / _0.45_	

4c

Donor	Acceptor	$\langle E\rangle^a$	$\langle E\rangle^b$
n1(O8)	n* (C3)	**0.28** / _0.39_	.... / ....
n1(O8)	π* (C3-C4)	**1.76** / _2.11_	**1.50** / _1.76_
n2(O8)	π* (C3-C4)	**10.20** / _13.75_	**12.75** / _17.67_
π (C4-O8)	n* (C3)	**5.21** / _5.15_	.... / ....
π (C1-C2)	n* (C3)	**8.80** / _9.10_	.... / ....
π (C1-C2)	π* (C3-C4)	**9.54** / _12.45_	**8.03** / _10.85_
n2(O8)	π* (C1-C2)	**14.90** / _20.50_	**14.03** / _19.17_
π* (C1-C2)	π* (C3-C4)	**25.19** / _26.23_	.... / ....
n* (C3)	σ* (C2-H6)	**0.30** / _0.25_	
n* (C3)	σ* (C4-H7)	**0.40** / _0.36_	

	5b				5c				6b				6c		
Donor	Acceptor	$\langle E\rangle^a$	$\langle E\rangle^b$	Donor	Acceptor	$\langle E\rangle^a$	$\langle E\rangle^b$	Donor	Acceptor	$\langle E\rangle^a$	$\langle E\rangle^b$	Donor	Acceptor	$\langle E\rangle^a$	$\langle E\rangle^b$
$n_{(P8)}$	$n^*_{(C1)}$	**0.75** / *0.54*	...... /	$n_{(P8)}$	$\pi^*_{(C1-C2)}$	**1.28** / *1.92*	**1.66** / *2.72*	$n1_{(S8)}$	$n^*_{(C4)}$	**0.43** /	...... /	$n1_{(S8)}$	$\pi^*_{(C3-C4)}$	**1.18** / *1.42*	**0.85** / *0.99*
$n_{(P8)}$	$\pi^*_{(C1-C2)}$	**0.94** / *1.09*	**2.34** / *3.08*	$\pi_{(C1-P8)}$	$n^*_{(C2)}$	**17.37** / *18.73*	...... /	$n1_{(S8)}$	$\pi^*_{(C3-C4)}$	**2.03** / *2.26*	**1.93** / *2.12*	$n2_{(S8)}$	$\pi^*_{(C3-C4)}$	**7.44** / *10.83*	**9.63** / *14.29*
$\pi_{(C2-C3)}$	$n^*_{(C1)}$	**8.57** / *9.28*	...... /	$\pi_{(C3-C4)}$	$n^*_{(C2)}$	**6.01** / *6.36*	...... /	$n2_{(S8)}$	$\pi^*_{(C3-C4)}$	**12.84** / *17.92*	**11.24** / *15.64*	$\pi_{(C1-C2)}$	$n^*_{(C3)}$	**7.33** / *7.60*	...... / ......
$\pi_{(C4-P8)}$	$n^*_{(C1)}$	**7.55** / *8.11*	...... /	$\pi_{(C3-C4)}$	$\pi^*_{(C1-C2)}$	**8.36** / *9.97*	**7.19** / *8.58*	$\pi_{(C2-C3)}$	$n^*_{(C4)}$	**9.92** / *10.34*	...... /	$\pi_{(C1-C2)}$	$\pi^*_{(C3-C4)}$	**9.52** / *12.17*	**8.13** / *10.64*
$\pi_{(C3-C4)}$	$\pi^*_{(C1-C2)}$	**4.94** / *5.59*	**6.39** / *8.20*	$n_{(P8)}$	$\pi^*_{(C3-C4)}$	**1.90** / *2.96*	**2.10** / *3.16*	$\pi_{(C1-S8)}$	$n^*_{(C4)}$	**8.52** / *9.09*	...... /	$\pi_{(C4-S8)}$	$n^*_{(C3)}$	**10.45** / *10.68*	...... / ......
$n_{(P8)}$	$\pi^*_{(C3-C4)}$	**2.00** / *2.77*	**1.93** / *2.89*	$\pi^*_{(C3-C4)}$	$\pi^*_{(C1-C2)}$	**14.29** / *13.94*	**23.95** / *31.47*	$\pi_{(C1-C2)}$	$\pi^*_{(C3-C4)}$	**5.26** / *6.93*	**7.32** / *10.05*	$\sigma_{(C4-H7)}$	$n^*_{(C3)}$	**0.56** / *0.83*	...... / ......
$\pi^*_{(C3-C4)}$	$\pi^*_{(C1-C2)}$	**24.24** / *18.90*	...... /	$\sigma_{(C1-H5)}$	$n^*_{(C2)}$	**0.61** / *0.99*		$\sigma_{(C3-H7)}$	$n^*_{(C4)}$	**0.56** / *0.84*	...... /	$n2_{(S8)}$	$\pi^*_{(C1-C2)}$	**12.36** / *18.32*	**11.54** / *16.87*
$n^*_{(C1)}$	$\sigma^*_{(C2-H5)}$	**0.69** / *0.66*		$n^*_{(C2)}$	$\sigma^*_{(C1-H5)}$	**1.06** / *0.94*		$n2_{(S8)}$	$\pi^*_{(C1-C2)}$	**10.01** / *14.53*	**10.81** / *15.96*	$\pi^*_{(C1-C2)}$	$\pi^*_{(C3-C4)}$	**31.33** / *34.84*	**66.79** / *112.54*
				$n^*_{(C2)}$	$\sigma^*_{(C3-H6)}$	**0.81** / *0.73*		$\pi^*_{(C1-C2)}$	$\pi^*_{(C3-C4)}$	**41.86** / *46.67*	...... /	$n^*_{(C3)}$	$\sigma^*_{(C2-H6)}$	**0.56** / *0.50*	
								$n^*_{(C4)}$	$\sigma^*_{(C3-H7)}$	**0.58** / *0.55*		$n^*_{(C3)}$	$\sigma^*_{(C4-H7)}$	**0.67** / *0.60*	

[a]Interaction energies when radical electron resides in α orbital.
[b]Interaction energies when radical electron resides in β orbital

4.2.3.3 Resonance energy and aromaticity character

Due to the presence of conjugated π–bonds, all of the radical isomers are stabilized by resonance, which can be enhanced with the participation of the heteroatom. In order to understand the involvement of the heteroatom, the resonance energies[12-15] and the aromaticity have also been estimated for all of the parent compounds and their respective radical isomers. For resonance energy estimation, a hypothetical reaction has been considered, where a saturated heterocycle/heterocyclic radical analogue and cyclohexadiene are the reactants. [26] This led to the formation of an unsaturated parent heterocycle/heterocyclic radical (our desired radical) and cyclohexene as the products. The enthalpy change (ΔH) accompanying such reactions is calculated as a measure of as the resonance energy. More negative or less positive ΔH value indicates the presence of greater resonance stabilization. In all of the cases, β-centered radicals are found to have higher resonance energy values than their corresponding α-centered radical isomers. Thus, resonance energy calculations support the higher stability of β-centered radicals. Based on the resonance stabilization energy alone, the *B*-centered radical **1a** is found to be more stable than its parent, despite the attainment of non-planarity. On the other hand, cyclopentadiene and phosphole are non-planar due to the presence of sp^3 center and the deviation from planarity of P-H bond, respectively. However, their analogous radicals (**2a** and **5a**) are found to be planar and gain extra stability due to the enhanced delocalization or resonance. Conversely, the resonance stabilization lowers in the *N*-centered pyrrolyl radical due to the loss of aromaticity as compared to the parent pyrrole.

In this regard, the aromaticity character in the parent heterocycles and their respective radical isomers has also been estimated through nucleus-independent chemical shifts (NICS). Based on the NICS method, aromatic, antiaromatic and non-aromatic characters of the

various heterocycles and their radical isomers have been evaluated using the computed magnetic shielding. The resulting NICS indices are useful in the classification of the ring currents as diatropic (negative, aromatic) and paratropic (positive, antiaromatic). NICS (1.0) indices for all of the heterocyclic/carbocyclic radicals have been estimated at (U)B3LYP/cc-pVTZ as shown in **Figure 4.4**. NICS (0), NICS (0.5), NICS (1.0), NICS (1.5) and NICS (2.0) indices are obtained by varying the position of probe atom along the perpendicular axis to the molecular plane at (U)B3LYP/cc-pVTZ and (U)M06-2X/cc-pVTZ levels of theory as listed in **Table 4.5**. Moreover, resonance energy for all of the heterocyclic/carbocyclic radicals have been estimated at (U)B3LYP/cc-pVTZ and (U)M06-2X/cc-pVTZ levels of theory and are given in **Table 4.6.**
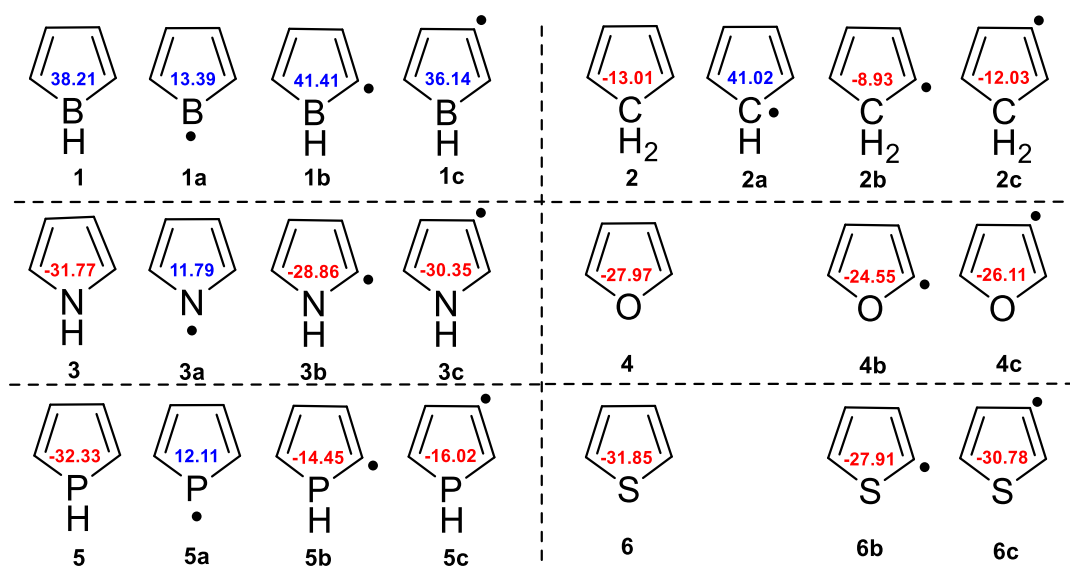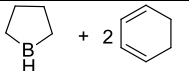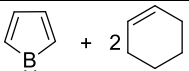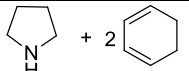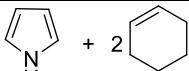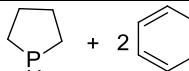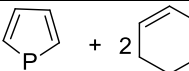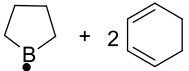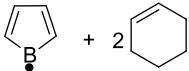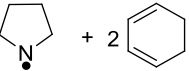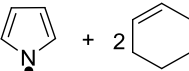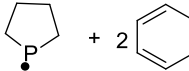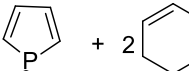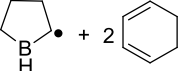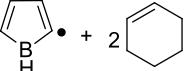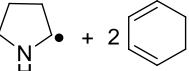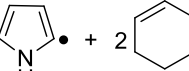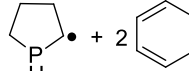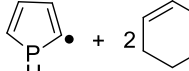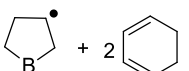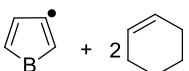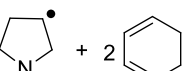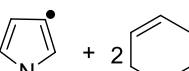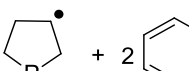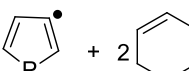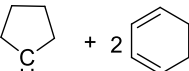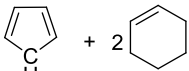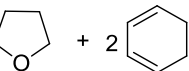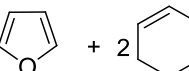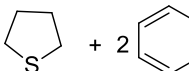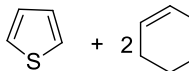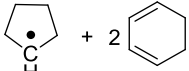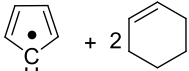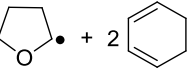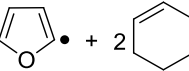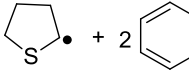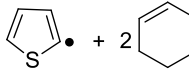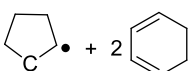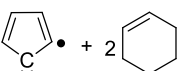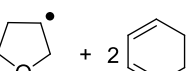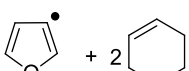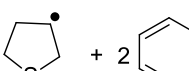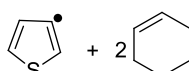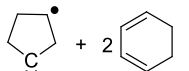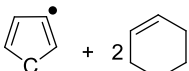
Figure 4.4 NICS (1.0) indices for borole **1**,cyclopentadiene **2**, pyrrole **3**, furan **4**, phosphole **5**, thiophene **6** and their corresponding radical isomers **1a-c**, **2a-c**, **3a-c**, **4b-c**, **5a-c** and **6b-c** performed at (U)B3LYP/cc-pVTZ level of theory. (Blue – Positive NICS values; Red – Negative NICS values)

Table 4.5 Estimated NICS Indices for Understanding the Aromatic Character of all the Isomeric Radicals and Their Respective Parent at (U)B3LYP/cc-pVTZ and (U)M06-2X/cc-pVTZ Levels of Theory. NICS Indices in Bold Indicates (U)B3LYP and in Italics Represent (U)M06-2X.

Species	NICS (0)	NICS (0.5)	NICS (1.0)	NICS (1.5)	NICS (2.0)	Species	NICS (0)	NICS (0.5)	NICS (1.0)	NICS (1.5)	NICS (2.0)
1	**63.94**	**59.67**	**38.21**	**17.17**	**6.47**	**2**	**9.05**	**−1.55**	**−13.01**	**−13.93**	**−10.75**
	62.67	*58.01*	*36.48*	*15.82*	*5.56*		*9.82*	*−1.33*	*−13.37*	*−14.36*	*−11.08*
1a	**27.71**	**27.19**	**13.39**	**2.74**	**−1.22**	**2a**	**69.90**	**65.81**	**41.02**	**17.40**	**6.09**
	27.66	*27.54*	*13.37*	*2.58*	*−1.35*		*72.42*	*68.37*	*42.64*	*17.98*	*6.22*
1b	**64.88**	**61.99**	**41.41**	**19.85**	**8.42**	**2b**	**10.55**	**1.59**	**−8.93**	**−10.67**	**−8.50**
	63.46	*59.62*	*39.49*	*18.50*	*7.54*		*10.46*	*1.23*	*−9.56*	*−11.22*	*−8.89*
1c	**58.09**	**55.24**	**36.14**	**16.57**	**6.47**	**2c**	**6.64**	**−2.47**	**−12.03**	**−12.49**	**−9.53**
	55.97	*52.95*	*34.13*	*15.14*	*5.56*		*6.95*	*−2.48*	*−12.39*	*−12.89*	*−9.83*
3	**−14.29**	**−26.44**	**−31.77**	**−24.13**	**−15.88**	**4**	**−10.51**	**−22.51**	**−27.97**	**−21.26**	**−13.98**
	−14.64	*−27.52*	*−33.13*	*−25.10*	*−16.49*		*−10.79*	*−23.33*	*−29.01*	*−22.01*	*−14.45*
3a	**37.09**	**29.76**	**11.79**	**0.50**	**−2.79**	**4b**	**−8.68**	**−19.46**	**−24.55**	**−18.73**	**−12.31**
	36.21	*28.33*	*10.23*	*−0.64*	*−3.51*		*−9.25*	*−20.53*	*−25.95*	*−19.62*	*−12.87*
3b	**−13.66**	**−24.42**	**−28.86**	**−21.74**	**−14.22**	**4c**	**−11.44**	**−22.27**	**−26.11**	**−19.26**	**−12.46**
	−14.57	*−25.85*	*−30.35*	*−22.76*	*−14.85*		*−12.42*	*−23.43*	*−27.20*	*−20.00*	*−12.92*
3c	**−16.81**	**−27.22**	**−30.35**	**−22.31**	**−14.44**	**5**	**−20.19**	**−28.09**	**−32.33**	**−25.83**	**−17.74**
	−17.61	*−28.52*	*−31.71*	*−23.25*	*−15.01*		*−20.75*	*−29.20*	*−33.80*	*−26.98*	*−18.49*
6	**−17.16**	**−26.82**	**−31.85**	**−25.15**	**−17.11**	**5a**	**29.25**	**24.81**	**12.11**	**2.02**	**−1.90**
	−18.00	*-28.06*	*−33.25*	*−26.19*	*−17.78*		*24.99*	*19.78*	*7.40*	*−1.13*	*−3.79*
6b	**−15.69**	**−23.82**	**−27.91**	**−21.96**	**−14.90**	**5b**	**−1.52**	**−8.06**	**−14.45**	**−13.87**	**−10.57**
	−17.18	*−25.44*	*−29.39*	*−22.99*	*−15.55*		*−2.26*	*−8.84*	*−15.19*	*−14.46*	*−10.97*
6c	**−18.44**	**−27.23**	**−30.78**	**−23.62**	**−15.81**	**5c**	**−3.93**	**−9.43**	**−16.02**	**−15.20**	**−11.50**
	−19.76	*−28.76*	*−32.23*	*−24.65*	*−16.45*		*−4.34*	*−10.30*	*−17.01*	*−15.95*	*−11.98*

NICS (1.0) value for each parent molecule and their respective radical isomers are shown in **Figure 4.4.** These values are in line with our initial claim on the preferential stabilization of the β-centered radicals over the α-centered radical. Based on the resonance energy and NICS calculations thus far, the radicals **2a, 3a** and **5a** can be interesting candidates with respect to aromaticity character. Independent to the aromaticity character of their respective parents (aromatic for N, and P containing heterocycle, non-aromatic for CH_2 and antiaromatic for B), the resulting *X*-centered radicals (X = B, C-H, N and P) exhibit a common way in flipping of unpaired electron from the σ- to π-orbital. Thus, all of them led to π−centered, cyclic, 4n+1 π−delocalized and planar radicals. Apparently, all of the heteroatom-centered/C-centered radicals containing (4n+1) π−electrons, the NICS (1.0) values clearly showed the evidences for a weak antiaromatic character. Thus, heteroatom centered/C-centered radicals containing odd number of delocalized π−electrons can be classified as "quasi-antiaromatic" systems.

Table 4.6 Resonance Energies of Borole **1**, Cyclopentadiene **2**, Pyrrole **3**, Furan **4**, Phosphole **5**, Thiophene **6** and their Corresponding Radical Isomers at (U)B3LYP/cc-pVTZ (Bold) and (U)M06-2X/cc-pVTZ (Italics) Levels of Theory.

Reactants	Products	Resonance energy (ΔH) (kcal/mol)	Reactants	Products	Resonance energy (ΔH) (kcal/mol)	Reactants	Products	Resonance energy (ΔH) (kcal/mol)
		11.7/*10.1*			**−27.2**/*−30.0*			**−3.4**/*−4.4*
		7.9/*6.0*			**−20.9**/*−24.4*			**−7.4**/*−8.7*
		37.2/*34.2*			**3.8**/*−1.9*			**17.4**/*14.0*
		26.2/*22.8*			**−3.5**/*−8.3*			**10.5**/*8.1*
		−2.3/*−4.1*			**−17.9**/*−20.5*			**−16.8**/*−18.8*
		−15.4/*−17.1*			**10.9**/*5.5*			**11.1**/*6.4*
		19.7/*16.0*			**6.2**/*1.6*			**2.0**/*−1.7*
		18.8/*15.3*						

4.2.3.4 Ring strain
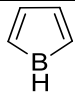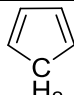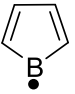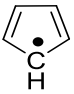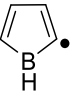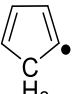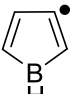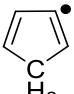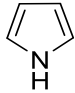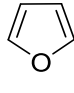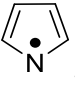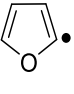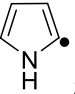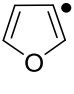
Since all of the parent compounds and their isomeric radicals are five-membered ring systems, one of the important destabilizing factors is the ring strain. It will be very intriguing to understand the influence of the radical center in the ring strain. Also, for understanding the relative stability of various radical isomers, estimation of the strain energy is inevitable. In this regard, group equivalence reactions have been considered to quantify the ring strain for the parent heterocycle and their respective radical isomers (**Scheme 4.2**). The group equivalence reactions are found to be advantageous over the other alternative methods such as homodesmotic and isodesmic reactions in determining the strain energies.[27] In principle, group equivalence reactions are both isodesmic and homodesmotic, and are capable of separating resonance from the destabilization due to strain.[28] For constructing a group equivalence reaction,[29,30] the following criteria have been considered: (i) Pairing (each individual equivalent group in the cyclic molecule must be paired with an equivalent group with a short acyclic counterpart) (ii) Heavy atoms (at least three heavy atoms should be part of each molecular fragment that can be considered as product) (iii) Balancing (each atom/fragments in the product should be balanced for the type and numbers of bonds and also the hybridization). Indeed, this method can work only when the reactions containing rings only on the reactant side. Due to the absence of ring in the product side, the group equivalence reactions cancel out the effect of resonance.[19] Using these group equivalent reactions, the ring strain energies for the parent and their respective isomeric radicals have been estimated at (U)B3LYP/cc-pVTZ and (U)M06-2X/cc-pVTZ levels of theory as listed in **Table 4.7.** If the enthalpy change accompanying the group equivalence reactions is more negative, it indicates that the ring strain will be more. Upon creating a radical center by
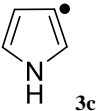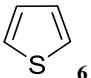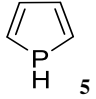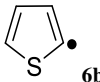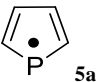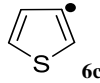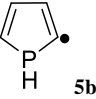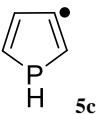
homolysis of C-H or X-H (X = B, CH, N, O, P and S) bonds, the resulting species gather more strain relative to their respective parent. The only exception is **1a**, which possesses 2.7 kcal/mol lower strain energy than its parent **1**. The *B*-centered **1a** and *P*-centered **5a** radicals are found to be less strained among their isomeric radicals, whereas the *C*-centered **2a** and *N*-centered **3a** are the most strained among their respective isomeric radicals. In general, we observed that the β-centered radicals are found to be the least strained radicals among each set of heterocyclic/carbocyclic isomeric radicals.
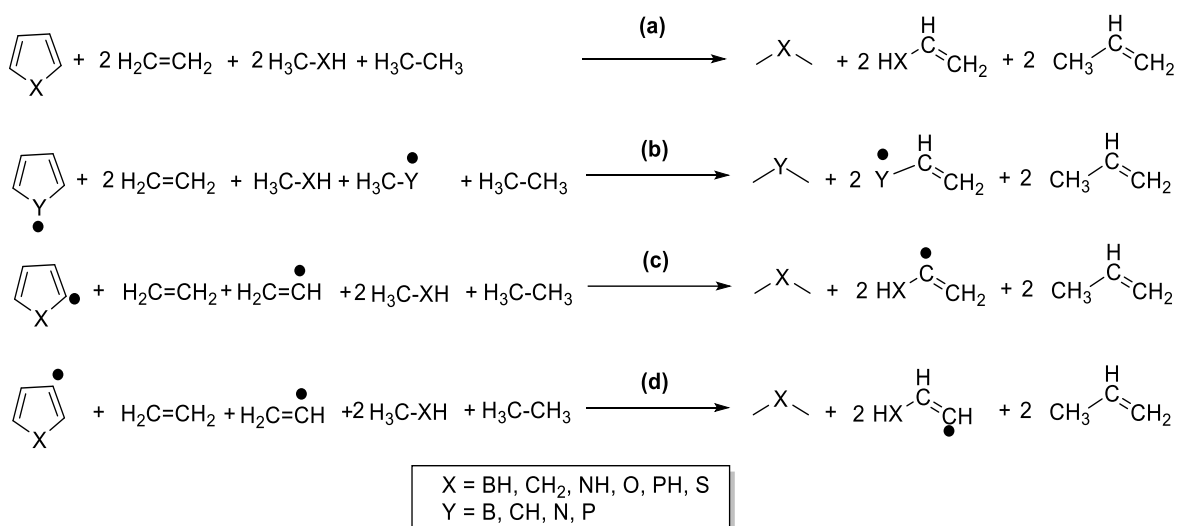
Scheme 4.2 Group Equivalence Reactions Used for the Estimation of Ring Strain of (a) Parent Heterocycle (b) Heteroatom-Centered (c) α-Centered and (d) β-Centered Radical Isomers.

Table 4.7 Ring Strain and Relative Ring Strain for Borole **1**, Cyclopentadiene **2**, Pyrrole **3**, Furan **4**, Phosphole **5**, Thiophene **6** and Their Corresponding Radical Isomers **1a-1c**, **2a-2c**, **3a-3c**, **4b-4c**, **5a-5c** and **6b-6c** with Respect to ∠CXC Performed at (U)B3LYP/cc-pVTZ and (U)M06-2X/cc-pVTZ Levels of Theory.

Species	∠CXC (degrees)	Ring Strain (ΔH) (kcal/mol)	Relative Ring Strain[a] (kcal/mol)	Species	∠CXC (degrees)	Ring Strain (ΔH) (kcal/mol)	Relative Ring Strain[a] (kcal/mol)
1 (B, H)	104.7/*104.7*	−20.2/*−20.2*	0.0/*0.0*	**2** (CH₂)	103.2/*103.1*	−2.4/*−4.3*	0.0/*0.0*
1a (B•)	119.9/*122.5*	−17.5/*−16.3*	−2.7/*−3.9*	**2a** (CH•)	109.0/*109.0*	−22.2/*−20.7*	19.8/*16.3*
1b (B, H)	101.9/*102.2*	−60.0/*−59.2*	39.8/*39.0*	**2b** (CH₂)	100.7/*100.8*	−16.6/*−16.3*	14.2/*12.0*
1c (B, H)	106.5/*106.2*	−24.2/*−24.3*	4.0/*4.1*	**2c** (CH₂)	103.9/*103.7*	−5.3/*−6.9*	2.9/*2.6*
3 (N, H)	109.8/*109.8*	10.0/*9.8*	0.0/*0.0*	**4** (O)	106.8/*107.0*	3.9/*2.8*	0.0/*0.0*
3a (N•)	104.6/*104.6*	−6.3/*−5.3*	16.3/*15.1*	**4b** (O)	105.5/*105.8*	−10.1/*−8.4*	14.0/*11.2*
3b (N, H)	107.9/*108.0*	−4.8/*−5.3*	14.8/*15.1*	**4c** (O)	107.2/*107.2*	2.2/*1.9*	1.7/*0.9*

122

Species	∠CXC (degrees)	Ring Strain (ΔH) (kcal/mol)	Relative Ring Strain[a] (kcal/mol)	Species	∠CXC (degrees)	Ring Strain (ΔH) (kcal/mol)	Relative Ring Strain[a] (kcal/mol)
3c	**110.1**/*110.1*	**8.5**/*8.8*	**1.5**/*1.0*				
5	**90.4**/*90.3*	**4.9**/*2.8*	**0.0**/*0.0*	**6**	**91.7**/*91.8*	**15.7**/*14.6*	**0.0**/*0.0*
5a	**90.3**/*90.4*	**0.6**/*0.7*	**4.3**/*2.1*	**6b**	**89.6**/*89.9*	**−2.5**/*−2.5*	**18.2**/*17.1*
5b	**88.0**/*88.1*	**−17.6**/*−15.8*	**22.5**/*18.6*	**6c**	**92.1**/*92.2*	**11.6**/*11.0*	**4.1**/*3.6*
5c	**91.1**/*91.0*	**0.7**/*−1.5*	**4.2**/*4.3*				

[a]Relative ring strain within the same set of heterocyclic system

123

As previously reported by Bach et al., the estimated strain energies of α-centered and β-centered radicals correlate very well with C-H BDE's, indicating that the strain energy increases as the BDE values increase.[18]

(a)

Equation	y = a + b*x
Plot	B
Weight	No Weighting
Intercept	-11.81887 ± 2.3473
Slope	0.89454 ± 0.08034
Residual Sum of Squares	1.05757
Pearson's r	0.99599
R-Square(COD)	0.992
Adj. R-Square	0.984

(b)

Equation	y = a + b*x
Plot	B
Weight	No Weighting
Intercept	27.48619 ± 4.342
Slope	-0.3945 ± 0.15463
Residual Sum of Squar	16.73087
Pearson's r	-0.82735
R-Square(COD)	0.68451
Adj. R-Square	0.57935

(c)

Equation	y = a + b*x
Plot	B
Weight	No Weighting
Intercept	6.97737 ± 0.7857
Slope	-0.15675 ± 0.02905
Residual Sum of Squares	0.60985
Pearson's r	-0.95214
R-Square(COD)	0.90658
Adj. R-Square	0.87544

Figure 4.5 Relationship between the relative ring strain energies (with respect to their respective parent) and the %s character of the "X" atoms (X = C, N, O, P, and S) in (a) X-centered, (b) α-centered and (c) β-centered radicals at (U)B3LYP/cc-pVTZ level of theory. (In these relationship, boron radicals were not considered)

Recently, Alabugin et al. reported that %s character has a very good correlation with the strain energy. In order to understand the effect of heteroatom in the influence of strain energy, we correlated the %s character of the heteroatom (based on the NBO hybridization

analysis) with that of strain energy of the individual radicals relative to their respective parent. The plots are shown in **Figure 4.5**. Except for boron based radicals, we found out that all of the radical isomers showed a linear correlation. Presumably, the presence of an empty orbital and a slight electropositive nature of boron might be responsible for the deviation from the linearity.

Apart from these, the change in the $\angle$CXC (X=heteroatom) angle at the heteroatom junction (relative to their respective parent) is a clear indicator of the estimated strain in the molecule. If the bond angle at heteroatom increases, the strain energy decreases and *vice versa* (**Figure 4.6** and **Table 4.7**). The strain energies of the parent molecules change in the following order: B > C > O > P > N > S. However, this trend changes upon introducing the radical centers, viz, for β-centered radicals, it is a slightly varied (B > C > P > O > N > S). Whereas the changes are more pronounced in the case of α-centered radicals (B > P > C > O > N > S) and heteroatom centered radicals (C > B > N > P). Apparently, the interactions of the heteroatoms with the radical centers play a significant role in the strain energies of the radicals.
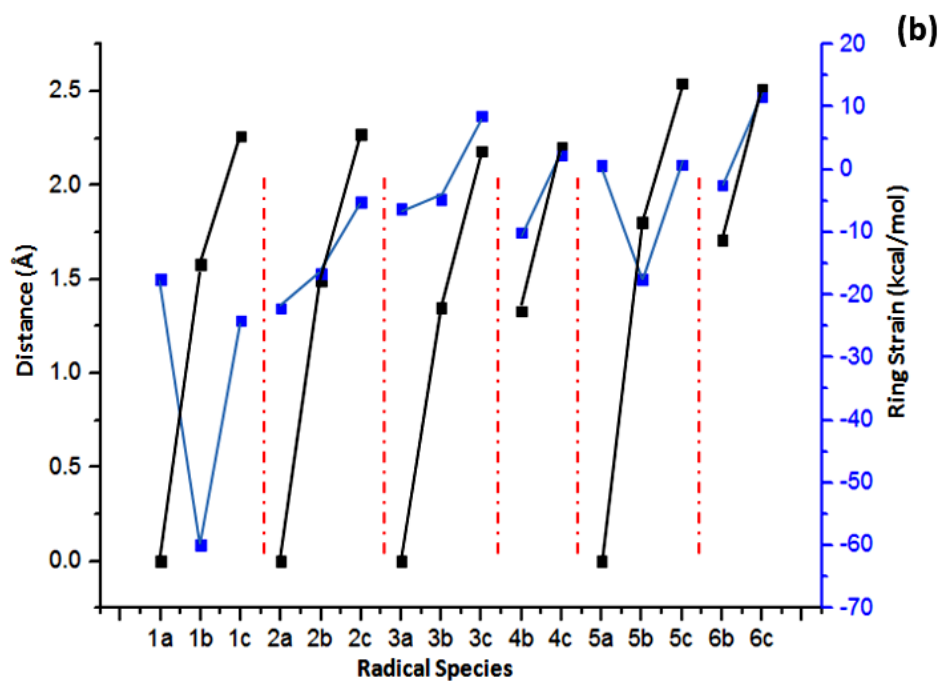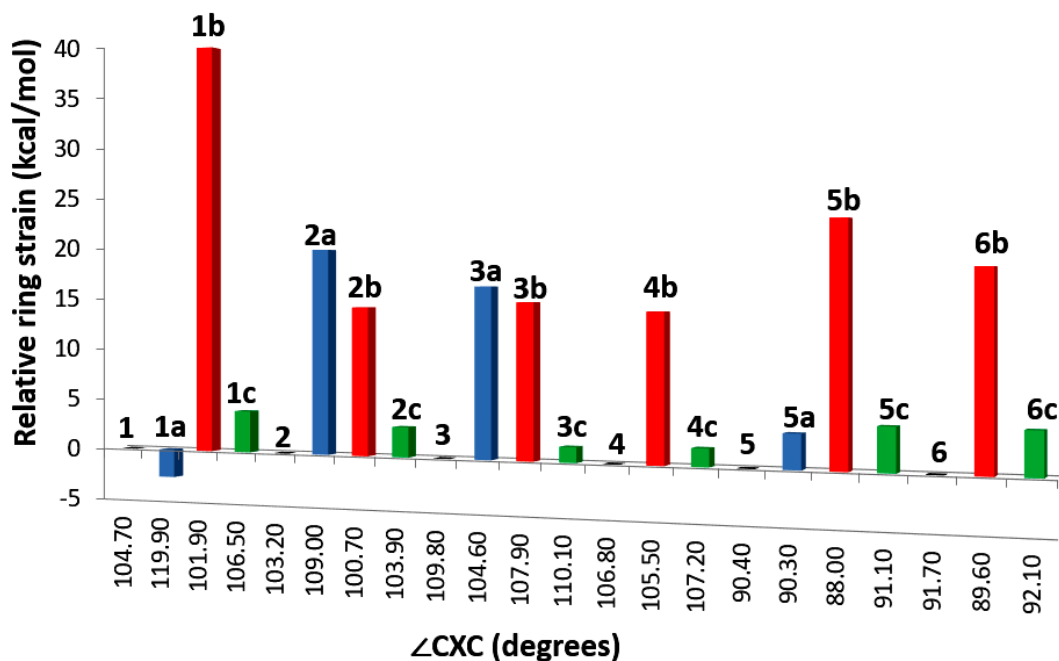
Figure 4.6 Correlation charts of ring strain energies with (a) bond angle at ∠CXC, where X=heteroatom or CH₂; (Black – Parent; Blue – X-centered radicals; Red – α-centered radicals; Green – β-centered radicals) (b) Internuclear distance between radical center and the X.

Despite the presence of more strain energy in destabilizing the *C*- and *N*-centered radicals than their respective isomers, both of them are found to be more stable. On the other hand, *B*- and *P*-centered radicals have lesser ring strains relative to their respective radical analogues. In all of the cases, the π- delocalization could be responsible for the higher stability of the heteroatom- or *C*-centered radicals. Similarly, due to the dominating π-delocalization and/or low ring strain, the β-centered radicals are found to be more stable relative to their α-centered analogues. It is evident that the delocalization (stabilizing effect) competes with the strain energy (destabilizing effect) in all of the radical isomers. Eventually the heteroatom- and β-centered radical isomers are stabilized on the basis of dominating radical delocalization.

4.3 CONCLUSIONS

In summary, sixteen heterocyclic and carbocylic radical isomers have been extensively studied, out of which, four are heteroatom centered and the remaining are C-centered radicals. All of the heteroatom radicals and **2a** were found to be π-centered, however, singly occupied molecular orbitals (SOMO) and their spin density values demonstrate a variable amount of σ−character in the *B*- and *P*-centered radicals. On the basis of high localization of spin values, all of the α-and β-centered radicals are found to be σ-radicals. Among all ofthe radicals that we investigated, the π-centered radicals are found to be the most stable. On the other hand, the β-centered radicals are relatively more stabilized relative to their corresponding α-centered σ-radicals. Particularly the estimated C-H BDE's fit very well with the trend shown in the stability of α-centered and β-centered radicals. Various factors like spin density, SOMO, strain energy, resonance energy and aromaticity have been accounted

for their stability. Except for boron based radicals, we found out that all of the radical isomers showed linear correlation between the relative strain energy and the %s character of the hetero and carbon atoms. Despite the higher ring strain, the dominating π-delocalization of the radical electron leading to higher stabilization of all the heteroatom centered and **2a** radicals. Similarly, more delocalization and lower ring strain can be accounted for relatively higher stability of β-centered over α-centered radical isomers. Interestingly, the delocalization of radical electron in π-centered radicals leads to a *quasi*-antiaromatic system. Overall, a competition between delocalization of radical electron or spin and the ring strain exists that dictates the overall stability of the five membered heterocyclic/carbocyclic radicals.

4.4 REFERENCES

1. Conjugated Carbon Centered Radicals, High-Spin System and Carbenes; Fischer, H.; Eds.; Academic: Berlin, 2002.

2. Trinquier, G.; Malrieu, J. − P. Spreading out Spin Density in Polyphenalenyl Radicals. *Phys. Chem. Chem. Phys.* **2017**, *19*, 27623−27642.

3. Hoffmann, R. Interaction of Orbitals Through Space and Through Bonds. *Acc. Chem. Res*. **1971**, *4*, 1−9.

4. Dougherty, D. A. Spin Control in Organic Molecules. *Acc. Chem. Res*. **1991**, *24*, 88−94.

5. Rajca, A. Organic Diradicals and Polyradicals: From Spin Coupling to Magnetism? *Chem. Rev*. **1994**, *94*, 871−893.

6. Mitoraj, M.; Zhu, H.; Michalak, A.; Ziegler, T. Relating the Radical Stabilization Energy and Steric Bulk of a Hydrocarbyl Group to the Strength of its Bonds with Metals and Hydrogen: A Theoretical Study. *Organometallics*. **2007**, *26*, 1627−1634.

7. Hicks, R. G. Stable Radicals: Fundamentals and Applied Aspects of Odd-Electron Compounds; John Wiley & Sons, Ltd: Wiltshire, U.K., 2010.

8. Xie, C. J.; Lahti, P. M.; George, C. Modulating Spin Delocalization in Phenoxy Radicals Conjugated with Heterocycles. *Org. Lett.* **2000**, *2*, 3417−3420.

9. Leitch, A. A.; Brusso, J. L.; Cvrkalj, K.; Reed, R. W.; Robertson, C. M.; Dube, P. A.; Oakley, R. T. Spin-canting in Heavy Atom Heterocyclic Radicals. *Chem. Commun.* **2007**, *32*, 3368−3370.

10. Sah, C.; Jacob, L.; Saraswat, M.; Venkataramani, S. Does a Nitrogen Lone Pair Lead to Two Centered−Three Electron (2c−3e) Interactions in Pyridyl Radical Isomers? *J. Phys. Chem. A.* **2017**, *121*, 3781−3791.

11. Saraswat, M.; Venkataramani, S. Through Bond and Through Space Interactions in Dehydro-Diazine Radicals: A Case Study of 3c-5e Interactions. *Phys. Chem. Chem. Phys.* **2018**, *20*, 4386−4395.

12. Mo, Y. The Resonance Energy of Benzene: A Revisit. *J. Phys. Chem. A.* **2009**, *113,* 5163–5169.

13. Schleyer, P. V. R.; Pu1hlhofer, F. Recommendations for the Evaluation of Aromatic Stabilization Energies. *Org. Lett.* **2002**, *4*, 2873−2876.

14. Mandado, M.; Otero, N.; Mosquera, R. A. Local Aromaticity Study of Heterocycles Using *N*-Center Delocalization Indices: The Role of Aromaticity on the Relative Stability of Position Isomers. *Tetrahedron.* **2006**, *62*, 12204–12210.

15. Campbell, P. G.; Abbey, E. R.; Neiner, D.; Grant, D. J.; Dixon, D. A.; Liu, S. Y. Resonance Stabilization Energy of 1,2-Azaborines: A Quantitative Experimental Study by Reaction Calorimetry. *J. Am. Chem. Soc.* **2010**, *132*, 18048–18050.

16. Gordon, M. S. Ring Strain in Cyclopropane, Cyclopropene, Silacyclopropane, and Silacyclopropene. *J. Am. Chem. Soc.* **1980**, *102*, 7419−7422.

17. Borst, M. L. G.; Ehlers, A. W.; Lammertsma, K. G3(MP2) Ring Strain in Bicyclic Phosphorus Heterocycles and Their Hydrocarbon Analogues. *J. Org. Chem.* **2005**, *70*, 8110−8116.

18. Bach, R. D.; Dmitrenko, O. The Effect of Carbonyl Substitution on the Strain Energy of Small Ring Compounds and Their Six-Member Ring Reference Compounds. *J. Am. Chem. Soc.* **2006**, *128*, 4598−4611.

19. Mukhopadhyay, A.; Jacob, L.; Venkataramani, S. Dehydro-Oxazole, Thiazole and Imidazole Radicals: Insights into the Electronic Structure, Stability and Reactivity Aspects. *Phys. Chem. Chem. Phys*. **2017**, *19*, 394−407.

20. Alabugin, I. V.; Bresch, S.; Manoharan, M. Hybridization Trends for Main Group Elements and Expanding the Bent's Rule Beyond Carbon: More than Electronegativity. *J. Phys. Chem. A*. **2014**, *118* (20), 3663–3677.

21. Alabugin, I. V.; Bresch, S.; Gomes, G. D. P. Orbital Hybridization: A Key Electronic Factor in Control of Structure and Reactivity. *J. Phys. Org. Chem*. **2015**, *28,* 147–162.

22. Izgorodina, E. I.; Coote, M. L.; Radom, L.Trends in R-X Bond Dissociation Energies (R = Me, Et, i-Pr, t-Bu; X = H, CH3, OCH3, OH, F): A Surprising Shortcoming of Density Functional Theory. *J. Phys. Chem. A*. **2005**, *109* (33), 7558–7566.

23. Lu, D.; Wu, C.; Li, P. 3-Center-5-Electron Boryl Radicals with $\sigma^0\pi^1$ Ground State Electronic Structure. *Org. Lett.* **2014**, *16*, 1486−1489.

24. Alabugin, I. V. *Stereoelectronic Effects: A Bridge Between Structure and Reactivity*; John Wiley & Sons, Ltd.: Chichester, UK, 2016.

25. Alabugin, I. V.Stereoelectronic Interactions in Cyclohexane, 1,3-Dioxane, 1,3-Oxathiane, and 1,3-Dithiane: W-Effect, $\sigma_{C-X} \leftrightarrow \sigma^*_{C-H}$ Interactions, Anomeric Effect − What is Really Important? *J. Org. Chem.* **2000**, *65* (13), 3910–3919.

26. Ponomarev, D. A.; Takhistov, V. V. What are Isodesmic Reactions? *J. Chem. Educ*. **1997**, *74,* 201−203.

27. Bachrach, S. M. *Computational Organic Chemistry*; John Wiley & Sons, Inc: New Jersey, 2014.

28. Steven M. Bachrach. On the Destabilization (Strain) Energy of Biphenylene. *J. Phys. Chem. A*. **2008**, *112*, 7750–7754.

29. Tuttle, T.; Kraka, E.; Cremer, D. Docking, Triggering, and Biological Activity of Dynemicin A in DNA: A Computational Study. *J. Am. Chem. Soc*. **2005**, *127*, 9469−9484.

30. Bachrach, S. M. The Group Equivalent Reaction: An Improved Method for Determining Ring Strain Energy. *J. Chem. Educ*. **1990**, *67,* 907−908.

Chapter 5

Photochemistry of 2-hydroxyphenylazo-3,5-dimethylisoxazole under matrix isolation conditions

5.1 Introduction

Azoheteroarenes are one of the most popular classes of photoswitches in recent times. The presence of five-membered heterocyclic rings gives additional benefits such as better separation in the electronic spectra of *E*- and *Z*-isomers, photoswitching efficiency, reversibility and also the thermal stabilization of *Z*-isomers.[1-3] Several groups have introduced different heterocycles for tuning the properties towards obtaining the most efficient azoheteroarene based photoswithces. The photochemistry of azoarenes have been largely explored in solution form. The photochromic behaviour associated with them have been constantly followed by UV-Vis spectroscopy and NMR spectroscopy. However, infrared spectroscopic investigation on such effect will be interesting. Unlike the commonly observed broad spectral feature arising in the electronic spectroscopy or the time averaged spectral features arising in NMR spectroscopic techniques associated with the photoswitching of azoarenes, the infrared spectroscopy will provide unique features. Although infrared spectroscopy is associated with the spectral broadening, under matrix isolation conditions, the spectral features are generally sharp. This can be mainly attributed to the restriction in the molecular rotations, limitations to the intermolecular interactions and also the lower temperature (4 K) that avoids the collisional broadening. This will provide unique opportunities in undermining the photochemistry, and also characterization of the photoproducts.

Recently, Reva and co-workers have explored the possibility of photoisomerization of azobenzene in argon matrices. Based on their reports, the simple azobenzene (AB) did not exhibit the forward *E-Z* photoisomerization in argon matrix.[4] On the other hand, the isolation of *Z*-isomer in the matrix can allow it to show photochemistry in the reverse direction (*Z-E*). However, both *E-Z* and *Z-E* isomerization processes were observed in xenon matrix.[5] The photoisomerization efficiency increases at elevated temperature (60 K). In yet another work, the same group have explored the photochemistry of 2,2'-dihydroxyazobenzene (DAB) and azotoluene (AT).[5] On irradiation, DAB exhibited reversible *E-E* isomerization. No *Z* form was observed due to the presence of strong intramolecular hydrogen bond (OH…N) interactions. On the other hand, forward isomerization (*E-Z*) and reversible photoisomerization (*Z-E*) was observed in the case of azotoluene (AT). The photoisomerization may be attributed to the repulsive interactions of two methyl groups with azo fragment.

During our recent explorations on azoheteroarenes in our group, we reported a new class of azoisoxazole based photoswitch (i.e. 2-hydroxyphenylazo-3,5-dimethylisoxazole **1**), which showed excellent photoswitching and light induced phase transition.[6] On irradiation, the molecule **1** can undergo three possible channels; (a) It can undergo tautomerism due to the presence of *o*-hydroxy group (potential hydrogen bonding group) (b) It can undergo *E-Z* photoisomerization due to the presence of two methyl groups in the isoxazole unit (possibly prevent the stacking and provide room for photoswitching) and (c) It can also undergo *E-E* conformational change as shown in **scheme 5.1** In this regard, we wanted to explore the competition between tautomerism, photoswitching and conformational change channels, and find out the dominating channel. We intended to explore this using matrix isolation IR

spectroscopy in combination with computations, which can clearly exhibit majorly sharp vibrational features that can be used to differentiate between the competing channels. Through this investigations, we report the matrix isolation infrared spectroscopic and computational studies on the photoisomerization of 2-hydroxyphenylazo-3,5-dimethylisoxazole **1** in argon matrix at 4 K.
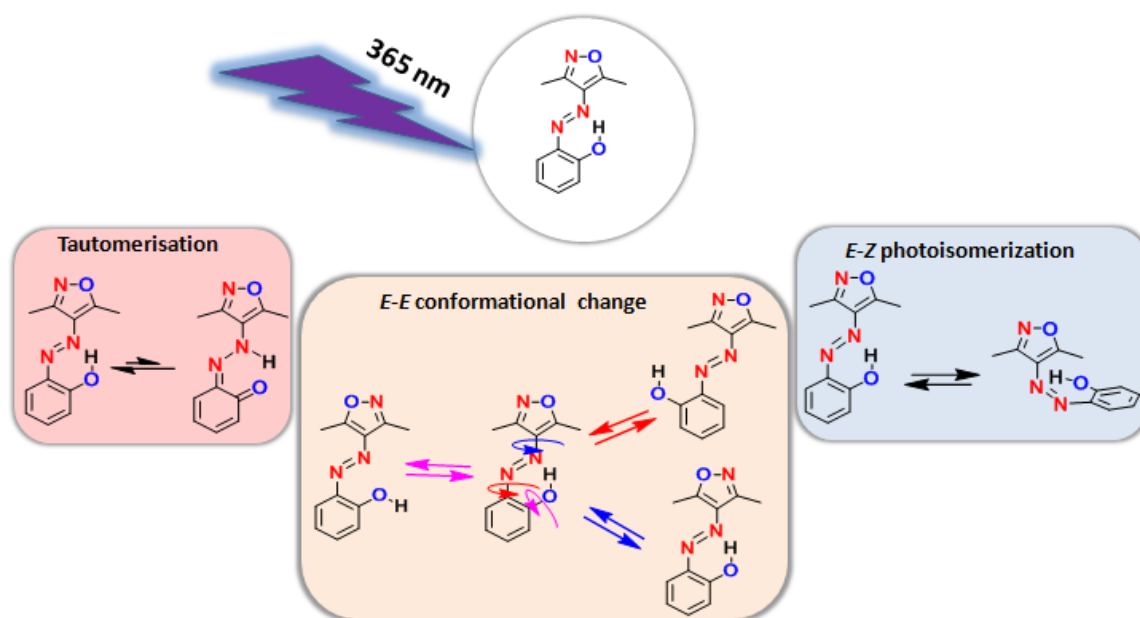
Scheme 5.1 Possible competing channels on photolysis of 2-hydroxyphenylazo-3,5-dimethylisoxazole.

5.2 Motivation

In our group, we are working on arylazo-3,5-dimethylisoxazole photoswitches. Interestingly, the parent molecule (i.e. phenylazo-3,5-dimethylisoxazole) exhibited light induced phase transition. The unsubstituted phenylazo-3,5-dimethylisoxazole in its native state got converted from yellow solid to molten red liquid on irradiation with 365 nm light[6] as depicted in **scheme 5.2**.
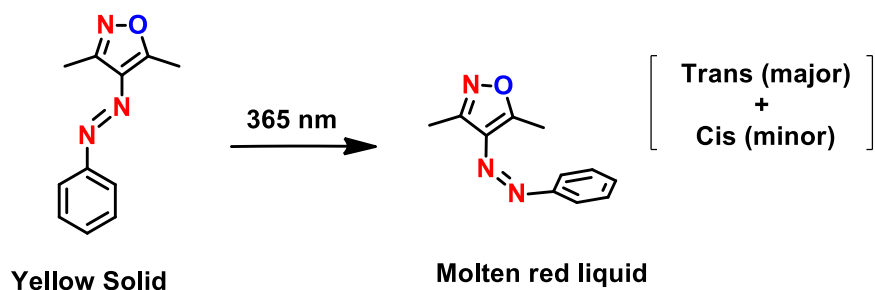
Scheme 5.2 Light induced phase transition exhibited by phenylazo-3,5-dimethylisoxazole on irradiation with 365 nm light.

Figure 5.1 Matrix isolation infrared spectroscopic studies on phenylazo-3,5-dimethylazoisoxazole. **(a)** Deposition spectrum (Ar, 4 K, Deposition conditions: 60 $^\circ$C, 75 min); **(b)** After irradiation at 365 nm for 50 min.

In order to understand the light induced phase transition phenomenon in the phenylazo-3,5-dimethylisoxazole, we intended to ascertain whether the conformational changes or the molecule undergoes photoisomerization. This gave us the motivation to study this particular molecule to look into the conformational changes or photoisomerization under matrix isolation condition. In this regard, the sample was heated at 60 $^\circ$C ″using buchi″ oven for 75 minutes and was deposited on to the KBr window at 4 K with a large excess of argon gas.

The matrix was irradiated with 365 nm light for 50 minutes duration. On inducing photochemistry; instead of the bleaching of precursor signals, the signal intensity got enhanced as shown in **figure 5.1**.

Moreover, the signals obtained were broad, presumably the conformational changes along with photoisomerization might be responsible for such changes. For this reason we couldn't continue with this particular molecule. Instead of this, we have chosen another system. In order to bring the complexity, we introduced hydroxy group in the *ortho* position of the phenyl ring. This opens up the possibilities such as (a) *E-E* conformational change, (b) *E-Z* photoisomerization and (c) tautomerization on photolysis. The detailed insights for the molecule (i.e. 2-hydroxyphenylazo-3,5-dimethylisoxazole) is discussed in the proceeding sections of this chapter.

5.3 Materials and Methods
5.3.1 Synthesis and Matrix isolation IR spectroscopy

2-Hydroxyphenylazo-3,5-dimethylisoxazole (HPAI) was synthesized from 2-hydroxyaniline using the already reported procedure,[6] as per the **Scheme 5.3**. Matrix IR spectrum was recorded on a Bruker Tensor II FTIR instrument in absorbance mode. The compound vapor was codeposited with a large excess of Ar gas on to a KBr window cooled at 4 K using a closed cycle Helium compressor. The deposition and irradiation temperature were maintained at 4 K. The Infrared spectra was recorded in the mid IR range from 4000-400 cm^{-1}. All spectra were recorded for 128 scans with a 0.5 cm^{-1} resolution.

The sample was heated at 170 $^{\circ}$C ″using buchi″ oven for 70 minutes and was deposited on to the KBr window kept at 4 K with large excess of argon gas. The matrix was irradiated

through quartz window using 365 nm light. The experimental results were assisted by computations using the Gaussian 09 program package. All the calculations were performed using the M06-2X functional and cc-pVTZ as the basis set. Vibrational frequencies in the harmonic approximation calculations have been performed to confirm the minima and also to obtain thermochemistry data including zero-point energy corrections.
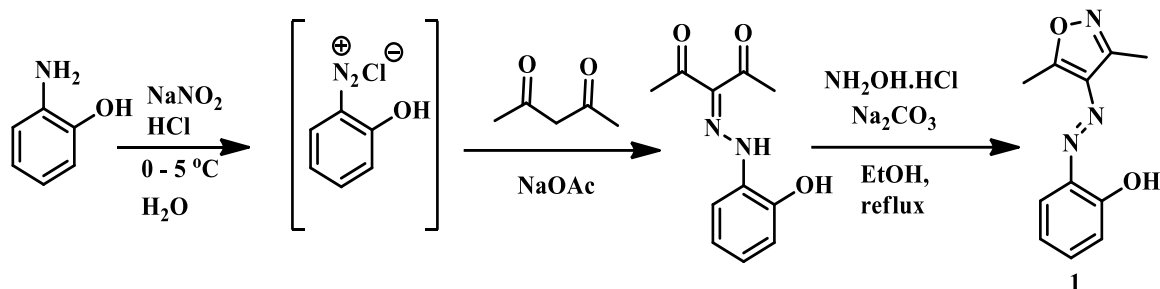
Scheme 5.3 Synthesis of 2-hydroxyphenylazo-3,5-dimethylisoxazole (HPAI).

5.4 Results and Discussion

5.4.1 Geometries and energies

HPAI possess a hydroxy group at the *ortho* position of phenyl ring. It can adopt azo-enol and keto-hydrazone as the tautomeric forms. Azo-enol can have *syn* (OH towards N=N) and *anti* (OH away from N=N) conformers, denoted by *s* and *a* in the nomenclature for the optimized geometries in **figure 5.2**. Taking all this into consideration we have optimized 12 possible conformers for the *trans* form. Here, C1 and C2 denotes the N-O and O-N orientation of isoxazole unit with the hydroxy group on the right. Whereas, C3 and C4 denotes the N-O and O-N orientation of the isoxazole unit with the hydroxy group on the left. All these conformers can undergo isomerization to *cis* form around the CNNC moiety. The optimized geometries and the relative energies of the 12 possible conformers are shown in **Figure 5.2** and **Table 5.1**.

1E-C1-a   1E-C1-s   1E-C1-s-keto   1E-C2-a   1E-C2-s   1E-C2-s-keto

1E-C3-a   1E-C3-s   1E-C3-s-keto   1E-C4-a   1E-C4-s   1E-C4-s-keto
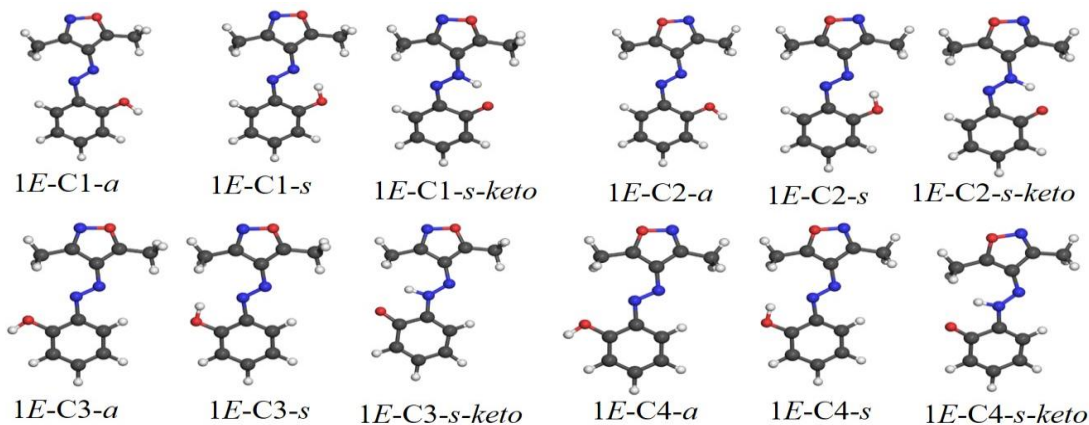
Figure 5.2 The optimized geometries of different conformers of *E*-isomeric forms of 2-hydroxyphenylazo-3,5-dimethylisoxazole (HPAI) calculated at M06-2X/cc-pVTZ level of theory.

As per the calculations, the *E* conformers are lower in energy than their *Z* counterparts. Among all the conformers of HPAI, the most stable is **1E-C1-s** followed by **1E-C2-s**, bearing six-membered quasi ring stabilized by intramolecular hydrogen bond (OH…N) interactions. The other two *syn* conformers (**1E-C3-s** and **1E-C4-s**) are stabilized by five-membered H-bonded quasi ring. The *anti* conformers of *E*-form had relatively higher energy than their corresponding *syn* forms. After understanding the structural and stability aspects of the *E*-conformers, we estimated the relative population by taking the population ratio of the other possible conformers with respect to the most stable conformer (i.e.1*E*-C1-*s*) by using the Gibbs free energy (ΔG) at 298.15 K as follows:

$$N_{1E\text{-}C1\text{-}s} = e^{-G_{1E-C1-s}/k_B.T} \quad \text{..............(1)}$$

$$N_{1E\text{-}C2\text{-}s} = e^{-G_{1E-C2-s}/k_B.T} \quad \text{...............(2)}$$

Dividing equation (2) by equation (1) we get

$$N_{1E\text{-}C2\text{-}s}/ N_{1E\text{-}C1\text{-}s} = e^{-\Delta G/k_B.T}$$

Here, $\Delta G = G_{1E\text{-}C2\text{-}S} - G_{1E\text{-}C1\text{-}S}$

1E-C1-s with a relative population 93.8% is expected to be the major contributor in the

deposited matrices. The other conformers (**1E-C2-s** and **1E-C3-s**) could also be present in the deposited matrices as per their relative population 1.9 and 3.8% respectively. The total contribution of all the *anti* and *keto* forms of *E* conformer is 0.5%. We have also estimated the population analysis for the Gibbs free energy at the deposition temperature (i.e. 443 K). The relative population of 1*E*-C1-*s* was 98.5% and the rest of the conformers contributed 1.5% as shown in **Table 5.2.**

Table 5.1 Relative energy (in kcal/mol) of isomeric forms of 2-hydroxyphenylazo-3,5-dimethylisoxazole (HPAI) calculated at M06-2X/cc-pVTZ level of theory. The absolute energies are zero-point corrected.

HPAI	Relative Energy (kcal/mol)	HPAI	Relative Energy (kcal/mol)
1*E*-C1-*s*	0.0	1Z-C4-*s*	15.6
1*E*-C2-*s*	1.2	1Z-C1-*s*	18.1
1*E*-C3-*s*	1.4	1Z-C2-*s*	18.2
1*E*-C4-*s*	2.8	1Z-C2-*a*	18.4
1*E*-C3-*a*	6.1	1Z-C1-*a*	18.7
1*E*-C4-*a*	7.4	1Z-C3-*a*	19.3
1*E*-C1-*a*	9.3	1Z-C4-*a*	19.6
1*E*-C1-*s-keto*	9.3	1*E*-C3-*s-keto*	21.9
1*E*-C2-*s-keto*	10.1	1*E*-C4-*s-keto*	22.8
1*E*-C2-*a*	11.0	1Z-C2-*s-keto*	25.9
1Z-C3-*s*	14.9	1Z-C1-*s-keto*	26.2

5.4.2 Infrared spectra of matrix-isolated HPAI

The matrix isolated IR data of HPAI in argon matrix at 4 K exhibited prominent features at 1627.0, 1487.0, 1279.0 and 754.5 cm^{-1}. In order to analyze the spectrum, various conformers of the HPAI have been considered. Since HPAI has the hydroxy group at the proximal position to the azo group, tautomeric structures (i.e. keto-hydrazone) associated with this conformations have also been considered. The resulting keto structure is expected to have a prominent carbonyl stretching around 1650-1750 cm^{-1} range. Upon examining the resulting spectral data, no such signals was observed that can be attributed to the carbonyl stretching.

Hence, the possibility of keto tautomer in the matrix is ruled out. The experimental infrared spectra of HPAI in argon matrix at 4 K had correspondences with calculated spectra **1*E*-C1-*s*,** **1*E*-C2-*s*** and **1*E*-C3-*s*** at M06-2X/cc-pVTZ level of theory. The region below 1800 cm^{-1} had a good resemblance with the calculated spectra of **1*E*-C1-*s***. Most of the signals of the *trans* conformers falls around similar frequencies. Based on the relative population at room temperature, estimated from the calculated Gibbs free energy at 298.15 K and the Boltzmann distribution (93.8 %), **1*E*-C1-*s*** has been identified as the major contributor to the gas-phase equilibrium, which could also be dominant conformer in the deposited matrices. At higher frequencies, the absence of free OH peak around 3600 cm^{-1} and the presence of broad feature around 3200-2700 cm^{-1} signifies the involvement of OH in strong intramolecular OH…N hydrogen bonds through six-membered quasi ring (i.e. **1*E*-C1-*s*** and **1*E*-C2-*s***). Indeed such large shifts in the OH stretching due to hydrogen bonding have been reported for 2-nitrophenol and 2,2'-dihydroxyazobezene.[5,7] Whereas, a weak signal at 3480 cm^{-1} corresponds to the presence of relatively weaker OH…N interactions through five-membered quasi ring (i.e. **1*E*-C3-*s***). In this regard, **1*E*-C1-*s*,** **1*E*-C2-*s*** and **1*E*-C3-*s*** were the contributors among the various possible *E*-conformers that can be accountable to the observed features of HPAI as shown in **Figure 5.3** and were in good agreement with the relative population analysis as given in **Table 5.2**. Due to the presence of three conformers in the deposited matrix, we considered the relative population at 298.15 K over the deposition temperature (443 K)[5]. The peaks around 1600 cm^{-1} also showed broadening due to strong hydrogen bonding. Similar observations were also reported on a study on the isomerization of 2-nitrophenol molecule by Nakata et al.[7] The frequencies and the relative intensity of the calculated and the experimental spectra has been tabulated as **Table 5.3**.
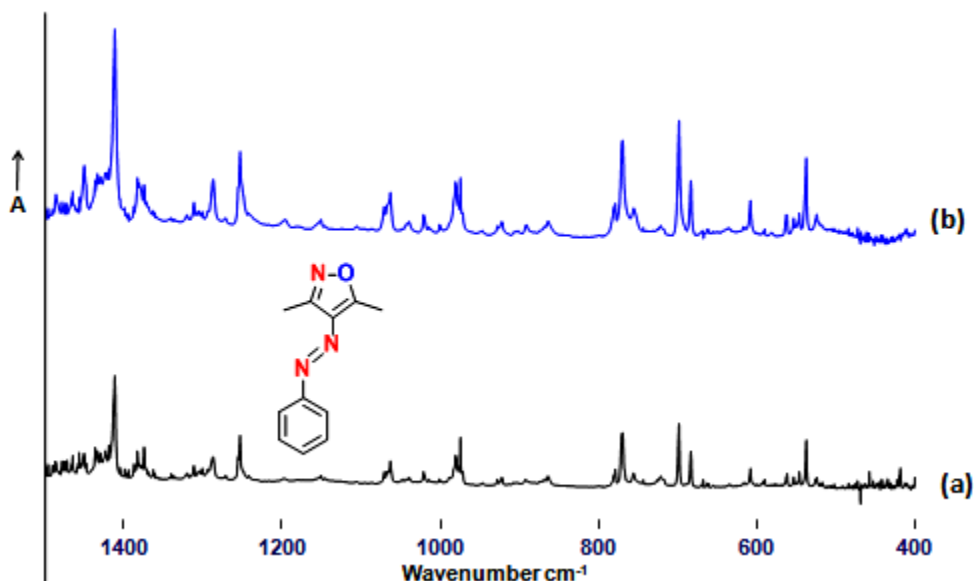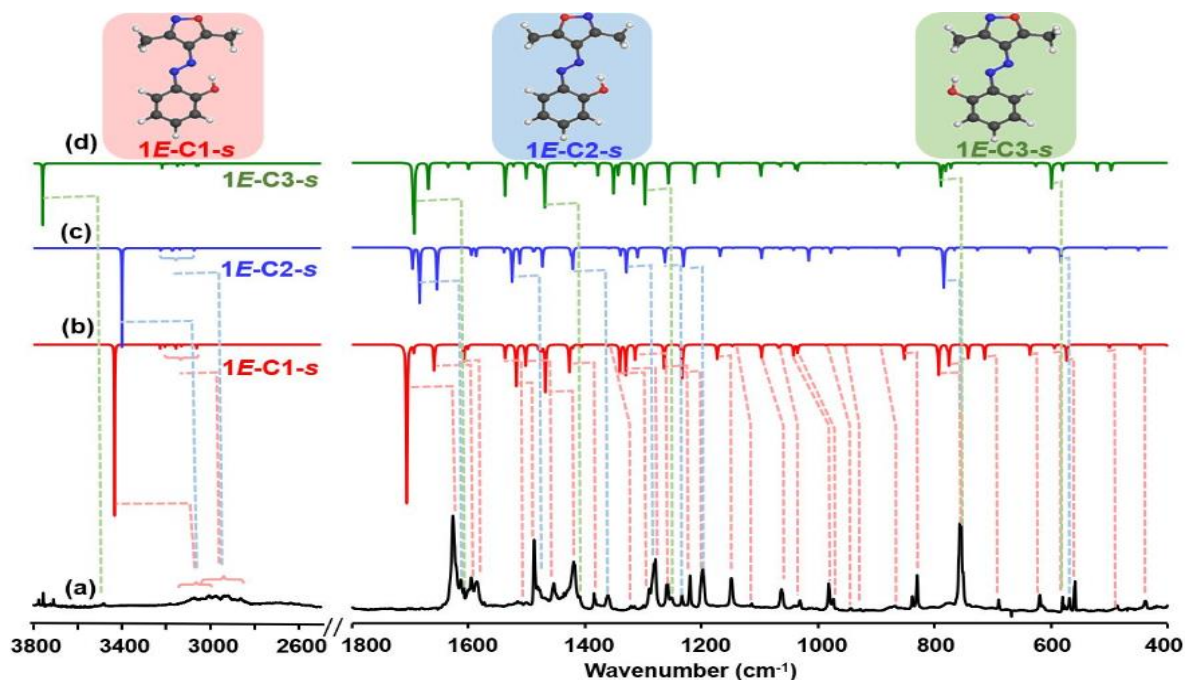
Figure 5.3 Matrix isolation infrared spectroscopic studies on HPAI. (**a**) Deposition spectrum (Ar, 4 K, Deposition conditions: 170 $^{\circ}$C, 70 min); (**b-d**) Computed spectra of the conformers 1*E*-C1-*s,* 1*E*-C2-*s* and 1*E*-C3-*s (*M06-2X/cc-pVTZ level of theory, unscaled).

Table 5.2 Relative population of *E-* isomeric forms of 2-hydroxyphenylazo-3,5-dimethylisoxazole (HPAI) calculated at M06-2X/cc-pVTZ level of theory. For the relative energy, absolute energies are zero-point corrected. Thermal corrections to the Gibbs free energies has been considered for the relative population estimation.

S.NO	HPAI	Relative Energy (kcal/mol)	Relative Population (%)[a]	Relative Population (%)[b]
1	1*E*-C1-*s*	0.0	93.8	98.5
2	1*E*-C2-*s*	1.2	1.9	0.6
3	1*E*-C3-*s*	1.4	3.8	0.8
4	1*E*-C4-*s*	2.8	4.9×10^{-1}	2.0×10^{-1}
5	1*E*-C3-*a*	6.1	1.0×10^{-2}	2.5×10^{-2}
6	1*E*-C4-*a*	7.4	4.2×10^{-4}	5.3×10^{-4}
7	1*E*-C1-*a*	9.3	8.3×10^{-6}	6.5×10^{-6}
8	1*E*-C1-*s-keto*	9.3	3.6×10^{-5}	5.3×10^{-5}
9	1*E*-C2-*s-keto*	10.1	1.5×10^{-6}	8.0×10^{-7}
10	1*E*-C2-*a*	11.0	6.3×10^{-7}	5.4×10^{-7}
11	1*E*-C3-*s-keto*	21.9	3.2×10^{-15}	1.5×10^{-15}
12	1*E*-C4-*s-keto*	22.8	1.0×10^{-15}	6.0×10^{-16}

[a]Gibbs free energies at 298.15 K; [b]Gibbs free energies at 443 K

Table 5.3 Computed frequency and intensity of 1*E*-C1-*s*, 1*E*-C2-*s* and 1*E*-C3-*s* at M06-2X/cc-pVTZ level of theory along with the experimental frequency and intensity of the deposited HPAI.

Normal Mode	Symmetry	Computed				Experimental (Ar, 4 K)		Tentative Assignments
		$\tilde{\upsilon}_{calcd.}$ (cm^{-1}) 1*E*-C1-*s*	$\tilde{\upsilon}_{calcd.}$ (cm^{-1}) 1*E*-C2-*s*	$\tilde{\upsilon}_{calcd.}$ (cm^{-1}) 1*E*-C3-*s*	I_{rel}	$\tilde{\upsilon}$ (cm^{-1})	I_{rel}	
75	A			3759.6	49	3484.0	2	ν(OH)
						3072.0	5	
						3041.5	4	
75	A+ A′	3434.5	3401.7		100	3007.5	7	ν(OH)
						2987.5	6	
						2974.5	6	
						2944.5	6	
						2936.5	7	
						2921.0	6	
						2864.0	4	
64	A	1706.1			90	1627.0	100	ν_{ph}(CC)+$\boldsymbol{\delta}_{ph}$(CH)+$\boldsymbol{\delta}$(OH)+$\boldsymbol{\delta_{ph}}$(NNC)+ ν_{iso}(CC)+ν_{iso}(CN)
63	A′		1684.0		53	1613.0	29	ν_{ph}(CC) + ν_{iso}(CC) +ν_{iso}(CN)+ν(NN)+$\boldsymbol{\delta}_{iso}$(CH$_3$)+$\boldsymbol{\delta}$(OH)
63	A			1693.8	51	1608.0	19	ν_{ph}(CC)+ν_{iso}(CC)+ ν_{iso}(CN)+ν(NN)+$\boldsymbol{\delta}_{iso}$(CH$_3$)+$\boldsymbol{\delta_{iso}}$(CNN$_{azo}$)
62	A	1659.6			15	1595.0	31	ν_{ph}(CC)+$\boldsymbol{\delta}_{ph}$(CH)+$\boldsymbol{\delta}$(OH)+ν(NN)
						1585.5	27	
						1573.0	5	
58	A	1518.6			23	1487.0	73	ν_{ph}(CC)+$\boldsymbol{\delta}_{ph}$(CH)+ν(NN)+ν_{ph}(CO)
57	A	1502.7			12	1481.5	21	ν_{iso}(CC)+$\boldsymbol{\delta}_{iso}$(CH$_3$)
						1477.0	18	
53	A	1468.6			27	1453.5	25	ν_{iso}(CC)+$\boldsymbol{\delta}_{iso}$(CH$_3$)
						1436.0	10	
58	A′		1525.4		33	1419.5	49	ν_{ph}(CC)+ν_{iso}(CC)+$\boldsymbol{\delta}_{iso}$(CH$_3$)+$\boldsymbol{\delta}$(OH)+$\boldsymbol{\delta}_{ph}$(CH)
						1409.0	15	

Normal Mode	Symmetry	Computed				Experimental (Ar, 4 K)		Tentative Assignments
		$\tilde{\upsilon}_{calcd.}$ (cm^{-1}) 1E-C1-s	$\tilde{\upsilon}_{calcd.}$ (cm^{-1}) 1E-C2-s	$\tilde{\upsilon}_{calcd.}$ (cm^{-1}) 1E-C3-s	I_{rel}	υ (cm^{-1})	I_{rel}	
52	A	1427.4			16	1385.0	19	$\nu_{ph}(CC)+\delta_{ph}(CH)+\delta(OH)$
						1361.0	16	
						1321.5	5	
						1315.0	5	
						1300.0	5	
						1290.0	22	
						1281.5	50	
47	A	1330.7			17	1279.0	55	$\nu_{ph}(CO)+\nu_{ph}(CC)+\delta_{ph}(CH)+\delta(OH)$
46	A	1314.0			9	1258.0	28	$\nu_{ph}(CN_{azo}) +\nu_{iso}(CN_{azo})\delta(OH) +\delta_{ph}(CH) +\delta_{iso}(CH_3)$
46	A			1297.1	34	1251.5	12	$\nu_{ph}(CC)+\nu_{iso}(CC)+\nu_{ph}(CO)+\delta(OH)+\delta_{ph}(CH)$
						1233.5	15	
45	A	1264.5			14	1220.0	36	$\nu_{iso}(CN_{azo})+\delta(OH)+\delta_{ph}(CH)$
44	A	1233.5			19	1198.0	44	$\nu_{ph}(CN_{azo})+\delta(OH)+\delta_{ph}(CH)+\nu_{ph}(CC)$
43	A	1173.5			8	1149.0	31	$\delta_{ph}(CH)$
						1114.0	4	
41	A	1097.9			7	1062.5	21	$\nu_{iso}(C\text{-}CH_3)+\delta_{ph}(CH)+\delta_{iso}(CH_3)+\delta_{Ph}(ring)+\delta_{iso}(CCO)$
						1031.0	10	
37	A	1042.8			6	981.5	30	$\gamma_{iso}(CH_3)+\nu_{iso}(ON)$
						973.5	13	
						838.0	15	
30	A	852.6			8	830.0	38	$\delta_{Ph}(ring)+\delta_{ph}(CH)+\nu_{ph}(CO)+\delta(NN)+\nu_{iso}(CC)$
						756.5	93	
29+27+29	A + A''+A	793.5	784.4	789.3	17 + 38 + 19	754.5	98	$\gamma_{ph}(CH)+\gamma_{ph}(CN_{azo})+\gamma(OH)$

Normal Mode	Symmetry	Computed				Experimental (Ar, 4 K)		Tentative Assignments
		$\tilde{\nu}_{calcd.}$ (cm^{-1}) 1E-C1-s	$\tilde{\nu}_{calcd.}$ (cm^{-1}) 1E-C2-s	$\tilde{\nu}_{calcd.}$ (cm^{-1}) 1E-C3-s	I_{rel}	$\tilde{\nu}$ (cm^{-1})	I_{rel}	
24	A	714.5			8	690.0	11	
22	A	636.2			6	619.5	17	$\boldsymbol{\delta}_{\mathbf{Ph}}$(ring)+$\boldsymbol{\delta}_{\mathbf{iso}}$(ring)
22	A			599.4	21	580.0	16	γ(OH)
						576.5	7	
20	A′		583.5		14	568.5	15	γ_{iso}(CH$_3$)+$\boldsymbol{\delta}_{\mathbf{iso}}$(ring)+$\underline{\tau}$(CNNC)+$\underline{\tau}_{\mathbf{Ph}}$(ring)
19	A	573.6			9	559.0	34	$\underline{\tau}_{\mathbf{Ph}}$(ring)+$\boldsymbol{\delta}_{\mathbf{iso}}$(ring)+$\boldsymbol{\delta}_{\mathbf{ph}}$(N$_{azo}$CC)+ $\underline{\tau}$(OH)+$\underline{\tau}$(CNNC)
						531.5	1	
						509.5	2	
17	A	500.8			2	486.0	5	γ_{ph}(CH)+γ_{ph}(CN$_{azo}$)
16	A	447.9			3	438.0	9	$\underline{\tau}_{\mathbf{Ph}}$(ring)+$\underline{\tau}_{\mathbf{iso}}$(ring)+$\underline{\tau}$(CNNC)

ν, stretching; δ, in-plane-bending; γ, out-of-plane bending; τ, torsion.

5.4.3 AIM analysis

In order to estimate the extent of hydrogen bonding, we used AIM theory introduced by Bader.[8] Using the optimized geometry of the *trans* conformers computed at the M06-2X/cc-pVTZ level, we searched for a $(3, -1)$ bond critical point (BCP) as shown in **Figure 5.4**. The electron density, $\rho(rc)$, and $\nabla^2 \rho(rc)$ (defined as sum of the Hessian eigenvalues) were analyzed at the bond critical point for all the *trans* conformers. The hydrogen bond energy can be estimated using the Espinosa equation by considering the electron density at the BCP. From the calculations, we observed that the conformers **1*E*-C1-*s*** and **1*E*-C2-*s*** have a strong H-bonding of about 13.8 and 14.3 kcal/mol respectively, whereas for **1*E*-C3-*s*** and **1*E*-C4-*s*** exhibits weak hydrogen bonding around 5.8 kcal/mol.

1*E*-C1-*s*   **1*E*-C2-*s***   **1*E*-C3-*s***   **1*E*-C4-*s***
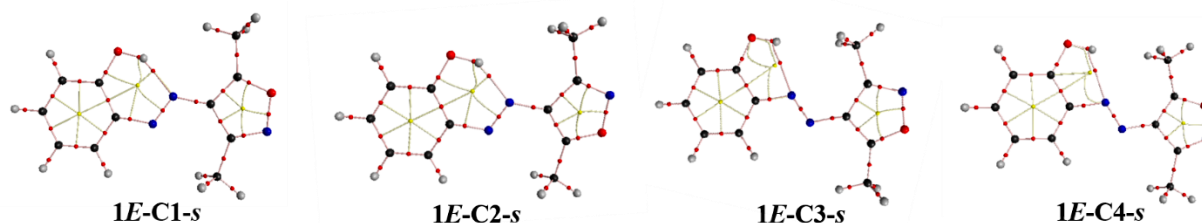
Figure 5.4 Hydrogen bond energy estimation at the bond critical point for the optimized geometry of the trans conformers computed at M06-2X level of theory.

5.4.4 Photochemistry of the matrix isolated HPAI in solid argon

Upon irradiation at 365 nm for 60 minutes, the matrix isolated HPAI showed photochemistry. Majority of the signals due to the sample showed decrease in intensity, whereas some of the signal intensity got increased and many additional signals appeared on irradiation. The decrease of broader region around 3200-2700 cm^{-1} indicates the consumption of OH…N stabilized **1*E*-C1-s** and **1*E*-C2-s** conformers. On the other hand,

increase in intensity at 3484 cm^{-1} is an indication of the formation of a conformer involving a weaker OH…N interaction.

As indicated by Reva and coworkers, we also considered the light induced conformational changes or tautomers, however none of them matched with the observed changes. On contrast, the spectral features of the Z-isomer showed a better agreement with the observed spectral features. To ascertain the product features, we also considered various conformations of the 1-*Z* as shown in **figure 5.5**. In the given nomenclatures, *s* and *a* denotes the *syn* and *anti* conformers. Whereas, C1/C3 and C2/C4 depicts the O-N and N-O orientations of the isoxazole unit.

1Z-C1-*s* 1Z-C1-*s-keto* 1Z-C1-*a* 1Z-C2-*s* 1Z-C2-*s-keto*

1Z-C2-*a* 1Z-C3-*s* 1Z-C3-*a* 1Z-C4-*s* 1Z-C4-*a*
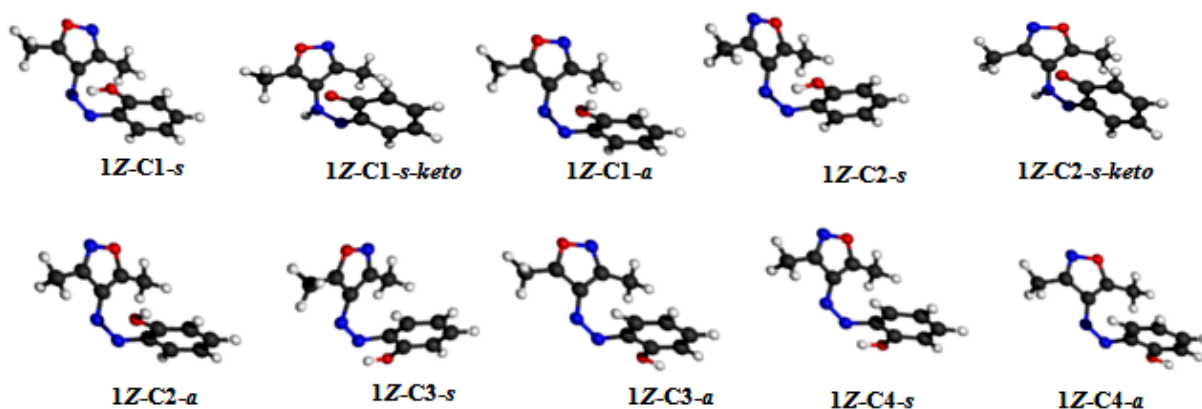
Figure 5.5 The optimized geometries of different conformers of Z-isomeric forms of 2-hydroxyphenylazo-3,5-dimethylisoxazole (HPAI) calculated at M06-2X/cc-pVTZ level of theory.

Once again, the absolute energies are zero-point corrected for the relative energies related to all the conformations. Whereas, thermal corrections to the Gibbs free energy has been considered for the estimation of the relative population. Based on the most populated conformations, the observed spectral features have been compared with the corresponding computed spectra as depicted in **figure 5.6**. The new set of peaks matched with **1Z-C3-*s*** and

1Z-C4-s and was found to be in good agreement with the relative population analysis as given in **Table 5.4**. However on careful examination, the patterns of **1Z-C3-s** fit in more to the newly appeared peaks. The frequencies for calculated and the experimental spectra has been mentioned in **Table 5.5** and **5.6**. On irradiation, the absence of carbonyl stretching and also the frequency shift in hydroxy region rules out the possibility of tautomerization and *E-E* isomerization. Interestingly, the reverse isomerization did not happen even after prolonged irradiation conditions at different wavelengths. Indeed, in solution phase photochemistry, only a partial reverse isomerization was observed.[6] Based on these experiments, the forward *E-Z* photoisomerization have been confirmed. Moreover, the observed photochemistry at 4 K proved that the arylazoisoxazoles are one of the important classes of photoswitches.
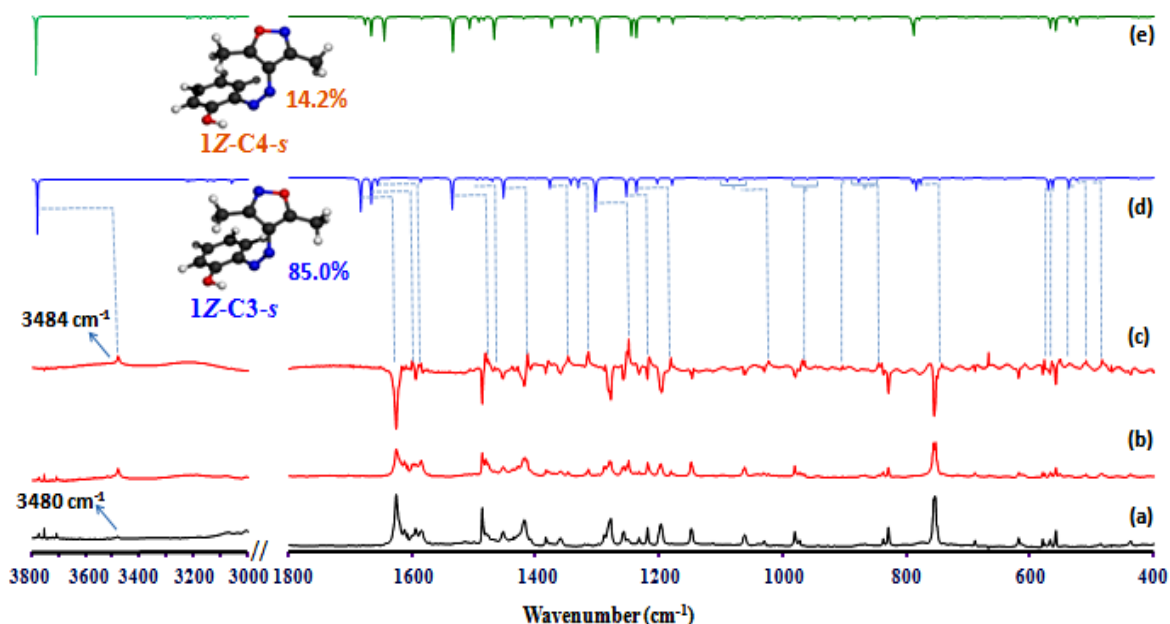
Figure 5.6 Photochemistry of HPAI in argon matrix at 4 K. (**a**) Deposition spectrum of HPAI (Ar, 4 K); (**b**) After irradiation at 365 nm for 60 minutes; (**c**) Difference spectrum; Bands pointing upwards are the new features, whereas the bands pointing downwards are due to the HPAI (*E*-isomer) upon 365 nm irradiation. Computed data of (**d**) 1Z-C3-*s* and (**e**) 1Z-C4-*s* (M06-2X/cc-pVTZ level of theory, unscaled).

Table 5.4 Relative population of Z-isomeric forms of 2-hydroxyphenylazo-3,5-dimethylisoxazole (HPAI) calculated at M06-2X/cc-pVTZ level of theory. For the relative energy, absolute energies are zero-point corrected. Thermal corrections to the Gibbs free energies has been considered for the relative population estimation.

S.NO	HPAI	Relative Energy (kcal/mol)	Relative Population (%)
1	1Z-C3-*s*	0.0	85.0
2	1Z-C4-*s*	0.7	14.2
3	1Z-C1-*s*	3.2	2.1×10^{-1}
4	1Z-C2-*s*	3.4	2.5×10^{-1}
5	1Z-C2-*a*	3.5	1.6×10^{-1}
6	1Z-C1-*a*	3.8	9.7×10^{-2}
7	1Z-C3-*a*	4.4	5.8×10^{-2}
8	1Z-C4-*a*	4.7	2.8×10^{-2}
9	1Z-C2-*s-keto*	11.0	1.0×10^{-6}
10	1Z-C1-*s-keto*	11.4	4.8×10^{-7}

Table 5.5 Computed frequency and intensity of 1Z-C3-*s* at M06-2X/cc-pVTZ level of theory along with the experimental frequency and intensity at 365 nm.

Normal Mode	Symmetry	Computed		Experimental (Ar, 4 K)		$\tilde{\upsilon}_{diff.}$ (cm^{-1})	Tentative Assignments
		$\tilde{\upsilon}_{calcd.}$ (cm^{-1}) 1Z-C3-*s*	I_{rel}	υ (cm^{-1})	I_{rel}		
75	A	3782.8	81	3484.0	39	298.8	ν(OH)
63	A	1684.8	99	1611.0	13	73.8	ν_{ph}(CC)+ ν_{iso}(CC) ν_{iso}(CN)+ ν(NN)+δ_{iso}(CH$_3$)
62	A	1667.2	76	1600.5	36	66.7	ν_{ph}(CC)+ ν_{iso}(CC)+ν(NN)+δ_{ph}(CH) +δ(OH)
61	A	1657.5	22	1587.0	25	70.5	ν_{ph}(CC)+ ν_{iso}(CC) ν(NN)+δ_{ph}(CH) +δ(OH)
59	A	1536.2	93	1482.0	58	54.2	ν_{ph}(CO)+ ν_{ph}(CC)+δ_{ph}(CH)
57	A	1496.5	6	1467.0	16	29.5	ν_{iso}(CO)+ ν_{iso}(CC)+δ_{iso}(CH$_3$)
56	A	1486.9	5	1439.0	16	47.9	δ_{iso}(CH$_3$)
54	A	1471.5	10	1431.0	15	40.5	δ_{iso}(CH$_3$)
53	A	1453	59	1414.0	67	39.0	ν_{iso}(CO)+ ν_{iso}(CC)+δ_{iso}(CH$_3$)
50	A	1378.4	31	1348.0	34	30.4	ν_{ph}(CC)+ δ_{ph}(CH) +δ(OH)
48	A	1332.6	29	1316.0	58	16.6	ν_{iso}(CO)+ ν_{iso}(CC)+δ_{iso}(CH$_3$)
47	A	1304.1	100	1250.0	100	54.1	ν_{ph}(CO)+ ν_{ph}(CC)+δ_{ph}(CH) +δ(OH)

Normal Mode	Symmetry	Computed		Experimental (Ar, 4 K)		$\vartheta_{diff.}$ (cm^{-1})	Tentative Assignments
		$\vartheta_{calcd.}$ (cm^{-1}) 1Z-C3-s	I_{rel}	ϑ (cm^{-1})	I_{rel}		
45	A	1238.6	42	1182.0	53	56.6	$\nu_{iso}(CN_{azo})$+ $\nu_{ph}(CN_{azo})$ +$\nu_{ph}(CC)$+$\delta_{ph}(CH)$ +$\delta(OH)$
40	A	1071.3	7	1024.0	26	47.3	$\nu_{ph}(CC)$+$\delta_{ph}(CH)$
34	A	983.9	5	970.0	40	13.9	$\gamma_{ph}(CH)$
33	A	962	5	966.0	41	−4.0	$\nu_{iso}(NO)$+$\gamma_{iso}(CH_3)$
32	A	905.8	4	905.0	16	0.8	$\gamma_{ph}(CH)$+ $\gamma_{ph}(CN_{azo})$
31	A	878	13	846.0	32	32.0	$\gamma_{ph}(CH)$+$\gamma_{ph}(CN_{azo})$
30	A	862.3	6	841.0	33	21.3	$\delta_{ph}(ring)$+$\nu_{ph}(CO)$
28	A	785.9	36	743.0	20	42.9	$\gamma_{ph}(CH)$+ $\gamma_{ph}(CN_{azo})$
20	A	571.5	35	577.0	34	−5.5	$\gamma(OH)$+$\delta_{ph}(ring)$
19	A	564.2	28	565.0	31	−0.8	$\gamma(OH)$
				553.0	28		
17	A	525.1	8	510.0	31	15.1	$\gamma(OH)$+$\delta_{ph}(ring)$
16	A	495	4	485.0	41	10.0	$\underline{\tau}_{iso}(ring)$+$\gamma_{ph}(CH)$+ $\gamma(OH)$+ $\gamma_{iso}(CH_3)$+ $\gamma_{ph}(CN_{azo})$

ν, stretching; δ, in-plane-bending; γ, out-of-plane bending; τ, torsion.

Table 5.6 Computed frequency and intensity of 1Z-C4-*s* at M06-2X/cc-pVTZ level of theory along with the experimental frequency and intensity at 365 nm.

Normal Mode	Symmetry	Computed		Experimental (Ar, 4 K)		$\tilde{\upsilon}_{diff.}$ (cm^{-1})	Tentative Assignments
		$\tilde{\upsilon}_{calcd.}$ (cm^{-1}) 1Z-C4-*s*	I_{rel}	υ (cm^{-1})	I_{rel}		
75	A	3787.9	86	3484.0	39	303.9	ν(OH)
63	A	1678	22	1611.0	13	67.0	ν_{iso}(CN)+ ν_{ph}(CC)+ ν_{iso}(CC)+ν(NN)+δ_{iso}(CH$_3$)+ δ(OH)
62	A	1667.7	53	1600.5	36	67.2	ν_{ph}(CC)+δ_{ph}(CH)+ δ(OH)
61	A	1646.1	67	1587.0	25	59.1	ν_{iso}(CN)+ ν_{ph}(CC)+ ν_{iso}(CC)+ν(NN)+δ(OH)
59	A	1535.8	98	1482.0	58	53.8	ν_{ph}(CC)+δ_{ph}(CH)
57	A	1508.3	33	1467.0	16	41.3	ν_{iso}(CC)+ ν_{iso}(CO)+δ_{iso}(CH$_3$)
56	A	1493.7	14	1439.0	16	54.7	δ_{iso}(CH$_3$)
54	A	1485.1	9	1431.0	15	54.1	δ_{iso}(CH$_3$)
53	A	1468.7	64	1414.0	67	54.7	ν_{iso}(CC)+δ_{iso}(CH$_3$)
50	A	1375	30	1348.0	34	27.0	ν_{ph}(CC)+δ_{ph}(CH)+ δ(OH)
48	A	1328.1	15	1316.0	58	12.1	ν_{iso}(CC)+ ν_{iso}(CO)+δ_{iso}(CH$_3$)
47	A	1301.8	100	1250.0	100	51.8	ν_{ph}(CC)+ ν_{ph}(CO)+δ_{ph}(CH)+δ(OH)
45	A	1238.3	58	1182.0	53	56.3	ν_{ph}(CN$_{azo}$)+δ_{ph}(CH)+ δ(OH)
39	A	1069.7	8	1024.0	26	45.7	ν_{ph}(CC)+δ_{ph}(CH)
34	A	985.7	6	970.0	40	15.7	γ_{ph}(CH)
33	A	974	10	966.0	41	8.0	γ_{iso}(CH$_3$)+ν_{iso}(NO)
32	A	910.7	8	905.0	16	5.7	γ_{ph}(CH)+ γ_{ph}(CN$_{azo}$)

Normal Mode	Symmetry	Computed		Experimental (Ar, 4 K)		$\tilde{\nu}_{diff.}$ (cm^{-1})	Tentative Assignments
		$\tilde{\nu}_{calcd.}$ (cm^{-1}) 1Z-C4-s	I_{rel}	$\tilde{\nu}$ (cm^{-1})	I_{rel}		
31	A	884.8	11	846.0	32	38.8	$\gamma_{ph}(CH)+\gamma_{ph}(CN_{azo})$
30	A	861.5	8	841.0	33	20.5	$\delta_{ph}(ring)+\nu_{ph}(CO)$
28	A	789.9	50	743.0	20	46.9	$\gamma_{ph}(CH)+\gamma_{ph}(CN_{azo})$
20	A	568.5	32	577.0	34	−8.5	$\gamma(OH)+\delta_{ph}(ring)+\underline{\tau}(CNNC)$
19	A	559.9	39	565.0	31	−5.1	$\gamma(OH)$
				553.0	28		
17	A	525.5	24	510.0	31	15.5	$\gamma(OH)+\delta_{ph}(ring)$
16	A	491.9	3	485.0	41	6.9	$\gamma_{ph}(CH)+\gamma_{ph}(CN_{azo})+$ $\gamma_{iso}(CH_3)+\underline{\tau}(CNNC)+$ $\tau_{ph}(ring)+\underline{\tau}_{iso}(ring)$

ν, stretching; δ, in-plane-bending; γ, out-of-plane bending; τ, torsion.

5.5 CONCLUSIONS

2-Hydroxyphenylazo-3,5-dimethylisoxazole (HPAI) was investigated by matrix-isolation infrared spectroscopy and the theoretical calculations were performed at M06-2X/cc-pVTZ level of theory. Among the 12 possible conformers for the *trans* form, **1E-C1-s** has been identified as the major contributor and the dominant conformer in the deposited matrices. Apart from **1E-C1-s**, **1E-C2-s** and **1E-C3-s** also acconted to the observed features of HPAI and were in good agreement with the relative population analysis. Irradiation at 365 nm, resulted in new features belonging to **1Z-C3-s** and **1Z-C4-s** among the 10 possible conformers for the *cis* form. **1Z-C3-s** was the dominant photoproduct on the basis of the relative population analysis. Through this investigation, despite the presence of hydrogen bond forming groups that is capable of hindering the isomerization channel through the potential tautomeric forms, we were able to successfully induce the *E-Z* photoisomerization in HPAI under cryogenic conditions in argon matrix at 4 K.

5.6 REFERENCES

1. Wendler, T.; Schuett, C.; Naether, C.; Herges, R. Photoswitchable azoheterocycles via coupling of lithiated imidazoles with benzenediazonium salts. *J. Org. Chem.* **2012**, *77*, 3284−3287.

2. Weston, C. E.; Richardson, R. D.; Haycock, P. R.; White, A. J. P.; Fuchter, M. J. Arylazopyrazoles: azoheteroarene photoswitches offering quantitative isomerization and long thermal half-lives. *J. Am. Chem. Soc.* **2014**, *136*, 11878−11881.

3. Weston, C. E.; Kramer, A.; Colin, F.; Yildiz, O.; Baud, M. G. J.; Meyer-Almes, F. J.; Fuchter, M. J. Toward Photopharmacological Antimicrobial Chemotherapy Using Photoswitchable Amidohydrolase Inhibitors. *ACS Infect. Dis.* **2017**, *3*, 152−161.

4. Duarte, L.; Fausto, R.; Reva, I. Structural and spectroscopic characterization of *E*- and *Z*-isomers of azobenzene. *Phys. Chem. Chem. Phys.* **2014**, *16*, 16919−16930.

5. Duarte, L.; Khriachtchev, L.; Fausto, R.; Reva, I. Photoisomerization of Azobenzenes Isolated in Cryogenic Matrices. *Phys. Chem. Chem. Phys.* **2016**, *18*, 16802−16811.

6. Kumar, P.; Srivastava, A.; Sah, C.; Devi, S.; Venkataramani, S. Azoheteroarene photoswitches exhibiting high Z-isomer stability, solid state photochromism and reversible light-induced phase transition. *Chem. Eur. J.* **2019**, *25*, 11924–11932.

7. Nagaya, M.; Kudoh, S.; Nakata, M. Infrared spectrum and structure of the aci-nitro form of 2-nitrophenol in a low-temperature argon matrix. *Chem. Phys. Lett.* **2006**, *427*, 67-71.

8. Bader, R. F. W.; Bader, R. F. *Atoms in Molecules: A Quantum Theory*; International series of monographs on chemistry; Clarendon Press, 1990.

Chapter 6
Materials and methods

6.1. Matrix Isolation

The characterization of reactive intermediates has been one of the challenge for physical chemists due to their reactive and short lived nature. To overcome this challenge, matrix isolation emerged as one of the best experimental spectroscopic technique for the characterization of the reactive intermediates. The technique had its beginning in early 1920 by Vegard[1] and was coined as "matrix isolation" 30 years later in 1954 by Pimentel and coworkers. Pimentel and coworkers used the technique for the study of free radical, unstable transient species and hydrogen bonding interactions.[2-5] Matrix isolation is a technique, in which the guests such as atoms, ions or molecules are trapped in the cavity of rigid host materials. In principle, the guest (i.e. molecule of interest) is deposited with excess of host gas (1:1000) such as argon, neon and nitrogen on a cold spectroscopic window and can be converted to desired reactive species. The matrix host gases used has the following advantages: (i) they are inert which makes them unreactive towards guest species (ii) it forms optically clear matrices which allows good quality electronic spectra to be recorded (iii) have no absorption on the IR region.

In general, the deposited precursor on the KBr window can be converted to reactive species by photolysis. Due to the extremely cold temperature of rigid matrix, the reactive species are well isolated which arrests the possibility of diffusion and intermolecular interactions. In this regard, the trapped molecules in the inert gas matrix can be studied by using spectroscopic techniques such as UV-visible,[6] infrared and ESR[7]. In general, the spectra obtained for the species bound in the matrix are very similar to that obtained for the same species in the gas

phase. Infact, the matrix isolated spectra obtained are much simpler because the rotational motion of the species are suppressed in comparision to the gas phase spectra. Matrix isolation technique was mainly developed for the study of unstable molecules. In principle, the study of unstable molecules is difficult due to their high reactivity and lower lifetime. Under matrix isolation technique, the lifetime for the trapped species is longer which makes the task of experimentalist much simpler. The matrix formed should be rigid, any kind of softness in the matrix will allow diffusion of species which can lead to recombination of radicals, dimers and higher aggregates. Thus, softening of matrix will lead to the formation of stable molecules which complicates the spectra.

6.1.1 Properties of matrices

The aim of matrix isolation technique is to study unstable molecular species. The technique provides necessary conditions such that the life time of trapped molecular species gets longer which makes the work of experimentalists much easier. Under the low temperature condition (i.e. 4 K–20 K) and low concentration of guest molecules, molecular collisions are inhibited which results in isolation of molecular species. Moreover, matrix properties also aids in the isolation of the unstable molecular species. Some of the matrix properties which need to be considered are as follows:

(i) The matrix formed by the host gas must be solid and inert. The best matrix materials which meet the matrix conditions are noble gases and nitrogen, being inert they have no infrared absorption.

(ii) The matrix formed must have high degree of purity, an impure matrix will mask the absorption peaks of molecule of interest.

(iii)   The matrix should be necessarily rigid otherwise diffusion of trapped radicals will occur leading to the recombination of free radicals forming stable aggregates. The process of diffusion complicates the spectra of unstable species to be studied.

(iv)   The matrices with small lattice energy (i.e. 2 kcal/mol for argon) results in weak interactions between the matrix atoms and the guest molecules. Hence for the matrices with smaller lattice energy, the molecules are well isolated.

6.2 Challenges involved in Matrix isolation technique

A sufficient vapor pressure of the sample is required to be deposited on the cold window. Sample deposition of low vapor pressure are difficult to deposit in sufficient amount under room temperature conditions. Therefore, for such samples heating conditions are required in order to raise the vapor pressure. For achieving this task, heating has to be carried out in controlled manner since higher temperature can also lead to sample decomposition. Also, the idea of "non-interacting matrix" is practically unrealizable. In principle, there do exist a minimal interaction between the matrix and the isolated species which cannot be ignored. This is addressed under the following sections.

6.2.1   Matrix Effects

Matrix effect describes the interaction between the guest molecule and the host gas forming the matrix. The infrared spectra of matrix isolated species are associated with small sub-bands, which are termed as "matrix splitting" or "site effect". The factors responsible for such splitting are as follows:

(i)   Guest-guest interactions: Even though the interaction between the guest molecule is weak; but still the interaction of two or more molecules (i.e. molecular aggregation) will give rise to a frequency different to that of a monomer. The molecular

aggregation can arise due to weak intermolecular interactions such as hydrogen bonding, van der waals associations and dipole-dipole alignment.

(ii)   Host-guest interactions: Depending upon the nature of the gas, the inert gases adopt either hexagonal close-packed (h.c.p) or face-centered cubic crystal (f.c.c) structure upon solidification. Therefore, the sample molecules experience different environment when trapped at different sites. Due to this phenomenon, either peak broadening or peak splitting into multiplets (i.e. site effects) is observed. The intensity of spectral features at different sites will be determined by the stability of each trapping site. The process of annealing removes the unstable sites, which helps in sharpening of the spectral features. The host-guest interactions can be minimized either by dilution or by changing the host gas.

6.2.2   Matrix Shifts

The interaction of the sample molecules with the matrix gas leads to the matrix shifts. During the course of interaction, the vibrational levels of guest molecule gets perturbed by the matrix and thus shift in vibrational frequencies are observed as compared to their gas phase values. The extent of perturbation on the vibrational levels of the trapped species by matrix molecules are reflected by the frequency shifts of sample molecules. The shifts in the vibrational frequency (Δv) of the trapped species relative to the gas phase value gives the magnitude of this interaction.

$$\Delta v = v_{matrix} - v_{gas}$$

Various factors, such as electrostatic (Δv_{elec}), inductive (Δv_{ind}), repulsive (Δv_{rep}) and dispersion (Δv_{disp}) interactions are responsible for the interaction of matrix gases with trapped

species. In principle, the long-range london dispersion (Δv_{disp}) and short-range repulsive forces (Δv_{rep}) are the major contributors to the interaction of rare-gas matrix molecules with the trapped species. A loose cage effect (i.e. host atom placed at a larger distance from matrix atoms) results in a negative Δv value and leads to the red shift. For polyatomic molecules, the high-frequency stretching vibration mimics loose cage effect owing to the small vibrational amplitudes and results in the red shift. Similarly, tight cage effect results in a positive Δv value, which leads to blue shift. The tight cage effect is reflected by the low-frequency modes such as bending and rocking showing large amplitude motion. Therefore, in order to infer the spectra of matrix isolated species with precision it is crucial to recognize the matrix effect.

6.3 Instrumental Setup

The main components of matrix isolation setup are comprised of cryostat, compressor, vacuum pumps, FTIR spectrometer and the light sources.

6.3.1   Cryostat

A cryostat is required to achieve low temperature for the sample deposition along with the inert gas. In principle, cryostat is the heart of matrix isolation set-up. Cryostats are generally classified into three types.

(a) Liquid refrigerant cryostat

The earlier cryostats had a tubular reservoir filled with liquid refrigerant such as helium (4.2 K) and liquid nitrogen (77 K). The reservoir was attached to a window for matrix deposition. The cryostat in which liquid helium was used had Double-Dewar construction. In this arrangement the liquid helium reservoir is surrounded by liquid nitrogen reservoir. Here,

liquid nitrogen reservoir acts as a heat shield to minimize the evaporation loss of liquid helium. The construction was modified later to continuous-flow cryostats by attaching the liquid helium reservoir to cold fingers. In this way, continuous-flow cryostats were economical and much more compact than the Double-Dewar cryostats.

(b) Joule-Thomson Open Cycle Cryostats

Open cycle cryostats using the Joule-Thomson principle became available in 1960's. In this type of cryostat, the incoming helium gas at high pressure is expanded through a small orifice to produce low temperatures. In these cryostats, the sample window connected to a cooling tube is surrounded by a radiation shield and a vacuum jacket. The liquid helium cools the copper tip of the cooling tube and thus cools the sample window on which the matrix is formed. These cryostats are more useful since they avoid the necessity of handling expensive liquid refrigerants. In a way they are much more compact and fits easily into the spectrometer area. The temperature range from 4-200 K can be controlled in the commercially available models.

(c) Closed cycle cryostats

The cryostat works on the principle of Gifford-McMahon cycle. The cooling is achieved by continuous compression and expansion of helium gas in an enclosed space. The cooling cycle takes place in four successive stages and is comprised of compression space, the cooler, the regenerator and an expansion space. The four stages are as follows:

(i)   In the first stage, the helium gas is compressed to a pressure of about 20 bar at room temperature.

(ii)   In the second stage, the compressed fluid passes the cooler where it dissipates the heat of compression. The fluid is now passed to the regenerator (i.e. heat exchanger), here the fluid is almost cooled to the refrigeration temperature.

(iii)   In the third stage, the fluid expands in the expansion space and does work against the expansion piston.

(iv)   In the fourth stage, the expansion piston moves the fluid back to the compression space and the cycle re-starts again.

In our matrix isolation setup, cryostat (RDX-408D2 from sumitomo) is used to achieve the cryogenic temperature, which is required to solidify the inert gas.

6.3.2   Vacuum pumps

Vacuum pumps are employed for the gas transfer from system to the atmosphere in order to create vacuum. The vacuum pumps for the matrix isolation setup are of two types:

(a) Rotary vane pump

These are widely used pumps in vacuum technology. The pumps works on the principle of positive displacement (i.e. directional flow) of gas from system to the atmosphere as shown in **figure 6.1.** It is mostly used to achieve a rough vacuum of 10^{-3} mbar and is backed by a diffusion pump. The pump consists of a stationary part (i.e. stator) and a moving part (i.e. slotted rotor) assembled in a casing. The rotor is driven by an electric motor with a pumping speed of 100 lit/min. The air at atmospheric pressure is drawn through an inlet due to pressure difference. The rotation of rotor compresses the incoming air through the inlet and passes the compressed air from slot A to slot B. Once the pressure at slot B just reaches above the atmospheric pressure, the exhaust valve opens up and the trapped air molecules are delivered to the atmosphere. In this way, the rotary vane pump brings the continuum level (1 atm) to a molecular level (10^{-3} mbar) for the operation of diffusion pump.
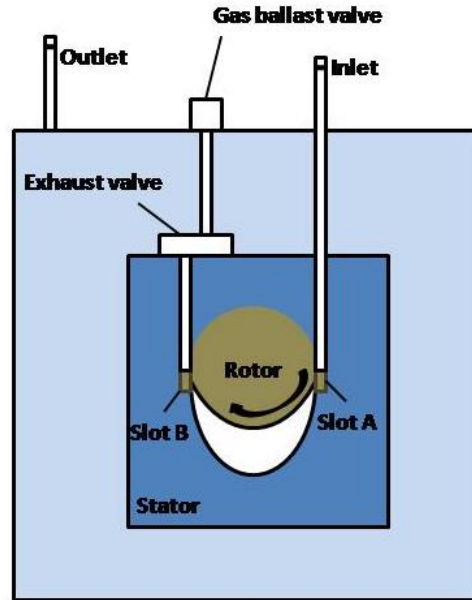
Figure 6.1 Working of a Rotary Vane Pump

(b) Diffusion pump

In practical applications, diffusion pumps are backed by a rotary vane pump. The rotary vane pump creates a molecular regime (10^{-3} mbar) for the working of a diffusion pump. Diffusion pump comes under the category of kinetic pumps. In these pumps, the kinetic energy or momentum are imparted to the gas molecules. The imparted momentum expels the gas molecules from the system and creates a vacuum of the order of 10^{-6} mbar.

Working

Diffusion pump consists of a chamber housing a oil vessel with a heater, nozzle and a chimney as represented in **figure 6.2.** The outer surface of the chamber is wounded by cooling coils carrying water. The heater vaporizes the silicon oil and the hot vapor rises to the chimney. The hot vapors are deflected downward by an annular nozzle mounted at the top of the chimney. The hot vapors travelling downward at a supersonic speed imparts

160

momentum to the gas molecules initially at molecular regime. The imparted momentum deflects the gas molecules towards pump outlet. The backing pump connected to the pump outlet delivers the gas molecules to the atmosphere. The hot oil condenses on the cold walls and returns back to the oil vessel. In this way, diffusion pumps dumps the gas molecules to the atmosphere and creates a vacuum of 10^{-6} mbar.
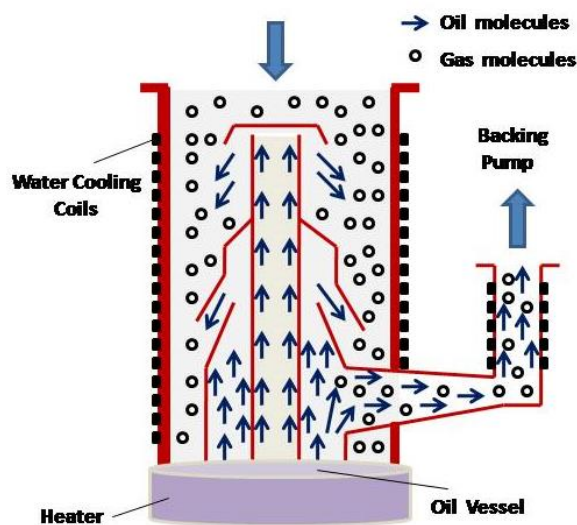
Figure 6.2 Working of a Diffusion Pump

6.3.3   Temperature Controller

The place of sample deposition (i.e. the optical window) at the cryostat is connected to a temperature controller (Lakeshore model No. 336) with a temperature sensor. The temperature controller enables to heat the window in order to achieve the desired temperature required for annealing. The process of annealing softens the solid inert gas matrix which enables the diffusion of the trapped molecular species.

6.3.4 FTIR Spectrometer

The term Fourier-transform infrared (FTIR) spectroscopy originates from "Fourier transform" (a mathematical process) which is required to convert the raw data into the actual spectrum. FTIR as a technique is used to obtain an infrared spectrum of absorption or emission of a solid, liquid or gas. An FTIR spectrometer simultaneously collects high-spectral-resolution data over a wide spectral range. Thus, it has a significant advantage over a dispersive spectrometer, which measures intensity over a narrow range of wavelengths at a time. The trapped species were studied using a Bruker Tensor II FTIR spectrometer. The instrument was operated at a resolution of 0.5 cm^{-1}.
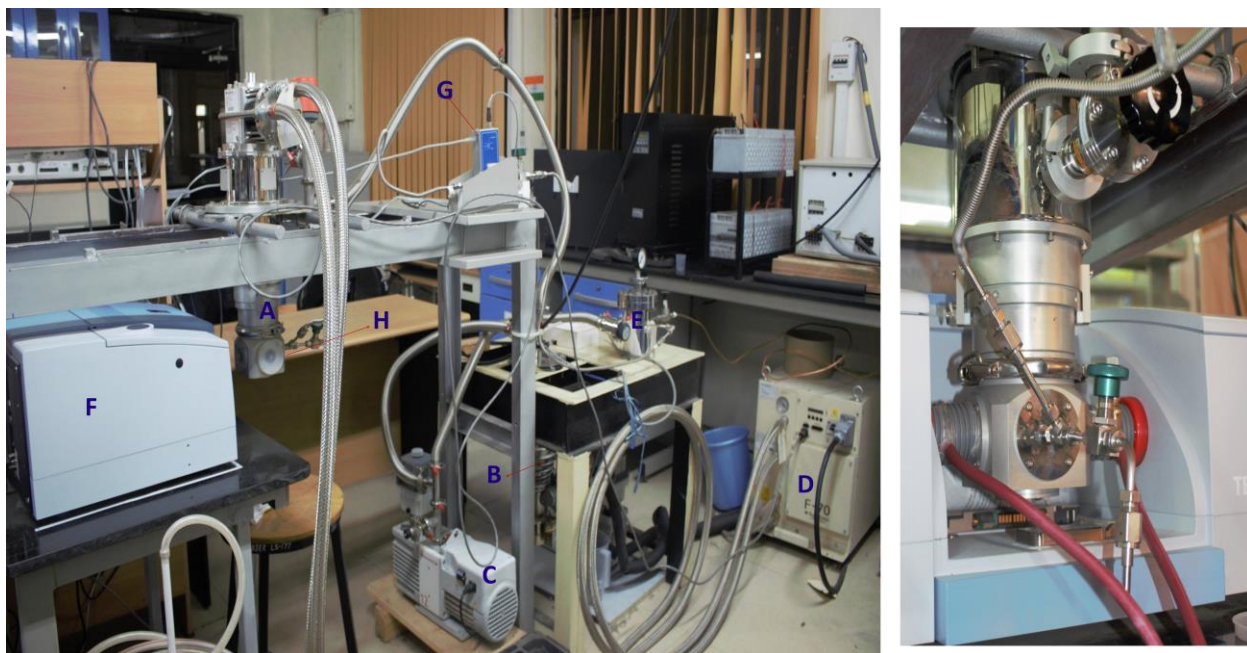
Figure 6.3 Matrix isolation infrared spectroscopic set up with its components. Components are labeled as **A:** Cryostat, **B:** Diffusion Pump, **C:** Rotary Vane Pump, **D:** Helium Compressor, **E:** Mixing Chamber, **F:** IR Spectrometer, **G:** Flow Controller and **H:** KBr Window

6.3.5 Light Sources

Various reactive intermediates and unstable species have been generated using the precursors that were deposited and isolated in an inert gas matrices by irradiation under suitable wavelengths. The choice of the wavelengths were depending on the solution phase absorption characteristics of the precursor. At intermediate stage, various wavelenghths will be tested. For such photochemical processes, mainly the following three light sources have been used:

(a) 1000 Watts high pressure Xenon lamp (Kiloarc Broadband Arc Lamp light source from HORIBA scientific) equipped with a monochromator that can be tuned between 250 and 900 nm.

(b) For 254 nm wavelength irradiation, a low pressure mercury lamp (UVP Pen ray lamp) was used.

(c) A commercial LED or the xenon lamp has been used for 365 nm.

6.4 Advantages of Matrix Isolation Technique

(i)   The technique is useful for isolation and characterization of free radicals, unstable and other transient species.

(ii)   In general, reactive intermediates have a fleeting existence which is of a timescale of femtoseconds. The reactive intermediates trapped in matrix under stable conditions provides detail insights regarding the electronic and molecular structure of the reactive intermediates.

(iii) The isolation of species under inert and low temperature environment reduces the intermolecular interactions which results in sharpening of absorptions.

(iv)   Much narrower bands are observed as compared to the gas phases since the rotational motion of species does not occur. The low temperature also results in small bandwidths.

(v)   It is also involved in the study of weakly bound systems such as H-bonded, molecular conformation, charge transfer and van der waal complexes.

(vi)   The non interference of the inert host gas allows for temperature dependent studies of reactive intermediates. Apart from this, transparency of inert gas provides higher resolution to the spectra which helps in decoding the complex structure in a much easier way.

6.5 Limitations of matrix isolation technique

Apart from several advantages, the technique is also bestowed with limitations. The limitations are as follows:

(i)   The most important one is the choice of precursor. The precursor of the reactive intermediate to be studied must be contaminant free, volatilizable without decomposition, and should have thermal or photochemical labile groups.

(ii)   The reactive intermediates formed by the attack of nucleophiles, electrophiles, oxidants or reductants in solution phase is not applicable for matrix isolation studies.

(iii)   The reactive intermediates to be studied by matrix isolation must be formed by unimolecular processes such as fragmentation and rearrangement of chemical bonds induced by photolysis or thermolysis.

(iv)   Cage effect: The precursors even capable of providing reactive intermediates, sometimes wont workout inside matrix due to cage effect. The fragments created during the cleavage of precursor remains trapped in the same matrix cavity and undergoes recombination immediately after their formation.

(v)   Polar substrates: Polar substrates have a higher tendency to form dimers or higher aggregates. Hence the isolation of reactive intermediates becomes difficult due to aggregation property of polar substrates.

Introduction to Computational Chemistry

6.6 Computational Chemistry

Computational chemistry is the branch of chemistry that applies the quantum mechanical equations or classical mechanics to generate information that is complimentary to experimental data. Theoretical chemists developed the art of computation for centuries in order to solve the problems associated with atoms and molecular species. Computational chemistry has developed enough to perform calculations on the properties such as determining the electronic structure, geometrical optimization, frequency calculation, protein calculations (docking), transition states, potential energy surfaces, rate constant calculation for kinetics and heat of reactions to assist the thermodynamics. The qualitative and quantitative analysis of molecules based upon the above properties is the sole objective of computational chemistry. It is beneficial to compute the properties of molecule before the experiment; and also to tune the experimental work accordingly to gain maximum output. Not only the experimental results can be compared to the theoretical one but it also helps to explain the reaction mechanism which is sometimes difficult to portray through the experimental observations.

Unfortunately, the work of computational chemistry as a unique field of study was recognized very late. In 1995, Paul Crutzen, Mario Molina, and F. Sherwood Rowland, won the Chemistry Nobel prize for explaining the ozone formation and decomposition in the atmosphere by constructing mathematical models that used chemical and thermodynamic laws. In 1998, Walter Kohn and John Pople won the Chemistry Nobel prize for their work on density functional theory and computational methods in quantum chemistry. For their work in 1970s, Martin Karplus, Michael Levitt, and Arieh Warshel won the 2013 Nobel Prize in Chemistry for laying the foundations for today's computer models that combine principles of classical and quantum physics.

At present, computational chemistry has almost covered all areas of research which includes:

(a) The contribution it has made in pharmaceutical industry in drug designing on the basis of docking experiments.

(b) The study of hydrogen bonding pathway and hydrogen transfer in biochemical processes.

(c) Exploration of structural, bonding and reactivity aspects of molecules in organometallic, organic and physical organic chemistry.

(d) Protein dynamics, modeling of protein and its electrostatics.

(e) Analyzing the properties of short-lived intermediates and several explosives that are difficult to handle in a laboratory.

(f) Valuable for the study of materials such as semiconductors, superconductors and ceramics in material science.

In this regard, computational chemistry eliminates time consumption and costly experimentations. Moreover, it is environmentally safe and clean chemistry.

6.6.1 The tools of Computational Chemistry

The main tools of the computational chemistry are broadly classified into five classes. These are as follows:

(a) **Molecular Mechanics (MM):** Molecular mechanics is a model which treats a molecule as a collection of balls (i.e. atoms) which are held together by springs (i.e. bonds). In this model, atom is considered to be spherical having a net charge and the interactions determines the geometry as well as the energy of the molecule. Geometrical optimization is achieved after changing the geometry (i.e. stretching and bending the bonds) until and unless the lowest energy is found. Molecular mechanics is very fast, even a large molecule like cholesterol can be optimized within seconds.

(b) *Ab initio* **calculations:** *ab initio* is latin derived that means "from the beginning" and reflects the calculations based on Schrodinger equation. The Schrodinger equation describes the behavior of electron in a molecule. The method solves the Schrodinger equation from which the wave function and the molecular energy is deduced. The wave function is used to calculate the electron distribution. The electron distribution helps to interpret the extent of polarity of molecule (a viable information with respect to a electrophilic or a nucleophilic attack). In general, *ab initio* calculations are slow.

(c) **Semiempirical Calculations (SEC):** Similar to *ab initio*; the semiempirical calculations are also based on the Schrodinger equation. The only difference being that the complicated integrals are not evaluated in SEC unlike in *ab initio* and the Schrodinger equation is parameterized with the experimental values. Infact, it is the

plugging of experimental values into a mathematical procedure (theory) that makes the method semiempirical. In general, semiempirical calculations are faster than *ab initio* and slower than Molecular Mechanics (MM).

(d) Density functional calculations: Density functional calculations are also based on the schrodinger equation similar to the ab initio and the semiempirical calculations. Density functional calculations derive electron density functional unlike ab initio and SEC calculations which calculates the wavefunction. In general, Density functional calculations are slower than SEC but usually faster than the *ab initio* calculations.

(e) Molecular Dynamics (MD): Molecular Dynamics is a versatile tool for investigating bimolecular interactions. It simulates natural motion to the molecular system under study. The energy provided allows the atom to move and collide with the neighbouring atoms. The numerical solution of classical Newtonian dynamic equation accounts for the simulation of motion. The motion of an enzyme binding to the substrate or the motion of water molecules around a solute molecule can be simulated using molecular dynamics.

6.7 Density Functional Theory (DFT)

Density functional theory is a theory based on the electron density distribution $\rho(r)$ rather than the many-electron wave function ψ (r_1, r_2, r_3, r_4….). DFT is regarded as one of the promising and successful level of theory for the computation of electronic structure of molecules. It is widely used for the accurate estimation of energies involved for determining the thermodynamics and kinetics of the reaction pathway.

In 1964, Hornberg and Kohn introduced the concept that the ground state properties are the functional of the electron density.[8-10] Electron density is referred as functional

because it is the function of the wavefunction. For a system of N electrons the electron density depends on 3N variables (i.e. Cartesian axes, x, y, and z). The total ground state energy of an electron system can be expressed as a functional of the electron density. The minimum energy of an electron system is possible if the density corresponds to the exact density for the ground state. Hornberg and Kohn proposed the two theorems which relates to the system consisting of electrons moving under the influence of external potential (i.e. V_{ext}).

Theorem 1: It states that the total energy and the external potential are unique functional of the electron density.

In this approach, the kinetic energy of electrons and the electron-electron interaction adjust themselves to the external potential (i.e. V_{ext}) in the Hamiltonian. This means that the external potential is the only variable and other things (including electron density) adjusts themselves in order to give the lowest energy to the system. The electron density determines the number of electrons (N) and also the V_{ext}.

$$N = \int \rho(\text{r})\text{dr}$$

Hence, the total electron density is as useful as the wavefunction ψ describing the state of the system. This is proved through a contradiction:

(a) The exact ground state density $\rho(\text{r})$ is nondegenerate (i.e. it has only one wavefunction ψ for the ground state.

(b) It is assumed that for the electron density $\rho(\text{r})$ there are two external potentials V_{ext} and V'_{ext}, producing two different Hamiltonians H and H′ with two different ground state wavefunctions ψ and ψ' respectively.

The energies are expressed as:

$$E_0 = \langle \psi | H | \psi \rangle \tag{1}$$

$$E'_0 = \langle \psi' | H' | \psi' \rangle \tag{2}$$

Using the variational theorem, the expectation value of energy is calculated for ψ' with the hamiltonian H.

$$E_0 < \langle \psi' | H | \psi' \rangle = \langle \psi' | H' | \psi' \rangle + \langle \psi' | H - H' | \psi' \rangle = E'_0 + \int \rho(r)[V_{ext} - V'_{ext}] \, dr$$

Hence, we have the relation:

$$E_0 < E'_0 + \int \rho(r)[V_{ext} - V'_{ext}] \, dr \tag{3}$$

Similarly, the expectation value of energy for ψ with the hamiltonian H' is

$$E'_0 < \langle \psi | H' | \psi \rangle = \langle \psi | H | \psi \rangle + \langle \psi | H' - H | \psi \rangle = E_0 + \int \rho(r)[V'_{ext} - V_{ext}] \, dr$$

i.e

$$E'_0 < E_0 + \int \rho(r)[V'_{ext} - V_{ext}] \, dr \tag{4}$$

On adding eqn (3) and (4), we obtain:

$$E_0 + E'_0 < E'_0 + E_0 \tag{5}$$

Eqn (5) leads to a contradiction. There cannot be two distinct V_{ext} that gives the same ground state electron density $\rho(r)$. Hence, for any given $\rho(r)$, there can be only one V_{ext}.

The total ground state energy is the functional of electron density. The energy is the summation of the kinetic energy of electrons (T_e), electron-electron interaction energy (U_{ee}) and the energy corresponding to the external potential (V_{ext}).

$$E(\rho) = Te(\rho) + U_{ee}(\rho) + V_{ext}(\rho) \tag{6}$$

Theorem 2: The density that minimizes the total energy is said to be exact ground state density.

The electron density $\rho(r)$ determines V_{ext}, V_{ext} determines hamiltonian (H) and ψ. Thus, ψ is a functional of $\rho(r)$. The expectation value of F is also a functional of $\rho(r)$.

i.e

$$F[\rho(r)] = \langle \psi | F | \psi \rangle \tag{7}$$

The energy functional which is v-representable of external potential $V_{ext}(r)$ is unrelated to another density $\rho'(r)$ is given as:

$$E_v[\rho(r)] = \int \rho'(r)V_{ext}(r)dr + F[\rho'(r)] \qquad (8)$$

With the assertion of variational principle we have the relation:

$$\langle \psi'|F|\psi' \rangle + \langle \psi'|V_{ext}|\psi' \rangle > \langle \psi|F|\psi \rangle + \langle \psi|V_{ext}|\psi \rangle \qquad (9)$$

Here, ψ is the wavefunction corresponding to the true ground state density $\rho(r)$. This leads to

$$\int \rho'(r)V_{ext}(r)dr + F[\rho'(r)] > \int \rho(r)V_{ext}(r)dr + F[\rho(r)] \qquad (10)$$

Eqn (10) can also be expressed in the form of energy as

$$E_v > E_v[\rho(r)] \qquad (11)$$

6.8 Potential Energy Surface (PES)

The concept of potential energy surface has its roots in the Molecular Mechanics and Born Oppenheimer approximation. The simple diatomic molecular model AB, behaves like balls (i.e. atoms) held together by springs (i.e. bonds). Any distortion in geometry by compression and stretching the bonds will lead to increase in the potential energy of the molecule. The potential energy surface is the plot of molecular energy against the bond length (i.e. nuclear coordinates). The molecular energy corresponds to the energy of all the electrons and nuclei that constitutes the molecule. The important question which arises here is; if the molecule is comprised of both nuclei and electrons, why plot the molecular energy versus nuclear coordinates (why not against the electron coordinates?). The answer lies in the Born Oppenheimer approximation, which states that nucleus are more sluggish than electrons due to their larger mass. The nuclei are not stationary, they do undergo vibrations of small

amplitudes about equilibrium positions. These equilibrium positions are referred to the fixed nuclear positions or the nuclear coordinates.

For a diatomic molecule like AB, the plot is Energy (E) versus q_1. On the other hand, for triatomic and tetra atomic molecules, the plot becomes E vs (q_1, q_2) and E vs (q_1, q_2, q_3). Here, q_1, q_2, q_3 signifies bond length, bond angle and dihedral angle as the geometrical parameters. The minimum in the potential energy for a diatomic molecule corresponds to a point at which $dE/dq_1 = 0$; for triatomic case $[dE/dq_1 = dE/dq_2 = 0]$. In a reaction pathway, the location of transition state which connects the reactant and product becomes crucial. In the PES, all the three species (i.e. reactant, transition state and the product) are the stationary points. Mathematically, it is defined as a point at which the first derivate of potential energy with respect to each geometrical parameter is zero.

$$dE/dq_1 = dE/dq_2 = dE/dq_3 = 0$$

The lowest energy pathway which connects the two minimum (i.e. reactant and product) and passes through a transition state by overcoming the activation barrier corresponds to the intrinsic reaction coordinate (IRC). The transition state represents a maximum along the direction of IRC and is termed as a ″saddle point″. Saddle point is similar to a stationary point because it resides at the center of a saddle-shaped surface which is flat. Mathematically speaking, both minima and saddle points are stationary points since the first derivative of energy is zero. The only difference being; a minima is a minimum in all directions, whereas a saddle point is a maximum along the IRC and a minimum in all other directions. The minima and maxima can be distinguished by taking the second derivative of energy.

For a minimum:

$$d^2E/dq^2 > 0$$

For a transition state:

$$d^2E/dq^2 < 0 \quad \text{(along the reaction coordinate)}$$

$$d^2E/dq^2 > 0 \quad \text{(along all other directions)}$$

On this basis, a transition state can be defined as a saddle point on the PES where the second derivative of energy with respect to one geometric coordinate is negative.

6.9 Geometry Optimization

Locating the stationary point on the PES and, calculating its geometry and energy is basically the geometry optimization. To our point of interest, the stationary point might be a minimum or a transition state. In general, geometry optimizations are carried out by starting with a input structure which resembles to the desired stationary point. On submitting the input structure, the computer algorithm changes the geometry until energy minimization is achieved. The second derivative of energy can be taken to characterize the structure as a minimum or a saddle point. In principle, one must go for the frequency calculations to get assured of the nature of a stationary point. On analysis, look for the number of imaginary frequencies present. A minimum has none, a transition state has one, and a hilltop (i.e. higher order saddle point) has more than one. Particularly, for a transition state following things should be taken care of:

(a) The structure of transition state should lie between that of reactant and the product.

(b) The structure must have only one imaginary frequency.

(c) The animation of the imaginary frequency must be visualized by the program so that it corresponds to the reaction coordinate.

(d) The energy of transition state should be higher than that of reactant and product.

6.10 Natural Bond Orbital (NBO) Analysis

The theory of natural bond orbital (NBO) was developed by Weinhold and co-workers for the understanding and quantification of orbital interactions in a molecule.[11] The Lewis-like bonding pattern of electron pairs is described by an orthogonal set of localized orbitals (i.e. NBO). The concerned atomic orbital basis set is transformed into natural atomic orbital (NAO), which in turn forms natural hybrid orbital and natural bonding orbital. The second-order perturbation energy E(2) gives the estimation of the stabilization achieved due to orbital delocalization interaction. The magnitude of E(2) of a given donor-acceptor orbital pair interactions depends on the overlap coefficient between donor (i) and acceptor (j) orbitals. The energy difference between donor and acceptor orbitals [E(j)-E(i)] is inversely related to the overlap coefficient denoted by F(i,j). The NBO analysis of the computed radicals was carried out with Gaussian 09 package.

6.11 Basis Sets

A basis set is defined as the mathematical description of orbitals by stacking the basis functions that can be used for theoretical calculations. Here, Stacking means taking the linear combinations of basis function, with each basis function multiplied to its normalization constant.

$$\psi = c_1\emptyset_1 + c_2\emptyset_2 + c_3\emptyset_3 + \cdots c_k\emptyset_k$$

Where $\emptyset_1$, $\emptyset_2$, $\emptyset_3$ .... $\emptyset_k$ are the basis functions and c_1, c_2, c_3 ...... c_k are the normalization constants. The first computation using Slater Type Orbitals (STO) was done by John C. Slater. The general expression for a STO basis function is given as:

$$STO = N \times e^{-\propto r}$$

Where $N = (\alpha^3/\Pi)^{1/2}$ is the normalization constant, α is the orbital exponent and r is the radius in angstroms. Slater Type Orbitals are best for solving one electron problem.

In order to solve the problem for a system containing more than one electrons, the wavefunction was modified by the introduction of Gaussian type functions. The general expression for a GTO basis function is given as:

$$GTO = N \times e^{-\alpha r^2}$$

Where $N = (2\alpha/\Pi)^{3/4}$ is the normalization constant.

STOs are more accurate but it takes longer time to compute the integral. The STO function can be mimicked for solving many electron problem by taking the linear combinations of several GTOs. Moreover, the GTO functions are easy to compute than the STO function due to the square of radius term in the exponent.

6.11.1 Minimal Basis Sets

The common minimal basis sets (i.e STO-nG) was devised by John Pople. For a minimal basis set we have one basis function for each atomic orbital. For example, Carbon atom has 1s orbital, a 2s orbital and three 2p orbitals, the basis set comprises of five basis functions. The STO-nG basis set is constructed by taking the linear combination of "n" GTOs. Lets take the example of STO-3G basis set

$$\text{STO-3G} = C_1 e^{-\alpha_1 r^2} + C_2 e^{-\alpha_2 r^2} + C_3 e^{-\alpha_3 r^2}$$

The individual GTOs are the primitive orbitals while the combined function are called the contracted function. In a STO-3G basis set, each basis function is a contraction of three primitive Gaussians. Similarly, in a STO-6G each basis function is a contraction of six primitive Gaussians. The linear combination of more and more GTOs in a STO function leads to energy minimization.

6.11.2 Split-Valence Basis Sets

In late 1970's John Pople and his group introduced the Split-valence basis sets. The split-valence basis is a minimal basis for the core orbitals and double or triple-zeta for the valence shell. A double or triple-zeta basis set consists of two and three basis function for the valence orbital. The basis set is more accurate than the minimal basis set since it treats core and valence electrons separately. The smallest split-valence basis set is 3-21G (i.e. double-zeta). For carbon atom, the inner core orbital 1s is represented by 3 primitive Gaussians and each of the four valence orbitals (2s, $2p_x$, $2p_y$ and $2p_z$) is comprised of 3 primitives (i.e. first basis function comprises of 2 contracted and the second basis function comprises of 1 uncontracted orbital). Hence, number of primitive Gaussians required are (3×1 (core) + 3×4 (valence) = 15). The other basis set 6-31 (doubly split valence/double-zeta) and 6-311 (triply split valence/triple-zeta) uses 22 and 26 primitive Gaussians for carbon atom respectively. The use of contracted and uncontracted basis functions to the valence orbitals, allows the orbitals to expand or contract during the molecular calculation.

6.11.3 Polarized Basis Sets

Gaussian functions which are one unit higher in angular momentum are added to the ground state of atom as a polarized functions. During the bond formation in a molecule, the atomic orbitals (i.e. s and p) are distorted from their original shape. The polarized "p" or "d" basis functions are added to describe the distortion of "s" and "p" orbitals and, increases the flexibility in the valence orbital of a molecule. The polarized function are designated by an asterisk (*). For example, the 6-311G(d) (or 6-311G*) basis sets adds d-type functions to all non-hydrogen atoms. On the other hand, a 6-311G(d,p) (or 6-311G**) adds a p-type function on hydrogen atoms as well. In principle, addition of polarized functions tend to increase the

basis functions in the basis set. The increased basis functions (i.e. extended basis sets) helps to improve geometry and energetic of a molecular system.

6.11.4 Diffused Basis Sets

Diffused functions are defined as the shallow Gaussian functions which represents the tail portion of the atomic orbitals (i.e. for the electrons which are distant from the atomic nuclei). The addition of a diffused function assists the split-valence basis set. The diffused functions are designated by a + sign. In 6-311++G, ++ indicates one set of p diffused functions added to heavy atoms and 1s diffuse function added to H atom. In general, the diffused orbitals occupies large region of space. Diffused functions are important to those systems for which the electrons are far away from the nucleus. These are used in the computation of anions, electronegative atoms, excited states and for the molecules with a higher bond length. The geometry of covalent bonded molecules are not much affected by the addition of a diffused function, but they do help in improving the energetics of molecules involved in weak interactions.

6.11.5 Correlation consistent basis sets

Basis sets cc-pVNZ where N=D, T, Q....n (D=double-zeta, T=triple-zeta, etc.). The 'cc-p', stands for 'correlation consistent polarized' and the 'V' indicates they are valence only basis sets. The basis set is built by adding shells of functions to a core set of atomic hartree-fock functions. For the 1st and 2nd row atoms, the cc-pVDZ basis set adds 1s, 1p and 1d functions. Similarly, cc-pVTZ basis set adds another s, p, d, and f functions. Thus, these basis sets include polarization functions. On the other hand, the introduction of augmentations to these basis sets (i.e. aug-cc-pVNZ) adds diffuse functions for the better description of anions and weakly interacting molecules.

6.12. REFERENCES

1. Vegard, L. The auroral spectrum and the upper atmosphere. *Nature.* **1924**, *114*, 357.

2. Whittle, E.; Dows, D. A.; Pimentel, G. C. Matrix Isolation Method for the Experimental Study of Unstable Species. *J. Chem. Phys.* **1954**, *22* (11), 1943.

3. Becker, E. D.; Pimentel, G. C. Spectroscopic Studies of Reactive Molecules by the Matrix Isolation Method. *J. Chem. Phys.* **1956**, *25* (2), 224–228.

4. Van Thiel, M.; Becker, E. D.; Pimentel, G. C. Infrared Studies of Hydrogen Bonding of Methanol by the Matrix Isolation Technique. *J. Chem. Phys.* **1957**, *27* (1), 95–99.

5. Van Thiel, M.; Becker, E. D.; Pimentel, G. C. Infrared Studies of Hydrogen Bonding of Water by the Matrix Isolation Technique. *J. Chem. Phys.* **1957**, *27* (2), 486–490.

6. Hobe, M. Von; Stroh, F.; Beckers, H. The UV / Vis Absorption Spectrum of Matrix-Isolated Dichlorine Peroxide , ClOOCl. *Phys. Chem. Chem. Phys.* **2009**, *11*, 1571–1580.

7. Costa, P.; Sander, W. Hydrogen Bonding Switches the Spin State of Diphenylcarbene from Triplet to Singlet. *Angew. Chemie Int. Ed.* **2014**, *53* (20), 5122–5125.

8. Hohenberg, P.; Kohn, W. Inhomogeneous Electron Gas. *Phys. Rev. B.* **1964**, *136*, 864.

9. Kohn, W.; Becke, A. D.; Parr, R. G. Density Functional Theory of Electronic Structure. *J. Phys. Chem.* **1996**, *100,* 12974–12980.

10. Ramachandran, K. I.; Deepa, G.; Namboori, K. *Computational Chemistry and Molecular Modeling;* Amrita Vishwa Vidyapeetham University: Springer, 2008.

11. Glendening, E. D.; Reed, A. E.; Carpenter, J. E.; Weinhold, F. NBO Version 3.1. *NBO Version 3.1.*

Chapter 7

Summary and Outlook

7.1 Summary

The research investigation deals with both computational as well as the experimental studies. The computational study focuses on the electronic structural, stability and the reactivity aspects of the heterocyclic radicals. Computational journey started with exploration of the relative stability pattern in pyridyl radical isomers. The primary objective was to interpret the interactions between the nitrogen lone pair and the radical center which influences the stability pattern. The objective was executed by performing spin density, electrostatic potential, bond dissociation energy calculations which gave insights regarding these interactions. The qualitative analysis of the mode of interactions (i.e. through space and through bond) was done by performing multireference calculations. Whereas, the natural bond orbital (NBO) gave the quantitative estimation of such interactions. Thus, the thermodynamic stability order (*o*-pyridyl > *p*-pyridyl > *m*-pyridyl) was justified by the above computational analysis. Moreover, for obtaining the evidences of lone-pair and radical interactions we investigated pyridyl-*N*-oxide and protonted analogues of the pyridyl radicals. The interactions were partially quenched by *N*-oxidation and were completely nullified by protonation of nitrogen lone pair which proves the involvement of nitrogen lone pair in stabilizing the radical center in pyridyl radical isomers.

Just like the thermodynamic stability in the pyridyl radical isomers, we also wanted to explore their kinetic stability through reactivity aspects. To execute this plan, we studied (a) Isomerization through 1, 2 H-shift (b) Second C-H bond scission leading to the formation of

biradicals (c) Unimolecular decomposition channels leading to fragmented products (d) Bimolecular reactions with small molecules as the possible reactivity channels. The channels (a) and (b) had higher energy barriers, thus we considered channels (c) and (d) for obtaining the kinetic stability. At this juncture, spin density value at the reactant and as well as transition state played a major role in deciding the bond cleavages in the unimolecular channels and also in explaining the reactivity pattern in the bimolecular reactions for pyridyl radical isomers. Once again, the study conducted on the *N*-oxidation and protonated analogues justified the kinetic stability trend for the pyridyl radical isomers.

From six-membered heterocyclic radicals (i.e. pyridyl), we extended our study to five-membered heterocyclic radicals (B, N, O, P and S) containing one heteroatom. The relative stability order displayed the stability trend: Heteroatom-centered > β-centered > α-centered. The higher stability of heteroatom-centered (i.e π-radical) was accounted by the BDE and the spin density calculations. The orbital interactions revealed by the NBO analysis was not satisfactory to explain the higher stability of β-centered radicals over α. At this juncture, the major challenge was overcomed by calculating the resonance and ring strain energies. Thus, among the radical isomers; heteroatom-centered radical was the most stable owing to the dominating resonance energy whereas β-centered radical had higher resonance and lower ring strain energy as compared to its α counterpart. Overall, it is the resonance (i.e. stabilizing effect) which dominates over the ring strain (i.e. destabilizing effect) and dictates the overall stability order.

The photochemistry of azobenzene based derivatives under cryogenic conditions are limited in literature. In this regard, we wanted to explore 2-hydroxyphenylazo-3,5-dimethylisoxazole due to its interesting molecular properties. On irradiation with 365 nm, the molecule can

undergo (a) tautomerism due to the presence of ortho-hydroxy group (b) *E-E* conformational change and (c) *E-Z* photoisomerization due to the presence of two methyl groups in the isoxazole unit. Thus the objective was to explore the competition among tautomerism, conformational change and photoswitching channel and to find out the dominating channel. The molecule was successfully deposited in its stable *E*-form (i.e. **1E-C1-s**) and on irradiation with 365 nm it photoswitched to its *Z*-form (i.e. **1Z-C3-s**). The spectral features obtained on irradiation did not matched with *E*-conformers and also lacked the carbonyl stretching; which rules out the possibility of *E-E* conformational change and tautomerism. Through this investigation, we successfully induced *E-Z* photoisomerization in 2-hydroxyphenylazo-3,5-dimethylisoxazole in argon matrix at 4 K.

7.2 Outlook

During our investigations on the five-membered heterocyclic radicals, the heteroatom centered (B, N, P) radicals formed an interesting class of (4n+1) π delocalized systems, especially in the N-centered pyrrole radical. The creation of another radical center (i.e. σ) will give rise to orthogonality of orbitals in order to obtain high spin biradicals. In this regard, future work will focus on the biradical formation and its ground state (i.e. singlet or triplet); and in tuning the singlet-triplet energy gap by substituent effects. Design and development of such stable biradicals with high spin ground state multiplicity will have potential application in data storage and in making of organic based molecular magnets.

APPENDIX CHAPTER 2

Table A2.1 Electronic and thermodynamic parameters of all the radical isomers and their respective parents at both (U)B3LYP/cc-pVTZ and (U)M06/cc-pVTZ levels of theory. Normal font indicates (U)B3LYP and italics represent (U)M06.

Species	Absolute energy (Hartrees)	ZPVE (Hartrees)	Lowest Frequency	Spin Contamination		Point Group	Electronic State	Absolute free energy(G) (Hartrees)	Absolute Enthalpy(H) (Hartrees)
				Before Annihilation	After Annihilation				
1	−248.37319	0.088611	385.54	0.0000	0.0000	C_{2v}	$^1A_1$	−248.31131	−248.27937
	−248.17229	*0.088222*	*376.68*	*0.0000*	*0.0000*			*−248.11081*	*−248.07883*
1a	−247.69339	0.075746	386.75	0.7552	0.7500	C_s	$^2A'$	−247.64561	−247.61245
	−247.49468	*0.075448*	*376.52*	*0.7584*	*0.7500*			*−247.44720*	*−247.41400*
1b	−247.68336	0.075550	391.16	0.7570	0.7500	C_s	$^2A'$	−247.63577	−247.60262
	−247.48606	*0.075325*	*381.60*	*0.7626*	*0.7501*			*−247.43870*	*−247.40552*
1c	−247.68519	0.075321	380.29	0.7563	0.7500	C_{2v}	$^2A_1$	−247.63717	−247.60469
	−247.48811	*0.075106*	*365.84*	*0.7618*	*0.7501*			*−247.44032*	*−247.40779*
2	−248.74382	0.102891	393.19	0.0000	0.0000	C_{2v}	$^1A_1$	−248.66776	−248.63563
	−248.54114	*0.102296*	*384.93*	*0.0000*	*0.0000*			*−248.46568*	*−248.43350*
2a	−248.04299	0.089265	384.25	0.7573	0.7500	C_s	$^2A'$	−248.98179	−248.94844
	−248.84509	*0.088901*	*373.64*	*0.7623*	*0.7501*			*−248.78426*	*−248.75087*
2b	−248.04440	0.089526	379.22	0.7567	0.7500	C_s	$^2A'$	−248.98294	−248.94959
	−247.84697	*0.089131*	*367.24*	*0.7618*	*0.7501*			*−247.78591*	*−247.75251*
2c	−248.04825	0.089534	390.59	0.7564	0.7500	C_{2v}	$^2A_1$	−247.98611	−247.95345
	−248.85048	*0.089123*	*380.58*	*0.7629*	*0.7501*			*−247.78876*	*−247.75605*
3	−323.56750	0.092807	211.02	0.0000	0.0000	C_{2v}	$^1A_1$	−323.50274	−323.46870
	−323.32992	*0.092503*	*211.25*	*0.0000*	*0.0000*			*−323.26546*	*−323.23141*
3a	−322.86826	0.079324	198.66	0.7623	0.7501	C_s	$^2A'$	−322.81832	−322.78287
	−322.63503	*0.079289*	*200.16*	*0.7677*	*0.7501*			*−322.58511*	*−322.54967*
3b	−322.87665	0.079527	206.68	0.7581	0.7500	C_s	$^2A'$	−322.82642	−322.79113
	−322.64360	*0.079458*	*206.75*	*0.7637*	*0.7501*			*−322.59343*	*−322.55814*
3c	−322.87402	0.079597	218.88	0.7641	0.7501	C_{2v}	$^2A_1$	−322.82307	−322.78842
	−322.64134	*0.079481*	*219.47*	*0.7723*	*0.7502*			*−322.59049*	*−322.55585*

(a)

1a

1b

1c

(b)

2a

2b

2c

(c)
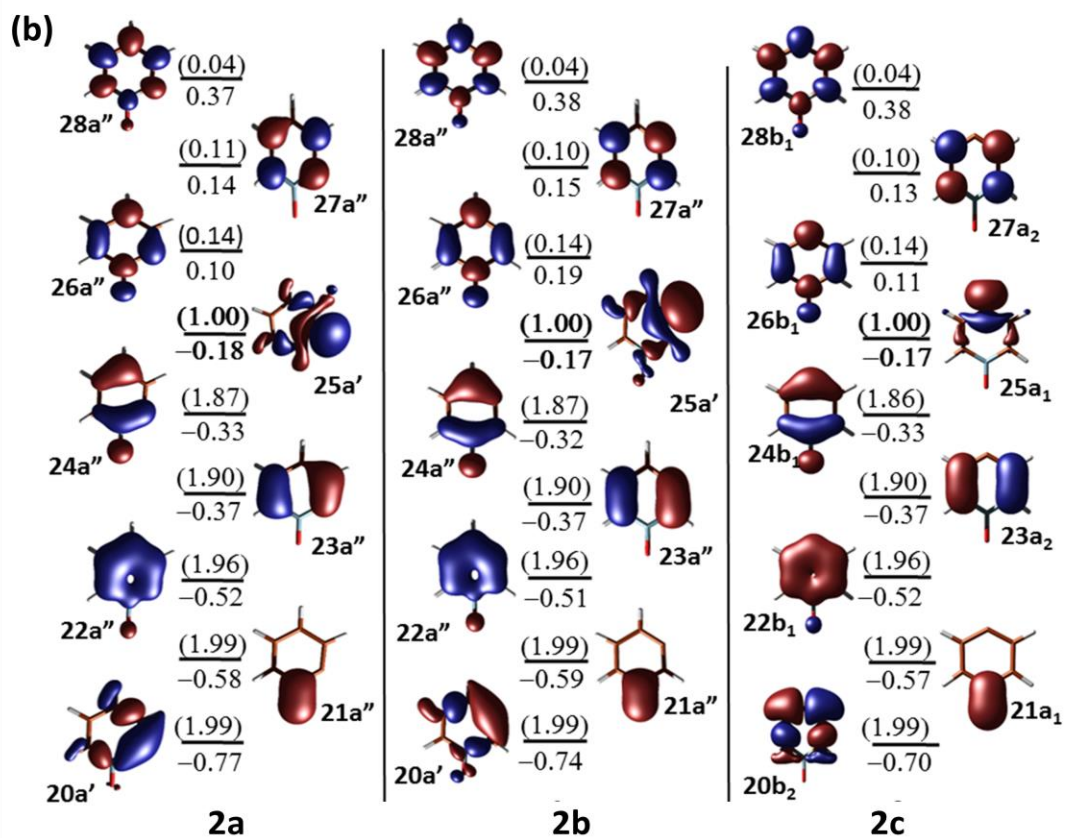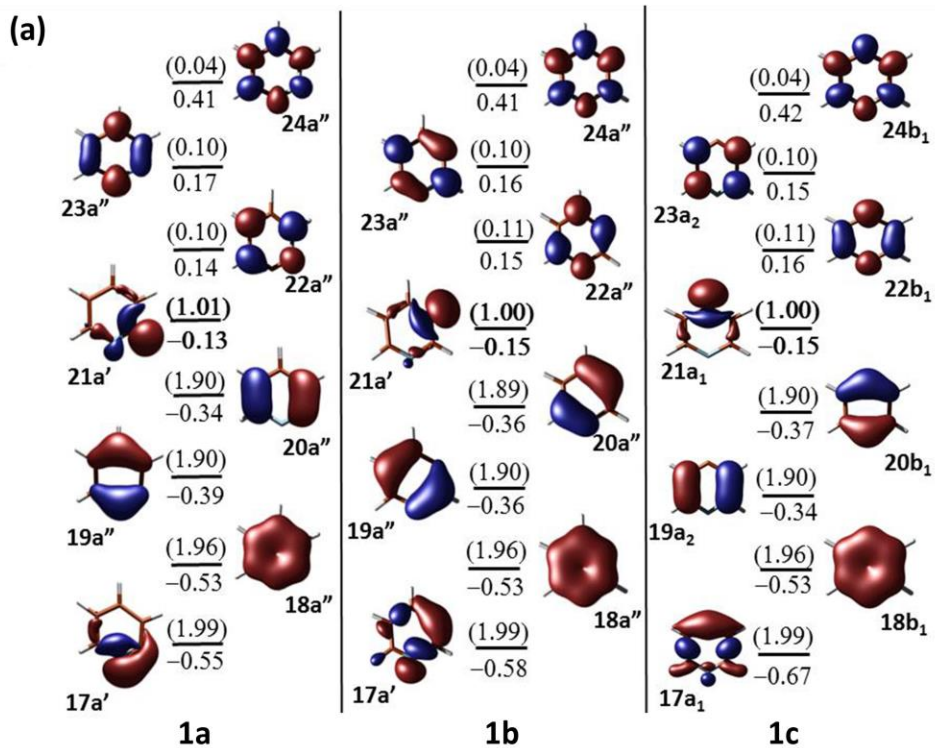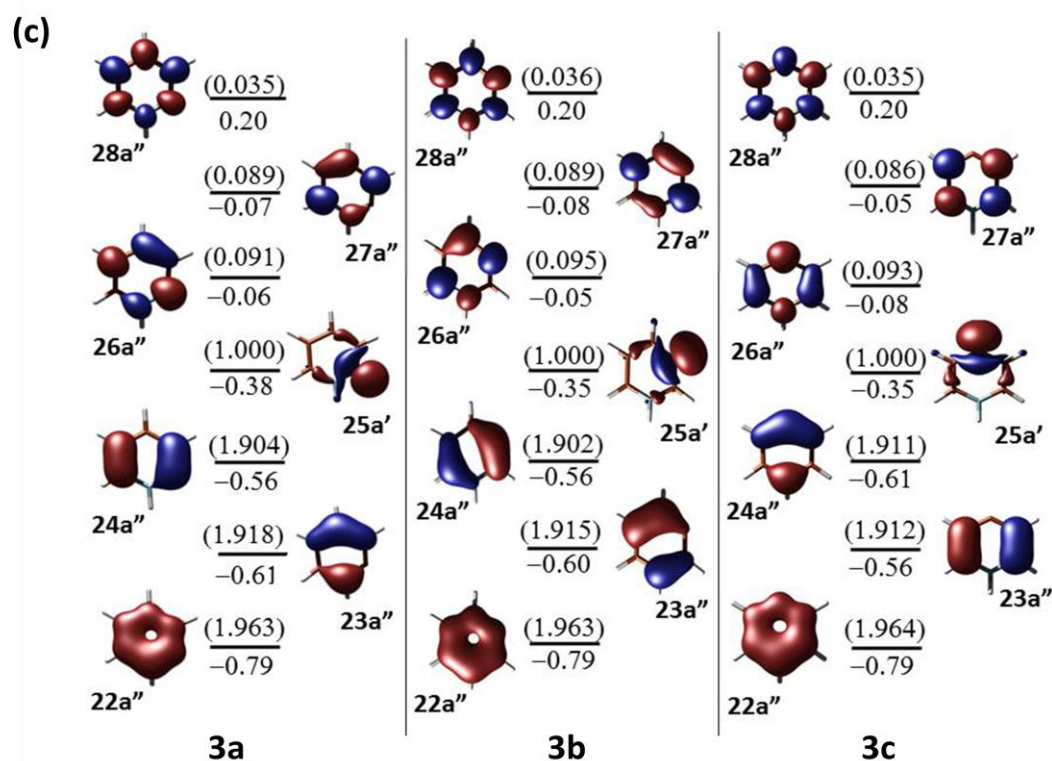
Figure A2.1 The complete active space molecular orbital diagrams of all the radicals at CASSCF/cc-pVTZ//(U)B3LYP/cc-pVTZ level of theory; (a) pyridyl radicals **1a-c** (b) pyridyl-*N*-oxide radicals **2a-c** (c) pyridinyl radicals **3a-c**. The values in normal font indicate orbital energies (hartree) and values in parenthesis represent the occupancies. Orbital number and their respective symmetry are designated in bold. All the orbitals are rendered at an isovalue 0.05.

VIE is the energy required to remove an electron from a radical to form a cation. Whereas, VDE is the energy required to detach an electron from anion to form a radical.

(a)

(b)

$$X = N, \overset{\oplus}{N}\text{-}\overset{\ominus}{O}, \overset{\oplus}{N}H$$
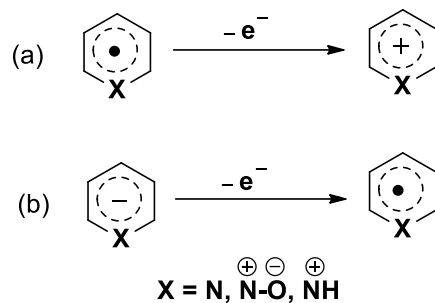
Scheme A.2.1 (a) VIE and (b) VDE of radical isomers of pyridine **1a-c**, pyridine-*N*-oxide **2a-c** and cationic pyridine **3a-c**.

$$(\text{VIE})^{\Delta E} = E_{N-1}(G_N) - E_N(G_N)$$

$$(\text{VDE})^{\Delta E} = E_N(G_{N+1}) - E_{N+1}(G_{N+1})$$

Where $E_{N-1}(G_N)$ and $E_N(G_N)$ are the total energies of (N-1) and N electron systems calculated at the G_N geometry; on the other hand, $E_N(G_{N+1})$ and $E_{N+1}(G_{N+1})$ are the total energies of N and (N+1) electron systems calculated at G_{N+1} geometry.

APPENDIX CHAPTER 3

Table A3.1 Activation Energy Barrier and the Spin Densities at Transition States for the Reactions of Phenyl, Dehydro-Pyridyl **1a-c**, Pyridyl-*N*-oxide **2a-c** and Pyridinyl **3a-c** Radical Isomers with Small Molecules H_2, H_2O, CO, CO_2, CH_4 and CH_3OH at(U)B3LYP/cc-pVTZ (bold), (U)M06-2X/cc-pVTZ (normal) and (U)CCSD(T)/cc-pVTZ//(U)B3LYP/cc-pVTZ (italics) Levels of Theory.

Radicals	H_2	H_2O (H radical)	H_2O (OH radical)	CO	CO_2	CH_4	CH_3OH
Phenyl Radical	**5.5** (0.670)	**35.4(0.239)**	**4.2 (0.424)**	**0.9(0.843)**	**10.3(0.538)**	**8.3(0.582)**	**−0.4(0.547)**
	7.7 (0.692)	39.1(0.237)	8.8(0.373)	0.9(0.891)	10.3(0.499)	9.6(0.601)	2.7 (0.533)
	8.6 (1.335)	*52.7 (0.958)*	*19.2 (0.733)*	*1.9 (1.491)*	*14.4 (1.157)*	*13.4(1.229)*	*8.5 (1.194)*
1a	**8.1 (0.528)**	**35.0 (0.274)**	**7.3 (0.295)**	**2.0 (0.677)**	**11.5 (0.425)**	**11.9 (0.500)**	**1.0 (0.407)**
	10.4 (0.557)	36.4(0.292)	11.7(0.302)	2.1(0.741)	13.9(0.126)	12.5(0.504)	3.8(0.387)
	11.6(1.183)	*106.0(0.404)*	*15.2(0.768)*	*4.2(1.345)*	*16.7(1.041)*	*16.7(1.119)*	*10.5(1.012)*
1b	**5.5 (0.648)**	**35.4 (0.225)**	**3.9 (0.410)**	**1.2 (0.803)**	**9.9 (0.536)**	**8.0 (0.572)**	**−0.7 (0.525)**
	7.5 (0.676)	38.2(0.216)	8.3(0.380)	1.1(0.873)	10.0(0.552)	8.8(0.594)	2.2(0.531)
	8.6 (1.340)	*49.5 (1.047)*	*12.4(0.968)*	*2.3(1.491)*	*14.4(1.216)*	*12.8(1.236)*	*8.4(1.206)*
1c	**6.1 (0.646)**	**35.0 (0.240)**	**4.9 (0.403)**	**1.5 (0.809)**	**11.6 (0.497)**	**8.7 (0.571)**	**0.1 (0.525)**
	8.2(0.646)	37.4(0.235)	9.6(0.353)	1.6(0.846)	12.0(0.451)	9.7(0.568)	**3.2(0.502)**
	9.3(1.315)	*49.4(1.030)*	*13.5(0.930)*	*2.8(1.467)*	*16.5(1.152)*	*13.6(1.214)*	*9.3(1.180)*
2a	**4.2 (0.746)**	–	**−0.7 (0.555)**	**0.6 (0.866)**	**12.5 (0.586)**	**4.0 (0.643)**	**−2.8 (0.628)**
	6.9(0.745)		2.5(0.525)	0.6(0.878)	13.2(0.629)	4.9(0.652)	−0.3(0.638)
	7.1(1.488)		–	*1.4(1.581)*	*13.9(0.702)*	*9.0(1.388)*	–
2b	**5.4 (0.662)**	**35.1 (0.231)**	**4.4 (0.432)**	**1.3 (0.823)**	**29.3 (−0.035)**	**7.3 (0.580)**	**−0.3 (0.550)**
	7.9(0.684)	37.7(0.212)	8.8(0.409)	1.3(0.887)	28.7(-0.057)	8.2(0.603)	2.7(0.561)
	8.5(1.390)	*60.5 (1.153)*	–	*2.3(1.533)*	*18.0(1.567)*	*12.1(1.288)*	–
2c	**4.8 (0.723)**	**32.4 (0.132)**	**3.3 (0.480)**	**0.9 (0.887)**	**10.8 (0.608)**	**6.5 (0.623)**	**−1.0 (0.605)**
	7.0(0.719)	35.2(0.106)	8.2(0.426)	0.9(0.915)	25.7(0.235)	8.1(0.629)	2.2(0.588)
	8.0(1.478)	*60.2(-0.728)*	–	*1.8(1.608)*	*25.1(0.256)*	*10.8(0.626)*	–
3a	**2.8 (0.721)**	**20.5 (0.214)**	**2.4 (0.504)**	**−0.4 (0.830)**	**16.8 (0.538)**	**−1.2(0.638)**	**−4.5 (0.576)**
	5.2(0.696)	23.5(0.201)	6.6(0.480)	0.5(0.852)	17.7(0.541)	0.8(0.625)	−1.1(0.601)
	6.0(1.209)	*32.7(0.106)*	*10.7(0.899)*	*1.0(1.309)*	*20.8(0.872)*	*4.4(1.107)*	*4.5(1.182)*
3b	**3.2 (0.714)**	**22.7 (0.014)**	**3.4 (0.432)**	**−0.4 (0.840)**	**17.6 (0.534)**	**0.2 (0.618)**	**−2.3 (0.408)**
	5.5(0.702)	25.5(-0.023)	7.8(0.489)	0.5(0.875)	18.3(0.549)	2.1(0.615)	1.1(0.646)
	6.3(1.275)	*39.2(-0.393)*	*12.0(0.984)*	*0.8(1.400)*	*21.5(0.903)*	*5.6(1.067)*	*6.3(1.267)*
3c	**4.1 (0.684)**	**16.9 (0.197)**	**4.8 (0.505)**	**0.4 (0.821)**	**18.8 (0.540)**	**1.6 (0.600)**	**−1.1 (0.616)**
	6.4(0.645)	19.8(0.181)	9.5(0.457)	1.3(0.843)	20.2(0.488)	3.5(0.574)	2.2(0.620)
	7.6(1.218)	*28.3(0.082)*	*13.8(0.912)*	*2.0(1.358)*	*24.0(1.071)*	*7.2(1.084)*	*8.0(1.244)*

A3.1 Computing spin density:

$$\rho_s(r) = \rho_\alpha(r) - \rho_\beta(r)$$

Spin density is the difference between the α electron density and the β electron density. Electron spin density is positive in areas where an electron is more likely to be in α spin state, and negative where an electron is more likely to be in β spin state. Spin density is an important parameter which helps us to understand whether the spins are localized at the radical center or delocalized. In general, localized radicals have high positive spin density values. Lowering of the spin density values at the radical center gives insights regarding the extend of delocalization. Experimentally, electron spin density is measured by electron paramagnetic resonance (EPR). Polarized neutron diffraction is a major experimental technique for spin density estimation. Computationally, spin density values corresponding to individual atoms in a molecule can be obtained from the output file of the optimized radical structure.

Table A.3.2 Comparison of first unimolecular decomposition channels in pyridyl radical isomers **1a-c** with previously reported literature data.

Species (First unimolecular Bond cleavage)	Present Work			Literature
	(U)B3LYP/cc-pVTZ	(U)M06-2X/cc-pVTZ	(U)CCSD(T)/cc-pVTZ//(U)B3LYP/cc-pVTZ	QCISD(T)/cc-pVDZ +ZPE
1a$_{C-N}$	42.5	45.3	43.8	40.3
1a$_{C-C}$	72.4	75.4	78.8	76.0
1b$_{C-N}$	45.2	50.0	49.6	51.4
1b$_{C-C}$	69.7	72.2	75.2	77.5
1c$_{C-C}$	57.6	61.3	66.6	66.2

Section 1A Unimolecular decomposition channels with spin density values indicated in purple color.
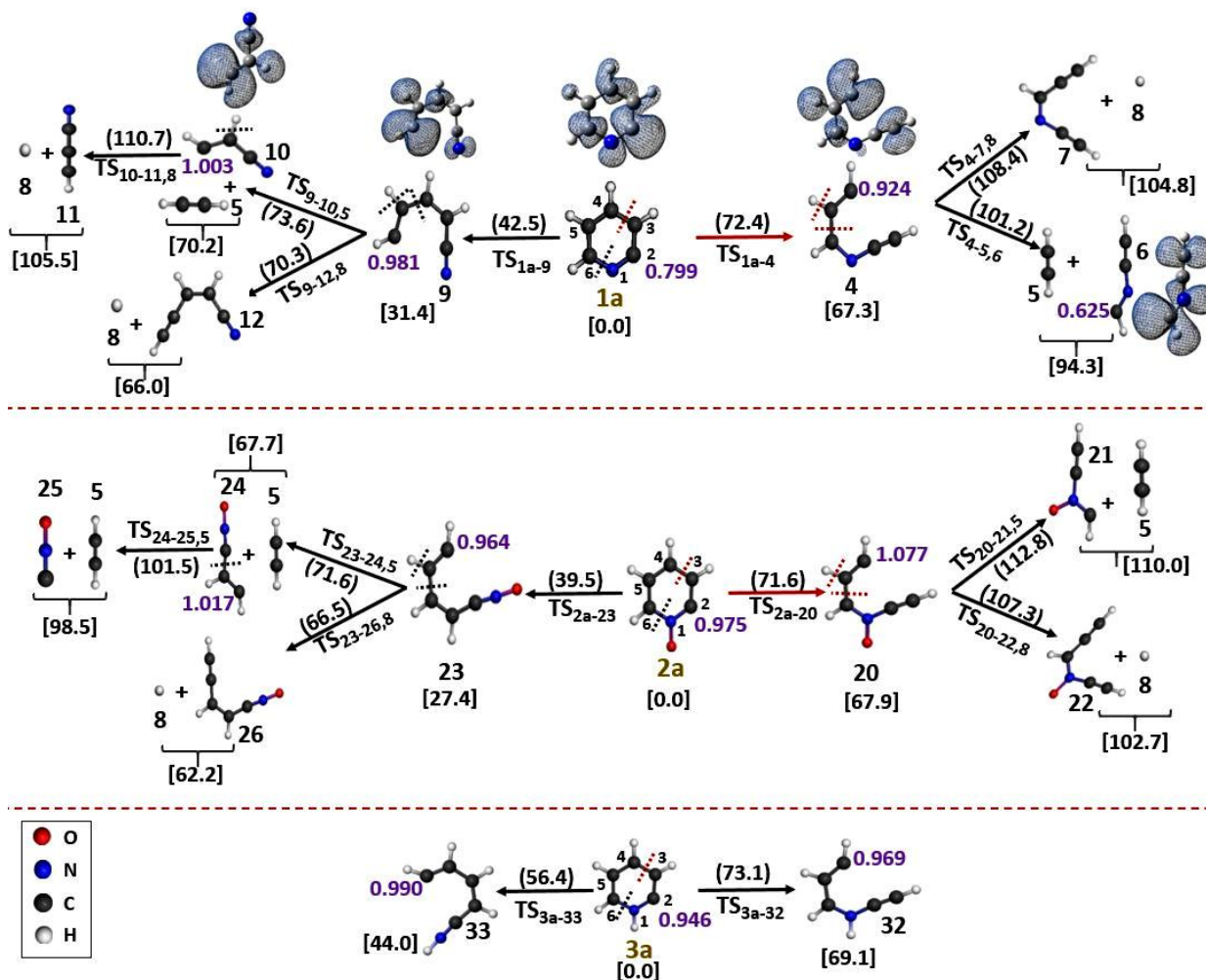

Figure A3.1 Unimolecular decomposition channels of 2-pyridyl **1a**, 2-pyridyl-*N*-oxide **2a**, and 2-pyridinyl **3a** radicals with spin densities indicated in purple color at (U)B3LYP/cc-pVTZ level of theory.
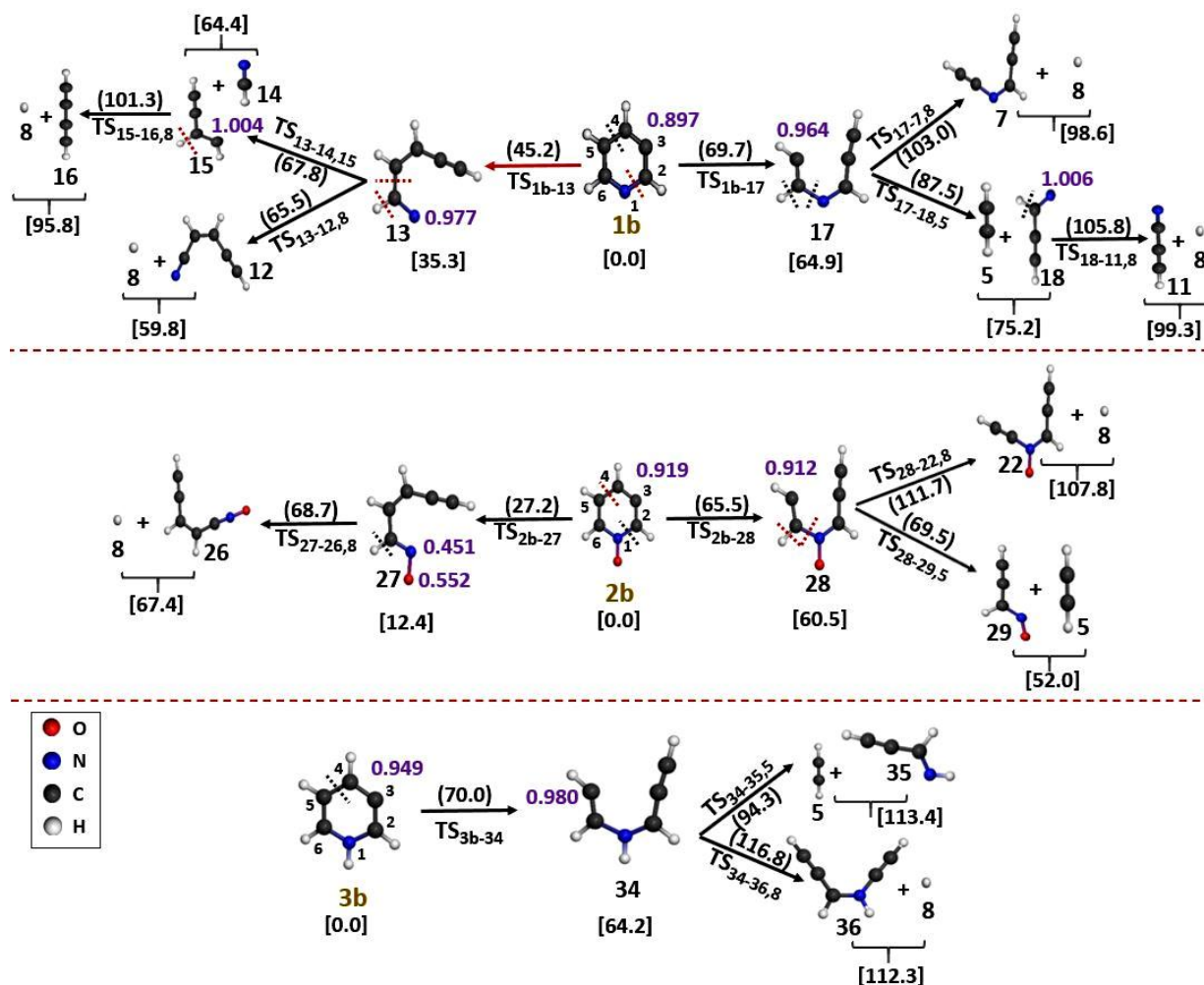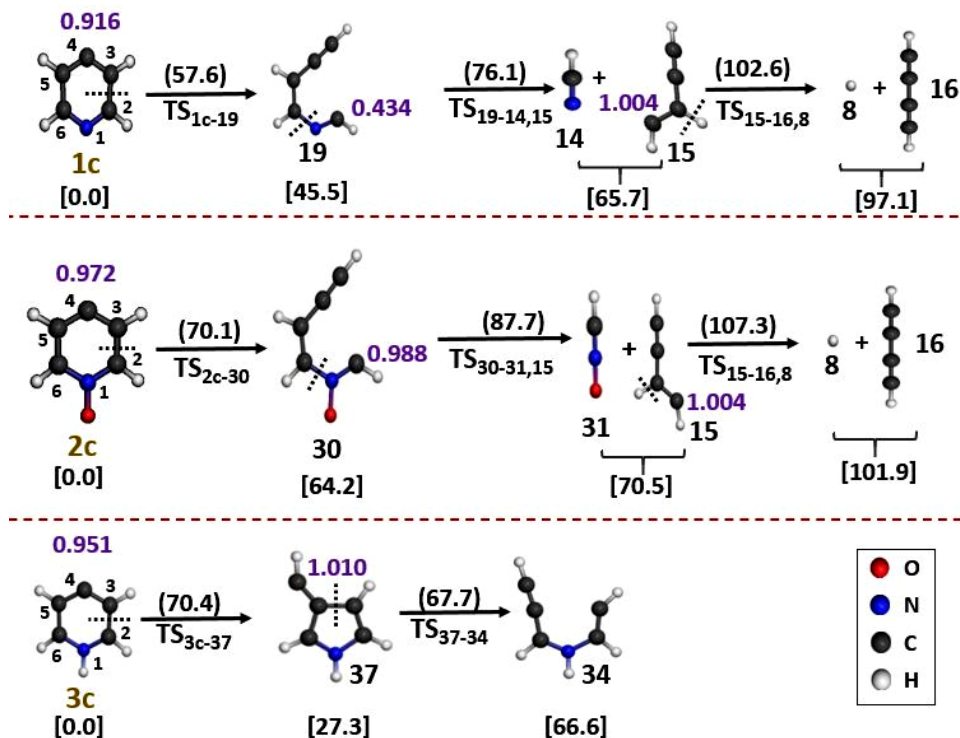
Figure A3.2 Unimolecular decomposition channels of 3-pyridyl **1b**, 3-pyridyl-*N*-oxide **2b**, and 3-pyridinyl **3b** radicals with spin densities indicated in purple color at (U)B3LYP/cc-pVTZ level of theory.
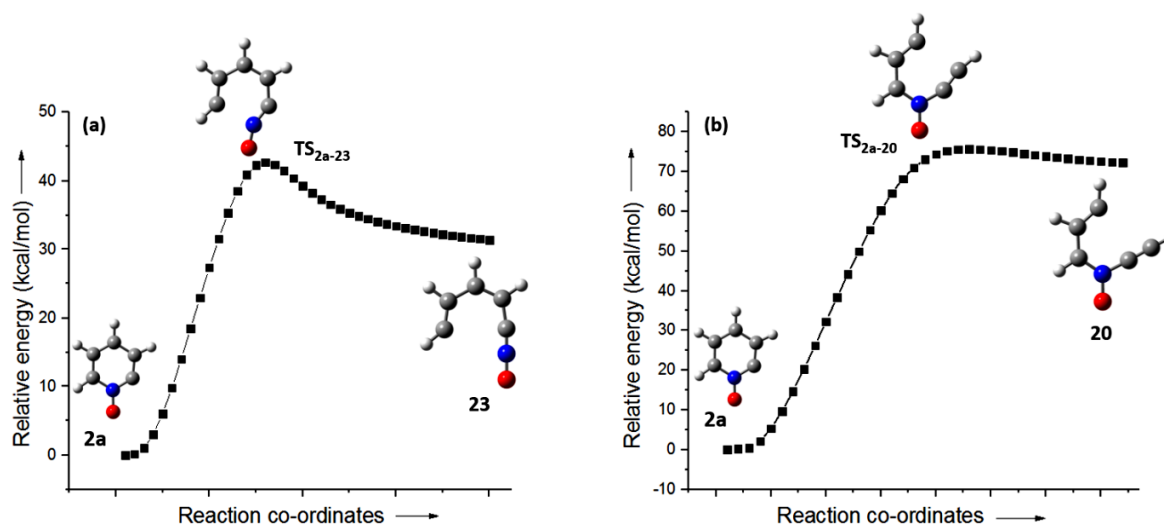
Figure A3.3 Unimolecular decomposition channels of 4-pyridyl **1c**, 4-pyridyl-*N*-oxide **2c**, and 4-pyridinyl **3c** radicals with spin densities indicated in purple color at (U)B3LYP/cc-pVTZ level of theory.

Section 2A IRC for Unimolecular decomposition channels

Figure A3.4 IRC corresponding to (a) C-N bond breaking and (b) C-C bond breaking step in 2-dehydro pyridyl-*N*-oxide (**2a**) radical at (U)B3LYP/cc-pVTZ level of theory.
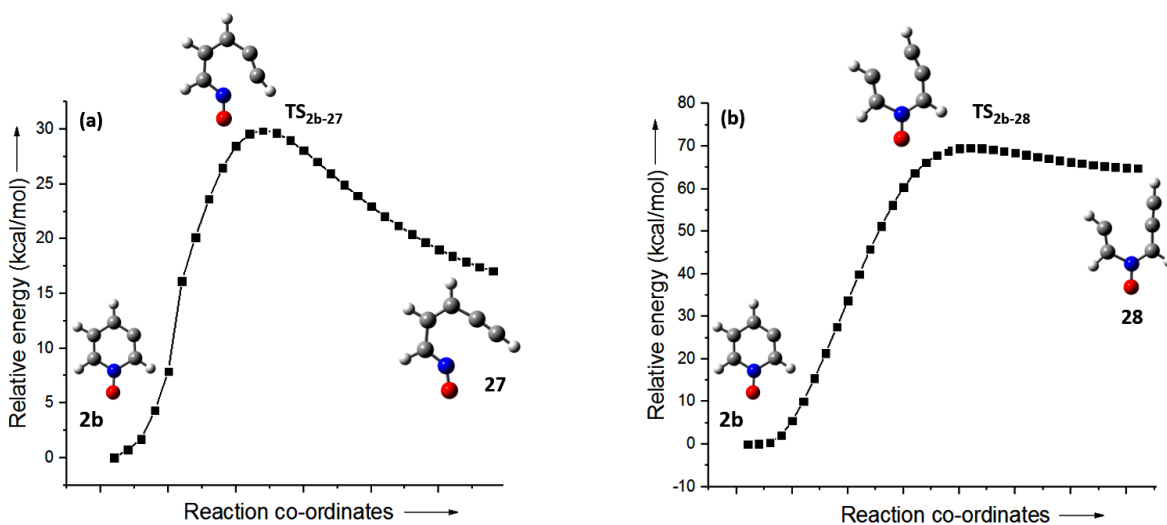
Figure A3.5 IRC corresponding to (a) C-N bond breaking and (b) C-C bond breaking step in 3-dehydro pyridyl-*N*-oxide (**2b**) radical at (U)B3LYP/cc-pVTZ level of theory.
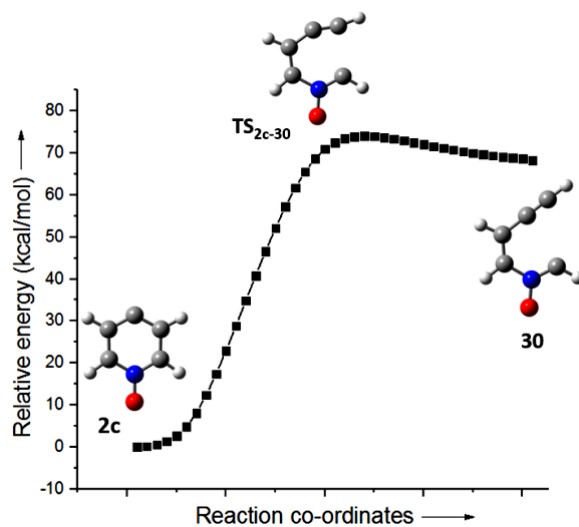

Figure A3.6 IRC corresponding to C-C bond breaking step in 4-dehydro pyridyl-*N*-oxide (**2c**) radical at (U)B3LYP/cc-pVTZ level of theory.
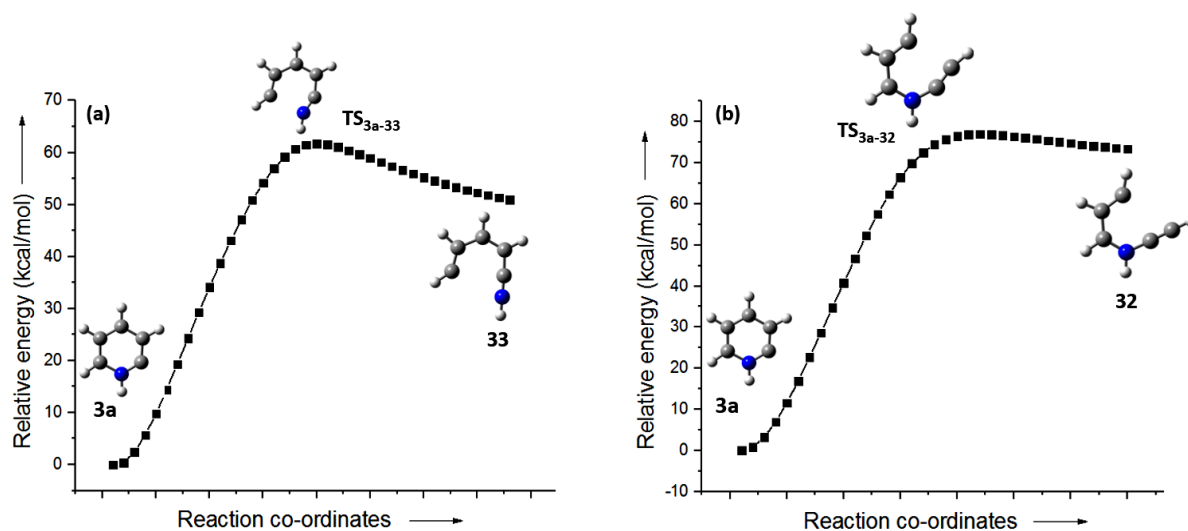
Figure A3.7 IRC corresponding to (a) C-N bond breaking and (b) C-C bond breaking step in 2-dehydropyridinyl (**3a**) radical at (U)B3LYP/cc-pVTZ level of theory.
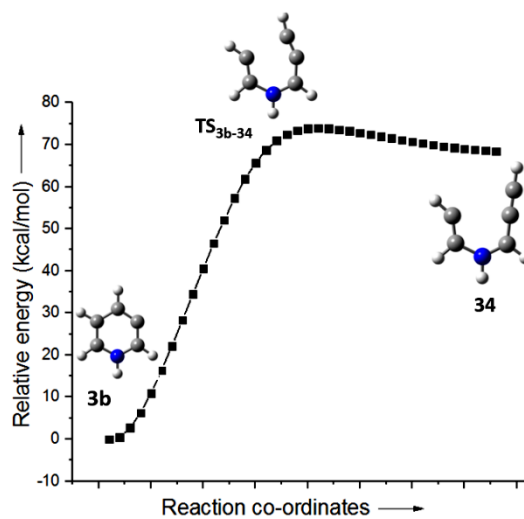

Figure A3.8 IRC corresponding to C-C bond breaking step in 3-dehydropyridinyl (**3b**) radical at (U)B3LYP/cc-pVTZ level of theory.
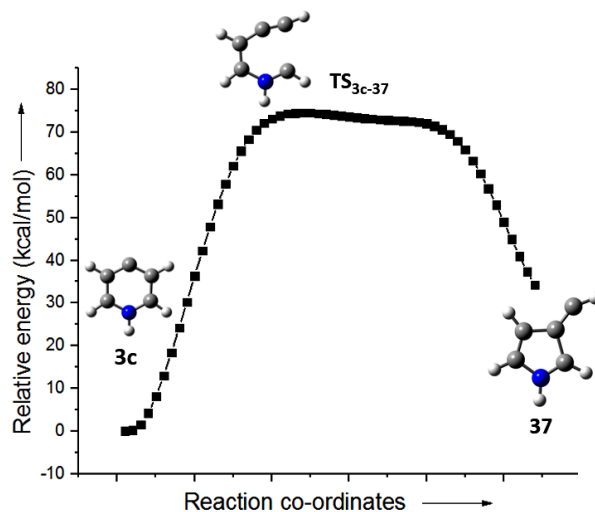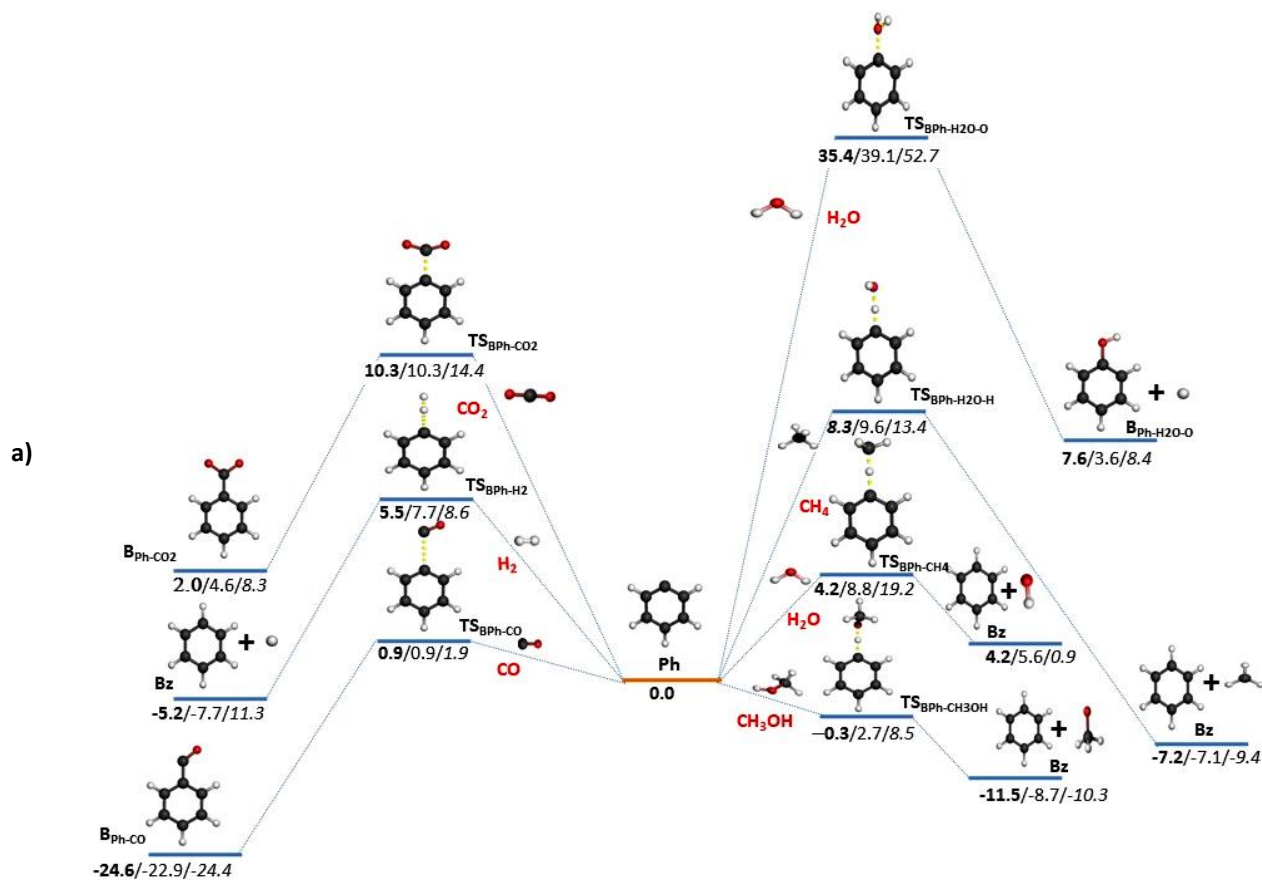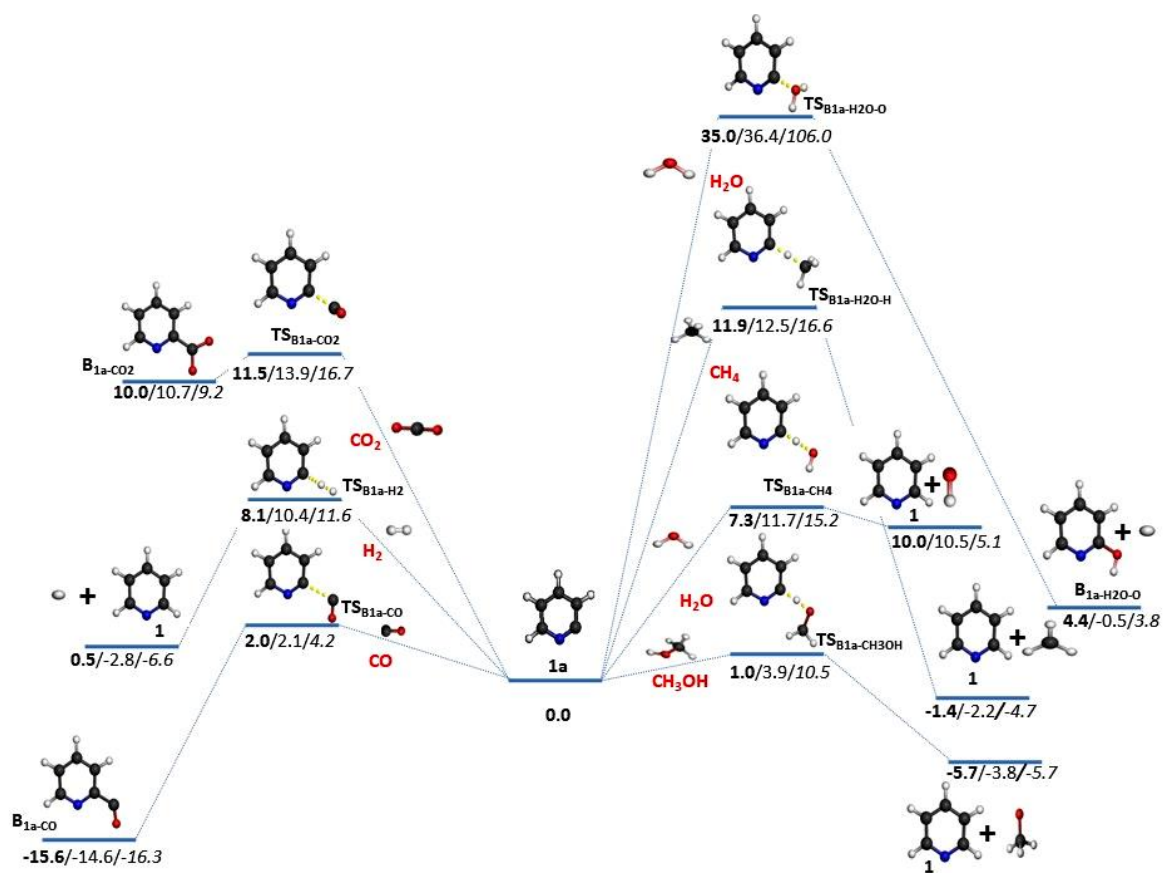
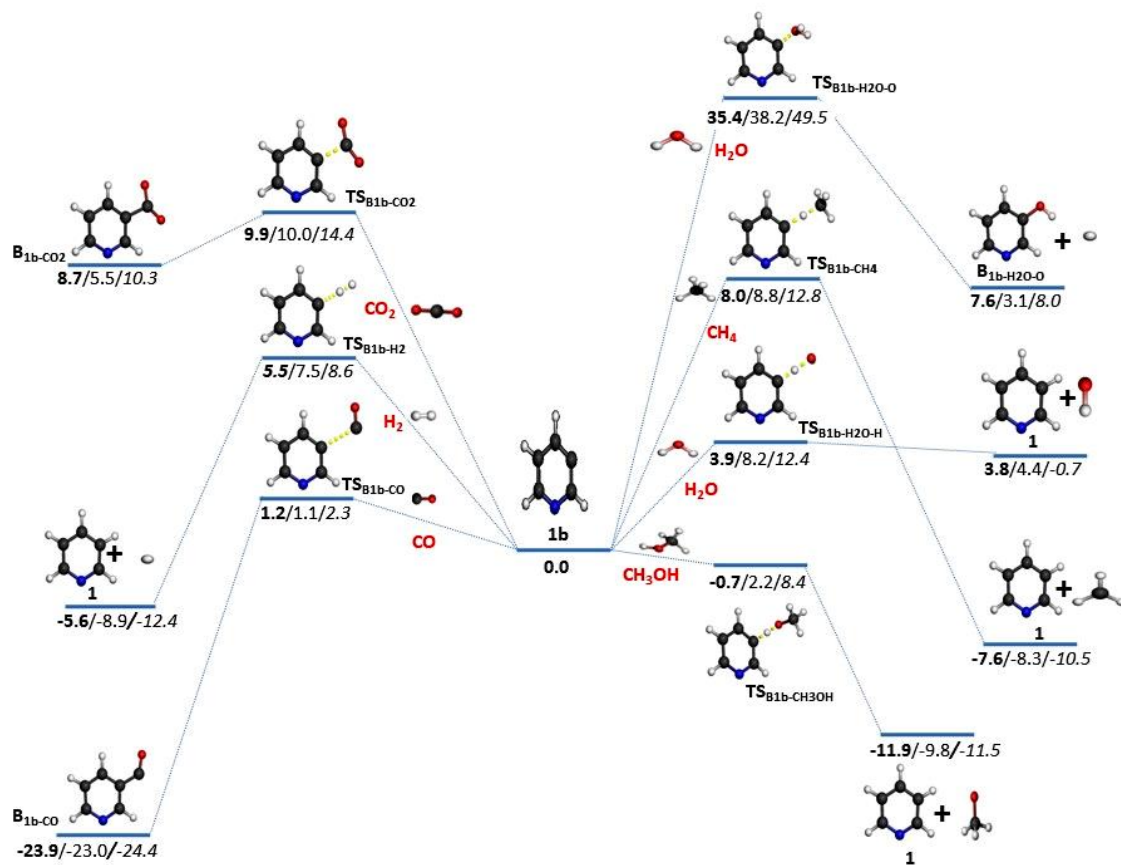**Figure A3.9** IRC corresponding to C-C bond breaking step in 4-dehydropyridinyl (**3c**) radical at (U)B3LYP/cc-pVTZ level of theory.

Section 3A Bimolecular reactions with small molecules

b)

TS$_{B1a-H2O-O}$
35.0/36.4/*106.0*

H$_2$O

TS$_{B1a-H2O-H}$
11.9/12.5/*16.6*

CH$_4$

B$_{1a-CO2}$
10.0/10.7/*9.2*

TS$_{B1a-CO2}$
11.5/13.9/*16.7*

CO$_2$

TS$_{B1a-H2}$
8.1/10.4/*11.6*

H$_2$

1

+

TS$_{B1a-CO}$
2.0/2.1/*4.2*

0.5/-2.8/*-6.6*

CO

TS$_{B1a-CH4}$
7.3/11.7/*15.2*

H$_2$O

TS$_{B1a-CH3OH}$
1.0/3.9/*10.5*

CH$_3$OH

1a

0.0

1

+

10.0/10.5/*5.1*

B$_{1a-H2O-O}$
4.4/-0.5/*3.8*

+

1

+

-1.4/-2.2/*-4.7*

-5.7/-3.8/*-5.7*

1

+

B$_{1a-CO}$
-15.6/-14.6/*-16.3*

c)

d)

$TS_{B1c-H2O-O}$
35.0/37.4/*49.4*

H_2O

B_{1c-CO2}
10.9/8.0/*10.2*

$TS_{B1c-CO2}$
11.6/12.0/*16.5*

$TS_{B1c-CH4}$
8.7/9.7/*13.6*

$B_{1c-H2O-O}$
6.7/2.5/*6.8*

CH_4

TS_{B1c-H2}
6.0/8.2/*9.3*

CO_2

$TS_{B1c-H2O-H}$
4.9/9.6/*13.4*

1
5.1/6.2/*0.8*

H_2

H_2O

TS_{B1c-CO}
1.4/1.6/*2.8*

1
-4.4/-7.1/*-10.9*

1c
0.0

CO

CH_3OH

$TS_{B1c-CH3OH}$
0.1/3.2/*9.3*

1
-6.3/-6.6/*-9.0*

-10.6/-8.1/*-10.0*

B_{1c-CO}
-21.3/-19.9/*-21.6*

1

e)

TS$_{B3a-H2O-O}$
22.7/25.5/*32.7*

TS$_{B3a-CO2}$
16.8/17.7/*20.8*

B$_{3a-CO2}$
9.7/10.5/*9.6*

CO_2

H_2O

TS$_{B3a-H2}$
2.8/5.2/*6.0*

H_2

TS$_{B3a-CO}$
-0.4/0.5/*1.0*

3a
0.0

CO

H_2O

TS$_{B3a-H2O-H}$
2.4/6.6/*10.7*

TS$_{B3a-CH4}$
-1.2/0.8/*4.4*

CH_4

CH_3OH

-4.5/-1.1/*4.5*

B$_{3a-H2O-O}$
-1.2/-4.4/*0.9*

3
-2.7/-0.8/*-5.3*

3
-12.2/-14.2/*-17.4*

B$_{3a-CO}$
-20.4/-17.9/*-19.4*

TS$_{B3a-CH3OH}$

3
-14.2/-13.6/*-15.5*
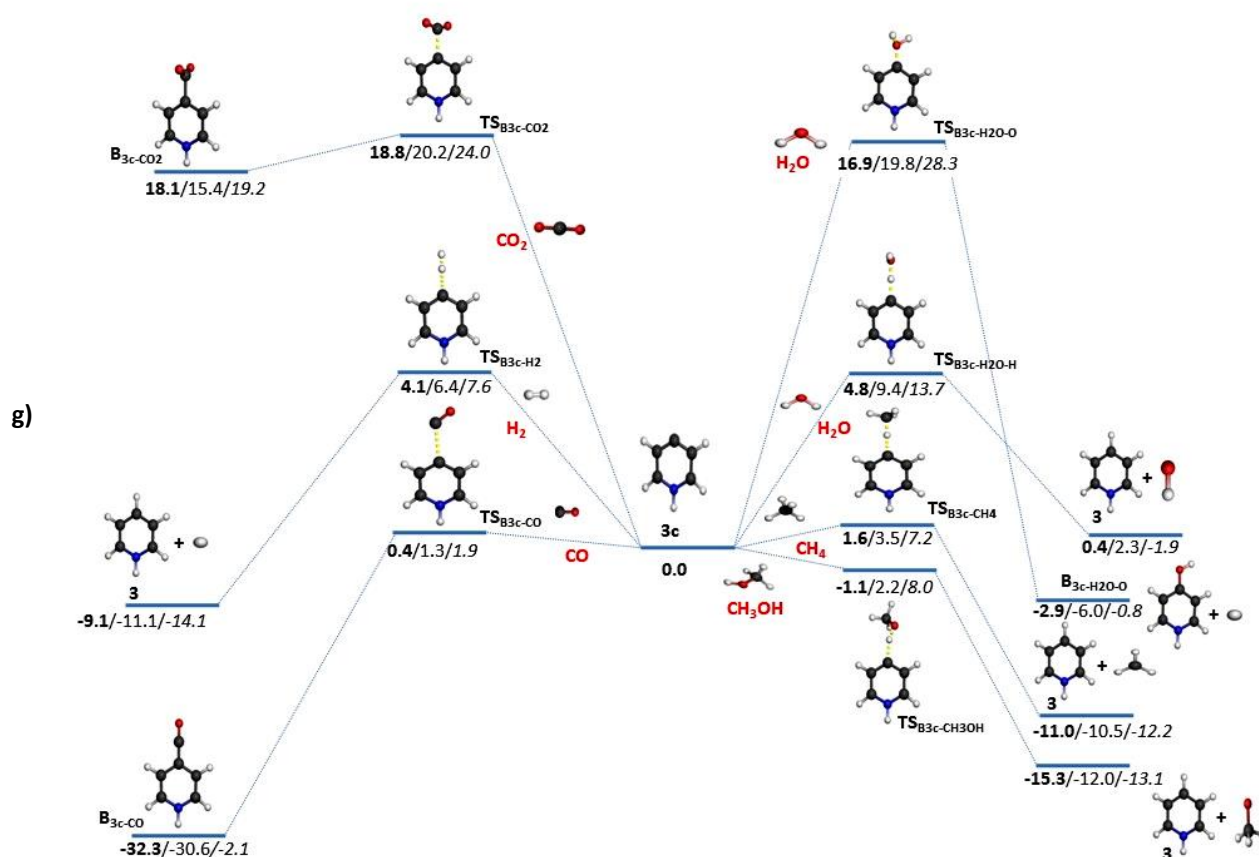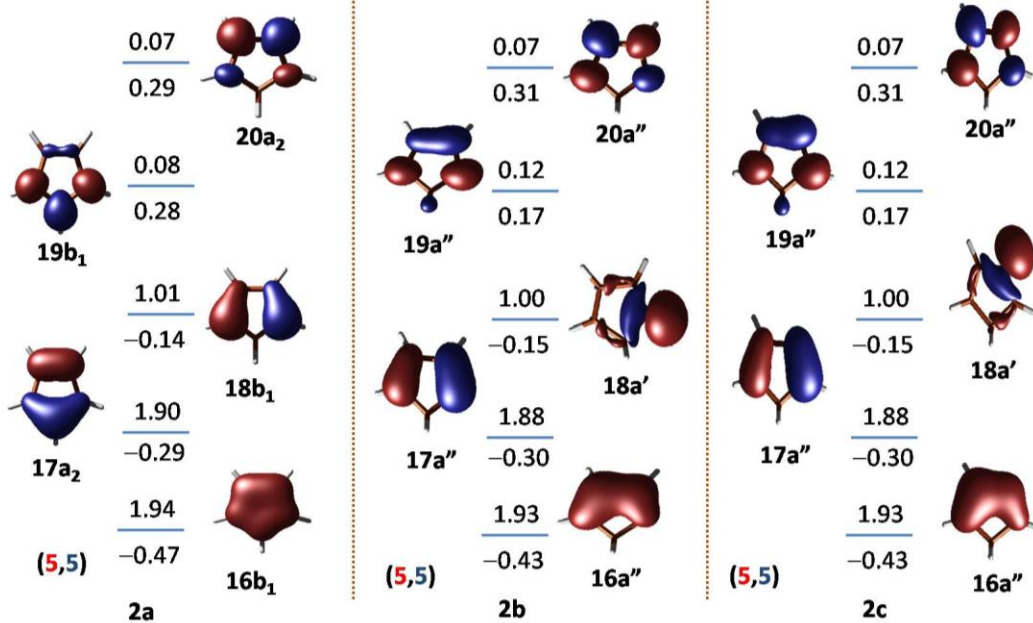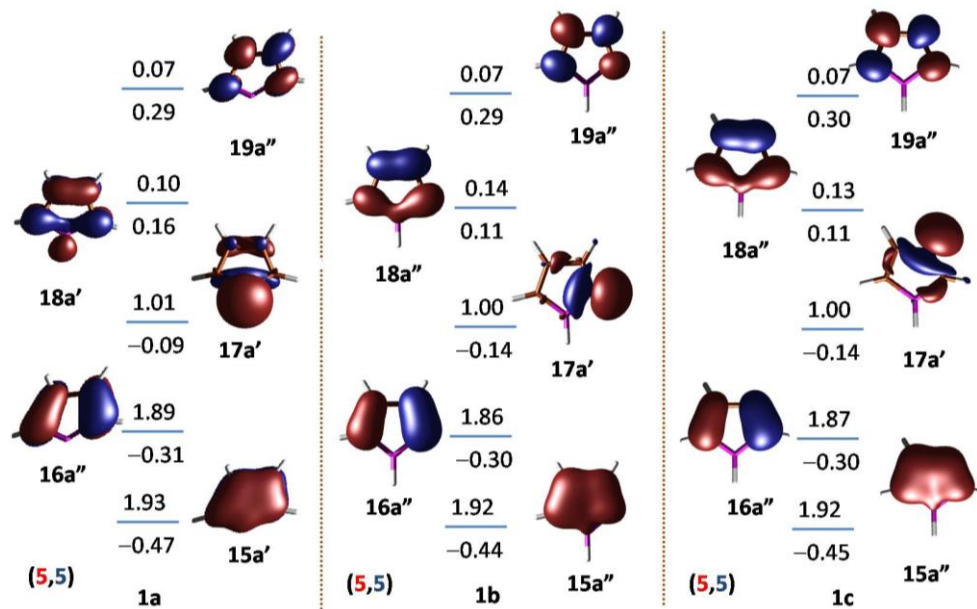
-18.4/-15.1/*-16.5*

3

f)

Figure A3.10 Bimolecular reactions of (a) phenyl radical **Ph**; (b) 2-pyridyl radical **1a**; (c) 3-pyridyl radical **1b**; (d) 4-pyridyl radical **1c**; (e) 2-pyridinyl radical **3a**; (f) 3-pyridinyl radical **3b** and (g) 4-pyridinyl radical **3c** with small molecules (CO, H_2, CO_2, H_2O, CH_4 and CH_3OH). (For water, both H-atom abstraction as well as OH abstraction channels by the radical isomers have been indicated separately; The energy values (in kcal/mol) are indicated in Bold – (U)B3LYP/cc-pVTZ; Normal font – (U)M06-2X/cc-pVTZ and italics – (U)CCSD(T)/cc-pVTZ//(U)B3LYP/cc-pVTZ)
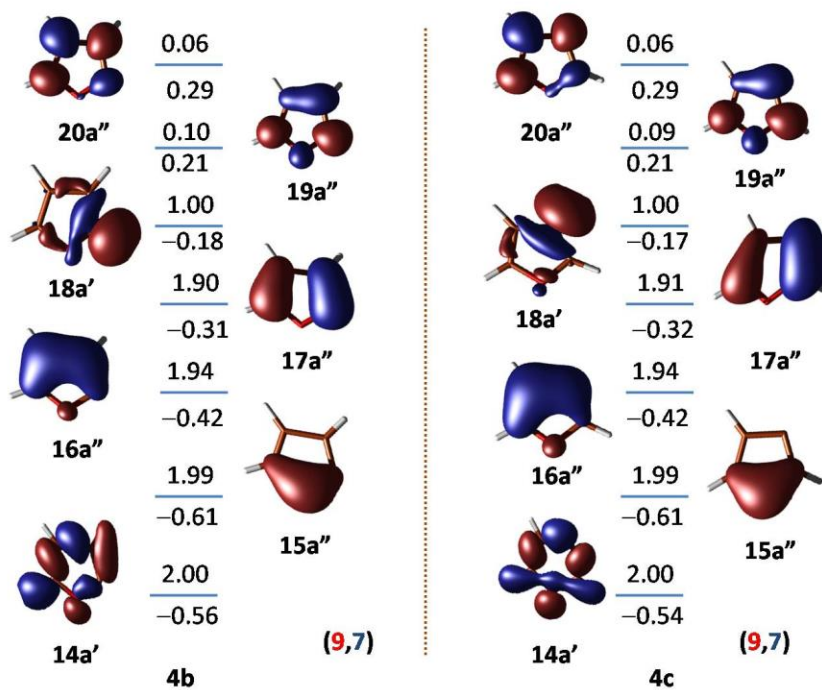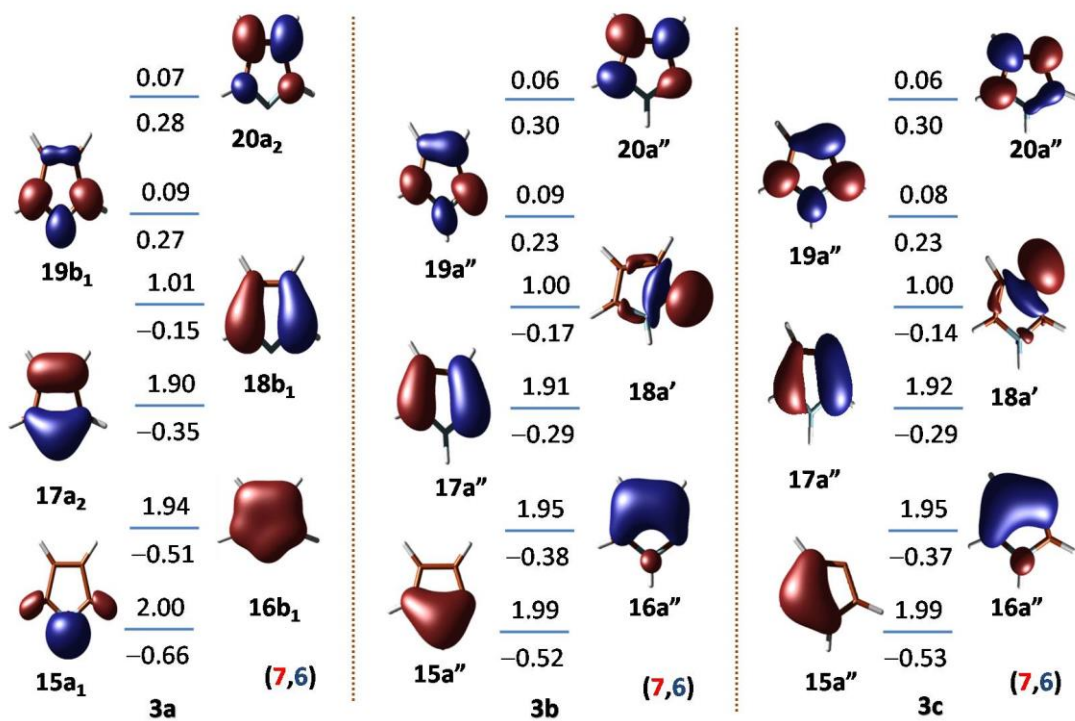
APPENDIX CHAPTER 4

Table A4.1 Electronic and thermodynamic parameters of parent and their radical isomers at (U)B3LYP/cc-pVTZ (normal font) and (U)M06-2X/cc-pVTZ (italics) level of theory.

Species	Absolute energy (Hartrees)	ZPVE (Hartrees)	Lowest frequency	Spin Contamination		Point group	Electronic state	Absolute free energy(G) (Hartrees)	Absolute Enthalpy(H) (Hartrees)
				Before annhilation	After annhilation				
1	−180.20647	0.076651	188.64	0.0000	0.0000	C_{2v}	$^1A_1$	−180.23276	−180.20097
	−180.11667	0.077512	193.63	0.0000	0.0000			−180.14294	−180.11120
1a	−179.54530	0.065054	350.99	0.7585	0.7500	C_S	$^2A'$	−179.57251	−179.53993
	−179.46111	0.065495	245.88	0.7594	0.7500			−179.48846	−179.45561
1b	−179.52767	0.063740	176.34	0.7966	0.7505	C_S	$^2A'$	−179.55529	−179.52211
	−179.44128	0.064749	189.40	0.7973	0.7505			−179.46881	−179.43581
1c	−179.53353	0.063326	65.87	0.7712	0.7501	C_S	$^2A'$	−179.56180	−179.52778
	−179.44656	0.064376	122.93	0.7811	0.7502			−179.47434	−179.44098
2	−194.08183	0.096426	352.61	0.0000	0.0000	C_{2v}	$^1A_1$	−194.10775	−194.07674
	−193.98542	0.093280	344.37	0.0000	0.0000			−194.01135	−193.98035
2a	−193.45570	0.077774	35.39	0.7679	0.7501	C_{2v}	$^2A_2$	−193.48447	−193.44994
	−193.35954	0.079412	323.45	0.7657	0.7501			−193.38676	−193.35430
2b	−193.39910	0.079606	313.06	0.7637	0.7501	C_S	$^2A'$	−193.42631	−193.39398
	−193.30665	0.080651	326.34	0.7703	0.7501			−193.33381	−193.30159
2c	−193.40052	0.079502	350.19	0.7590	0.7500	C_S	$^2A'$	−193.42767	−193.39544
	−193.30777	0.080514	344.83	0.7638	0.7501			−193.33491	−193.30274
3	−210.16667	0.082377	480.36	0.0000	0.0000	C_{2v}	$^1A_1$	−210.19240	−210.16176
	−210.07253	0.083465	515.22	0.0000	0.0000			−210.09822	−210.06770
3a	−209.51790	0.067838	495.34	0.7645	0.7501	C_{2v}	$^2A_2$	−209.54421	−209.51304
	−209.42342	0.06890	509.44	0.7645	0.7501			−209.44969	−209.41863
3b	−209.47857	0.069009	316.45	0.7579	0.7500	C_S	$^2A'$	−209.50570	−209.47346
	−209.38858	0.07042	439.07	0.7579	0.7500			−209.41554	−209.38370
3c	−209.47921	0.069586	443.51	0.7563	0.7500	C_S	$^2A'$	−209.50618	−209.47428
	−209.38918	0.07075	486.89	0.7563	0.7500			−209.41609	−209.38436

Species	Absolute energy (Hartrees)	ZPVE (Hartrees)	Lowest frequency	Spin Contamination		Point group	Electronic state	Absolute free energy(G) (Hartrees)	Absolute Enthalpy(H) (Hartrees)
				Before annhilation	After Annihilation				
4	−230.03888	0.069865	618.11	0.0000	0.0000	C$_{2v}$	$^1A_1$	−230.06448	−230.03423
	−229.94218	0.070955	623.20	0.0000	0.0000			−229.96776	−229.93758
4b	−229.35014	0.056852	493.99	0.7595	0.7500	C$_S$	$^2A'$	−229.37699	−229.34547
	−229.28497	0.058047	568.44	0.7628	0.7501			−229.28497	−229.25359
4c	−229.35030	0.057201	549.72	0.7569	0.7500	C$_S$	$^2A'$	−229.37712	−229.34566
	−229.25751	0.058326	577.45	0.7605	0.7500			−229.28430	−229.25295
5	−496.76033	0.074426	333.12	0.0000	0.0000	C$_S$	$^1A'$	−496.78789	−496.75485
	−496.64808	0.075300	322.31	0.0000	0.0000			−496.67563	−496.64262
5a	−496.14514	0.064737	325.32	0.7617	0.7501	C$_{2v}$	$^2B_1$	−496.17263	−496.13975
	−496.03640	0.065686	325.25	0.7608	0.7501			−496.06385	−496.03109
5b	−496.08016	0.061804	282.72	0.7603	0.7500	C$_1$	^2A	−496.10838	−496.07464
	−495.97126	0.062866	306.02	0.7671	0.7501			−495.99941	−495.96583
5c	−496.08560	0.061522	327.19	0.7588	0.7500	C$_1$	^2A	−496.11376	−496.08008
	−495.97586	0.062380	315.16	0.7640	0.7501			−496.00402	−495.97039
6	−553.03163	0.066562	461.70	0.0000	0.0000	C$_{2v}$	$^1A_1$	−553.05819	−553.02662
	−552.92821	0.067432	467.42	0.0000	0.0000			−552.95474	−552.92326
6b	−552.34612	0.053810	371.93	0.7595	0.7500	C$_S$	$^2A'$	−552.37399	−552.34106
	−552.24645	0.05479	422.88	0.7637	0.7501			−552.27424	−552.24150
6c	−552.35068	0.053793	444.51	0.7574	0.7500	C$_S$	$^2A'$	−552.37850	−552.34566
	−552.25035	0.05469	456.71	0.7616	0.7501			−552.27812	−552.24541

0.07
0.29
19a″

0.10
0.16
18a′

1.01
−0.09
17a′

1.89
−0.31
16a″

1.93
−0.47
15a′

(5,5)
1a

0.07
0.29
19a″

0.14
0.11
18a″

1.00
−0.14
17a′

1.86
−0.30
16a″

1.92
−0.44
15a″

(5,5)
1b

0.07
0.30
19a″

0.13
0.11
18a″

1.00
−0.14
17a′

1.87
−0.30
16a″

1.92
−0.45
15a″

(5,5)
1c

0.07
0.29
20a₂

0.08
0.28
19b₁

1.01
−0.14
18b₁

1.90
−0.29
17a₂

1.94
−0.47
16b₁

(5,5)
2a

0.07
0.31
20a″

0.12
0.17
19a″

1.00
−0.15
18a′

1.88
−0.30
17a″

1.93
−0.43
16a″

(5,5)
2b

0.07
0.31
20a″

0.12
0.17
19a″

1.00
−0.15
18a′

1.88
−0.30
17a″

1.93
−0.43
16a″

(5,5)
2c

203

Figure A4.1 The complete active space molecular orbital diagrams of all the radicals at CASSCF/cc-pVTZ level of theory. The values corresponding to orbital energies (in hartrees) and the occupancies are indicated. Orbital number and their respective symmetry are designated in bold. The active space is shown as (**a, b**) where **a** indicates number of electrons and **b** as number of orbitals. All the orbitals are rendered at an isovalue 0.05.

205

LIST OF PUBLICATIONS

1. Sah, C.; Jacob, L.; Saraswat, M.; Venkataramani, S. Does Nitrogen Lone Pair Lead to Two Centered - Three Electrons (2c-3e) Interactions in Pyridyl Radical Isomers? *J. Phys. Chem. A.* **2017**, *121* (19), 3781-3791.

2. Sah, C.; Saraswat, M.; Jacob, L.; Venkataramani, S. Insights on Unimolecular and Bimolecular Reactivity Patterns of Pyridyl, Pyridyl-*N*-oxide, and Pyridinyl Radicals Through Spin Density. *Comput. Theor. Chem.* **2020**, *1191,* 113025.

3. Sah, C.; Yadav, A. K.; Venkataramani, S. Deciphering Stability of Five-Membered Heterocyclic Radicals: Balancing Act Between Delocalization and Ring Strain. *J. Phys. Chem. A.* **2018**, *122* (24), 5464–5476.

4. Kumar, P.; Srivastava, A.; Sah, C.; Devi, S.; Venkataramani, S. Azoheteroarene photoswitches exhibiting high Z-isomer stability, solid state photochromism and reversible light-induced phase transition. *Chem. Eur. J.* **2019**, *25*, 11924–11932.

5. Rajamanickam, S.; Sah, C.; Mir, B. A.; Ghosh, S.; Sethi, G.; Yadav, V.; Venkataramani, S.; Patel, B. K. Bu$_4$NI Catalyzed Radical Induced Regioselective N-Alkylations and Arylations of Tetrazoles Using Organic Peroxides/Peresters. *J. Org. Chem.* **2020**, *85*, 2118−2141.

CONFERENCES AND WORKSHOPS

1. Presented poster 'Pyridine and pyridine-*N*-oxide radicals – A Computational study' in 18th CRSI National Symposium In Chemistry Feb 2016 at Punjab University, Chandigarh.

2. Presented poster 'Bimolecular reactions of pyridine and pyridine-*N*-oxide radicals with small molecules' in Modern Trends in Molecular Magnets which was held in May 2016 at IIT Bombay.

3. Attended a workshop on 'Electronic structure of Co-ordination Complexes' in May 2016 at IIT Bombay.

4. Presented poster 'Resonance stabilization in *N*-centered radicals- Utility in generating high spin systems' in 16th discussion Meeting of Spectroscopy and Dynamics of Molecules and Clusters held at Koti Resorts, Shimla, from 21st February to 24th February 2019.

5. Attended International E-workshop on "Electronic structure theory and application to chemical systems" during 02-06 November 2020 (online) organized by the Department of Chemistry, National Institute of Technology, Tiruchirappalli.

Insights on unimolecular and bimolecular reactivity patterns of pyridyl, pyridyl-N-oxide, and pyridinyl radicals through spin density

Author: Chitranjan Sah,Mayank Saraswat,Lilit Jacob,Sugumar Venkataramani

Publication: Computational and Theoretical Chemistry

Publisher: Elsevier

Date: 1 December 2020

Journal Author Rights

BACK   CLOSE WINDOW

Deciphering Stability of Five-Membered Heterocyclic Radicals: Balancing Act Between Delocalization and Ring Strain

ACS Publications
Most Trusted. Most Cited. Most Read.

Author: Chitranjan Sah, Ajit Kumar Yadav, Sugumar Venkataramani

Publication: The Journal of Physical Chemistry A

Publisher: American Chemical Society

Date: Jun 1, 2018

Copyright © 2018, American Chemical Society

PERMISSION/LICENSE IS GRANTED FOR YOUR ORDER AT NO CHARGE

This type of permission/license, instead of the standard Terms & Conditions, is sent to you because no fee is being charged for your order. Please note the following:

- Permission is granted for your request in both print and electronic formats, and translations.
- If figures and/or tables were requested, they may be adapted or used in part.
- Please print this page for your records and send a copy of it to your publisher/graduate school.
- Appropriate credit for the requested material should be given as follows: "Reprinted (adapted) with permission from (COMPLETE REFERENCE CITATION). Copyright (YEAR) American Chemical Society." Insert appropriate information in place of the capitalized words.
- One-time permission is granted only for the use specified in your request. No additional uses are granted (such as derivative works or other editions). For any other uses, please submit a new request.

BACK   CLOSE WINDOW

Chitranjan Sah

Address: Khazanchi Mohalla
Almora (Uttarakhand)
Email: chitranjansah43@gmail.com

EDUCATION

Ph.D., Indian Institute of Science Education and Research   (2015 – ongoing)
M.S., Indian Institute of Science Education and Research   (2013 – 2015)
CGPA: 8.9/10
B.Sc Chem (Hons)., Kirori Mal College (University of Delhi)   (2010 – 2013)
Percentage: 80.2 %
Class XII., Koormanchal Academy Almora   (2009 – 2010)
Percentage: 90.3%

RESEARCH EXPERIENCE

Summer Internship, IISER MOHALI   (05/2015 – 07/2015)
- Advisor: Dr. Sugumar Venkataramani
- Understanding the electronic structure and reactivity aspects of dehydro-triazole radicals

Masters project, IISER MOHALI   (01/2015 – 05/2015)
- Advisor: Dr. Sugumar Venkataramani
- Synthesis and characterization of substituted acetylacetone derivatives of phenylazobenzene

Summer Internship, IISER MOHALI   (05/2014 – 07/2014)
- Advisor: Dr. Angshuman Roy Choudhury
- In-situ crystallization of fluoro-phenols and anilines under cryogenic condition

ADDITIONAL SKILLS

Technical: Ultra-high Vacuum technology
Spectroscopy: Infrared spectroscopy, Matrix-isolation technique
Computational: Gaussian 09, MOLPRO

AWARD

Certificate of Academic Excellence: Highest grade point for the semester August 2013 – November 2013